Mathematical models of tumour-immune interactions: discrete and continuum approaches

Emma Leschiera

SORBONNE UNIVERSITÉ
CRÉATEURS DE FUTURS DEPUIS 1257

SORBONNE UNIVERSITÉ
LJLL

Doctoral School **École Doctorale Sciences Mathématiques de Paris Centre**

University Department **Laboratoire Jacques-Louis Lions**

Thesis defended by **Emma LESCHIERA**

Defended on **October 10, 2022**

In order to become Doctor from Sorbonne Université

Academic Field **Mathématiques appliquées**

Mathematical models of tumour-immune interactions: discrete and continuum approaches

Thesis supervised by	Luís ALMEIDA	Supervisor
	Chloé AUDEBERT	Co-Supervisor
	Tommaso LORENZI	Co-Supervisor

Committee members

Referees	Raluca EFTIMIE	Université de Franche-Comté	
	Noemi PICCO	Swansea University	
Examiners	Thierry GOUDON	Inria Sophia Antipolis	
	Thomas LEPOUTRE	Inria Rhone Alpes and Université Lyon 1	
	Benoît PERTHAME	Sorbonne Université	Committee President
Supervisors	Luís ALMEIDA	Sorbonne Université	
	Chloé AUDEBERT	Sorbonne Université	
	Tommaso LORENZI	Politecnico di Torino	

Keywords: tumour-immune interactions, immunotherapy, discrete models, continuum models, numerical simulations

Mots clés : interactions tumeur-système immunitaire, immunothérapie, modèles discrets, modèles continus, simulations numériques

This thesis has been prepared at

Laboratoire Jacques-Louis Lions
Sorbonne Université
Campus Pierre et Marie Curie
4 place Jussieu
75005 Paris
France

☎ +33 1 44 27 42 98
Web Site https://ljll.math.upmc.fr/

A tutte le persone che contribuiscono a rendere la mia vita così felice.

À toutes les personnes qui contribuent à rendre ma vie si heureuse.

Rare sono le persone che usano la mente... poche coloro che usano il cuore... e uniche coloro che usano entrambi.

Rita Levi Montalcini

Dans la vie, rien n'est à craindre, tout est à comprendre.

Marie Curie

Mathematical models of tumour-immune interactions: discrete and continuum approaches

Abstract

The past decade's technological advances have led to the development of immunotherapies, which differ from conventional anti-cancer therapies by targeting tumour-immune interactions to enhance the effectiveness of the anti-tumour immune response. However, these interactions are based on complex mechanisms that make it difficult to design treatments to effectively boost the immune response. For this reason, mathematical models are useful tools for reproducing and predicting the spatio-temporal dynamics of interactions between tumour cells and immune cells, in order to test the potential of new therapeutic techniques in a flexible and affordable way. In this thesis, we develop discrete and continuum models to describe the spatio-temporal dynamics of the interactions between a solid tumour and cytotoxic T cells, with the goal to investigate the biological settings which allow for the clearance or the escape of the tumour. The discrete models developed in this work track the dynamics of single cells, thus permitting the representation of single cell-scale mechanisms, and are sufficiently detailed and specific to qualitatively investigate and reproduce empirical observations. The continuum models considered are not formulated on the basis of phenomenological arguments, which can hinder a precise mathematical description of crucial biological and biophysical aspects, but they are formally derived from the discrete models through suitable asymptotic methods. The results of computational simulations of the discrete models show that there is an excellent quantitative agreement between them and numerical solutions of the corresponding continuum models, and further clarify the conditions for successful and unsuccessful immune surveillance. Ultimately, the mathematical models presented in this thesis may provide a framework to help biologists and clinicians gain a better understanding of the mechanisms that are responsible for immune escape, and they may be promising tools in the exploration of therapeutic strategies to improve the effectiveness of the overall anti-tumour immune response.

Keywords: tumour-immune interactions, immunotherapy, discrete models, continuum models, numerical simulations

Résumé

Au cours de la dernière décennie, les progrès technologiques ont permis la conception d'immunothérapies qui, contrairement aux thérapies anticancéreuses classiques, ciblent les interactions entre cellules tumorales et cellules immunitaires, dans le but de renforcer l'efficacité de la réponse immunitaire. Cependant, ces interactions reposent sur des mécanismes complexes, ce qui rend difficile la conception de traitements efficaces. Par conséquent, les modèles mathématiques sont des outils utiles pour reproduire la dynamique spatio-temporelle des interactions entre les cellules tumorales et les cellules immunitaires, afin de tester le potentiel de nouvelles techniques thérapeutiques de manière flexible et non coûteuse. Dans cette thèse, nous développons des modèles discrets et continus pour décrire la dynamique spatio-temporelle des interactions entre une tumeur solide et les cellules T cytotoxiques, dans le but d'étudier les paramètres biologiques qui permettent l'élimination, ou bien l'échappement, de la tumeur. Les modèles discrets développés dans ce travail décrivent la dynamique de chaque cellule, permettant ainsi la représentation de mécanismes à l'échelle cellulaire. De plus, ils sont suffisamment détaillés et spécifiques pour reproduire qualitativement les résultats d'études expérimentales. Quant aux modèles continus, ils ne sont pas formulés sur la base d'arguments phénoménologiques, qui peuvent limiter une description mathématique précise d'aspects biologiques et biophysiques cruciaux, mais ils sont dérivés formellement des modèles discrets par le biais de méthodes asymptotiques appropriées. Les résultats des simulations numériques des modèles discrets montrent qu'il existe un excellent accord quantitatif entre eux et les solutions des modèles continus correspondants, et clarifient les conditions de réussite, ou bien d'échec, de la surveillance immunitaire. Enfin, les modèles mathématiques présentés dans cette thèse peuvent fournir un cadre pour aider les biologistes et les cliniciens à mieux comprendre les mécanismes par lesquels les tumeurs échappent au système immunitaire, et peuvent être des outils prometteurs pour explorer des stratégies thérapeutiques conçues pour améliorer l'efficacité de la réponse immunitaire anti-tumorale.

Mots clés : interactions tumeur-système immunitaire, immunothérapie, modèles discrets, modèles continus, simulations numériques

Laboratoire Jacques-Louis Lions
Sorbonne Université – Campus Pierre et Marie Curie – 4 place Jussieu – 75005 Paris – France

Acknowledgements

I like to compare the PhD thesis to a journey across the ocean: when we start sailing, the sea is smooth and allows us to navigate with confidence and enthusiasm. Then, after a while, we find ourself out on the open sea, going through storms, thinking we have lost our way. But when we finally see the final destination, whatever it may be, we realize the great achievements we have made. Despite few big waves, my journey went smoothly, and certainly also thanks to all the people who were by my side.

First of all, my sincere thanks go to my PhD advisors: Luís Almeida, Chloé Audebert and Tommaso Lorenzi. Thank you for giving me the opportunity to work on this fascinating subject and for guiding me throughout this thesis. I thank you for the time and attention you payed to my work, for the many discussions and ideas you gave me, for your patience and enthusiasm. Learning from you has been a real pleasure and your kindness and advice have provided the best possible environment for the success of my journey.

I am honored that Raluca Eftimie and Noemi Picco have accepted the role of referees for this thesis, and I deeply thank them for the precious time they have spent on the manuscript. Also, I would like to thank Thierry Goudon, Thomas Lepoutre and Benoît Perthame for having accepted to be part of the jury: your work is a real source of inspiration for me.

During these years I have also had the chance to meet, discuss and work with people from different communities. A big thanks to my master professors in Lyon, for having allowed me to discover this fascinating area of mathematics applied to biology and medicine. A special thanks to Thomas Lepoutre, for having been the first one to introduce me to the research in the math-bio world and for having encouraged me to pursue this path. I would like to thank Shensi Shen, Melanie Flint and Chandrasekhar Venkataraman for the fruitful and interesting conversations and for the valuable collaboration. I would also like to thank all the members of the Inria Mamba team for their kindness and the organisation of the mamba seminar, which gave meaning to my Monday afternoons during confinement ;-) I am grateful to Florence Hubert and Jacqueline Marvel for your enriching discussion and advice.

The PhD journey is never completed alone, so I would like to thank all those who made the experience even more exciting. Prima di tutto, vorrei ringraziare le mie patate dell'LJLL, croccanti fuori e morbide dentro: la nono-nonna e la Gioggetta, un amore a prima (s)vista e la Kikina, il gioiellino più bello che mi ha regalato St. Andrews. Senza di voi questo viaggio non avrebbe avuto lo stesso sapore. Grazie per le serate pazzerelle, gli spettegolezzi e il sostegno quotidiano. Spero di condividere ancora un'infinità di avventure insieme a voi, in ambito professionale e non solo. Un énorme merci/gracias/grazie à mes collègues du bureau: Jesús, Nicolas e Eugenio, con cui ho condiviso quotidianamente il mio viaggio, i miei momenti felici e quelli più difficili, ainsi que Fabrice, pour les pauses gourmandes à parler de focaccia. Seguramente no olvidaré a todos los demás del grupo italiano-latino-español, autrement dit le groupe des mange-tard ou du thé de 17h: Elena, Agustin, Ramon, Chourouk (porque ahora tienes un nivel C2 de español, no?), María. Et bien sûr, 1000 mercis vont à tous les doctorants avec qui j'ai eu la chance de

partager une petite ou grande partie de ces trois années: les responsables doctorants presents et passé, Antoine, Juliette, Rémi, Gabriela et David; les GTTeams, Charles, Guillaume, Lise, Lucas, Pierre, Matthieu, Yipeng, Jules, sans oublier les responsables bière et soirées, certains dejà cité en haut, bien que ils soient très actifs dans ce rôle aussi, et je rajouterais Anatole, Thomas, Robin, Elise, Alex (x2), Christophe, Nga. Merci pour les soirées clandestines à danser Sean Paul et pour m'avoir laissé chanter les chansons italiennes quand c'était mon anniversaire. Merci pour les moments conviviaux et chaleureux pendant les poses midi et en dehors du labo!

Et si le voyage est si agréable à vivre, c'est aussi grâce aux personnes qui font en sorte que le vent souffle toujours dans la bonne direction: merci à Kashayar pour avoir résolu mes petits et grands problèmes informatiques, et merci à Malika, Salima, Catherine et Nathalie pour leur rigueur (et patience) à gérer l'organisation administrative du laboratoire.

Place maintenant à la catégorie hors-LJLL. Les premiers remerciements vont à 'l'aperitif floor' de Rue Barrault. Je tiens à remercier Nico, Jul et Clémence (+ les deux petites princesses) parque que sans vous les confinements n'auraient pas eu le même gout, et je souligne que le gout était plutôt bon. Un grazie speciale a Lollo, che mi ha fatto sempre sentire un po' a casa, mi ha istruita sull'attualità italiana e mi ha fatto venire l'acquolina in bocca con le sue prelibatezze. Et merci à Celine et Arnauld (+ le petit prince), parce que tous ensemble on a formé une belle équipe et on s'est bien amusé.

Et on n'oubli pas les amis qui étaient dejà la ancore avant de commencer ce voyage. Grazie a Elena, che nonostante sei lontana mi sei sempre vicina. Merci à Alice, que au contraire cette année a été littéralement très proche et ça a été trooop cool. A Ling Zi, qui gagne le prix mondial de meilleure coloc pour la vie et qui a toujours des bons plans à proposer. Une grande pensé va à Elias, Anais, Yannou et Claire, qui continuent à m'envoyer un message chaque fois qui passent par Paris. Vous êtes des personnes exceptionnelles et je suis contente de garder le lien avec vous ! Alle mie amiche del cuore, Chiara, Bea e Marta, che anche se ci vediamo poco so che ci saranno per sempre. E alle amiche pazze, Luli, Mari, Silvs e Marti: quando sono con voi, le risate e le figure di merd* sono assicurate.

Je suis reconnaissante envers ma famille bretonne, ma mamie pour sa douceur, mon papi pour sa soif de connaissance et ma tata Anne pour sa gentillesse et son sens de l'humour. Grazie a zia Paola per l'amore che mi trasmette, e per accogliermi e coccolarmi ogni volta che sono una profuga in Italia. Al mio caro Pepi, so che quando mi stritoli, lo fai anche perché mi vuoi (un po') bene. Grazie a Chiaretta, per prenderti cura della tua Muzza, dalle serate marce in discoteca alle serate detox con la tisana. Ringrazio anche Otta, solo perché mi sento in dovere di metterla nei ringraziamenti, ma alla fine è simpatica quindi ci sta (scheeerzo baby).

Alla mia mamma e il mio papà, grazie per il miglior regalo che avreste potuto farmi: la vita, accompagnata da grandi valori che mi hanno permesso di viverla fino ad adesso così passionalmente e felicemente. Grazie per avermi tenuto la mano quando ce n'era bisogno e avermela lasciata quando sapevate che ero pronta a continuare da sola. Siete la mia forza, il mio faro e il mio porto sicuro. E grazie a mio fratello Matteo, come sono stata fortunata a crescere insieme a te. Sei il mio orgoglio, energia pura, la mia grande fonte di inspirazione e motivazione.

Et enfin, merci à Abou d'être mon bonheur quotidien, la luce che illumina i miei occhi et le feu qui réchauffe mon coeur. Tu es celui qui me rend *deliriously happy*.

Contents

Biological glossary

antigen Any substance that causes the body to make an immune response against that substance. Antigens include toxins, chemicals, bacteria, viruses, or other substances that come from outside the body. Body tissues and cells, including tumour cells, also have antigens on them that can trigger an immune response. 1, 2, 3, 5, 6, 7, 8, 9, 10, 12, 13, 14, 16, 18, 20, 21, 22, 24, 25

antigen presenting cell (APC) Heterogeneous group of immune cells that mediates the cellular immune response by processing and presenting antigens for recognition by certain lymphocytes such as T cells. Classical APCs include dendritic cells and macrophages 4, 5, 7

chemoattractant A chemical (chemotactic) agent that induces an organism or a cell to migrate towards it. In the context of tumours, the chemoattractant can represent a mixture of small soluble proteins called chemokines (*e.g.* CCL3, CCL5, CCL20, and CXCL10). During the anti-tumour immune response, cytotoxic T lymphocytes migrate via chemotaxis towards the tumour, in the directions of stronger gradients of the chemokines produced by both tumour and immune cells. 6, 16, 19, 25

cytokine A type of protein produced by certain immune and non-immune cells which has an effect on the immune system. Some cytokines, the pro-inflammatory cytokines, stimulate the immune system, helping the body fight tumours, infections, and other diseases. Other cytokines, the anti-inflammatory cytokines, slow down the immune system, inhibiting its function. Examples of cytokines are interleukins, such as IL-2 and IL-10, interferons, such as INF$-\gamma$, and growth factors. 4, 5, 8, 9, 12, 13, 14, 17, 18

cytotoxic A substance, a cell, a drug that kills cells, including tumour cells. Cytotoxic agents may stop tumour cells from dividing and growing and may cause tumours to shrink in size. For example: cytotoxic T lymphocyte, cytotoxic chemotherapy. 1, 5, 6, 22

cytotoxic T lymphocyte (CTL) A type of cells of the adaptive immune system that has the capacity to directly kill other cells. It plays a major role in host defense against tumour cells 3, 5, 6, 7, 8, 9, 10, 11, 12, 13, 14, 16, 17, 18, 19, 20, 21, 22, 24, 25

dendritic cell A special type of immune cell that boosts immune responses by showing antigens on its surface to other cells of the adaptive immune system. A dendritic cell is a type of phagocyte and also an antigen-presenting cell (APC). 4, 5, 7, 8, 20

immune checkpoint A type of protein produced by some types of immune system cells, such as cytotoxic T lymphocytes, and some tumour cells, which helps prevent immune responses

from being too strong. During tumour development, immune checkpoints can keep T cells from killing tumour cells. Examples of checkpoint proteins found on T cells or tumour cells include PD-1/PD-L1 and CTLA-4/B7-1/B7-2. 8, 11

immune checkpoint inhibitor A type of drug that blocks proteins called immune checkpoints. When these checkpoints are blocked, T cells can kill tumour cells more efficiently. Examples of immune checkpoint inhibitors include anti-PD-L1 or anti-PD-1 (which block the binding of PD-L1 to PD-1) and anti-CTLA-4 antibody (which block the binding of CTLA-4 to B7-1/B7-2) 2, 8, 11, 13

immunogenic Relating to or denoting substances able to produce an immune response. For example: immunogenic tumours, immunogenic antigens. 12, 18, 20, 25

intra-tumour heterogeneity (ITH) It refers to distinct tumour cell populations (with different molecular and phenotypical profiles) within the same tumour specimen. It differs from inter-tumour heterogeneity, which refers to the differences found between similar tumours in different patients. 8, 10, 25

macrophage A type of cell of the innate immune response that surrounds and kills microorganisms, removes dead cells, and stimulates the action of other immune system cells, acting as antigen-presenting cell (APC). Some macrophages have a tumour-promoting phenotype, and can drive pathological phenomena including tumour cell proliferation, tumour angiogenesis, invasion and metastasis, immunosuppression, and drug resistance. 4, 7

major histocompatibility complex (MHC) A group of genes that codes for proteins found on the surface of cells that helps the immune system recognize foreign substances. During an immune response, it allows T lymphocytes to detect antigen presenting cells that have ingested infectious microorganisms and display peptide fragments on their surface. 5, 7, 8, 9, 10

natural killer cell (NK cell) A type of cell of the innate immune system that has granules (small particles) with enzymes that can kill tumour cells or cells infected by a virus. 4, 21

solid tumour An abnormal mass of tissue that usually does not contain cysts or liquid areas. Solid tumours may be benign (not cancer), or malignant (cancer). Different types of solid tumours are named for the type of cells that form them. Examples of solid tumours are sarcomas, carcinomas, and lymphomas. Leukemias (cancers of the blood) generally do not form solid tumours. 4, 11, 12, 20, 25

T cell receptor (TCR) A group of proteins found on T cells. TCRs bind to certain antigens found on abnormal cells, tumour cells, cells from other organisms. This interaction causes the T cells to attack these cells and helps the body fight infection, tumour cells, or other diseases. 5, 6, 9, 16, 24

telomere The ends of a chromosome. Each time a cell divides, telomeres lose a small amount of DNA and become shorter. Over time, the chromosomes become damaged and the cells die. However, tumour cells express high levels of telomeraze, an enzyme preventing the shortening of the telomere, allowing for a longer or infinite survival of cells. 3, 4

tumour microenvironment (TME) The normal cells, immune cells, molecules, and blood vessels that surround, feed and interact with tumour cells. A tumour can change its microenvironment, and the microenvironment can affect how a tumour grows and spreads. 6, 7, 8, 9, 13, 17

Mathematical glossary

hybrid discrete-continuum model A modelling approach which combines individual-based modelling techniques (usually to describe individuals) with ordinary or partial differential equations (usually to describe continuum fields). 14, 15, 17, 20

individual-based model A discrete and stochastic modelling approach which attempts to describe how individuals behave and interact over time by specifying rules for each individual. These rules depend on the probability of events occurring. 10, 14, 16, 17, 20, 22, 24, 25

integro-differential equation (IDE) mathematical equation that involves one or more independent variables, an unknown function and both derivatives (with respect to one variable) and integrals of the function. A partial integro-differential equation is an equation for a function of two or more variables which appear as arguments both of integral and of partial differential operators. 15, 16, 18, 23

ordinary differential equation (ODE) mathematical equation that involves one independent variables, usually time, an unknown function (dependent on this variable), and partial derivatives of the unknown function with respect to the independent variable. 15, 17, 18, 20, 21, 23

partial differential equation (PDE) mathematical equation that involves two or more independent variables, usually time and space, an unknown function (dependent on those variables), and partial derivatives of the unknown function with respect to the independent variables. 15, 16, 17, 19, 20, 21, 22, 23

Chapter 1

Introduction

1.1 Motivation

Cancer can be described as a disease in which some abnormal or damaged cells of the body grow uncontrollably and spread to other parts of the body[1]. The first, possibly disputable, evidence of this disease was found in the fossil records of a human ancestor as old as 1.7 million years [162], and that of a dinosaur, dated back more than 75 million years ago [201]. Cancer was a quite rare disease in ancient human societies, but today in France it is the first cause of death in men and the second in women[2]. There are two probable reasons for that: (1) the harmful environmental and lifestyle factors that trigger its emergence, and (2) the increase in life expectancy, since the risk of developing a tumour increases with age. Today, cancer results in approximately ten million annual deaths, only taking into account official data [159]. Despite technological developments and major advances in cancer research, it is clear that this disease is still enduring.

It seems that the best choice of treatment that humans used for centuries, was the surgical removal of malignant tumours, and even nowadays it frequently remains the best treatment option. However, it was already known to ancient Romans and Greeks that surgery could only be successful for superficial tumours, and that in many cases it could even worsen the conditions of the patient [50]. The first major breakthrough happened at the turn of the 19th and 20th centuries with the discovery of X-rays and the introduction of radiotherapy treatments, which use high doses of radiation to kill tumour cells and shrink tumours. In fact, at high doses, radiation therapy is able to kill tumour cells or slow their growth by damaging their DNA. In the 1940s, the introduction of chemotherapy to treat tumours proved to be another considerable breakthrough in oncology. Chemotherapy uses one or more *cytotoxic* anti-cancer drugs (chemotherapeutic agents), which inhibit cell mitosis (*i.e.* division) or induce DNA damage. Surgery, radiotherapy and chemotherapy are still the most widespread modalities in tumour treatment. However, the side effects of these traditional treatment approaches can be severe. They include: sustained damage to healthy cells, nausea, fertility issues, hair loss and psychological issues.

More recently, the focus of cancer therapy research has turned to developing targeted and more personalised treatments. The development of some of these new treatment approaches relies on the fact that the immune system plays a primary and critical role in the prevention and eradication of tumours. In fact, tumour cells express antigens on their surface which allow them not only to be identifiable by cells of the immune system but also enable an effective immune response to be triggered. This finding implies that clinically observable, and often

[1] https://www.cancer.gov
[2] https://www.santepubliquefrance.fr

aggressive, tumours are those that have escaped control of the immune system. In this context, designing immunomodulatory treatments to enhance or restore anti-tumour immune responses may be beneficial in the treatment of multiple types of tumours. The development of these new therapeutic approaches is based on understanding the key mechanisms, or hallmarks, that enable the tumour to avoid immune destruction. There can be multiple mechanisms that lead to the suppression of the immune response; moreover, these immunosuppressive mechanisms can vary between patients. Consequently, immunotherapy techniques have been, and continue to be, developed by targeting the key mechanisms that are responsible for immune escape, to offer a more personalised form of cancer treatment. These techniques can be active, *i.e.* specifically targeting tumour cells, like cancer vaccines that contain specific antigens, or passive, *i.e.* enhancing the ability of the immune system to attack tumour cells, like immune checkpoint inhibitors, whose authors were awarded the Nobel Prize in Medicine in 2018. However, many of the biological phenomena that foster the escape of tumour cells from the action of immune cells and the failure of immunotherapy treatments are still not fully understood to this day. And the causes of this lack of understanding are diverse. One reason is the complex nature of the interactions between tumour cells and immune cells, which involve various molecules, proteins, receptors and cells that promote or inhibit the immune action. Moreover, the development and testing of new therapy techniques can be an expensive and time-consuming process, and often associated with ethical difficulties, as the result of changes in clinical protocols may reduce the overall treatment efficacy.

One option to tackle these problems is to develop mathematical models capable of describing and synthesising these complex phenomena in order to carry out numerical experiments (known as *in silico*). The added value of mathematical modelling and computer simulations are their reproducibility and flexibility. On the one hand, their reproducibility makes it possible to replicate various experiment in shorter periods of time than those required for clinical trials. On the other hand, their flexibility allows to add various biological phenomena as desired, in order to describe increasingly complex mechanisms or to vary unknown parameters. This last quality will allow us, in this thesis, to describe different mechanisms involved in tumour-immune interactions and to analyse the duality of the anti-tumour immune response, as well as the role of treatment strategies based on immunotherapy. Mathematical models represent a simplification of reality and, therefore, do not allow to draw absolutely accurate conclusions on the underlying biological dynamics. However, their study allows to assess the value of certain biological parameters, as well as the reliability of certain hypotheses.

The inherent complexity, not only of the interactions between tumour cells and the immune system, but also in the mathematical modelling of this phenomenon, requires a clear definition of the underlying biological framework. Thus, in this chapter, a first part will be devoted to the description of the biological context. After a brief introduction on tumour development, we will describe the mechanisms governing the interactions between malignant tumour cells and cells of the immune system. We will then introduce some mechanisms leading the tumour cells to evade the immune response, and provide a short review of some current immunotherapies. In the second part, we will give an overview of the existing mathematical models in the literature used to describe tumour-immune interactions, and discuss how they can be adapted to include the effects of immunotherapies. Finally, a third part will be devoted to a summary of the contributions of the thesis.

1.2 Biological overview of the immune response to tumours

In this section, we introduce the key biological mechanisms involved in the immune response to solid tumours. As previously said, the interactions between tumour cells and cells of the immune system constitute a very complex system, which involves cells and molecules of different types. Therefore, some of the concepts described in the following sections may represent a simplification of the real mechanisms underlying the immune response to tumours. These simplifications are directly related to the assumptions that have led to the development of our mathematical models.

The first part briefly describes the general mechanisms that must be overcome in order for a normal cell to develop into a tumour cell. In the second part, we present an overview of the immune system, focussing on different types of cells which take part in the immune response in tumour development.

> While being aware of the fact that a variety of different cells and molecules take part in the anti-tumour immune response, in this thesis we are mainly interested on a particular type of immune cells: cytotoxic T lymphocytes (CTLs). Such cells are the major anti-tumour effector cells and represent the immune cells that are most commonly stimulated by immunotherapies.

Additionally, we describe some of the key biological and immunological mechanisms involved in the recognition of tumour cells, such as the expression of tumour antigens, and how the immune system is activated to fight tumour cells. In the third part, we present some of the properties of tumour cells which allow them to evade the immune response. We will conclude the section by considering some immunotherapy techniques which have been developed to target these aspects.

1.2.1 Tumour development

Normal cells grow and divide, but have many mechanisms that control their growth. They only grow when stimulated by growth factors. If they are damaged, a molecular brake stops them from dividing until they are repaired. If they cannot be repaired, they commit programmed cell death (apoptosis) [64]. Moreover, thanks to a specific enzyme, the telomerase, which shortens their telomeres at the end of the chromosomes at each cell division, normal cells can only divide a limited number of times [115]. Cells are part of a tissue structure, and remain where they belong. Each of these mechanisms is controlled by several proteins, which ensure the proper functioning of all our cells [64].

All these mechanisms must be overcome in order for a normal cell to develop into a tumour cell. A critical protein must malfunction in each of those mechanisms. These proteins become non-functional when they acquire somatic mutations (mutations that are not inherited but occur after conception). This occurs in a series of steps, which in [94] have been referred to as 'hallmarks of cancer'. These include the ability of tumour cells to: sustain or enhance replication and growth (cell proliferation), avoid growth suppressors, avoid or suppress the immune response, be able to divide/replicate indefinitely, recruit immune cells to cause inflammation, invade another area of the body (formation of metastasis), create new blood vessels (angiogenesis), mutate, resist apoptosis (cell death) and alter their metabolic processes to avoid the need for oxygen.

Through cell division, the altered cells cluster together to form a growing tumour. In the early stages of tumorigenesis, tumour cells stay close to the original site where they have formed [94]. However, once the tumour has developed and is large enough, it can begin to create a blood

supply through angiogenesis. This allows single cells to leave the initial site and travel to other sites of the body, through the blood stream, which can ultimately lead to the formation of metastasis [62]. Furthermore, most tumour cells express high levels of telomerase, an enzyme preventing the shortening of the telomeres and allowing for a longer or infinite division, and thus survival, of cells [115].

In this thesis, we focus on solid tumours in the early stages of development (*i.e.* small pre-angiogenic tumours) and, in particular, on the ability of tumours to evade immune destruction.

In the following sections we will briefly describe the mechanisms governing immune surveillance and some mechanisms used by tumour cells to escape the control of the immune system.

1.2.2 Tumour immunology

The immune system is the body's natural defence mechanism against any foreign attack. Through the immune response, the body is able to attack these foreign and harmful materials and destroy them. It has also become evident that the immune system plays a role in the protection from harmful substances within the body, including tumour cells. This makes the immune system a very important mechanism for controlling and treating tumours. However, both the functioning of the immune system and the growth of tumours involve highly complex processes, making the interactions between tumour cells and immune cells an elaborate system that is not yet fully understood by either experimentalists or theoreticians [142].

In the case of the human immune system, there are two different types of barriers, namely, the innate and adaptive immune systems. Both of them have their own individual methods and abilities to help our bodies stay healthy, and interact with one another to kill harmful invaders, including tumour cells.

Innate immune system and tumour antigen presentation Briefly, the *innate immune system* is the first line of defence against pathogens and malignant cells and its role is to recognize and respond to them in a generic way. It recruits specific immune cells at the site of infection, provides an immediate defense mechanism through the initiation of inflammation, removes foreign substances, and activates the adaptive immune response [37]. Innate immune cells include different types of cells. In the context of tumours, the two most important one are the natural killer cells (NK cells) and the professional phagocytes.

NK cells are part of a class of white blood cells called lymphocytes. When NK cells receive signals from other immune cells, they secrete proteins called *cytokines*, which in turn signal other immune cells to come and help defend an infected area. Also, NK cells can destroy tumour cells without requiring activation by other cells via cell lysis (*i.e.* disintegration) which results in cell debris within the microenvironment [143].

The professional phagocytes consist of different types of cells, whose role is to engulf and remove invaders through a process called "phagocytosis". Moreover, particular types of professional phagocytes, the dendritic cells and the macrophages, play an important role in the initial steps of the immune response to tumours. Whilst undergoing phagocytosis, dendritic cells and macrophages secrete pro-inflammatory cytokines, such as the tumour necrosis factor (TNF), which can kill tumour cells, as well as activate other immune cells [191]. Secondly, dendritic cells and macrophages can act as *antigen presenting cells (APCs)* [37]. When the defences are

put under pressure and APCs have engulfed an invader, they present specific proteins, called antigens, on their surface [151]. In immunology, an antigen can represent a protein, a molecule or any substance that causes the body to make an immune response against that substance. In the context of tumours, such antigens are usually composed of fragments of proteins belonging to tumour cells, reflecting changes or mutations that the latter have undergone during cancer formation. Once collected, the APCs can process the antigens and load them on their cell surface through *major histocompatibility complex (MHC)* molecules, allowing them to be recognised by the adaptive immune system [22, 21].

Activation of the adaptive immune system While the innate immune response is a general defence reaction, the adaptive immune response is highly specific to the particular pathogen that induced it, and it provides long-lasting protection. The *adaptive immune system* requires more time to develop an effective response. However, it recognizes and remembers specific pathogens, and, therefore, its efficacy increases each time the same pathogen is encountered [191]. In the case of an anti-tumour immune response, the most important adaptive immune cell types are the *T lymphocytes*, the specific functions of which will be described later in this paragraph.

Adaptive immune cells must be activated to produce an effective anti-tumour immune response. The activation of the adaptive immune response requires the expression of antigens on the surface of tumour cells, and their presentation on the surface of APCs by MHC molecules. Once the APCs have processed the antigens, they move to the lymph nodes to present them to adaptive immune cells, specifically to naive T lymphocytes (or T cells). Naive T lymphocytes, which can be distinguished in naive CD4+ and naive CD8+ lymphocytes, are immature T cells that have differentiated and been released by the thymus, but have not yet encountered their corresponding antigens and are not activated. These cells are endowed with particular receptors, the *T cell receptor (TCR)*, on the surface of their membrane, which allow them to recognise specific antigens, activate, and initiate an antigen-specific immune response [45, 151]. The activation process relies on co-stimulatory (e.g CD28) and co-inhibitory (e.g CTLA-4, PD-1) proteins [143]. Depending on such complementary proteins and the antigen-MHC complex, subsequently, naive T lymphocytes can mature into distinct groups. The most important groups of T lymphocytes participating in the anti-tumour immune response include: the helper CD4+ T lymphocytes, the cytotoxic CD8+ T lymphocytes, and the regulatory T lymphocytes. The first group promotes the activation of a larger number of APCs and CD8+ T cells by secreting a variety of pro-inflammatory cytokines, like interleukin 2 (IL-2) and interferon gamma (INF$-\gamma$), and displaying a variety of co-stimulatory proteins on their surface. The cytotoxic CD8+ T lymphocytes are the main players of the anti-tumour immune response, as they are able to directly eliminate tumour cells causing their apoptosis. The third type, the regulatory T lymphocytes, suppresses other cells of the immune system, preventing them from attacking normal tissue [191].

Particular proteins, the CD8 glycoproteins, on the surface of naive CD8+ T cells enhance the interaction with the B7 receptor expressed by dendritic cells and results in the maturation of CD8+ T lymphocytes, also known as CTLs [191].

In the hypothesis that lead to the development of our models, we also take into account the fact that the *level of presentation of the antigens* to the MHC may play a critical role in the effectiveness of the anti-tumour immune response [45, 151]. By 'level of antigen presentation' we refer to different mechanisms that may affect the recognition of antigens by APCs, the activation of CTLs, and the efficacy of immune action. On the one hand, if the level of presentation of the antigens is too low, APCs will hardly recognize them, and CTLs will be poorly activated [80]. In addition, we assume that a low or incorrect presentation of antigens on the surface of tumour cells may result in potential difficulties for CTLs to bind to them, thus decreasing the efficacy of their immune action. On the other hand, if the level of antigen presentation is sufficiently high,

CTLs will be well activated and may eventually mount a more efficient immune response.

Immune action After their activation, CTLs proliferate and migrate to the tumour site through blood vessels. Once in the *tumour microenvironment (TME)*, the presence of small soluble proteins called chemokines (*e.g.* CCL3, CCL5, CCL20, and CXCL10) produced by both tumour cells and immune cells, will help the movement and infiltration of CTLs into the tumour (see [20, 68, 230]). This particular form of movement is governed by the ability of cells that are sensitive to an attractive chemical signal (*e.g.* the chemokines) to move in the directions of stronger gradients of it. Throughout this thesis we will refer to this form of movement as *chemotaxis*, while the chemical signal will be referred to as *chemoattractant*.

Following the influx of CTLs in the TME and their infiltration inside the tumour, the CTLs recognise tumour cells through the interaction of their TCR with an antigen-MHC complex on the surface of the tumour cell. Note that CTLs only produce one type of TCR, which recognises and binds specifically to a certain antigen (*i.e.* the cognate antigen) [45], and possibly other antigens within a certain affinity range [144, 224]. This enables CTLs to exert an antigen-specific cytotoxic activity against tumour cells, whose efficacy may depend on the affinity range of TCRs and the level of antigen presentation. Upon recognition of the cognate antigen, CTLs can trigger tumour cell death by direct interaction with tumour cells, releasing cytotoxic factors (*i.e.* granzyme B, INF$-\gamma$) [117], causing their apoptosis. The apoptosis of tumour cells results in the release of additional antigens, which enhance the immune action.

In general, in the final step of immune response, CTLs must undergo apoptosis to prevent any damage to normal cells. The apoptosis of CTLs prevents the risk of autoimmune diseases occurring and the formation of a memory population which allow for a faster response if the same antigen is recognised in the future [119].

Overall, many experimental studies have concluded that the immune system is able to fight tumour cells and remove early stage tumours by a loop called the cancer-immunity cycle [39] (see Figure 1.1). However, through antigenic changes and other evolutionary mechanisms this cycle is subject to various obstacles, and tumour cells can adapt to evade the immune response through a process known as *immunoediting*.

In this thesis, we focus on the interaction dynamics occurring between tumour cells and CTLs. We use different properties of these cell types, *e.g.* the level of presentation of tumour antigens, the affinity between tumour antigens and TCRs and the movement of CTLs, to develop the mathematical models described in Chapters 2-5.

1.2.3 Immunoediting

Despite the important role played by the immune system in eliminating tumour cells, it is clear that, most of the time, the cancer-immunity cycle does not perform optimally in cancer patients. This is because, as tumour cells grow, they inhibit the protective functions of the immune system and use some mechanisms that promote tumour development.

In [60], Dunn and collaborators proposed a new theory to describe the three different stages of the immune response to tumours: elimination, equilibrium and escape. These stages have been named the "*three Es of cancer immunoediting*". Elimination refers to the inflammatory response of the immune system to tumour cells and subsequent tumour eradication. If the tumour mass is able to evade immune eradication in the elimination stage, it enters the equilibrium stage. Here, the tumour is kept at roughly the same size and is prevented from inducing an angiogenic

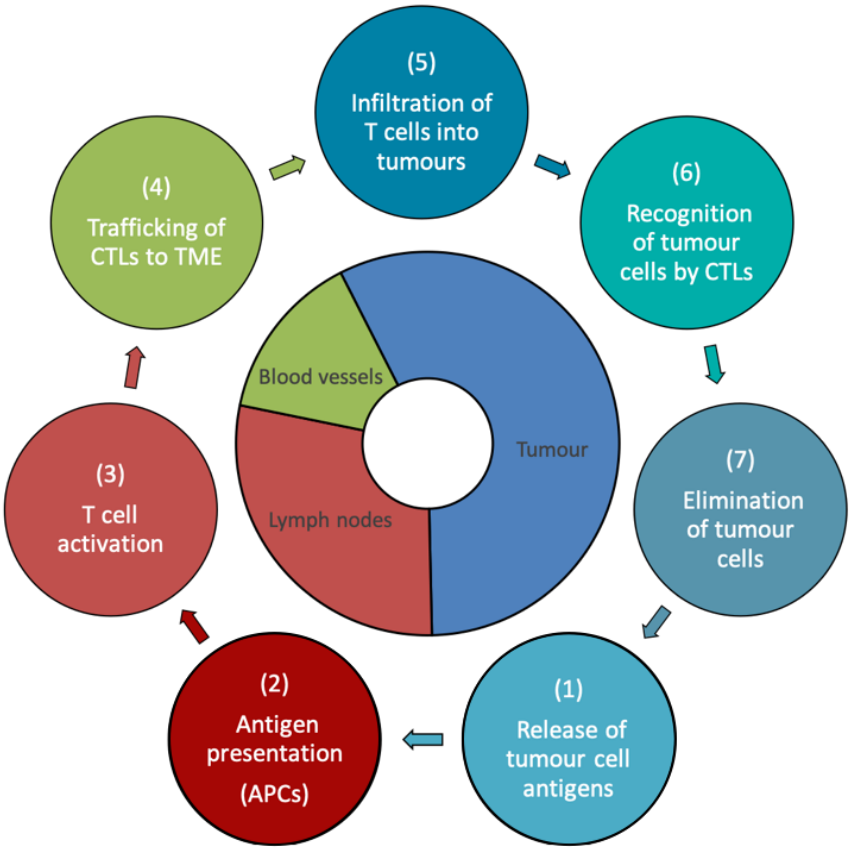

Figure 1.1: **The cancer-immunity cycle.** The cancer-immunity cycle is a 7-step framework used to describe how the immune system recognizes and eliminates tumour cells. In step-**1**, the transformation of normal cells to tumour cells causes the release of antigens. The antigens are then captured by antigen presenting cells (APCs), such as macrophages and dendritic cells, which process the antigens and load them on major histocompatibility complex (MHC). APCs move to the lymph nodes and present the antigens to naive T cells (step-**2**). This prepares and activates cytotoxic T lymphocytes (CTLs) and their response against tumour-specific antigens (step-**3**). The activated CTLs migrate to the tumour microenvironment (TME) (step-**4**) and infiltrate (step-**5**) the tumour. Within the tumour, the CTLs recognize and bind to tumour cells expressing the cognate antigens (step-**6**) and subsequently eliminate the target tumour cells (step-**7**). Killing the tumour cells releases additional antigens and begins the cycle again. Adapted from [39].

response. The last "E" of immunoediting is escape. Whilst in the equilibrium stage, interactions between tumour cells and immune cells can produce two possible outcomes: tumour elimination or tumour escape. In the first, the tumour is eliminated by the immune system, making this outcome equivalent to the elimination stage. The second outcome is when the tumour cells have managed to, through different factors, escape the immune action. The interaction between immune cells and tumour cells over a long period of time neutralises immune attack, leading the tumour to grow uncontrollably.

In the following paragraphs, we highlight some of the key evasion mechanisms which may lead tumour cells to avoid immune destruction, which are also schematically illustrated in Figure 1.2. Then, a new classification of tumours, based on the immune context, rather than on the tumour anatomical extent, is discussed.

Immune checkpoints Immune checkpoints are regulators of the immune system. In general, these pathways are crucial for self-tolerance, which prevents the immune system from attacking cells indiscriminately. However, in the context of cancers, some tumour cells can evade immune response by upregulating these immune checkpoint targets [49, 210].

For example, tumours may evade immune responses using negative feedback mechanisms to prevent apoptosis and downregulate the immune response either before or after its activation [49, 210]. These include immunosuppressive cytokines such as IL-10 and tumour growth factor (TGF)-β, inhibitory cell types such as regulatory T lymphocytes (Treg) or Myeloid-derived suppressor cells (MDCSs) and inhibitory receptors such as PD-1 and CTLA-4 (*cf.* Figure 1.2**(B)**). For example, the interaction between the CTLA-4 (cytotoxic T lymphocyte-associated antigen 4) protein with the activating receptor B7 expressed by dendritic cells may prevent CTL activation in secondary lymphoid organs, therefore limiting the number of activated CTLs and their efficiency at eliminating tumour cells. Similarly, after the arrival of CTLs in the TME, increased expression of PD-L1 (programmed death ligand 1) allows tumour cells to bind to the PD-1 (programmed death 1) receptor on CTLs, causing immune cell death or inhibition (*cf.* Figure 1.2**(C)**).

Alternatively, tumour cells can evade cell-cell recognition by immune cells through manipulating the binding process. The binding between the MHC molecule and the tumour antigen is the first step in antigen recognition. However, tumour cells can cause downregulation of MHC molecules, preventing presentation of the antigen (*cf.* left and central panel of Figure 1.2**(D)**). This may limit the activation of CTLs and their ability to recognise tumour cells, ultimately resulting in tumour escape [77, 76, 126].

With the aim of targeting the immune resistant mechanisms of tumour cells, immune checkpoint inhibitors have been developed as a method of treatment to allow for a stronger immune response.

Presence of sub-populations of tumour cells expressing sub-clonal antigens As tumours grow, they acquire mutations that can aid in immune resistance and immune evasion. In particular, these mutations may create *neoantigens*, potentially preventing CTLs from recognising them. There are many possible reasons for this, such as loss of antigen expression, creation of antigen variants not recognized by CTLs, etc. It has recently been reported that many of these neoantigens arise from sub-clonal branching mutations and could potentially increase *intratumour heterogeneity (ITH)* [149, 150, 180]. ITH describes the existence of distinct tumour cell populations with specific genetic, epigenetic and phenotypic features within the same tumour. It has recently been found to affect the effectiveness of the anti-tumour immune response in several tumour types, such as lung adenocarcinomas [180], breast cancer [149] and melanoma [150].

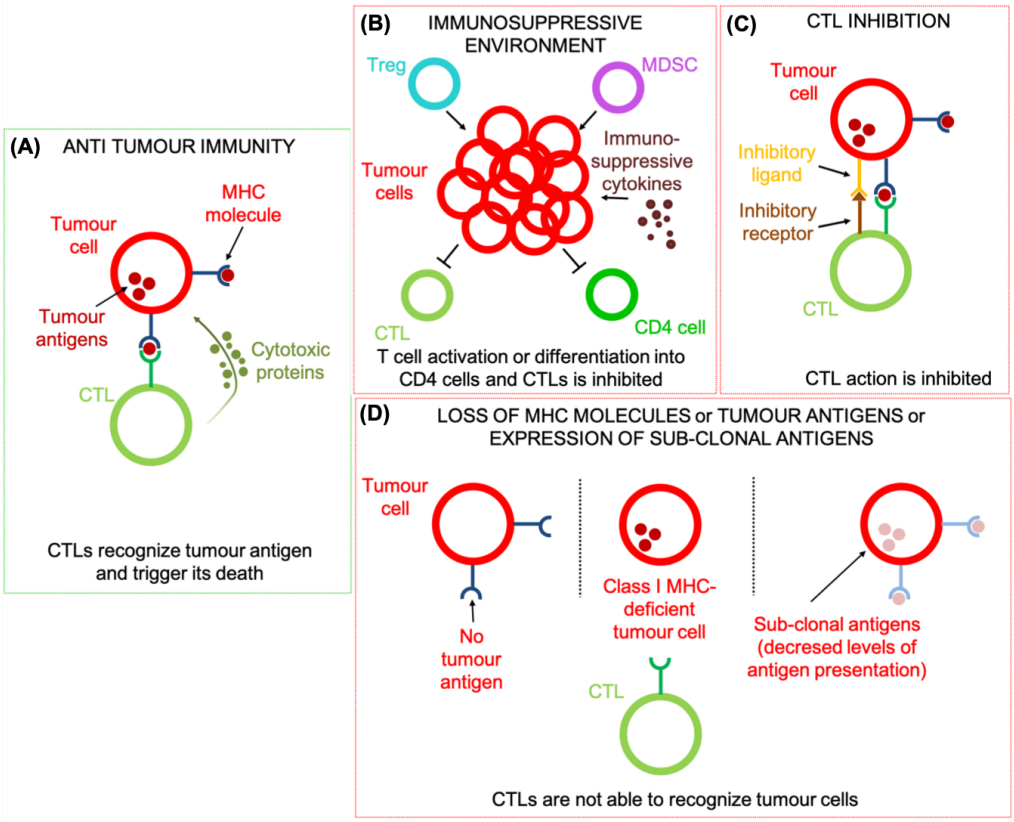

Figure 1.2: **Overview of immune response to tumours (panel (A)) vs. immune evasion mechanisms by tumours in the context of CTLs (panel (B)-(C)-(D)). (A)** Cytotoxic T lymphocytes (CTLs) are the preferred immune cells which play a role in the immune response against tumour cells. CTLs are able to eliminate malignant tumour cells upon the recognition by T cell receptor (TCR) of specific tumour antigens presented on the surface of major histocompatibility complex (MHC) molecules. **(B)** Regulatory T lymphocytes (Tregs) suppress the T cell responses to tumours. Myeloid-derived suppressor cells (MDCSs) accumulate in the TME and suppress anti-tumour T cell responses. Also, the release of immunosuppressive cytokines (for example IL-10) lead to suppression of the anti-tumour immune response. **(C)** T cell responses are inhibited by the involvement of inhibitory receptors and their corresponding ligands. An example of these inhibitory receptors are the PD-1 receptor on the surface of CTLs and its PD-L1 ligand on the surface of tumour cells. **(D)** The prevention of antigen expression or presentation by tumour cells leads to lack of tumour recognition by CTLs. Furthermore, MHC class I molecules can be downregulated on tumour cells, decreasing the ability of CTLs to recognize tumour cells. Finally, the expression of sub-clonal antigens decreases the effectiveness of immune response as they are associated with a reduced level of antigen presentation [80]. Adapted from [168].

Tumours with high ITH are characterised by *clonal antigens* (presented by all tumour cells), and *sub-clonal antigens* (presented only by sub-populations of tumour cells) [150]. Moreover, such sub-clonal antigens may be associated with a reduced level of antigen presentation by the MHC molecules, decreasing or preventing presentation of the antigen. This may limit the ability of CTLs to activate or recognise tumour cells, possibly leading to tumour survival [80] (*cf.* right panel of Figure 1.2**(D)**). In contrast, more homogeneous tumours (*i.e.* tumours with low ITH) express few clonal antigens in all tumour cells and appear to trigger a more efficient immune response across a wide range of tumour types [65, 150]. Furthermore, CTLs activated against clonal antigens are more commonly found at the tumour site than CTLs reactive to sub-clonal antigens [150]. These findings suggest that ITH may strongly affect the effectiveness of the anti-tumour immune response.

In Chapter 3, we present a spatial stochastic individual-based model of tumour-immune interaction dynamics that can be used to explore the effect of ITH on immune surveillance. The model makes it possible to dissect the specific impact of two expressions of ITH on anti-tumour immune response. Through computational simulations of our model, the effect of ITH is investigated at different levels, in order to assess its impact on anti-tumour immunity in a controlled manner.

Immune contexture and Immunoscore The tumour site is a complex and continuously evolving entity, which include immune cells, signalling molecules and extracellular matrix. In particular, it has been observed that type, density and location of immune cells within the tumour site correlate with prognosis in different types of cancer [70]. As a result, the *immune contexture*, which is determined by the type, density, immune functional orientation and localization of immune cells within a tumour, can yield information that is relevant to prognosis and prediction of a treatment response [10, 25]. 'Contexture' refers to the act of assembling parts into a whole, as an arrangement of interconnected parts.

Derived from the immune contexture, a simple and powerful immune-classification has been termed as the '*Immunoscore*' and is now used as a prognostic marker in cancer patients [10, 70, 72, 71]. The Immunoscore provides a score that increases with the density of CD8+ and CD3+ T cells both in the centre and at the margin of the tumour. In this vein, a new immune-based, rather than a cancer-based, classification of tumours based on the Immunoscore has been proposed in [72], where the authors have classified tumours in four categories. The "hot" category is characterized by tumours infiltrated with a large number of CTLs in the centre of it and, therefore, have a high Immunoscore. Such tumours present dysfunctions in the last steps of the cancer-immunity cycle (see Figure 1.1). In particular, infiltrated CTLs are exhausted or dysfunctional and express a number of inhibitory receptors, most notably CTLA-4 and PD-1 [70]. The category "altered-immunosuppressed" denotes tumours with a small amount of infiltrated CTLs. Here, the lack of adequate innate immune response constitutes a limiting factor restraining the development of an effective, adaptive anti-tumour response, therefore originating an immunosuppressed tumour. Tumours in the "altered-excluded" category are characterized by two different regions: their margin is infiltrated by activated CTLs while the centre is not. One reason for T cell exclusion is the lack of T cell-recruiting signals, such as chemokines directing T cell trafficking, or the presence of physical barriers. Tumours in this two categories have an intermediate Immunoscore. Moreover, such tumours present dysfunctions in the intermediate steps of the cancer-immunity cycle. Finally, "cold" tumours have a low Immunoscore and are often correlated to a poor response to immunotherapies since CTLs are absent both within the

centre of the tumour and at its margin. Such tumours completely lack a pre-existing immune response.

In Chapter 4, we develop an hybrid discrete-continuum modelling approach to explore the role of T cell infiltration in the immune response against solid tumours. Abstracting from the 'immunoscore' based classification of tumours developed by Galon and collaborators [72], we classify different tumour scenarios depending on the spatial distribution of CTLs within the tumour. Moreover, we investigate the impact of CTL infiltration on the response of tumour cells to different types of anti-cancer immunotherapy.
Also, in Chapter 5, we develop a stochastic individual-based model to investigate the effects of physiological stress on immune infiltration. Moreover, we develop an 'infiltration score' to quantitatively evaluate immune cell infiltration into the tumour. The results of numerical simulations of this model are able to qualitatively reproduce the experimental results presented in [99].

Given the extremely large amount of data showing the prognostic and predictive power of specific immune components (such as degree of immune infiltration, presence of immune suppressive cells or T cell checkpoint, low expression of antigens), it is important to assess individual immune determinants and/or a combination of immune determinants. This would allow for a more accurate patient assessment that would guide the design of effective tumour therapies [70].

1.2.4 Immunotherapy

Traditional treatments for tumours include chemotherapy and radiotherapy, which aim at attacking all rapidly-dividing cells within the body, effectively targeting fast-growing tumour cells. These types of treatments have proven to be beneficial in many cases and are widely used to treat most types of tumours. However, these treatments can potentially have severe side effects. For example, the damage caused to healthy cells as well as tumour cells can result in further illness or even fatalities [31].

Targeted therapies, like immunotherapy, may be able to reduce the damage to normal cells. Generally, the goal of immunotherapies is to initiate or reinitiate a self-sustaining cancer-immunity cycle (see Figure 1.3), enabling it to restore or amplify immune response, but not so much as to generate unrestrained autoimmune inflammatory responses. Tumour immunotherapies must therefore be carefully configured to overcome the negative feedback mechanisms that block the proper functioning of the cancer-immunity cycle.

Monoclonal antibodies Monoclonal antibodies are antibodies designed to bind to specific proteins. The aim of therapies based on these antibodies is to block immune checkpoints [49, 102, 181, 208]. For this reason, they are also called *immune checkpoint inhibitors*. As previously mentioned, overexpression of the checkpoint proteins CTLA-4 and PD-1 by CTLs, as well as overexpression of PD-L1 ligands by tumour cells, is a major factor in suppressing the anti-tumour immune response. In particular, CTLs that have been in contact with tumour cells possessing PD-L1 ligands are inhibited and become exhausted, *i.e.* tolerant to the presence of the tumour. Therefore, treatments (such as nivolumab, pembrolizumab, and lambrolizumab) that block PD-1 and PD-L1 interactions are able to restore the effector activity of exhausted CTLs. Similarly, monoclonal antibodies capable of blocking interactions between the checkpoint proteins CTLA-4 and B7 are able to restore the mechanism of T cell activation in secondary

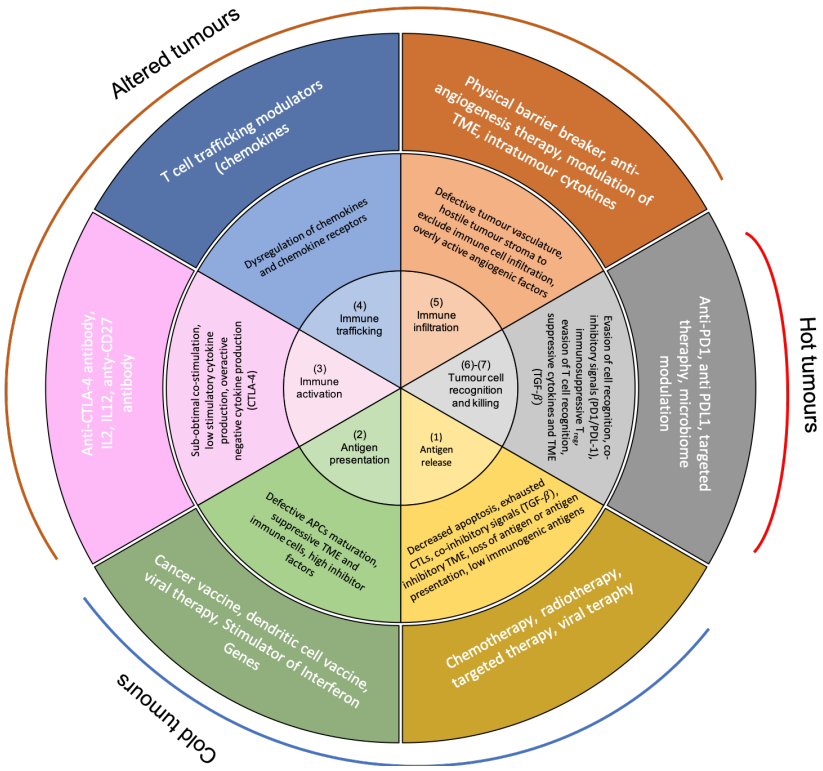

Figure 1.3: **Immune-resistant mechanisms of the cancer-immunity cycle and immunotherapy strategies to counteract immune inhibition.** Solid tumours can be classified in three main categories based on their immunoscore: cold tumours, altered tumours and hot tumours. Each category is associated with specific underlying biological mechanisms that may prevent the host immune response from eradicating the tumour. Cold tumours are the result of immunological ignorance, the induction of tolerance or a lack of appropriate T-cell priming or activation. Altered tumours may reflect a specific chemokine state, the presence of particular vascular factors or barriers, or sub-optimal stimulation of CTLs. Hot tumours can demonstrate infiltration by a number of subtypes of immune cells, including immune-inhibitory regulatory T lymphocytes and myeloid-derived suppressor cells. CTLs may also demonstrate a dysfunctional state such as exhaustion. Tumour cells in hot tumours can also express inhibitory signals (*e.g.* PD1), suppressive cytokines, and other pathways that de-sensitize them to anti-tumour immunity. Each immune-resistant mechanism (middle circle) is placed in the step of the cancer-immunity cycle (innermost circle) in which its mainly acts. For example, low immunogenic (*i.e.* able to produce an immune response) antigens or loss of antigen presentation are highly important for T cell activation. Current anti-tumour immunotherapy approaches (outermost circle) have been targeting and harnessing various mechanisms along this tumour-immunity circle. Adapted from [70].

lymph nodes. Various monoclonal antibodies have been designed, for example ipilimumab, which can bind to the CTLA-4 protein and prevent CTLA-4/B7 binding. In clinical trials, therapies

employing these monoclonal antibodies have exhibited durable responses and improved survival of patients across a range of cancers including advanced melanoma [222], Non-small cell lung cancer (NSCLC) [96] and renal cancer [156], and have thus been granted regulatory approval from the Food and Drug Administration [210] and the European Medicines Agency [91] for those indications.

Adoptive T cell therapy The effectiveness of monoclonal antibody therapies relies on the fact that the immune system already produces sufficient tumour antigen-specific CTLs. However, in many tumours the amount of these CTLs is very limited. Two immunotherapy strategies can address this problem: adoptive cell transfer and modified cell transfer therapies [66]. Adoptive cell transfer consists in taking tumour-infiltrating CTLs from the patient that are specific to the tumour antigens and then culturing them in the presence of particular cytokines (such as IL-2) to induce their proliferation. Once the required number of CTLs has been reached, the cultured cells are then re-injected into the patient. The use of the patient's own CTLs allows this therapy to become more adaptable and personalised for each patient.

However, in some more severe cases, it is very difficult to isolate cells specific to the tumour antigens. Additionally, by targeting common antigens there is a risk of attacking healthy cells, leading to severe side effects [92]. Therefore, modified cell transfer therapy involves genetically modifying the patient's CTLs so that they can better recognise the tumour antigens. One of the best known treatment based on modified cell transfer therapy today is the one based on CAR-T cells [216]. Chimeric antigen receptors (CARs, also known as chimeric T cell receptors or artificial T cell receptors) are receptor proteins that have been engineered to give CTLs the new ability to target a specific antigen. The receptors are chimeric because they combine both antigen-binding and T cell activating functions into a single receptor. There have been extensive experiments and clinical trials based on CAR-T cell therapies with successful initial results; however, very few have been approved as viable options for tumour treatment. This is caused by the potential risk of CAR-T cells attacking non-tumour cells that express the target antigen [92].

Combinatorial immune parameters Despite the clinical success of immune checkpoint blockade and adoptive CAR T-cell therapy, these approaches have shown substantial benefit to only some of the patients, while the rest have not responded due to immune evasion [170]. For example, in cold tumours, the lack of CTLs in the TME can lead to a failure of immune checkpoint inhibitor therapies, such as the anti-PD-1/PD-L1 therapy. Also, the mutations that create new sub-clonal antigens or an immunosuppressed TME can inhibit or limit the effects of adoptive T cell therapy [16].

As previously said, the analysis of the main immune determinants shaping tumour development, as well as the Immunoscore and immune contexture parameters, are useful prognostic (associated with survival) and predictive (associated with response to treatment) tools that should be used to guide the choice of the most effective therapeutic strategy. In this sense, it is reasonable to assume that the colder the tumour is, the more approaches are needed [70]. For example, hot tumours, which display a high degree of T cell infiltration [70], are associated with increased response to anti-PD-1 or anti-PD-L1 monotherapy (*cf.* Figure 1.3). In altered tumours, the combination of therapeutic epigenetic modulation directed to increase the level of chemokines for T cell trafficking and infiltration, with anti-PD-L1 treatment, has shown to slower tumour progression in preclinical models [158]. Finally, cold tumours, characterized by low Immunoscore, are the most challenging to eradicate and are invariably associated with poor prognosis. A proposed approach to overcome the lack of a pre-existing immune response is to combine a priming therapy that enhances T cell responses (such as chemotherapy or radiotherapy) with the removal of co-inhibitory signals (*e.g.* immune checkpoint inhibitors) and/or the

supply of co-stimulatory signals [70]. For example, in [73] the authors found that the combination of chemotherapy, which increases the release of tumour-associated antigens and stimulates the activation of CTLs, with anti-PD1 treatment, had clinical benefits in NSCLC.

Given the pivotal role of CTLs against cancer, it is clear that the identification of key features, immune-related, at the moment of diagnosis is needed to build a solid classification strategy supporting subsequent therapy.

The mathematical model developed in Chapter 4 is used to explore potential causes for the emergence of cold, altered-immunosuppressed, altered-excluded and hot tumour scenarios. Then, it is used to investigate how the effects of combination immunotherapies, namely anti-PD-1 therapy, anti-PD1-CTLA4 dual therapy and chemotherapy combined with anti-PD1 therapy, may vary the success of the immune response against tumour cells in the different categories of tumour scenarios.

1.3 Review of modelling strategies

In this section, we discuss the literature on mathematical models that have been developed to describe the interactions between a nascent tumour and the immune system.

In this thesis, we will develop discrete and continuum models to describe the spatio-temporal dynamics of the interactions between a solid tumour and cytotoxic T cells. Therefore, we begin this section with a discussion on the different methods of mathematical modelling used to describe tumour-immune interactions, which include discrete individual-based models, deterministic homogeneous and spatial models, and combinations of the two approaches, *i.e.* hybrid discrete-continuum models. Then we discuss some of the key models, from the literature, that have been developed previously to describe tumour development and its interaction with the immune system.

1.3.1 Methods of mathematical modelling

Mathematical models for tumour-immune interactions have become increasingly popular over the past few decades and are used as a tool to aid in the understanding of the mechanisms of tumour escape. Incorporating in these models the effects of therapeutic strategies that boost anti-tumour immune response can help biologists and clinicians to predict the success of cancer treatment protocols, including immunotherapy protocols.

Cellular processes in the tumour environment exhibits multiscale properties and the interactions between tumour cells and immune cells can occur across various spatial and temporal scales. Generally, there are three spatial scales potentially considered in modelling: *the molecular scale* (*i.e.* $nm - \mu m$), *the microscopic scale* (*i.e.* $\mu m - mm$), and *the macroscopic scale* (*i.e.* $mm - cm$) [51]. The molecular scale is used to model intracellular processes, such as cell signaling mechanisms (in the context of tumours: cytokines, chemokines, etc.). The microscopic scale is used to model extracellular processes, representing for example the interactions between tumour and immune cells. Models at the macroscopic scale focus on the dynamics of the total tumour behaviour occurring at the tissue level including morphology, shape, extent of vascularization, and invasion. Note that these scales are sometimes referred to, respectively, as microscopic, mesoscopic and macroscopic [145]. Since many biological mechanisms in the immune response

to tumours involve processes spanning different spatio-temporal scales, in the past twenty years new multiscale models have been proposed, where these multiscale properties of tumour-immune interactions can be effectively incorporated [145].

Furthermore, the mathematical modelling of tumour-immune interactions can involve techniques that are discrete, continuum, or hybrid, *i.e.*, the integration of both. *Discrete models* usually rely on an explicit representation of individual cells in space and time, tracking and updating their internal states according to a predefined set of biological and biophysical rules. Therefore, they are often referred to as individual-based models. They can be stochastic and are particularly suited to describe processes occurring at the microscopic scale and over short timescales (minutes-hours). They involve the representation of populations of low cell numbers (usually $< \mathcal{O}(10^5)$), which makes it possible to represent stochasticity and heterogeneity of the dynamics observed in small-scale phenomena. However, their computational cost increases rapidly with the number of cells modelled and they are usually less amenable to mathematical analysis. On the other hand, *continuum models* are, generally, deterministic and less computationally expensive than discrete models, allowing for the investigation of larger cell population sizes, where the small scale stochastic effects can be neglected. For this reason continuum models are particularly popular for tissue level dynamics over longer timescales (days-years). They give a macroscopic description of the system under study, as the terms in the model equations provide a mean-field representation of the underlying cellular dynamics. However, they cannot easily capture the emergence of population-level phenomena that are induced by stochastic fluctuations in single-cell biophysical properties, which are relevant in the regime of low cellular densities. By using *hybrid discrete-continuum models* , we can integrate the strengths of both continuum and discrete descriptions. Usually, in hybrid models a multiscale description of the system under study is given, where individual cells are treated discretely, but extracellular factors, such as chemical signals, are often modeled as continuous quantities. Hybrid models, similarly to individual-based models, may still be computationally expensive and less amenable to analytical investigations.

Various mathematical methods are used to model tumour-immune interactions including deterministic continuum model formulated in terms of differential equations, stochastic discrete individual-based models and combinations of these. The choice of the modelling approach should depends on the biological phenomena under investigation, the way one would represent the system (discrete or continuous), the spatial and time scale, as well as the kind of information (from hypothesis-driven to data-driven) one has.

In this thesis, we develop discrete individual-based and hybrid discrete-continuum modelling techniques to describe tumour-immune interactions in Chapters 2-5. Moreover, in Chapters 2 and 4 we will formally derive the deterministic continuum limit of these models.

Deterministic continuum models The specific interactions between tumour cells and immune cells have mostly been modelled using three classical deterministic continuum techniques: Ordinary, Integro and Partial Differential Equation systems.

A system of *ordinary differential equations (ODEs)* considers the change of continuous variables over either time or space. In the the tumour-immune setting, systems of ODEs are often used to investigate the importance of certain underlying dynamics, for example cell-cell interactions, whereas spatial interactions are neglected. *Integro-differential equations (IDEs)* are similar to ODEs, but also involve integrals of the unknown variables.

On the other hand, a system of *partial differential equations (PDEs)* considers the change of

continuous variables which depend on both space and time. In the the tumour-immune setting, systems of PDEs can model cellular and chemical concentration at given times, allowing for the inclusion of a wider range of biological aspects, such as cell movement or chemical diffusion.

In the same way that space provides a structural variable to account for cell movement, other structural variables can be included in PDE systems. Such structure variables can represent the size of the cells, and, therefore, allow to model the mitosis of the cells (*i.e.* when one mother cell divides into two daughter cells), or internal traits (*i.e.* phenotypes), characteristic of a relevant diversity in a cell population. In the context of tumours, such internal trait can represent the antigenic expression of tumour cells or their sensitivity to a drug under study. Therefore, it can be used, for example, to study the evolution of cell traits with time under the effect of environmental pressures, *e.g.* due to the interaction with the immune system or the introduction of anti-cancer drugs.

The continuum model presented in Chapter 2 describes the coevolutionary dynamics between tumour cells and CTLs in a well-mixed system (*i.e.* spatial interactions are not incorporated into the model). It is structured by a variable representing a parameterisation of the antigen expression profiles for tumour cells and a parameterisation of the target antigens of T-cell receptors (TCRs) for CTLs. The model comprises a non-local PDE for the phenotype distribution of tumour cells coupled with an IDE for the phenotype distribution of CTLs.
The continuum model presented in Chapter 4 describes spatial interactions between tumour cells and CTLs and explicitly takes into account the chemotactic movement of CTLs towards the tumour. This model comprises an IDE for the density of tumour cells coupled with a PDE for the density of CTLs and a PDE for the concentration of a chemoattractant.

Stochastic discrete individual-based models Among other types of techniques that describe the interactions of tumour cells and its local environment there are stochastic and discrete *individual- (or agent-) based models*. These models can be subdivided into two different categories based on their geometry: on lattice and off lattice. In on lattice models, cells are distributed in a grid system modelling physical space, whereas in off lattice models cells are not confined by grid restriction allowing the representation of complex cell shapes. Individual-based models attempt to describe how cells behave and interact over time by specifying rules for the behaviour of each individual cell (individual-based), helping to address the role of diversity in cell populations and also within each individual cell. These rules are formulated in terms of the probability of events occurring and allow for the observation of any patterns in the dynamics of the biological system. Specifically, *cellular automata models* are a type of on lattice individual-based models where, usually, only one cell can occupy each grid position through volume exclusion. The movement of cells and interactions with other cells within the system then depend on the rules of the model and the cells occupying the grids in the cell's neighbourhood.

An extension to the cellular automata model has been created in the form of a *Cellular Potts model* [89]. Here, the model is comprised of pixels with each cell, or cellular compartment, made up of several connecting pixels. Therefore, cells are no longer modelled as single points, but as spatial objects whose size and shape can be altered. The simulation progresses through a series of Monte Carlo Steps (MCS), which attempt to minimise the overall effective energy within the system. At each MCS, attempts are made to transform neighbouring pixels at the boundary of each cell to increase its volume. If the transformation, known as a "flip", reduces the overall effective energy then the pixel in question will be changed. The use of this type of

model allows to include many biological aspects, such as cell adhesion, cell growth and mitosis, cell movement, etc, where each individual element of the system can be modelled actively using numerous different rules. This type of model has been successfully transformed into user friendly software. *CompuCell3D* is one of them [107], which is a very useful tool when modelling tumour-immune interaction dynamics.

For the computational implementation of the individual-based models developed in Chapter 3 and Chapter 5 we use a Cellular Potts approach, and simulations were developed and run using the software CompuCell3D. However, in order to have a deeper understanding and control over the dynamic produced, for the models presented in Chapter 2 and Chapter 4, we develop our own computational codes.

Apart from CompuCell3D, several major computational frameworks are available for studying 3D multicellular systems, such as Chaste [155], CellSys [100] or PhisyCell [85].

Hybrid discrete-continuum models Since many biological systems involve processes spanning different spatiotemporal scales, in recent years, it has become common to combine discrete and continuum approaches to develop hybrid discrete-continuum models. Such models combine individual-based models or cellular automata with ODEs or PDEs in order to provide a more in-depth description of the biological system under study. In hybrid discrete-continuum models for tumour-immune interactions, tumour cells and immune cells are usually treated as discrete entities which interact with other chemical continuum fields, representing for example the concentration of chemokines, cytokines or oxygen in the TME. Hybrid discrete-continuous models provide an appropriate method to study tumour-immune interactions; however, they present some limitations, related for example to the possibly low number of cells and to the usually large number of parameters, the values of at least some of which are difficult or impossible to estimate from experimental data.

1.3.2 Mathematical modelling of tumour-immune dynamics

There have been many attempts over the years to model the interaction of the immune system and a growing tumour to try and help clinicians and experimentalists carry out their studies. These include deterministic continuum models, in the form of ODEs and PDEs, stochastic discrete models and hybrid discrete-continuum models. In this section, we will briefly discuss some of the key models, from the literature, that have been developed previously to describe the immune response to tumours. In particular, the models presented henceforth use discrete or continuum approaches to describe the interactions between tumour cells and immune cells, and in particular CTLs.

Deterministic nonspatial models The first models developed to describe tumour-immune interactions were nonspatial models formulated in terms of ordinary differential equations (ODEs) or integro-differential equations (IDEs). Based on the prey-predator nature of the interactions between tumour cells and immune cells, such models describe the tumour as prey, whose predators are cells of the immune system (in particular, CTLs).

One of the first two-species model which focus on tumour-immune interactions is presented in the pivotal work of Kuznetsov and collaborators in [123], where the authors developed a system of

two ODEs to describe the interactions between CTLs and an immunogenic (*i.e.* able to produce an immune response) tumour. The Kuznetsov model is given as

$$\begin{cases} \dfrac{dc}{dt} = S + \dfrac{\alpha_c cn}{\zeta_c + n} - \gamma_c nc - \mu_c c & c \equiv c(t) : \text{CTLs} \\ \dfrac{dn}{dt} = \alpha_n n(1 - \mu_n n) - \gamma_n cn & n \equiv n(t) : \text{tumour cells} \end{cases} \tag{1.1}$$

where functions c and n denote, respectively, the densities of effector cells (*i.e.* CTLs) and tumour cells. CTLs enter the system with constant influx S, are recruited at rate $\frac{\alpha_c n}{\zeta_c + n}$, are killed or inactivated at a rate proportional to the density of tumour cells, with constant of proportionality γ_c, and die at rate μ_c due to natural death. Tumour cells grow at a logistic rate $\alpha_n(1 - \mu_n n)$ with carrying capacity $1/\mu_n$, and are killed at a rate proportional to the density of CTLs, with constant of proportionality γ_n. The model is used to describe the kinetics of growth and regression of the B-lymphoma BCL_1 in the spleen of mice. By comparing the model with experimental data, numerical estimates of parameters describing processes that cannot be measured *in vivo* are derived. Through numerical simulations of this model, the established behaviour of "sneaking through", in which larger tumours are eliminated but smaller ones remain and grow, is observed. Moreover, the analytical and numerical results of the model show the presence of stable limit cycles, meaning that the immune system and the tumour coexist and undergo oscillations. For tumours with low antigenicity (which is linked to the value of γ_c) these cycles may be relatively long, with the tumours kept under control in a dormant state for most of the time.

From this particular model, a general framework has been derived, defined in [48]. For particular choice of its terms, this general model has been used in the literature to describe different observed tumour-immune interaction dynamics [67, 123, 192, 195]. In particular, this general framework is very helpful for elucidating basic and generic mechanisms that can induce observed behaviours, such as tumour regression and evasion, as well as tumour dormancy, a mechanism for which a small tumour continues to exist but is maintained at a restricted size by the immune system.

From these generic two equation models, many models have been developed by including one or more components representing specific aspects of the tumour-immune environment interactions such as: the interactions with normal tissue cells [51], or with cytokines (*e.g.*, IL-2, IFN-γ) and chemokines [118].

In nonspatial models, the expression and recognition of tumour antigens is usually modelled by variation of the rates of activation and proliferation of CTLs and of killing of tumour cells [12, 18, 69]. More recently, these processes have been explicitly modelled by nonspatial models formulated in terms of either ODEs [1, 15, 34, 120, 136] or IDEs [54, 52, 132].

A good review of nonspatial models that study interactions between immune and tumour cells can be found in [61].

Deterministic spatial models While deterministic nonspatial models are a good basis for modelling research, key dynamics of tumour-immune interactions can be confirmed or expanded in a wider range of biological aspects through the inclusion of spatial phenomena, *e.g.* random motility or chemotaxis, of the cells. This can be obtained by extending ODEs models into deterministic spatial models using partial differential equations [14, 148, 147, 200].

In particular, following the work of Kuznetsov and collaborators [123], in [148], Matzavinos and collaborators used a Fisher-Kolmogorov type model to describe the logistic growth of a tumour coupled with a chemotaxis model to describe the movement of CTLs into the tumour

microenvironment and an equation describing the dynamics of tumour cell-CTLs complexes. The Matzavinos model is given as

$$\begin{cases} \dfrac{dc}{dt} = \beta_c \Delta_x c - \chi_c \nabla_x (c \nabla_x \phi) + Sh(x) + \dfrac{\alpha_c r}{\zeta_c + n} & c \equiv c(x,t) : \text{CTLs} \\ \dfrac{d\phi}{dt} = \beta_\phi \Delta_x \phi + \alpha_\phi r - \kappa_\phi \phi & \phi \equiv \phi(x,t) : \text{chemoattractant} \\ \dfrac{dn}{dt} = \beta_n \Delta_x n + \phi_n n(1 - \mu_n n) - \gamma_n cn + \alpha_n r & n \equiv n(x,t) : \text{tumour cells} \\ \dfrac{dr}{dt} = \gamma_r cn - \mu_r r & r \equiv r(x,t) : \text{tumour cell-CTLs complexes} \end{cases} \tag{1.2}$$

Compared to model (1.1), the spatial structure included in this model allows one to describe the random motion of tumour cells and CTLs, as well as the chemotactic motion of CTLs towards the tumour. In particular, ϕ is the concentration of a specific substance, *i.e.* chemoattractant, along the gradient of which CTLs move with characteristic motility χ_c. Tumour cells and CTLs move via undirected, random movement with diffusion coefficients β_n and β_c. Chemoattractant production is proportional to tumour cell–CTLs complex (denoted by the letter r). Once produced, the chemoattractant is assumed to diffuse throughout the domain with diffusion coefficient β_ϕ and to decay with linear decay kinetics at rate κ_ϕ. Moreover, the parameter S represents the inflow of CTLs into the tissue (non-enhanced by the presence of tumour cells). The function $h(x)$ models the blood vessels through which new CTLs can enter the domain. The other parameters represent the local kinetics between tumour cells, CTLs and tumour cell-CTLs complexes. Numerical simulations of the model show that eventually the tumour cells develop very small-amplitude oscillations about a 'dormant' state, indicating that the CTLs have successfully managed to keep the tumour under control. Moreover, they demonstrate the existence of cell distributions that are quasi-stationary in time and heterogeneous in space. A linear stability analysis of the underlying spatially homogeneous ODE kinetics coupled with a numerical investigation of the ODE system reveals the existence of a stable limit cycle. This is verified further by the authors undertaking a bifurcation analysis. These results allow to explain the complex heterogeneous spatio-temporal dynamics observed in the PDE system, and reveal the key parameter regimen in which the onset of tumour dormancy may occur.

In Chapter 4, we develop a spatial hybrid discrete-continuum modelling framework for the interaction dynamics between tumour cells and CTLs. We formally derive the deterministic continuum limit of this model. In the obtained deterministic continuum model, the motility of CTLs is described by modified forms of the terms of random motion and chemotactic motion of CTLs used in system (1.2). These modified forms of motility allow us to take into account volume-filling effects [167], which take into account possible reduction in cell motility at high cell densities.

Apart from purely spatial models, many others PDE models investigate the dynamics of the immune response to tumours, using other structured variables than space. For example, in [14], the authors have developed a system of PDEs structured in space and size to describe the early interactions between tumour cells and CTLs. In this model, the displacement of CTLs is governed by chemotaxis, according to signals emitted by the tumour. Numerical simulations of the model reveal the importance of space-structuration: space heterogeneities of the sources of naive

immune cells, that provide, once activated, the CTLs that eliminate the tumour, dramatically influence the immune response efficiency. In particular, it is shown that replacing the homogeneous distribution of immune cells by a few spots makes the immune response less efficient. Instead of the control of the tumour, that would be kept at a fixed mass, the authors observe that there is a periodic succession of rapid growth and remission phases.

Discrete models By using discrete models, such as individual-based models and cellular automata models, a wider spectrum of biological phenomena can be translated into mathematical terms and described, such as cell-cell interactions, intracellular behaviour and individual cell properties. These models can be posed on a spatial domain (*e.g.* a grid), and a set of rules can be given to each cell with certain probabilities to achieve a detailed description of the interactions of tumour cells and the local tumour environment [43, 113, 140, 139]. For example, in [139] the authors used an individual-based approach to study the interactions between CTLs, dendritic cells and tumour cells. In their model, each tumour cell is characterised by an antigen profile which can change over time due to either epimutations or mutations. In this model, the immune response against tumour cells is initiated by the dendritic cells that recognise the tumour antigens and present them to the CTLs. Consequently, CTLs become activated against the tumour cells expressing such antigens. Moreover, in the modelling strategies developed in [139], the differences in movement between inactive and active immune cells are explicitly taken into account. The results obtained indicate that antigenic heterogeneity within a tumour determines the efficacy of immune action and highlight the complex interplay between spatial interactions and adaptive mechanisms that underpins the immune response against solid tumours.

CompuCell3D [107] is a very useful tool when modelling tumour-immune interactions. It allows the user to easily model an idealistic tumour environment where individual cells interact with one another. For example, in Tough PhD Thesis [205], two Cellular Potts models have been developed and implemented within CompuCell3D to try and explore the dynamics between CTLs and tumour cells. The first model is based on the ODE and PDE models presented in [123, 148, 147, 200]; however, the extension of these works into a Cellular Potts model allows the inclusion of more precise biological aspects (such as cell adhesion, cell growth and mitosis, motility, competition for space, etc). Numerical simulations of the model are used to portray the three Es of immunoediting described in Section 1.2.3: elimination, equilibrium and escape. The model begins with a central tumour mass, which is attacked by CTLs. Tumour cells are allowed to divide when they reach a certain size, determined by how much oxygen is available to them. This creates different tumoural zones, whereby the tumour mass forms a proliferating rim, quiescent zone and necrotic core. CTLs are constantly supplied to the domain and can eliminate tumour cells at a certain success rate. As this success rate is varied, the three Es of immunoediting are realised. The second individual-based model try again to detect the three Es of immunoediting; however, this time considering two types of immune cells, c_1 and c_2, and two types of tumour cells, n_1 and n_2. Tumour cells n_1 are only attacked by immune cells c_1, whereas tumour cells n_2 are killed by both c_1 and c_2. These hypothesis try to investigate the idea that a tumour, when in interaction with a host immune system, can become less efficient. The idea stems from the hypothesis of immunoediting. As tumour cells are of mixed type, it is thought that the immune system actively kills cells that are more immunogenic, allowing cells that are less immunogenic to proliferate. Hence, the tumour evades "immune destruction". The model also investigate the impact of the "Warburg Effect", *i.e.* the ability of tumour cells to use aerobic glycolysis to generate the energy needed for cellular processes, on tumour growth [213].

Hybrid discrete-continuum models Hybrid discrete-continuum models are also used to a great extent to study the immune response to tumours. In particular, the interaction between

tumour cells and immune cells has been modelled using a combination between PDE and cellular automata models. In particular, in [142] the authors use PDEs to describe the evolution of pro-tumour nutrients within the tumour microenvironement and describe tumour cell, CTL and NK cell movement and interactions through the cellular automata approach. Using this framework, they explore the role of nutrients, cell-cell adhesion and immune cell infiltration capabilities on a growing tumour. The results of numerical simulations of the model demonstrate different types of tumour growth depending on key model parameters related to the tumour–immune system interactions. In the absence of the immune system, the model is able to reproduce tumours of both compact-circular and papillary (branchy) morphologies. Introducing the immune system to the model leads to various results, which display either stable or unstable oscillatory tumour growth, tumour elimination, or the infiltration of CTLs into the growing tumour.

1.3.3 Mathematical modelling of immunotherapies

Most of the works on modelling anti-tumour immunotherapy are based on systems of ODEs and are focused mainly on the last steps of cancer-immunity cycle, *i.e.*, interaction of tumour cells with CTLs, death of tumour cells and inactivation of CTLs [18, 118, 163, 186]. The works in this direction are often based on the general prey-predator model presented in [48], where the number or properties of competing immune cells change due to therapy [12, 121, 69, 67, 192]. The general outcomes of this type of models is that the immune system can effectively eradicate small tumours, whereas large enough tumours are able to escape immune surveillance. From a mathematical point of view, this corresponds to the presence of an unstable manifold, that separates the basins of attraction of two stable points, which correspond to the scenarios of immune clearance or immune escape. Under such mathematical formulation, an important question is how it can be possible, with the help of a therapeutic intervention, to move the initial state of the system, located in a immune escape area, to the immune clearance one. Such problems are in general formulated as optimal control problems and are solved analytically [32, 101].

Additionally, key markers for therapies to target, such as tumour antigens, can also be discovered through ODE models [15, 136]. The account for the heterogeneity of antigens and the evolution of their expression profile has also been realized through IDEs. Such approach are implemented for example in the work [132], which develops a prey-predator model in which general T cell and target cell populations are structured by their respective target-antigenic and antigenic expression. The model is given as:

$$\begin{cases} \dfrac{dc}{dt} = [1+T_{c1}(t)]\alpha_c c - \dfrac{\mu_c}{1+T_{c2}(t)}\rho_c(t)c \\ \qquad\qquad + [1+T_{c3}(t)]\,\beta_c c \displaystyle\int_0^1 g(x,y;\gamma,\theta)n\,\mathrm{d}y \qquad c \equiv c(x,t) : \text{CTLs} \\ \dfrac{dn}{dt} = [\alpha_n - \mu_n\rho_n(t)]n - \beta_n n \displaystyle\int_0^1 g(y,x;\gamma,\theta)c\,\mathrm{d}x \qquad n \equiv n(y,t) : \text{Target cells} \end{cases} \tag{1.3}$$

In system (1.3), variables $x \in [0,1]$ and $y \in [0,1]$ model the target-antigenic expressions of CTLs and the antigenic expressions of target cells. It is supposed that: (i) target cells proliferate at rate α_n and die due to competition for limited space and resources with constant of proportionality μ_n; (ii) CTLs undergo antigen-independent proliferation at rate α_c; and (iii) CTL numbers are kept under control through homeostatic regulation mechanisms with constant of proportionality μ_c. Functions $\rho_c(t)$ and $\rho_n(t)$ respectively represent the total number of CTLs and target cells. Moreover, interactions between antigen-specific CTLs and their targets result in antigen-driven

T-cell expansion at rate β_c as well as selective action against target cells at rate β_n. Furthermore, up to three hypothetical classes of immunotherapies are presented, that are respectively designed to enhance antigen-independent proliferation (T_{c1}-agents), interfere with homeostasis to promote self-renewal of antigen-specific CTLs (T_{c2}-agents), and stimulate antigen-driven expansion (T_{c3}-agents).

First, the model is able to reproduce the three phases of the immune response orchestrated by CTLs: expansion, contraction and memory. Then, the model is devoted to the search for methods to counteract the dynamics of "chase and escape", which can develop under heterogeneous time-varying expression of antigens. The results of numerical simulations show that the three hypothetical classes of immunotherapies under study can reduce the likelihood of immune evasion. Moreover, they suggest that therapeutic protocols relying on the simultaneous delivery of sufficiently high concentrations of T_{c1}-agents and T_{c2}-agents are the most effective of the therapeutic protocols considered here. This implies that the success of an immunotherapy protocol correlates strongly with its ability to shorten the duration of the contraction phase and stabilize as many CTLs as possible inside the long-lived memory reservoir.

In Chapter 2, we develop an individual-based model for the coevolutionary dynamics between tumour cells and CTLs. We show that a generalised version of the mathematical model (1.3) can be formally obtained as the deterministic continuum limit of such stochastic discrete model. In addition to the biological phenomena incorporated into the model (1.3), the continuum model obtained takes also into account the effect of changes in antigen expression profiles of tumour cells and more general forms of competitive feedback mechanisms regulating the growth of the numbers of tumour cells and CTLs.

Moreover, PDE models have been used, for example, to describe tumour growth in the presence of cytotoxic drugs, *i.e.* drugs that directly kill tumour cells, and cytostatic drugs, which instead slow down the velocity of the cell division cycle [42, 41, 134, 194]. Many other discrete individual-based models and hybrid discrete-continuum models have also been utilized to predict the success of immunotherapy techniques [113, 175], such as PD-L1 inhibition therapies [87], antibody treatment [169] and cancer vaccines [116].

1.3.4 Mathematical models in clinical oncology

Mathematical modelling of tumour-immune interactions has great potential. For example, it can help to reveal non-obvious or non-intuitive mechanisms which may lead to immune escape and allows new treatment strategies to be proposed and tested in an affordable way. Also, the study of such models can help to suggest optimization of anti-cancer therapies already introduced into clinical practice. However, compared with traditional, widely empirical methods of cancer research, methods based on mathematical modelling of tumour-immune interactions have not led to significant success in clinical oncology. There are many reasons for this, such as finding the right balance between the reductionalism of mathematical models and the level of complexity prevailing in the clinical environment. The interactions between tumour and immune cells can be mathematically reproduced with models of different types and complexity. Developing more and more detailed models can be a tempting activity, however, it is usually associated with certain difficulties. For example, models of increasing complexity are associated with the problem of incomplete calibration. On the other hand, due to the difficulty in estimating parameter values, many models consider simple systems of equations and instead identify potential parameter

spaces of interest. However, mathematical modelling has already led to several predictions, validated using retrospective data [43, 187, 174, 214], preclinical successes [7, 125] as well as initiated clinical trials [63, 228].

Despite a present great interest in modelling for immunotherapy, most of the relevant mathematical models are of purely theoretical interest. What greatly complicates their development is the fact that immunotherapy itself often lacks a precise understanding of when it works, when it does not, and when it worsens the clinical scene. However, there is a small number of works in which biological experiments have been feed into the model, which can help to predict the next step for new experiments, and can then be tested [179, 215].

Inspired by experimental observations in co-culture between breast cancer spheroids and activated immune cells, which reproduce *in vivo* behaviours as described in [99], in Chapter 5 we explore a simple setting to study the effect of psychological stress on immune infiltration. To study the effect of stress on immune infiltration, we use a simplified version of the mathematical model developed in Chapter 3, which has been calibrated to reproduce *in silico* the results presented in [99].

1.3.5 Formal derivation of continuum models

In their nature, deterministic continuum models are amenable not only to numerical simulations but also to analytical approaches, which enable a complete exploration of the model parameter space. This allows a precise identification of the validity domain of the results obtained and ensures higher robustness and precision of the conclusions to be drawn. This in turn provides a more in-depth theoretical understanding of the underlying cellular dynamics. The analysis and numerical simulation of deterministic continuum models for tumour-immune interactions, which may help identifying the determinants of tumour development, progression and response to therapy, pose a series of mathematical challenges. Overcoming these challenges may require the use of a wide range of methods and techniques from different research areas of mathematics. In fact, the study of the qualitative and quantitative properties of the solutions of ODEs and PDEs, motivated by the need to address open questions in cancer research, has stimulated the extension of existing mathematical tools as well as the development of novel analytical techniques and numerical methods [157, 171, 172].

Ideally, instead of defining such continuum models for tumour-immune interactions on the basis of population- and tissue-scale phenomenological assumptions, one wants to derive them from first principles, that is, as the deterministic continuum limits of stochastic discrete models that track the dynamics of single cells [9, 212]. This is to ensure that the terms comprised in the model equations provide a faithful representation of the underlying cellular dynamics. In fact, although being computationally intensive to simulate for large cell numbers and, for most of them, inaccessible to analytical techniques, single-cell-based models allow the representation of fine details of cell-scale mechanisms and capture stochastic intercellular variability in spatial and evolutionary trajectories [130]. These aspects, which cannot be directly incorporated into deterministic continuum models, become especially important in scenarios where cell numbers and densities are low (*e.g.* in the early stages of tumour development or when tumour size is severely reduced after therapy), due to the stronger impact that single-cell processes and demographic stochasticity have on cellular dynamics.

For this reason, the derivation of continuum models formulated in terms of PDEs or IDEs

from underlying individual-based models has attracted the attention of a considerable number of mathematicians and physicists. Examples in this active field of research, whereby a range of asymptotic techniques, probabilistic methods and limiting procedures are used to systematically derive continuum models from their stochastic discrete counterparts, can be found, for instance, in [28, 35, 40, 110, 133].

1.4 Contributions of the thesis

As mentioned in Section 1.2, a strong connection may exist between tumour progression and immune dysfunction that, however, remains to be fully explained. Mathematical modelling and numerical simulations may help us to describe different mechanisms involved in tumour-immune interactions, as well as to analyse possible ways in which tumour cells may escape immune surveillance. This in turn may provide possible different frameworks to help biologists and clinicians design immunotherapy strategies which significantly improve the effectiveness of the overall anti-tumour immune response. In this thesis, we develop discrete and continuum models to describe the spatio-temporal dynamics of the interactions between a solid tumour and cytotoxic T cells, with the goal to investigate the biological settings which allow for the clearance or the escape of the tumour.

This thesis is organized in four chapters. Each chapter focusses on a different mechanism involved in tumour-immune interactions and is composed of three main sections: the first one briefly resumes relevant biological background to inform the reader on the empirical evidence motivating the model assumptions; the second one is dedicated to the presentation of the mathematical framework together with analytical and numerical results; the final section is dedicated to the discussion of the model and research perspectives, both in terms of applicability to empirical systems and mathematical tractability. As shown in Section 1.3, in the literature many models of tumour-immune interactions exist. However, the mathematical models developed in this thesis, include a new or more precise representation of some mechanisms involved in tumour-immune interactions.

Throughout the different chapters of the thesis, the contributions at the mathematical and biological level are diverse.

Chapter 2 - Modelling the coevolutionary dynamics between cytotoxic T lymphocytes and tumour cells In Chapter 2, we develop an individual-based model for the coevolutionary dynamics between CTLs and tumour cells in a well-mixed system (*i.e.* spatial interactions are not incorporated into the model). In this model, the phenotypic state of each cell is modelled by a discrete variable, which represents a parameterisation of the antigen expression profiles for tumour cells and a parameterisation of the target antigens of T-cell receptors (TCRs) for CTLs. We formally derive the deterministic continuum limit of this stochastic discrete model, which comprises a non-local partial differential equation for the phenotype distribution of tumour cells coupled with an integro-differential equation for the phenotype distribution of CTLs. We find the biologically relevant homogeneous steady-state solutions of the continuum model equations, and study their linear stability, in order to identify possible conditions on the model parameters leading to different outcomes of immune competition and to the emergence of patterns of phenotypic coevolution between tumour cells and CTLs. The results presented in this chapter support the idea that TCR-tumour antigen binding affinity may be a good intervention target for immunotherapy and offer a theoretical basis for the development of anti-cancer therapy, such as adoptive T cell therapy, aiming at engineering TCRs in order to shape their affinity for cancer targets.

For the sake of simplicity, in this first model we ignore spatial interactions between tumour cells and CTLs. Moreover, we consider a unique tumour cell population, characterized by the same antigen expression profile. However, solid tumours can be heterogeneous, characterized by different sub-populations of tumour cells expressing different antigens. Moreover, such antigens can be presented at different levels. These aspects, as well as spatial interactions between tumour cells and CTLs, may affect the efficacy of immune action and the outcomes of immune response, making it an interesting problem to investigate on its own. Therefore, these aspects are further included in the mathematical model presented in Chapter 3.

Chapter 3 - Modelling the impact of intra-tumour heterogeneity on immune response In Chapter 3, we extend the individual-based model developed in Chapter 2 further to explicitly include a spatial structure and tumour antigen expression and presentation. This allows us to investigate the impact of intra-tumour heterogeneity (ITH) on the immune response to tumours. Therefore, in Chapter 3, we develop a new spatially individual-based model of the interaction dynamics between tumour cells and CTLs which makes it possible to dissect the specific impact of two expressions of ITH on anti-tumour immune response. Such expressions of ITH are (i) the number of sub-populations of cancer cells expressing different antigens and (ii) the percentage of immunogenic cells (*i.e.* tumour cells that are effectively targeted by immune cells). The originality of this model lies in the characterisation of antigen presentation levels by tumour cells, which drive, by the means of a chemoattractant, the influx of CTLs in the tumour micro-environment and their movement towards tumour cells. In our model, the effectiveness of the anti-tumour immune response is directly linked to the level of presentation of tumour antigens. The set-up of numerical simulations of the model is defined so as to mimic scenarios considered in previous experimental studies reported in the literature [80, 223]. First, the results of numerical simulations of this model indicate that the presence of a larger number of sub-populations of tumour cells that express different antigens is associated with a reduced ability of CTLs to mount an effective anti-tumour immune response. Secondly, the presence of a larger percentage of tumour cells that are not effectively targeted by CTLs may reduce the effectiveness of anti-tumour immunity.

One potential limitation of individual-based models is their lack of amenability to mathematical analysis and their huge computational cost. To overcome this, we aimed to derive the continuum counterparts of the individual-based model introduced in this chapter. However, due to the complexity of the biological mechanisms included, in Chapter 4 we first consider a simpler biological situation.

Chapter 4 - Modelling the role of T cell infiltration in the immune response In Chapter 4, we present a spatial hybrid discrete-continuum modelling framework for the interaction dynamics between tumour cells and CTLs. Building on the modelling strategies developed in the previous chapter, in this framework, a stochastic individual-based model for cell dynamics is coupled with a reaction-diffusion equation for the evolution of a chemoattractant, which dictates the movement of CTLs towards the tumour. In order to take into account possible alterations in the infiltration capabilities of CTLs within the tumour, we let the probability of CTL movement be modulated by a decaying function of the densities of tumour cells and CTLs. We formally derive the deterministic continuum limit of this model, which comprises an integro-differential equation for the density of tumour cells coupled with a partial differential equation for the density of CTLs. We report on computational results of the hybrid model, and show that there is an excellent agreement between them and numerical results of the corresponding continuum model. The results presented in this chapter shed light on the mechanisms that underlie the emergence of different levels of infiltration of CTLs into the tumour and elucidate how CTL infiltration

shapes anti-tumour immune response. Moreover, exploiting the computational efficiency of the continuum model, we carry out extensive numerical simulations to investigate the impact of CTL infiltration on the response of tumour cells to different types of anti-cancer immunotherapy.

The different models of tumour-immune interactions developed in Chapters 2, 3 and 4 attempt to describe or explore different mechanisms of the anti-tumour immune response. The different models have been parametrised using parameter values drawn from the extant literature wherever possible and aim to reproduce or investigate observed behaviours. However, at this stage, they have not been calibrated to any particular type of data. Hence, they cannot be employed to generate predictions that can directly be used in the clinic. In Chapter 5, we address this, by proposing a simplified version of the mathematical model presented in Chapter 3, and calibrating it to qualitatively reproduce experimental observations.

Chapter 5 - Modelling the effect of psychological stress on immune infiltration In Chapter 5, we develop, in collaboration with biologists, a simple individual-based model to study the effect of physiological stress on immune infiltration. The development of this model is motivated by *in vitro* experimental observations in co-culture between breast cancer spheroids and activated immune cells, which study the effect of the glucocorticoid stress hormone, cortisol, on immune infiltration [99]. In this *in vitro* study, it is found that cortisol decreases the levels of the pro-inflammatory cytokine IFN-γ and increases the levels of the anti-inflammatory cytokine IL-10. Therefore, in our model, we suppose that the effect of stress on the anti-tumour immune response is directly linked to the change of levels of these two cytokines in the tumour microenvironment. Using a method similar to the one employed in [99], we define a score to quantify the effects of stress on immune infiltration in a controlled manner. The results of numerical simulations of this model are able to qualitatively reproduce the results of *in vitro* experiments presented in [99], and demonstrate the importance of including the effect of different factors when exploring the impact of physiological stress on immune infiltration into tumours.

Chapter 6 - Potential future directions In Chapter 6, we present a global conclusion of the thesis and we comment possible research perspectives.

1.5 List of publications

1.5.1 Accepted publications

- Luis Almeida, Chloe Audebert, E. L. and Tommaso Lorenzi, *Discrete and continuum models for the coevolutionary dynamics between CD8+ cytotoxic T lymphocytes and tumour cells*, Mathematical biology and medicine, 2022.

- E. L., Tommaso Lorenzi, Shensi Shen, Luis Almeida, Chloe Audebert, *A mathematical model to study the impact of intra-tumour heterogeneity on anti-tumour CD8+ T cell immune response*, Journal of Theoretical Biology, 2022.

- Luis Almeida, Chloe Audebert, E. L. and Tommaso Lorenzi, *A hybrid discrete-continuum modelling approach to explore the impact of T-cell infiltration on anti-tumour immune response*, Bulletin of Mathematical Biology, 2022.

1.5.2 In preparation

- Luis Almeida, Chloe Audebert, Melanie S. Flint, E. L., Tommaso Lorenzi and Chandrasekhar Venkataraman, *A mathematical model to investigate the effect of psychological stress on immune infiltration.*

Chapter 2

Discrete and continuum models for the coevolutionary dynamics between cytotoxic T lymphocytes and tumour cells

2.1 Motivation

In this chapter, we present an individual-based model for the coevolutionary dynamics between cytotoxic T lymphocytes (CTLs) and tumour cells. In this model, every cell is viewed as an individual agent whose phenotypic state is modelled by a discrete variable. For tumour cells this variable represents a parameterisation of the antigen expression profiles, while for CTLs it represents a parameterisation of the target antigens of T-cell receptors (TCRs).

In general, individual-based models are useful for observing emergent dynamics from interactions between single cells. However, they can be computationally time consuming and do not allow for analysis to be completed on the model. Considering the continuum counterpart of stochastic discrete individual-based models may allow for mathematical analysis. Therefore, we formally derive the deterministic continuum limit of this individual-based model, which comprises a non-local partial differential equation for the phenotype distribution of tumour cells coupled with an integro-differential equation for the phenotype distribution of CTLs. The biologically relevant homogeneous steady-state solutions of the continuum model equations are found. The linear-stability analysis of these steady-state solutions is then carried out in order to identify possible conditions on the model parameters that may lead to different outcomes of immune competition and to the emergence of patterns of phenotypic coevolution between tumour cells and CTLs.

We report on computational results of the individual-based model, and show that there is a good agreement between them and analytical and numerical results of the continuum model. These results shed light on the way in which different parameters affect the coevolutionary dynamics between tumour cells and CTLs. Moreover, they support the idea that TCR-tumour antigen binding affinity may be a good intervention target for immunotherapy and offer a theoretical basis for the development of anti-cancer therapy, such as adoptive T cell therapy, aiming at engineering TCRs so as to shape their affinity for cancer targets.

The models described in this chapter and the results shown have been published in Luis Almeida, Chloe Audebert, E. L. and Tommaso Lorenzi, *Discrete and continuum models for the coevolutionary dynamics between CD8+ cytotoxic T lymphocytes and tumour cells*, Mathematical biology and medicine, 2022.

2.2 Background

2.2.1 Biological background

As explained in Section 1.2, cytotoxic T lymphocytes (CTLs) play a key role in the immune response against cancer. CTLs carry a specific receptor on their surface, the T-cell receptor (TCR), which can recognise and bind to non-self antigens expressed by tumour cells [151]. Each TCR recognises and binds specifically to a certain antigen (*i.e.* the cognate antigen) [45], and possibly other antigens within a certain affinity range [144, 224]. This enables CTLs to exert an antigen-specific cytotoxic activity against tumour cells, whose efficacy may depend on the affinity range of TCRs and the strength of TCR-tumour antigen binding (*i.e.* TCR-tumour antigen binding affinity) [112, 197].

The presence of tumour cells expressing non-self antigens triggers the clonal expansion of CTLs with matching TCRs. Thereupon, CTL numbers are kept under control by self-regulation mechanisms [78, 154, 196, 227, 207], which play a key role in the prevention of autoimmunity.

Furthermore, epigenetic and genetic processes inducing stochastic and heritable changes in the antigen expression profiles of tumour cells foster dynamical intercellular variability in the expression levels of tumour antigens [29, 188, 209]. Due to limitations posed by self-regulation mechanisms upon the numbers of CTLs targeted against different antigens at the same tumour site, such a form of intratumour heterogeneity creates the substrate for adaptation of tumour cells to the antigen-specific cytotoxic activity of CTLs and triggers adaptive changes in the repertoire of CTLs. This results in coevolutionary dynamics whereby CTLs dynamically sculpt the antigenic distribution of tumour cells, and tumour cells concurrently reshape the repertoire of CTLs [173].

The observation that the numbers of CD8+ and CD3+ T lymphocytes at the tumour site correlate with prognosis in different types of cancer led to the development of the 'immunoscore' as a prognostic marker in cancer patients [10, 72, 71, 70]. The immunoscore provides a score that increases with the density of CD8+ and CD3+ T lymphocytes both in the centre and at the periphery of the tumour. A possible tumour classification based on the immunoscore has been proposed in [72], where tumours with a high immunoscore are classified as 'hot tumours', tumours with an intermediate immunoscore are classified as 'altered tumours', and tumours with a low immunoscore are classified as 'cold tumours'.

2.2.2 The mathematical model

In this vein, in this chapter, we develop an individual-based model for the coevolutionary dynamics between tumour cells and CTLs in a well-mixed system (*i.e.* spatial interactions are not incorporated into the model). Every cell is viewed as an individual agent whose phenotypic state is modelled by a discrete variable, which represents a parameterisation of the antigen expression profiles for tumour cells and a parameterisation of the target antigens of the TCRs for CTLs.

The model takes into account the effects of the following biological processes: proliferation and death of tumour cells and CTLs; heritable, spontaneous phenotypic changes of tumour cells resulting in variation of antigenic expression; antigen-driven expansion of CTLs (*i.e.* *in situ* clonal

expansion following antigen recognition); death of tumour cells due to antigen-specific cytotoxic activity of CTLs. These processes are incorporated into the model through a set of rules that correspond to a discrete-time branching random walk on the space of phenotypic states [40, 104].

We show that a generalised version of the mathematical model of immune competition presented in [132] can be formally obtained as the deterministic continuum limit of the individual-based model presented here. This continuum model comprises a non-local partial differential equation (PDE) for the phenotype distribution of tumour cells coupled with an integro-differential equation (IDE) for the phenotype distribution of CTLs, and shares some similarities with non-local predator-prey models such as those considered in [53, 81, 185, 202]. In addition to the biological phenomena incorporated into the model considered in [132], the deterministic continuum counterpart of the individual-based model developed here takes also into account the effect of changes in antigen expression profiles of tumour cells and more general forms of competitive feedback mechanisms regulating the growth of the numbers of tumour cells and CTLs.

The biologically relevant homogeneous steady-state solutions of the continuum model equations are found. Then, their linear stability analysis is studied in order to identify possible conditions on the model parameters leading to different outcomes of immune competition and to the formation of patterns of phenotypic coevolution between tumour cells and CTLs. We report on computational results of the individual-based model, and show that there is an excellent agreement between them and analytical and numerical results of the continuum model. Moreover, we explore possible scenarios in which differences between the outcomes of the discrete and continuum models may emerge. The results obtained disentangle the role of different cell parameters in the coevolutionary dynamics between tumour cells and CTLs.

2.2.3 Structure of the chapter

In Section 2.3, the individual-based model is introduced. In Section 2.4, the deterministic continuum counterpart of this model is presented (a formal derivation is provided in Appendix B.1). In Section 2.5, the homogeneous steady-state solutions of the continuum model equations are identified and their linear stability is investigated. In Section 2.6, computational results of the individual-based model are discussed and integrated with numerical solutions of the continuum model. In Section 2.7, key biological implications of the main findings of this study are summarised and directions for future research are outlined.

2.3 The individual-based model

We model the coevolutionary dynamics between a population of tumour cells and a population of CTLs in a well-mixed system. The population of tumour cells is labelled by the letter n, while the population of CTLs is labelled by the letter c. Building on the modelling approach developed in [52, 54, 132], at any time $t \in [0, t_f] \subset \mathbb{R}^+$, the phenotypic state of every tumour cell is modelled by a variable $x \in \overline{\mathcal{I}}$, where $\overline{\mathcal{I}} := [-L, L] \subset \mathbb{R}$ is the closure of the set $\mathcal{I} := (-L, L) \subset \mathbb{R}$ with $L > 0$, and the phenotypic state of every CTL is modelled by a variable $y \in \overline{\mathcal{I}}$. We make the following modelling assumptions.

Assumption 1. The variable x represents a parameterisation of the antigen expression profiles of tumour cells, while the variable y represents a parameterisation of the target antigens of the TCRs (see Figure 2.1). As a result, CTLs in the phenotypic state y will be primarily capable of recognising tumour cells in the phenotypic state $x = y$.

Assumption 2. Tumour cells will have higher antigenic similarity if their phenotypic states are modelled by closer value of x. Hence, depending on the range of TCR affinity, CTLs in the

phenotypic state $y = x$ may also be capable of recognising tumour cells in phenotypic states which are sufficiently close to x.

Assumption 3. Tumour cells in similar phenotypic states (*i.e.* phenotypic states that are modelled by sufficiently close values of x) will occupy similar niches and, therefore, a form of intra-population competition (*i.e.* clonal competition) will occur between them. Moreover, self-regulation mechanisms act on CTLs in similar phenotypic states (*i.e.* phenotypic states that are modelled by sufficiently close values of y). Hence, a form of intra-population competition will occur between these cells as well.

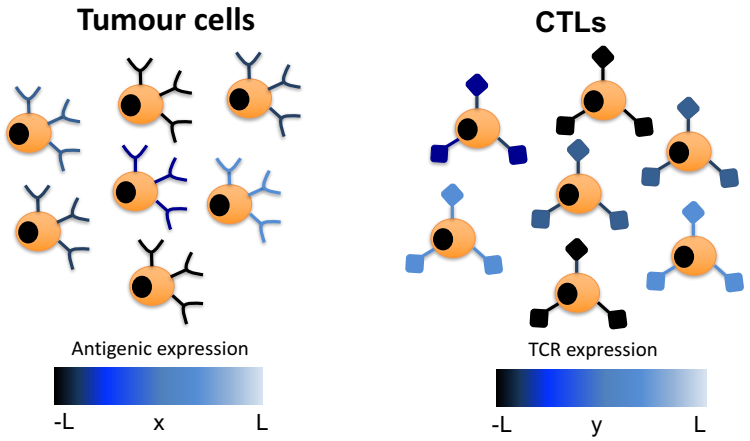

Figure 2.1: **Schematic illustration of the phenotypic expression of tumour cells and CTLs.** On the left: the value of the antigen expression profile of each tumour cell (variable x) is represented by the colour of the antigens on its surface. Likewise, on the right, the value of the target antigens of the TCRs that characterizes each CTL (*i.e.* variable y) is represented by the colour of the TCRs on its surface.

Building upon the ideas presented in [13, 40, 194], we model each cell as an agent that occupies a position on a lattice, which represents the space of phenotypic states. We discretise the time variable and the phenotypic states, respectively, as

$$t_k = k\tau \in [0, t_f], \quad x_i = i\chi \in \overline{\mathcal{I}} \quad \text{and} \quad y_j = j\chi \in \overline{\mathcal{I}}, \quad k \in \mathbb{N}_0,\ i, j \in \mathbb{Z},$$

where $\tau \in \mathbb{R}_*^+$ and $\chi \in \mathbb{R}_*^+$ are the time- and phenotype-step, respectively. We introduce the dependent variables $N_i^k \in \mathbb{N}_0$ and $C_j^k \in \mathbb{N}_0$ to represent, respectively, the number of tumour cells on lattice site i (*i.e.* in the phenotypic state x_i) and the number of CTLs on lattice site j (*i.e.* in the phenotypic state y_j) at time-step k. The population density functions of tumour cells and CTLs (*i.e.* the phenotype distributions of the two cell populations) are defined, respectively, as

$$n_i^k \equiv n(x_i, t_k) := \frac{N_i^k}{\chi} \quad \text{and} \quad c_j^k \equiv c(y_j, t_k) := \frac{C_j^k}{\chi}, \tag{2.1}$$

while the total numbers of tumour cells and CTLs (*i.e.* the sizes of the phenotype distributions

of the two cell populations) are defined, respectively, as

$$\rho_n^k \equiv \rho_n(t_k) := \sum_i N_i^k \quad \text{and} \quad \rho_c^k \equiv \rho_c(t_k) := \sum_j C_j^k. \tag{2.2}$$

In the mathematical framework of our model, the function

$$I_h \equiv I(t_k) := \frac{\rho_c(t_k)}{\rho_n(t_k)} \tag{2.3}$$

provides a possible simplified measure of the immune score at the k^{th} time-step in the well-mixed system considered here. In particular, abstracting from the immune-score based classification of tumours recalled in Section 2.2, throughout the chapter we will refer to situations in which the average value of I, *i.e.* the quantity

$$\overline{I} = \frac{\tau}{t_f} \sum_h I_h, \tag{2.4}$$

is smaller than 1 or at least about one order of magnitude larger than 1 as '*cold tumour-like scenarios*' and '*hot tumour-like scenarios*', respectively, whereas the remaining situations will be classified as '*altered tumour-like scenarios*'.

Remark 1. A more precise definition of the immunoscore, based on the spatial distribution of CTLs within the tumour and not just by their number, will be given in Chapter 4.

As mentioned earlier, we focus on a biological scenario whereby: (i) cells in the two populations divide and die due to intra-population competition (*i.e.* clonal competition amongst tumour cells and self-regulation of CTLs); (ii) tumour cells undergo heritable, spontaneous phenotypic changes which result in variation of antigen expression profiles; (iii) CTLs undergo antigen-driven expansion (*i.e. in situ* clonal expansion following antigen recognition); (iv) tumour cells die due to the antigen-specific cytotoxic activity of CTLs. These biological phenomena are incorporated into the model via the modelling strategies described in the following subsections, which are also schematised in Figure 2.2.

2.3.1 Mathematical modelling of cell division and death due to intra-population competition

We assume that a dividing cell is replaced by two identical cells that inherit the phenotypic state of the parent cell (*i.e.* the progenies are placed on the same lattice site as their parent), while a dying cell is removed from the population.

At every time-step k, we allow tumour cells and CTLs to undergo cell division at rates $\alpha_n > 0$ and $\alpha_c > 0$, respectively. Moreover, on the basis of Assumption 3, at every time-step k, we allow tumour cells in the phenotypic state x_i and CTLs in the phenotypic state y_j to die due to intra-population competition at rates $\mu_n\, K_{n_i}^k$ and $\mu_c\, K_{c_j}^k$, respectively, where $\mu_n, \mu_c > 0$ and

$$K_{n_i}^k \equiv K_n(x_i, t_k) := \sum_h g(x_i, x_h; \theta_n)\, N_h^k, \qquad K_{c_j}^k \equiv K_c(y_j, t_k) := \sum_h g(y_j, y_h; \theta_c)\, C_h^k. \tag{2.5}$$

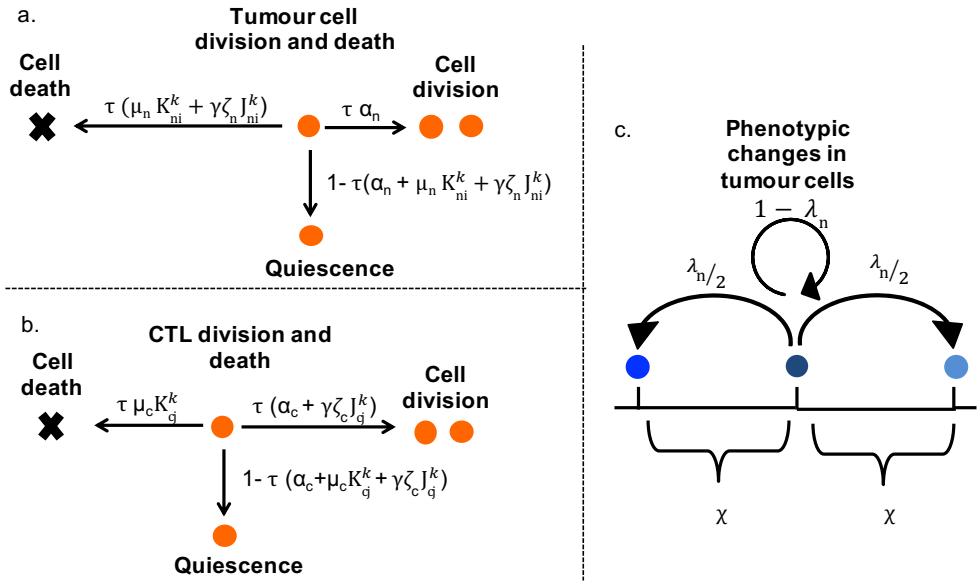

Figure 2.2: **Schematic representation of the algorithmic rules governing the coevolutionary dynamics between tumour cells and CTLs in the stochastic individual-based model.** Panel **a.**: for a tumour cell in the phenotypic state x_i we let α_n model the rate of cell division, $\mu_n K_{n_i}^k$ the rate of cell death due to intra-population competition, with the quantity $K_{n_i}^k$ defined via (2.5)-(2.7). Moreover, tumour cells can die due to antigen-specific cytotoxic activity of CTLs at rate $\zeta_n \gamma J_{n_i}^k$, with $J_{n_i}^k$ defined via (2.6)-(2.8). Therefore, during the time interval of length $\tau \ll 1$, between the time step k and the time step $k+1$ we let a tumour cell in a phenotypic state x_i divide with probability $\tau\alpha_n$ or die with probability $\tau(\mu_n K_{n_i}^k + \zeta_n \gamma J_{n_i}^k)$ or remain quiescent with probability $1 - \tau(\alpha_n + \mu_n K_{n_i}^k + \zeta_n \gamma J_{n_i}^k)$. Panel **b.**: for a CTL in the phenotypic state y_j we let α_c model the rate of cell division and $\mu_c K_{c_j}^k$ the rate of cell death due to intra-population competition, with the quantity $K_{c_j}^k$ defined via (2.5)-(2.7). Moreover, CTLs can undergo antigen-driven expansion at rate $\zeta_c \gamma J_{c_j}^k$, with $J_{c_j}^k$ defined via (2.6)-(2.8). Therefore, between the time step k and the time step $k+1$ we let a CTL in a phenotypic state y_j divide with probability $\tau(\alpha_c + \zeta_c \gamma J_{c_j}^k)$ or die with probability $\tau\mu_c K_{c_j}^k$ or remain quiescent with probability $1 - \tau(\alpha_c + \zeta_c \gamma J_{c_j}^k + \mu_c K_{c_j}^k)$. Panel **c.**: a tumour cell in the phenotypic state x_i that undergoes a phenotypic change can either enter into the phenotypic state x_{i-1} with probability $\frac{\lambda_n}{2}$, enter into the phenotypic state x_{i+1} with probability $\frac{\lambda_n}{2}$ or remain in its current phenotypic state with probability $1 - \lambda_n$.

The function g is defined as follows

$$g(x, y; \xi) := \begin{cases} \dfrac{1}{|\mathcal{L}_\xi(x)|} & \text{if} \quad |y - x| \leqslant \xi \\ 0 & \text{if} \quad |y - x| > \xi, \end{cases} \qquad \text{for } (x, y; \xi) \in \mathcal{I} \times \mathcal{I} \times (0, |\mathcal{I}|], \tag{2.6}$$

where $|\mathcal{I}|$ denotes the size of the interval $\mathcal{I}$ (*i.e.* $|\mathcal{I}| = 2L$) and $|\mathcal{L}_\xi(x)|$ denotes the size of the interval

$$\mathcal{L}_\xi(x) := \{y \in \mathcal{I} : |y - x| \leqslant \xi\}, \quad (x; \xi) \in \mathcal{I} \times (0, |\mathcal{I}|]. \tag{2.7}$$

The quantity $K_{n_i}^k$ defined via (2.5)-(2.7) represents the number of tumour cells whose phenotypic states are modelled by values of the variable x_h at a distance smaller than or equal to θ_n from x_i, rescaled to $|\mathcal{L}_{\theta_n}(x_i)|$. Similarly, the quantity $K_{c_j}^k$ defined via (2.5)-(2.7) represents the number of CTLs whose phenotypic states are modelled by values of the variable y_h at a distance smaller than or equal to θ_c from y_j, rescaled to $|\mathcal{L}_{\theta_c}(y_j)|$. Hence, the inverse of the parameter $0 < \theta_n \leqslant |\mathcal{I}|$ (*i.e.* $1/\theta_n$) provides a measure of the level of selectivity of clonal competition amongst tumour cells and the inverse of the parameter $0 < \theta_c \leqslant |\mathcal{I}|$ (*i.e.* $1/\theta_c$) provides a measure of the level of selectivity of self-regulation mechanisms acting on CTLs (*i.e.* the smaller θ_n and θ_c, then the higher the corresponding levels of selectivity). Furthermore, the parameters μ_n and μ_c represent the rates of death of tumour cells and CTLs due to these forms of intra-population competition.

2.3.2 Mathematical modelling of phenotypic changes in tumour cells

We account for spontaneous, heritable phenotypic changes which result in variation of antigen expression profiles by allowing tumour cells to update their phenotypic states according to a random walk. More precisely, between the time-steps k and $k+1$, every tumour cell enters a new phenotypic state, with probability $0 < \lambda_n < 1$, or remains in its current phenotypic state, with probability $1 - \lambda_n$. When a tumour cell in the phenotypic state x_i undergoes a phenotypic change, it enters into either the phenotypic state x_{i-1} or the phenotypic state x_{i+1} with probability $\lambda_n/2$. This models the fact that phenotypic changes occur randomly due to non-genetic instability, rather than being induced by selective pressures [103]. No-flux boundary conditions are implemented by aborting any attempted phenotypic variation of a tumour cell if it requires moving into a phenotypic state outside the interval $\overline{\mathcal{I}}$.

2.3.3 Mathematical modelling of tumour-immune competition

Similarly to cell division, we assume that a CTL undergoing antigen-driven expansion is replaced by two identical cells that inherit the phenotypic state of the parent cell. Moreover, similarly to cell death due to intra-population competition, we assume that a tumour cell dying due to the antigen-specific cytotoxic activity of CTLs is removed from the population.

On the basis of Assumptions 1 and 2, at every time-step k we allow CTLs in the phenotypic state y_j to undergo antigen-driven expansion at rate $\zeta_c\,\gamma\,J_{c_j}^k$, while tumour cells in the phenotypic state x_i will die due to antigen-specific cytotoxic activity of CTLs at rate $\zeta_n\,\gamma\,J_{n_i}^k$. Here, $\zeta_n, \zeta_c, \gamma > 0$ and

$$J_{c_j}^k \equiv J_c(y_j, t_k) := \sum_i g(y_j, x_i; \eta)\, N_i^k, \qquad J_{n_i}^k \equiv J_n(x_i, t_k) := \sum_j g(x_i, y_j; \eta)\, C_j^k, \tag{2.8}$$

where the function g is defined via (2.6) and (2.7). The quantity $J_{c_j}^k$ defined via (2.6)-(2.8) represents the number of tumour cells whose phenotypic states are modelled by values of the variable x_i at a distance smaller than or equal to η from y_j, rescaled to $|\mathcal{L}_\eta(y_j)|$. Similarly, the quantity $J_{C_i}^k$ defined via (2.6)-(2.8) represents the number of CTLs in phenotypic states which are modelled by values of the variable y_j at a distance smaller than or equal to η from x_i, rescaled to $|\mathcal{L}_\eta(x_i)|$. Hence, the parameter $0 < \eta \leqslant |\mathcal{I}|$ provides a measure of the affinity range of TCRs. Furthermore, the parameter γ provides a measure of the TCR-tumour antigen binding affinity (*i.e.* the strength of TCR-tumour antigen binding), while the parameter ζ_c represents the rate at which a CTL undergoing antigen-driven expansion divides (*i.e.* the rate of cell division corresponding to *in situ* clonal expansion), and the parameter ζ_n represents the rate at which a

tumour cell can die due to the antigen-specific cytotoxic activity of a CTL.

2.3.4 Computational implementation of the individual-based model

Numerical simulations of the individual-based model are performed in MATLAB. At each time-step, we follow the procedures described hereafter to simulate phenotypic variation, cell division and death of tumour cells, and cell division and death of CTLs. All random numbers mentioned below are real numbers drawn from the standard uniform distribution on the interval $(0, 1)$ using the built-in function RAND.

Computational implementation of spontaneous, heritable phenotypic changes of tumour cells For each tumour cell, a random number, r_1, is generated and used to determine whether the cell undergoes a phenotypic change (*i.e.* $0 < r_1 < \lambda_n$) or not (*i.e.* $\lambda_n \leqslant r_1 < 1$). If the cell undergoes a phenotypic change, then a second random number, r_2, is generated. If $0 < r_2 < 1/2$, then the cell moves into the phenotypic state to the left of its current state (*i.e.* a cell in the phenotypic state x_i will move into the phenotypic state $x_{i-1} = x_i - \chi$), whereas if $1/2 \leqslant r_2 < 1$ then the cell moves into the phenotypic state to the right of its current state (*i.e.* a cell in the phenotypic state x_i will move into the phenotypic state $x_{i+1} = x_i + \chi$). No-flux boundary conditions are implemented by aborting attempted phenotypic changes that would move a cell into a phenotypic state outside the interval $\overline{\mathcal{I}}$.

Computational implementation of cell division and death of tumour cells and CTLs For each population, the number of cells in each phenotypic state is counted. The quantities K_n and K_c are computed via (2.5) and the quantities J_n and J_c are computed via (2.8), and the following definitions are used to calculate the probabilities of cell division, death and quiescence (*i.e.* no division nor death) for every phenotypic state of cells in the two populations, respectively,

$$\mathrm{P}_n^b := \tau\,\alpha_n, \quad \mathrm{P}_n^d := \tau\,\left(\mu_n\,K_{n_i}^k + \zeta_n\,\gamma\,J_{n_i}^k\right), \quad \mathrm{P}_n^q := 1 - \left(\mathrm{P}_n^b + \mathrm{P}_n^d\right) \tag{2.9}$$

and

$$\mathrm{P}_c^b := \tau\,\left(\alpha_c + \zeta_c\,\gamma\,J_{c_j}^k\right), \quad \mathrm{P}_c^d := \tau\,\mu_c\,K_{c_j}^k, \quad \mathrm{P}_c^q := 1 - \left(\mathrm{P}_c^b + \mathrm{P}_c^d\right). \tag{2.10}$$

Notice that we are implicitly assuming that the time-step τ is sufficiently small that $0 < \mathrm{P}_n^k < 1$ and $0 < \mathrm{P}_c^k < 1$ for all $h \in \{b, d, q\}$. For each cell, a random number, r_3, is generated and the cells' fate is determined by comparing this number with the probabilities of division, death and quiescence corresponding to the phenotypic state of the cell. In more detail, for a cell in population C: if $0 < r_3 < \mathrm{P}_n^d$ then the cell is considered dead and is removed from the population; if $\mathrm{P}_n^d \leqslant r_3 < \mathrm{P}_n^d + \mathrm{P}_n^b$ then the cell undergoes division and an identical daughter cell is created; whereas if $\mathrm{P}_n^d + \mathrm{P}_n^b \leqslant r_3 < 1$ then the cell remains quiescent (*i.e.* does not divide nor die). Similarly, for a cell in population T: if $0 < r_3 < \mathrm{P}_c^d$ then the cell is considered dead and is removed from the population; if $\mathrm{P}_c^d \leqslant r_3 < \mathrm{P}_c^d + \mathrm{P}_c^b$ then the cell undergoes division and an identical daughter cell is created; whereas if $\mathrm{P}_c^d + \mathrm{P}_c^b \leqslant r_3 < 1$ then the cell remains quiescent.

2.4 Corresponding deterministic continuum model

In the case where cell dynamics are governed by the rules described in Sections 2.3.1-2.3.3, between time-steps k and $k + 1$ a tumour cell in the phenotypic state x_i may divide, die or remain quiescent (*i.e.* not divide nor die) with probabilities defined via (2.9), while a CTL in the phenotypic state y_j may divide, die or remain quiescent with probabilities defined via (2.10).

Hence, recalling that between time-steps k and $k+1$ a tumour cell in the phenotypic state x_i may also enter into either of the phenotypic states x_{i-1} and x_{i+1} with probabilities $\lambda_n/2$, the principle of mass balance gives the following system of coupled difference equations for the population densities n_i^k and c_j^k:

$$\begin{cases} n_i^{k+1} = \left(2\,\mathrm{P}_n^b + \mathrm{P}_n^q\right)\left[\dfrac{\lambda_n}{2}\left(n_{i+1}^k + n_{i-1}^k\right) + (1-\lambda_n)\,n_i^k\right], \quad (x_i, t_k) \in \mathcal{I} \times (0, t_f], \\ \\ c_j^{k+1} = \left(2\,\mathrm{P}_c^b + \mathrm{P}_c^q\right)\,c_j^k, \quad (y_j, t_k) \in \overline{\mathcal{I}} \times (0, t_f]. \end{cases} \tag{2.11}$$

The difference equation $(2.11)_1$ for n_i^k is subject to no-flux boundary conditions due to the fact that, as mentioned in Section 2.3.2, any attempted phenotypic variation of a tumour cell is aborted if it requires moving into a phenotypic state outside the interval $\overline{\mathcal{I}}$.

Starting from the system of coupled difference equations (2.11), letting the time-step $\tau \to 0$ and the phenotype-step $\chi \to 0$ in such a way that

$$\lambda_n \frac{\chi^2}{2\tau} \to \beta_n \quad \text{with} \quad 0 < \beta_n < \infty, \tag{2.12}$$

where the parameter β_n is the rate of spontaneous, heritable phenotypic changes of tumour cells, using the method employed in [13, 40, 194], it is possible to formally show (see Appendix B.1) that the deterministic continuum counterpart of the stochastic discrete model comprises the following PDE-IDE system for the cell population density functions $n(x,t)$ and $c(y,t)$

$$\begin{cases} \partial_t n - \beta_n\,\partial_{xx}^2 n = \Big[\alpha_n - \mu_n\,K_n(x,t) - \zeta_n\,\gamma\,J_n(x,t)\Big]n, \quad (x,t) \in \mathcal{I} \times (0,t_f], \\ \partial_t c = \Big[\alpha_c - \mu_c K_c(y,t) + \zeta_c\,\gamma\,J_c(y,t)\Big]c, \quad (y,t) \in \overline{\mathcal{I}} \times (0,t_f], \\ J_n(x,t) := \displaystyle\int_{\mathcal{I}} g(x,y;\eta)\,c(y,t)\,\mathrm{d}y, \quad K_n(x,t) := \int_{\mathcal{I}} g(x,z;\theta_n)\,n(z,t)\,\mathrm{d}z, \\ J_c(y,t) := \displaystyle\int_{\mathcal{I}} g(y,x;\eta)\,n(x,t)\mathrm{d}x, \quad K_c(y,t) := \int_{\mathcal{I}} g(y,z;\theta_c)\,c(z,t)\,\mathrm{d}z, \end{cases} \tag{2.13}$$

with $\mathcal{I} = (-L, L)$. Here, the function g is defined via (2.6) and (2.7), and the non-local PDE $(2.13)_1$ for n is subject to the following no-flux boundary conditions

$$\partial_x n(-L,t) = 0 \quad \text{and} \quad \partial_x n(L,t) = 0 \quad \text{for all } t \in (0,t_f]. \tag{2.14}$$

2.5 Steady-state and linear-stability analyses of the continuum model equations

In this section, we first identify the biologically relevant homogeneous steady-state solutions of the continuum model equations. Then, we carry out linear-stability analysis to: (i) determine conditions that may lead to the eradication of tumour cells by CTLs or to the coexistence between the two cell populations, and (ii) identify sufficient conditions for the emergence of patterns of phenotypic coevolution between tumour cells and CTLs.

2.5.1 Biologically relevant steady-state solutions

A biologically relevant steady-state solution of the PDE-IDE system (2.13) subject to the boundary conditions (2.14) is given by a pair of real, non-negative functions $n^*(x)$ and $c^*(y)$ that satisfy the following system of differential equations

$$\begin{cases} -\beta_n \, \partial^2_{xx} n^* = \Big[\alpha_n - \mu_n \, K^*_n(x) - \zeta_n \, \gamma \, J^*_n(x)\Big] n^*, \quad x \in \mathcal{I}, \\ \Big[\alpha_c - \mu_c K^*_c(y) + \zeta_c \, \gamma \, J^*_c(y)\Big] c^* = 0, \quad y \in \overline{\mathcal{I}}, \end{cases} \tag{2.15}$$

with $\mathcal{I} = (-L, L)$, subject to the boundary conditions

$$\partial_x n^*(-L) = 0 \quad \text{and} \quad \partial_x n^*(L) = 0. \tag{2.16}$$

In the system (2.15),

$$J^*_n(x) := \int_{\mathcal{I}} g(x, y; \eta) \, c^*(y) \, \mathrm{d}y, \quad K^*_n(x) := \int_{\mathcal{I}} g(x, z; \theta_n) \, n^*(z) \, \mathrm{d}z \tag{2.17}$$

and

$$J^*_c(y) := \int_{\mathcal{I}} g(y, x; \eta) \, n^*(x) \, \mathrm{d}x, \quad K^*_c(y) := \int_{\mathcal{I}} g(y, z; \theta_c) \, c^*(z) \, \mathrm{d}z. \tag{2.18}$$

The components of homogeneous steady-state solutions satisfy the following system of equations

$$\begin{cases} \Big[\alpha_n - \mu_n \, K^*_n(x) - \zeta_n \, \gamma \, J^*_n(x)\Big] n^* = 0, \quad x \in \overline{\mathcal{I}}, \\ \Big[\alpha_c - \mu_c K^*_c(y) + \zeta_c \, \gamma \, J^*_c(y)\Big] c^* = 0, \quad y \in \overline{\mathcal{I}} \end{cases} \tag{2.19}$$

and are of the form

$$n^*(x) = \frac{\rho^*_n}{|\mathcal{I}|} \ \ \forall x \in \overline{\mathcal{I}} \quad \text{and} \quad c^*(y) = \frac{\rho^*_c}{|\mathcal{I}|} \ \ \forall y \in \overline{\mathcal{I}}, \tag{2.20}$$

where $\rho^*_n \geqslant 0$ and $\rho^*_n \geqslant 0$ satisfy the following system of algebraic equations

$$\begin{cases} \Big(\alpha_n \, |\mathcal{I}| - \mu_n \, \rho^*_n - \gamma_n \, \rho^*_c\Big) \rho^*_n = 0, \\ \Big(\alpha_c \, |\mathcal{I}| - \mu_c \, \rho^*_c + \gamma_c \, \rho^*_n\Big) \rho^*_c = 0, \end{cases} \quad \text{with} \quad \gamma_n := \zeta_n \, \gamma \quad \text{and} \quad \gamma_c := \zeta_c \, \gamma. \tag{2.21}$$

The system of algebraic equations (2.21) is obtained by first integrating the PDE $(2.13)_1$ over $\mathcal{I}$ and imposing the boundary conditions (2.14), then integrating the IDE $(2.13)_2$ over $\mathcal{I}$, next substituting ansatz (2.20) into the resulting equations and equating to zero their right-hand sides, and finally using the fact that, when the function g is defined via (2.6) and (2.7),

$$\int_{\mathcal{I}} g(x, y; \xi) \, \mathrm{d}y = 1, \ \ \forall (x; \xi) \in \mathcal{I} \times (0, |\mathcal{I}|]. \tag{2.22}$$

In particular, since we are studying tumour-immune competition, we are interested in solutions of the system of equations (2.21) whose ρ^*_c component is strictly positive. There exist two solutions

of this type, that is, the semitrivial solution

$$(\rho_{n1}^*, \rho_{c1}^*) = \left(0, \frac{|\mathcal{I}|\alpha_c}{\mu_c}\right), \tag{2.23}$$

and, provided that the following condition on the model parameters is met

$$\gamma < \frac{\mu_c}{\alpha_c}\frac{\alpha_n}{\zeta_n}, \tag{2.24}$$

the nontrivial solution

$$(\rho_{n2}^*, \rho_{c2}^*) = \left(|\mathcal{I}|\,\frac{(\alpha_n\mu_c - \alpha_c\gamma_n)}{\gamma_c\gamma_n + \mu_n\mu_c}, |\mathcal{I}|\,\frac{(\alpha_c\mu_n + \alpha_n\gamma_c)}{\gamma_c\gamma_n + \mu_n\mu_c}\right). \tag{2.25}$$

The semitrivial steady-state solution given by (2.20) and (2.23) corresponds to biological scenarios whereby tumour cells are eradicated by CTLs, while the nontrivial steady-state solution given by (2.20) and (2.25) corresponds to situations where coexistence between tumour cells and CTLs occurs. Notice that condition (2.24) indicates that lower TCR-tumour antigen binding affinity (*i.e.* smaller values of γ) make it more likely that tumour cells survive the cytotoxic action of CTLs, thus promoting coexistence between the two cell populations.

2.5.2 Linear-stability analysis

Linearising the PDE-IDE system (2.13), subject to the boundary conditions (2.14), about a steady-state of components $n^*(x)$ and $c^*(y)$, and using the conditions given by equations (2.15), we obtain the following PDE-IDE system for the perturbations $\tilde{n}_n(x,t)$ and $\tilde{n}_T(y,t)$

$$\begin{cases} \partial_t\tilde{n} - \beta_n\,\partial_{xx}^2\tilde{n} = [\alpha_n - \mu_n K_n^*(x) - \gamma_n J_n^*(x)]\,\tilde{n} - \Big[\mu_n\,\tilde{K}_n(x,t) + \gamma_n\,\tilde{J}_n(x,t)\Big]n^*, \ (x,t) \in \mathcal{I}\times(0,t_f], \\ \partial_t\tilde{c} = [\alpha_c - \mu_c K_c^*(y) + \gamma_c J_c^*(y)]\,\tilde{c} - \Big[\mu_c\,\tilde{K}_c(y,t) - \gamma_c\,\tilde{J}_c(y,t)\Big]c^*, \quad (y,t) \in \overline{\mathcal{I}}\times(0,t_f], \end{cases} \tag{2.26}$$

subject to the boundary conditions

$$\partial_x\tilde{n}(-L,t) = 0 \quad \text{and} \quad \partial_x\tilde{n}(L,t) = 0 \quad \text{for all } t \in (0,t_f]. \tag{2.27}$$

In the system (2.26), $J_n^*(x)$ and $K_n^*(x)$ are defined via (2.17), $J_c^*(y)$ and $K_c^*(y)$ are defined via (2.18), and

$$\tilde{J}_n(x,t) := \int_{\mathcal{I}} g(x,y;\eta)\,\tilde{c}(y,t)\,\mathrm{d}y, \quad \tilde{K}_n(x,t) := \int_{\mathcal{I}} g(x,z;\theta_n)\,\tilde{n}(z,t)\,\mathrm{d}z, \tag{2.28}$$

$$\tilde{J}_c(y,t) := \int_{\mathcal{I}} g(y,x;\eta)\,\tilde{n}(x,t)\,\mathrm{d}x, \quad \tilde{K}_c(y,t) := \int_{\mathcal{I}} g(y,z;\theta_c)\,\tilde{c}(z,t)\,\mathrm{d}z. \tag{2.29}$$

Due to (2.19), if the steady-state solution (n^*, c^*) is given by (2.20) and (2.23) then the PDE-IDE system (2.26) reduces to

$$\begin{cases} \partial_t\tilde{n} - \beta_n\,\partial_{xx}^2\tilde{n} = \Big[\alpha_n - \gamma_n J_n^*(x)\Big]\tilde{n}, \quad (x,t) \in \mathcal{I}\times(0,t_f], \\ \partial_t\tilde{c} = -\Big[\mu_c\,\tilde{K}_c(y,t) - \gamma_c\,\tilde{J}_c(y,t)\Big]\dfrac{\rho_{c1}^*}{|\mathcal{I}|}, \quad (y,t) \in \overline{\mathcal{I}}\times(0,t_f], \end{cases} \tag{2.30}$$

whereas if condition (2.24) is met and the steady-state solution (n^*, c^*) is given by (2.20) and (2.25) then the PDE-IDE system (2.26) reduces to

$$\begin{cases} \partial_t \tilde{n} - \beta_n \, \partial^2_{xx} \tilde{n} = -\Big[\mu_n \, \tilde{K}_n(x,t) + \gamma_n \, \tilde{J}_n(x,t)\Big] \dfrac{\rho^*_{n2}}{|\mathcal{I}|}, \quad (x,t) \in \mathcal{I} \times (0, t_f], \\ \partial_t \tilde{c} = -\Big[\mu_c \, \tilde{K}_c(y,t) - \gamma_c \, \tilde{J}_c(y,t)\Big] \dfrac{\rho^*_{c2}}{|\mathcal{I}|}, \quad (y,t) \in \overline{\mathcal{I}} \times (0, t_f]. \end{cases} \tag{2.31}$$

Conditions for eradication of tumour cells by CTLs or coexistence between the two cell populations

In order to determine conditions on the model parameters that may lead to the eradication of tumour cells by CTLs or to the coexistence between the two cell populations, we study the stability of the steady-state solutions given by (2.20) and (2.23) or (2.25) to perturbations of the form

$$\tilde{n}(x,t) = \epsilon_n \, e^{\lambda t} \;\; \forall x \in \overline{\mathcal{I}} \quad \text{and} \quad \tilde{c}(y,t) = \epsilon_c \, e^{\lambda t} \;\; \forall y \in \overline{\mathcal{I}} \quad \text{with} \quad \epsilon_n, \epsilon_c \in \mathbb{R}_*, \; \lambda \in \mathbb{C}. \tag{2.32}$$

Substituting the ansatz (2.32) into the PDE-IDE system (2.30) and using property (2.22) along with the expression (2.23) of ρ^*_{c1} gives the following system of algebraic equations

$$\begin{cases} \lambda \epsilon_n = \Big(\alpha_n - \gamma_n \dfrac{\alpha_c}{\mu_c}\Big) \epsilon_n, \\ \lambda \epsilon_c = -\Big(\mu_c \, \epsilon_c - \gamma_c \, \epsilon_n\Big) \dfrac{\alpha_c}{\mu_c}, \end{cases} \tag{2.33}$$

which can be written in matrix form as

$$\begin{bmatrix} \alpha_n - \gamma_n \dfrac{\alpha_c}{\mu_c} - \lambda & 0 \\ \gamma_c \dfrac{\alpha_c}{\mu_c} & -\alpha_c - \lambda \end{bmatrix} \begin{bmatrix} \epsilon_n \\ \epsilon_c \end{bmatrix} = \begin{bmatrix} 0 \\ 0 \end{bmatrix}.$$

For a non-trivial solution of system (2.33) to exist, the determinant of the above matrix must be zero. This leads to the following quadratic equation for λ

$$\lambda^2 - B\lambda + C = 0$$

with

$$B := \alpha_n - \gamma_n \frac{\alpha_c}{\mu_c} - \alpha_c \quad \text{and} \quad C := \alpha_c \left(\gamma_n \frac{\alpha_c}{\mu_c} - \alpha_n\right).$$

Hence, the semitrivial steady-state solution given by (2.20) and (2.23) is locally asymptotically stable if the reverse of condition (2.24) holds, that is if

$$\gamma > \frac{\mu_c}{\alpha_c} \frac{\alpha_n}{\zeta_n}, \tag{2.34}$$

since in this case $B < 0$ and $C > 0$ (*i.e.* $\mathrm{Re}(\lambda) < 0$). On the other hand, performing similar

calculations on the PDE-IDE system (2.31) gives the the following system of algebraic equations

$$\begin{cases} \lambda\epsilon_n = -\Big(\mu_n\,\epsilon_n + \gamma_n\,\epsilon_c\Big)\,\dfrac{(\alpha_n\mu_c - \alpha_c\gamma_n)}{\gamma_c\gamma_n + \mu_n\mu_c}, \\ \lambda\epsilon_c = -\Big(\mu_c\,\epsilon_c - \gamma_c\,\epsilon_n\Big)\,\dfrac{(\alpha_c\mu_n + \alpha_n\gamma_c)}{\gamma_c\gamma_n + \mu_n\mu_c}, \end{cases} \tag{2.35}$$

which can be written in matrix form as

$$\begin{bmatrix} -\mu_n\dfrac{(\alpha_n\mu_c - \alpha_c\gamma_n)}{\gamma_c\gamma_n + \mu_n\mu_c} - \lambda & -\gamma_n\dfrac{(\alpha_n\mu_c - \alpha_c\gamma_n)}{\gamma_c\gamma_n + \mu_n\mu_c} \\ \gamma_c\dfrac{(\alpha_c\mu_n + \alpha_n\gamma_c)}{\gamma_c\gamma_n + \mu_n\mu_c} & -\mu_c\dfrac{(\alpha_c\mu_n + \alpha_n\gamma_c)}{\gamma_c\gamma_n + \mu_n\mu_c} - \lambda \end{bmatrix} \begin{bmatrix} \epsilon_n \\ \epsilon_c \end{bmatrix} = \begin{bmatrix} 0 \\ 0 \end{bmatrix}.$$

For a non-trivial solution of system (2.35) to exist, the determinant of the above matrix must be zero. This leads to the following quadratic equation for λ

$$\lambda^2 - B\lambda + C = 0$$

with

$$B := -\left[\mu_n\frac{(\alpha_n\mu_c - \alpha_c\gamma_n)}{\gamma_c\gamma_n + \mu_n\mu_c} + \mu_c\frac{(\alpha_c\mu_n + \alpha_n\gamma_c)}{\gamma_c\gamma_n + \mu_n\mu_c}\right]$$

and

$$C := \frac{(\alpha_n\mu_c - \alpha_c\gamma_n)(\alpha_c\mu_n + \alpha_n\gamma_c)}{(\gamma_c\gamma_n + \mu_n\mu_c)^2}\left[\mu_n\mu_c + \gamma_n\gamma_c\right].$$

Hence, if condition (2.24) is met, then the nontrivial steady-state solution given by (2.20) and (2.25) is locally asymptotically stable, since in this case $B < 0$ and $C > 0$ (*i.e.* $\mathrm{Re}(\lambda) < 0$).

Conditions for the emergence of patterns of phenotypic coevolution between tumour cells and CTLs

In order to identify sufficient conditions for the emergence of patterns of phenotypic coevolution between tumour cells and CTLs, we study the stability of the nontrivial steady-state solution given by (2.20) and (2.25) to perturbations of the form

$$\tilde{n}(x,t) = \epsilon_n\,e^{\lambda t}\,\varphi_h(x) \quad \text{and} \quad \tilde{c}(y,t) = \epsilon_c\,e^{\lambda t}\,\varphi_h(y) \quad \text{with} \quad \epsilon_n, \epsilon_c \in \mathbb{R}_*,\ \lambda \in \mathbb{C}. \tag{2.36}$$

Here, $\{\varphi_h\}_{h\geqslant 1}$ are the eigenfunctions of the Laplace operator on $\mathcal{I}$ with homogeneous Neumann boundary conditions indexed by the wavenumber h, that is,

$$\varphi_h(x) = \cos(h\,x) \quad \text{with} \quad h = \frac{m\pi}{|\mathcal{I}|}, \quad m \in \mathbb{N}, \quad x \in \overline{\mathcal{I}}. \tag{2.37}$$

Substituting the ansatz given by (2.36) and (2.37) into the PDE-IDE system (2.31), using the fact that

$$\int_{\mathcal{I}} g(x,y;\xi)\varphi_h(y)\,\mathrm{d}y = \frac{\sin(h\xi)}{h}\,\Psi(x;\xi)\,\varphi_h(x) \quad \text{with} \quad \Psi(x;\xi) := \frac{2}{|\mathcal{L}_\xi(x)|}$$

for all $x \in \mathcal{I}$ and $\xi \in (0, |\mathcal{I}|]$, we obtain the following infinite system of algebraic equations

$$\begin{cases} \lambda\,\epsilon_n = -h^2\,\beta_n\,\epsilon_n - \Big(\mu_n\,\dfrac{\sin(h\theta_n)}{h}\,\Psi(x;\theta_n)\,\epsilon_n + \gamma_n\,\dfrac{\sin(h\eta)}{h}\,\Psi(x;\eta)\,\epsilon_c\Big)\,\dfrac{\rho^*_{n2}}{|\mathcal{I}|}, \\ \lambda\,\epsilon_c = -\Big(\mu_c\,\dfrac{\sin(h\theta_c)}{h}\,\Psi(x;\theta_c)\,\epsilon_c - \gamma_c\,\dfrac{\sin(h\eta)}{h}\,\Psi(x;\eta)\,\epsilon_n\Big)\,\dfrac{\rho^*_{c2}}{|\mathcal{I}|}, \end{cases} \tag{2.38}$$

which can be written in matrix form as

$$\begin{bmatrix} -h^2\,\beta_n - \mu_n\dfrac{\sin(h\theta_n)}{h}\,\Psi(x;\theta_n)\dfrac{\rho^*_{n2}}{|\mathcal{I}|} - \lambda & -\gamma_n\dfrac{\sin(h\eta)}{h}\,\Psi(x;\eta)\dfrac{\rho^*_{n2}}{|\mathcal{I}|} \\ \gamma_c\dfrac{\sin(h\eta)}{h}\,\Psi(x;\eta)\dfrac{\rho^*_{c2}}{|\mathcal{I}|} & -\mu_c\dfrac{\sin(h\theta_c)}{h}\,\Psi(x;\theta_c)\dfrac{\rho^*_{c2}}{|\mathcal{I}|} - \lambda \end{bmatrix} \begin{bmatrix} \epsilon_n \\ \epsilon_c \end{bmatrix} = \begin{bmatrix} 0 \\ 0 \end{bmatrix}.$$

For each $x \in \mathcal{I}$, for a non-trivial solution of the system of algebraic equations (2.38) to exist the determinant of the above matrix must be zero. For each $x \in \mathcal{I}$, this leads to the following quadratic equation for λ

$$\lambda^2 - B\lambda + C = 0$$

where

$$B \equiv B(h,x) := -h^2\,\beta_n - \mu_n\frac{\sin(h\theta_n)}{h}\frac{\rho^*_{n2}}{|\mathcal{I}|}\,\Psi(x;\theta_n) - \mu_c\frac{\sin(h\theta_c)}{h}\frac{\rho^*_{c2}}{|\mathcal{I}|}\,\Psi(x;\theta_c) \tag{2.39}$$

and

$$\begin{aligned} C \equiv C(h,x) :&= h^2\,\beta_n\,\mu_c\frac{\sin(h\theta_c)}{h}\frac{\rho^*_{c2}}{|\mathcal{I}|}\Psi(x;\theta_c) + \\ &+ \frac{\rho^*_{n2}\,\rho^*_{c2}}{|\mathcal{I}|^2}\left[\gamma_n\gamma_c\left(\frac{\sin(h\eta)}{h}\Psi(x;\eta)\right)^2 + \mu_n\mu_c\frac{\sin(h\theta_n)}{h}\,\frac{\sin(h\theta_c)}{h}\Psi(x;\theta_n)\Psi(x;\theta_c)\right]. \end{aligned}$$

A sufficient condition for the nontrivial steady-state solution given by (2.20) and (2.25) to be driven unstable by perturbations of the form (2.36) (i.e. for patterns of phenotypic coevolution between tumour cells and CTLs to be formed) is that $B > 0$ and/or $C < 0$ so that $\mathrm{Re}(\lambda) > 0$ for all $x \in \mathcal{I}$. In particular, in the case where

$$\theta_n = \theta_c = \theta, \quad \theta \in (0, |\mathcal{I}|], \tag{2.40}$$

since k is defined via (2.37), for the condition $B(h,x) > 0$ to hold for all $x \in \mathcal{I}$ it suffices that

$$\beta_n < \frac{1}{|\mathcal{I}|}\min_{h\theta}\left\{-\frac{\sin(h\theta)}{h}\left(\frac{\rho^*_{n2}\mu_n + \rho^*_{c2}\mu_c}{h^2}\right)\right\}\min_{x\in\mathcal{I}}\Psi(x;\theta),$$

where $\mathcal{H} := \left\{h = \dfrac{m\pi}{|\mathcal{I}|},\, m \in \mathbb{N} : \sin(h\theta) < 0\right\}$. Since, under definition (2.7),

$$\min_{x\in\mathcal{I}}\Psi(x;\theta) = \frac{2}{\max\limits_{x\in\mathcal{I}}|\mathcal{L}_\theta(x)|} = \frac{1}{\theta},$$

the above condition on β_n reduces to

$$\beta_n < \frac{1}{|\mathcal{I}|} \min_{h\theta} \left\{ -\frac{\sin(h\theta)}{h\theta} \left(\frac{\rho^*_{n2}\mu_n + \rho^*_{c2}\mu_c}{h^2} \right) \right\}. \tag{2.41}$$

2.6 Numerical simulations

In this section, we report on computational results of the individual-based model along with numerical solutions of the corresponding continuum model given by the PDE-IDE system (2.13) and subject to the boundary conditions (2.14). Simulations are integrated with the results of steady-state and linear-stability analyses of the continuum model equations presented in Section 2.5. In particular, we investigate the way in which the outcomes of the models are affected by key parameters whose impact on the coevolutionary dynamics between tumour cells and CTLs is of particular biological interest. Such key parameters are: the TCR-tumour antigen binding affinity, γ, the level of selectivity of self-regulation mechanisms acting on CTLs, $1/\theta_c$, the level of selectivity of clonal competition amongst tumour cells, $1/\theta_n$, and the affinity range of TCRs, η. Moreover, we explore the existence of scenarios in which differences between the outcomes produced by the two models can emerge due to effects which reduce the quality of the approximation of the individual-based model provided by the continuum model.

2.6.1 Set-up of numerical simulations

Without loss of generality we choose $L = 1$, so that $\overline{\mathcal{I}} = [-1, 1]$ and $|\mathcal{I}| = 2$, and consider a discretisation of the interval $[-1, 1]$ consisting of 1500 points (*i.e.* the phenotype-step is $\chi \approx 0.0013$). Furthermore, we use the time-step $\tau = 0.05$ and, unless otherwise specified, we choose the final time $t_f = 30$ days.

Building on the results of steady-state and linear-stability analyses of the continuum model equations presented in Section 2.5, we carry out simulations using the following initial condition for the individual-based model

$$n^0(x_i) := 10^4(1 + a\,\cos(A\,x_i)), \qquad c^0(y_j) := 10^4(2 + a\,\cos(A\,y_j)), \quad a \geqslant 0,\ A > 0. \tag{2.42}$$

In Appendix B.2, we provide a detailed description of the methods employed to numerically solve the PDE-IDE system (2.13) complemented with the boundary conditions (2.14) and the continuum analogue of the initial condition (2.42), *i.e.* the initial condition

$$n^0(x) := 10^4(1 + a\,\cos(A\,x)), \qquad c^0(y) := 10^4(2 + a\,\cos(A\,y)), \quad a \geqslant 0,\ A > 0. \tag{2.43}$$

Unless otherwise specified, we use the parameter values listed in Table 2.1. Here, the values of the parameters α_n, α_c, ζ_n and ζ_c are consistent with previous measurement and estimation studies on the dynamics of tumour cells and CTLs [43, 176, 123, 184]. The values of the parameters μ_n and μ_c and the range of values of the parameters θ_n and θ_c are chosen so as to ensure that the equilibrium sizes and phenotype distributions of the two cell populations in isolation are biologically relevant. The range of values of the parameter η is consistent with experimental estimations of the precursor frequency of CTLs [19], while the values of the parameter γ are consistent with those used in [198, 199]. The value of the parameter λ_n is taken from [194] and corresponds to values of β_n that are consistent with experimental data reported in [56, 59].

Table 2.1: Parameter values used in numerical simulations and their sources

	Biological meaning	Value	Source
α_n	Rate of tumour cell proliferation	1.5/day	[43]
α_c	Rate of antigen-independent CTL proliferation	5×10^{-2}/day	[176]
μ_n	Rate of death of tumour cells due to clonal competition	$1.5 \times 10^{-6} \mu l$/day	*ad hoc*
μ_c	Rate of death of CTLs due to self-regulation mechanisms	$5 \times 10^{-6} \mu l$/day	*ad hoc*
ζ_n	Killing rate of tumour cells by CTLs	$5 \times 10^{-6} \mu l$/day	[123]
ζ_c	Rate of replication of CTLs following recognition	$3 \times 10^{-5} \mu l$/day	[184]
η	Affinity range of TCRs	[0.1, 2]	[19]
θ_n	Level of selectivity of clonal competition amongst tumour cells	[0.1, 2]	*ad hoc*
θ_c	Level of selectivity of self-regulation mechanisms of CTLs	[0.1, 2]	*ad hoc*
γ	TCR-tumour antigen binding affinity	[0.1, 3.5]	[198, 199]
λ_n	Probability of phenotypic variation of tumour cells	0.01	[194]

2.6.2 Main results

Eradication of tumour cells When γ is high enough so that condition (2.34) is satisfied (*i.e.* condition (2.24) does not hold), after initial growth, the total number of tumour cells decreases steadily over time until the tumour cell population is completely eradicated (*cf.* Figure 2.3**a**). This is due to the fact that, in response to a rapid growth in the size of the tumour cell population, the high TCR-tumour antigen binding affinity allows the population of CTLs to embark on rapid expansion in size that continues until CTLs have reached the critical mass required to push the population of tumour cells towards extinction. The expansion of the CTL population is followed by the transition to a contraction phase, which is characterised by a decline of the total number of CTLs to a level corresponding to the maintenance of a form of immunological memory. Moreover, the plots in Figure 2.3**a** demonstrate that there is a good agreement between numerical simulations of the individual-based and continuum models and, coherently with the analytical results presented in Section 2.5.2, the total numbers of tumour cells and CTLs converge to the steady-state values given by (2.23).

Hot tumour-like scenarios When γ satisfies condition (2.24) but is still sufficiently high, the total number of CTLs attains a value large enough to keep the total number of tumour cells steadily low. After initial growth, the total number of tumour cells decreases over time until it stabilises itself around a relatively small value (*cf.* Figure 2.3**b**). As a result, the average value of the immune score $\overline{I}$ defined via (2.3) and (2.4) is one order of magnitude larger than 1 (*i.e.* for the parameter values considered here $\overline{I} \approx 12.7$). In the framework of our model, this corresponds to the emergence of *hot tumour-like scenarios*.

Altered tumour-like scenarios For intermediate values of γ that satisfy condition (2.24), after initial growth, a certain number of tumour cells and a slightly larger number of CTLs stably coexist (*cf.* Figure 2.3**c**). In this case, the average value of the immune score $\overline{I}$ defined via (2.3) and (2.4) is just slightly larger than 1 (*i.e.* for the parameter values considered here $\overline{I} \approx 1.6$). In the framework of our model, this corresponds to the emergence of *altered tumour-like scenarios*.

Cold tumour-like scenarios For sufficiently small values of γ that satisfy condition (2.24), in the early stage of cell dynamics the total number of tumour cells overtakes the total number of CTLs, and keeps expanding until saturation (*cf.* Figure 2.3**d**). Accordingly, the average value of the immune score $\overline{I}$ defined via (2.3) and (2.4) is smaller than 1 (*i.e.* for the parameter values considered here $\overline{I} \approx 0.7$), which corresponds to the emergence of *cold tumour-like scenarios* in the framework of our model.

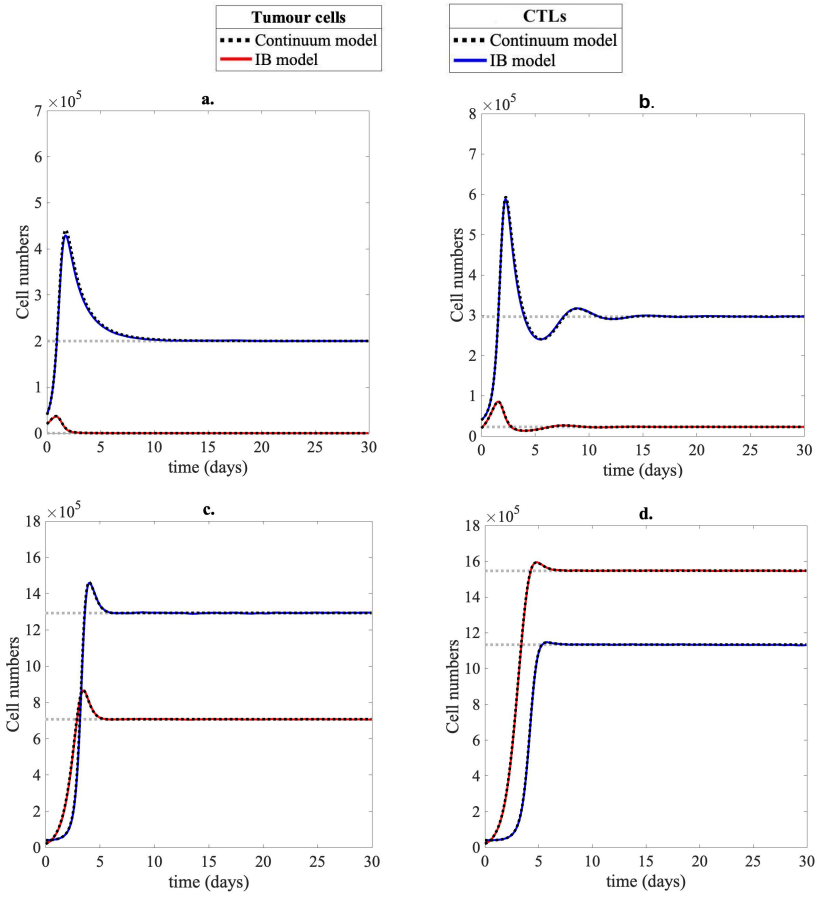

Figure 2.3: **Eradication of tumour cells and emergence of hot tumour-like, altered tumour-like and cold tumour-like scenarios.** Panel **a.** displays the plots of the time evolution of the total number of tumour cells (ρ_n) and CTLs (ρ_c) of the individual-based model (solid, coloured lines) and the continuum model (dashed, black lines) when γ is high enough that condition (2.34) is satisfied (*i.e.* condition (2.24) does not hold). Here, $\alpha_c = 0.5$/day and all the other parameters are as in Table 2.1 with $\gamma = 3.5$, $\eta = 1.8$ and $\theta_n = \theta_c = 1.8$. The grey dotted lines highlight the steady-state values of ρ_n and ρ_c given by (2.23). Panels **b.-d.** display similar plots for sufficiently large, intermediate and sufficiently small values of γ that satisfy condition (2.24) – *i.e.* $\gamma = 2$ (panel **b.**), $\gamma = 0.3$ (panel **c.**) and $\gamma = 0.12$ (panel **d.**). All the other parameters are as in Table 2.1 with $\eta = 1.8$ and $\theta_n = \theta_c = 1.8$. The grey dotted lines highlight the steady-state values of ρ_n and ρ_n given by (2.25). Initial conditions (2.42) and (2.43) with $a = 0$ were used to carry out numerical simulations. Analogous results hold when $a > 0$ in (2.42) and (2.43) (*cf.* Figure B.1 in Appendix B.3). The results from the individual-based model correspond to the average over two realisations of the underlying random walk and the related variance is displayed by the coloured areas surrounding the curves.

Robustness of numerical results The plots in Figure 2.3 demonstrate that there is an excellent quantitative agreement between the results of numerical simulations of the individual-based

model and numerical solutions of the corresponding continuum model. Moreover, consistently with the results of linear stability analysis of the continuum model presented in Section 2.5.2, these numerical results show that the total numbers of tumour cells and CTLs converge either to the steady-state values given by (2.23) (*cf.* Figure 2.3**a**), or the steady-state values given by (2.25) (*cf.* Figure 2.3**b-d**), depending on the fact that the choices of the model parameters are such that condition (2.34) or condition (2.24) holds, respectively. When convergence to the steady state $(\rho^*_{n2}, \rho^*_{c2})$ given by (2.25) occurs, in the long run, the value of the average immune score $\overline{I}$ defined via (2.4) reflects the value of the ratio ρ^*_{c2}/ρ^*_{n2}. Therefore, in the framework of our tumour classification based on the average immune score $\overline{I}$ (see page 5), if condition (2.24) is met: cold tumour-like scenarios and hot tumour-like scenarios will emerge when the values of the model parameters are such that the ratio ρ^*_{T2}/ρ^*_{C2} is smaller than 1 or at least about one order of magnitude larger than 1, respectively, whereas altered tumour-like scenarios will emerge in the remaining cases. This has been confirmed by the results of additional numerical simulations (results not shown). Hence, independently of the specific values of the model parameters, provided that assumption (2.24) is satisfied, cell dynamics qualitatively similar to those of Figure 2.3, and corresponding to hot, altered or cold tumour scenarios, will be observed depending on the value of the ratio ρ^*_{c2}/ρ^*_{n2}. This testifies to the robustness of the numerical results presented here.

Patterns of phenotypic coevolution between tumour cells and CTLs: impact of the parameters θ_n and θ_c Figure 2.4 displays the plots of the phenotype distributions of tumour cells (top panel) and CTLs (central panel) at the end of numerical simulations (*i.e.* close to numerical equilibrium) alongside the plots of the corresponding time evolution of the total cell numbers (bottom panel). In agreement with the analytical results presented in Section 2.5.2, when condition (2.24) is satisfied and conditions (2.40) and (2.41) are met as well, patterns of phenotypic coevolution between tumour cells and CTLs may emerge. Moreover, the top and central panels of Figure 2.4 show that, coherently with the shape of the function $B(h)$ defined via (2.39) (*cf.* the plots in Figure 2.5), smaller values of θ_n and θ_c correlate with the formation of more peaks in the phenotype distributions of the two cell populations. The plots in Figure 2.4 also demonstrate that there is a good agreement between numerical simulations of the individual-based and continuum models.

Sample temporal dynamics of such patterns are summarised by the plots in Figure 2.6, which show that clonal expansion leads to a rapid proliferation of CTLs that are targeted to the antigens mostly expressed by tumour cells, whereas self-regulation mechanisms induce formerly stimulated CTLs to decay. In turn, the antigen-specific cytotoxic action of CTLs causes the selection of those tumour cells that are able to escape immune recognition. As a result, immune competition induces the formation of multiple peaks in the phenotype distribution of tumour cells. This concurrently shapes the phenotype distribution of CTLs with a time shift corresponding to the time required for the CTLs to adapt to the antigenic distribution of tumour cells. The plots in Figure 2.6 demonstrate that there is again a good agreement between numerical simulations of the individual-based and continuum models.

Patterns of phenotypic coevolution between tumour cells and CTLs: impact of the parameter η The results of numerical simulations summarised by the plots in Figure 2.7 extend the analytical results presented in Section 2.5.2 by showing that, when condition (2.24) is satisfied and η is sufficiently small, smaller values of η may induce the formation of patterns of phenotypic coevolution between tumour cells and CTLs whereby less regular multi-peaked phenotype distributions of the two cell populations emerge (*cf.* top and central panels of Figure 2.7). The temporal dynamics of such patterns are qualitatively similar to those presented in Figure 2.6 (results not shown). Moreover, numerical simulations indicate that smaller val-

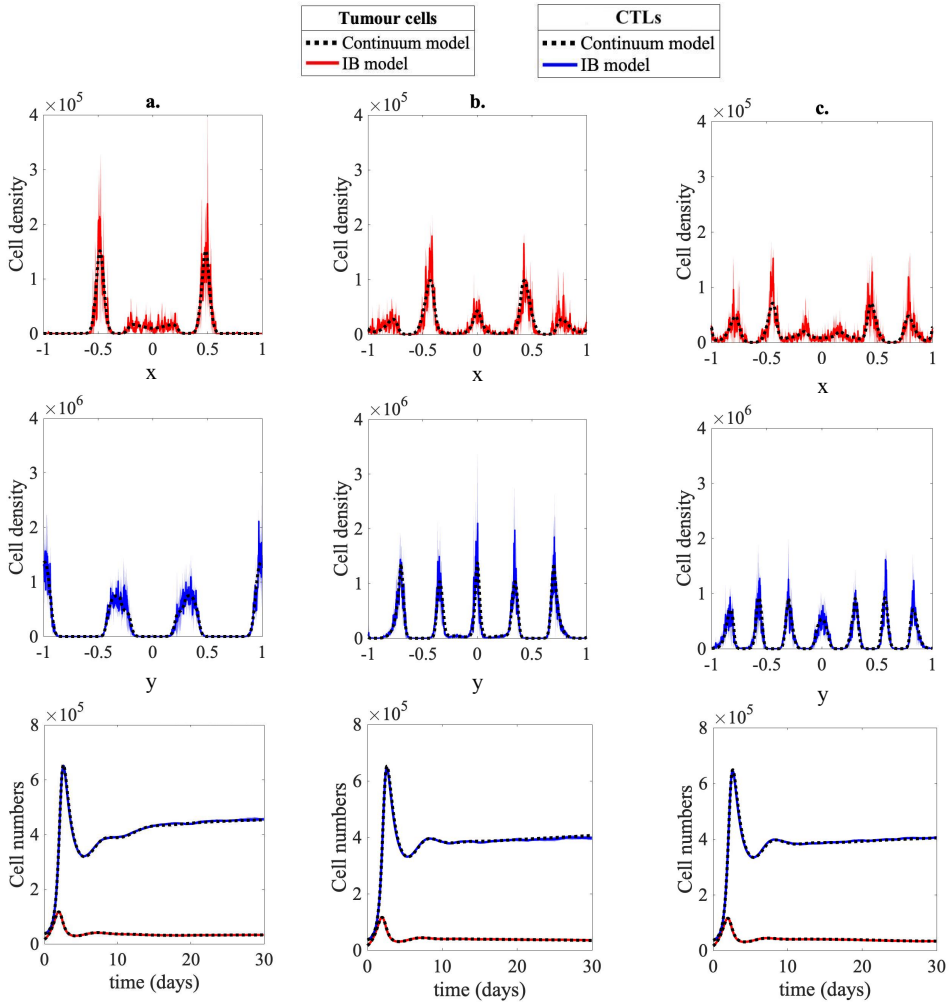

Figure 2.4: **Patterns of phenotypic coevolution between tumour cells and CTLs: impact of the parameters θ_n and θ_c.** Top panels display the plots of the population density function of tumour cells (n) and central panels display the plots of the population density function of CTLs (c) of the individual-based model (solid, coloured lines) and continuum model (dashed, black lines) at the end of numerical simulations (*i.e.* at $t = 30$) when conditions (2.24) and (2.41) are satisfied and progressively smaller values of θ_n and θ_c are considered – *i.e.* $\theta_n = \theta_c = 0.5$ (panels **a.**), $\theta_n = \theta_c = 0.3$ (panels **b.**) and $\theta_n = \theta_c = 0.2$ (panels **c.**). All the other parameters are as in Table 2.1 with $\gamma = 1.5$ and $\eta = 0.7$. Bottom panels display the corresponding plots of the time evolution of the total number of tumour cells (ρ_n) and CTLs (ρ_c). Initial conditions (2.42) and (2.43) with $a = 1$ and $A = 5$ were used to carry out numerical simulations. Analogous results were obtained when using different values of the parameter A (results not shown). The results from the individual-based model correspond to the average over two realisations of the underlying random walk and the related variance is displayed by the coloured areas surrounding the curves.

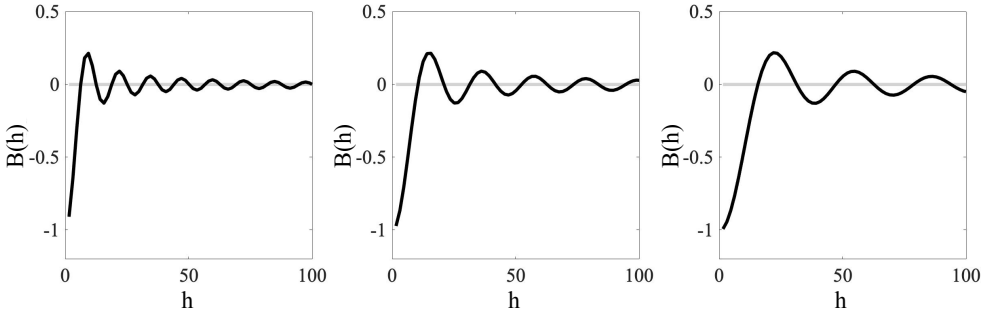

Figure 2.5: **Plots of $B(h,x)$ for different values of θ_n and θ_c.** Plots of the function $B(h)$ defined via (2.39) for the parameter values used in Figure 2.4 – *i.e.* $\theta_n = \theta_c = 0.5$ (left panel), $\theta_n = \theta_c = 0.3$ (central panel) and $\theta_n = \theta_c = 0.2$ (right panel).

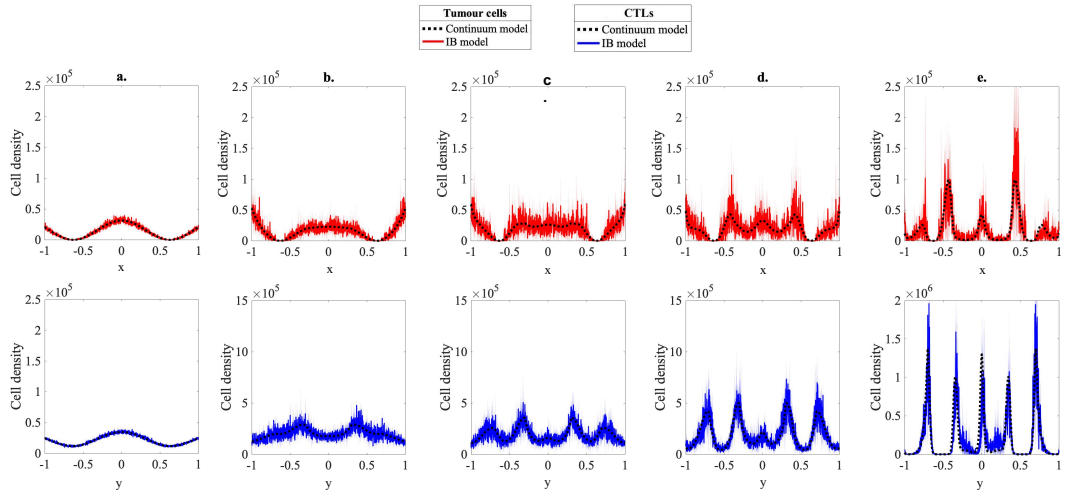

Figure 2.6: **Sample temporal dynamics of patterns of phenotypic coevolution between tumour cells and CTLs.** Top panels display the plots of the population density function of tumour cells (n) and bottom panels display the plots of the population density function of CTLs (c) of the individual-based model (solid, coloured lines) and continuum model (dashed, black lines) at five successive time instants – *i.e.* $t = 0.4$ (panels **a.**), $t = 4$ (panels **b.**), $t = 10$ (panels **c.**), $t = 16$ (panels **d.**), $t = 30$ (panels **e.**) – in the case where condition (2.24) is satisfied. Here, $\theta_n = \theta_c = 0.3$, $\gamma = 1.5$ and $\eta = 0.7$, and all the other parameters are as in Table 2.1. Initial conditions (2.42) and (2.43) with $a = 1$ and $A = 5$ were used to carry out numerical simulations. Analogous results were obtained when using different values of the parameter A (results not shown). The results from the individual-based model correspond to the average over two realisations of the underlying random walk and the related variance is displayed by the coloured areas surrounding the curves.

ues of η correlate with the emergence of oscillations in the total numbers of tumour cells and CTLs, that is, CTLs undergo a succession of expansion and contraction phases that result in

an alternate decay and growth of tumour cells (*cf.* bottom panel in Figure 2.7c). The plots in Figure 2.7 demonstrate that there is a good agreement between numerical simulations of the individual-based and continuum models.

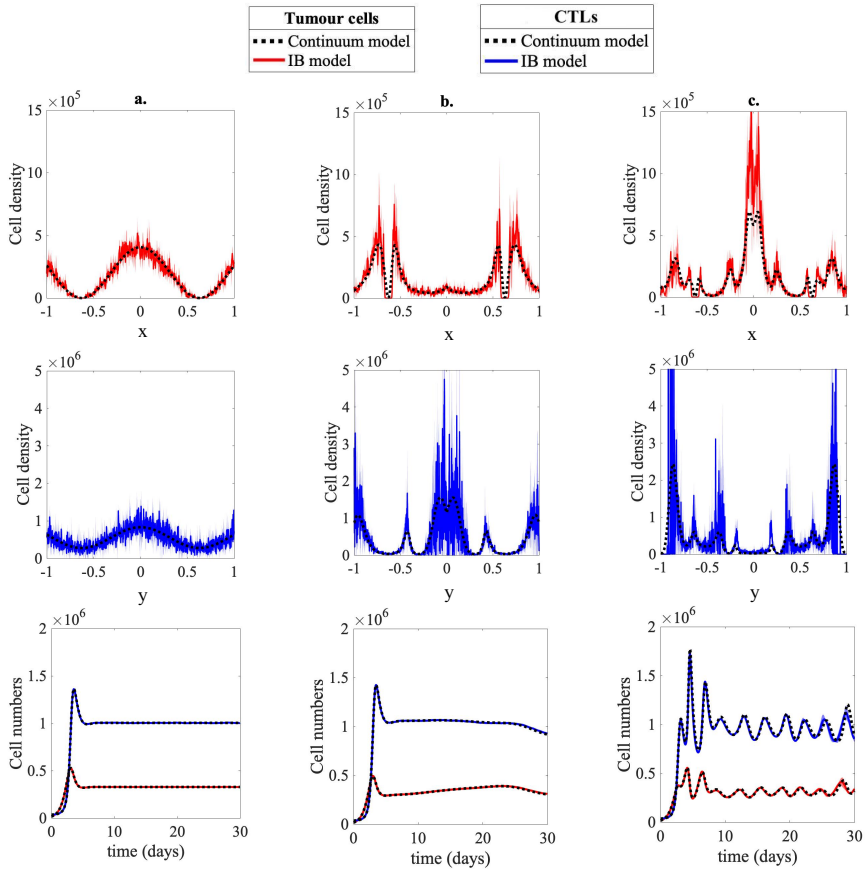

Figure 2.7: **Patterns of phenotypic coevolution between tumour cells and CTLs: impact of the parameter η.** Top panels display the plots of the population density function of tumour cells (n) and bottom panels display the plots of the population density function of CTLs (c) of the individual-based model (solid, coloured lines) and continuum model (dashed, black lines) at the end of numerical simulations (*i.e.* at $t = 30$) when condition (2.24) is satisfied and progressively smaller values of η are considered – *i.e.* $\eta = 1$ (panels **a.**), $\eta = 0.6$ (panels **b.**) and $\eta = 0.2$ (panels **c.**). All the other parameters are as in Table 2.1 with $\gamma = 1$ and $\theta_n = \theta_c = 0.7$. Bottom panels display the corresponding plots of the time evolution of the total number of tumour cells (ρ_n) and CTLs (ρ_c). Initial conditions (2.42) and (2.43) with $a = 1$ and $A = 5$ were used to carry out numerical simulations. Analogous results were obtained when using different values of the parameter A (results not shown). The results from the individual-based model correspond to the average over five realisations of the underlying random walk and the related variance is displayed by the coloured areas surrounding the curves.

Possible discrepancies between individual-based and continuum models The results that have been presented so far indicate that there is a good agreement between the results

of computational simulations of the individual-based model and the numerical solutions of the corresponding continuum model. However, we expect possible differences between the outcomes of the two models to emerge in the presence of lower tumour cell numbers, which may lead to more pronounced demographic stochasticity, and less regular multi-peaked cell phenotype distributions, which may cause a reduction in the quality of the approximations employed in the formal derivation of the deterministic continuum model from the individual-based model. In order to investigate this, we carried out numerical simulations of the two models for choices of parameter values such that condition (2.24) holds, evolution towards relatively small tumour cell numbers occurs, and less regular cell phenotype distributions with multiple peaks emerge. The results obtained are summarised by the plots in Figure 2.8, which show that the individual-based model predicts eradication of the tumour cell population, whereas the continuum model predicts coexistence between tumour cells and CTLs.

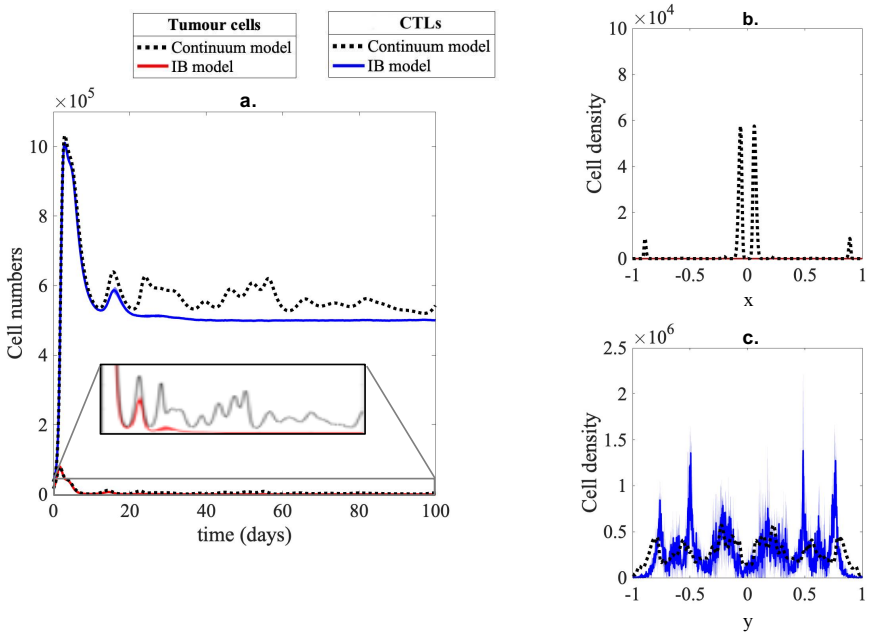

Figure 2.8: **Possible discrepancies between individual-based and continuum models.** Panel **a.** displays the plot of the time evolution of the total number of tumour cells (ρ_n) and CTLs (ρ_c) of the individual-based model (solid, coloured lines) and the continuum model (dashed, black lines) when condition (2.24) holds, evolution towards relatively small tumour cell numbers occurs, and the parameter η is sufficiently small so that less regular multi-peaked cell phenotype distributions emerge – *i.e.* $\alpha_c = 0.5/\text{day}$, $\mu_c = 2 \times 10^{-6} \mu l/\text{day}$, $\gamma = 1.1$, $\eta = 0.1$, and all the other parameters as in Table 2.1 with $\theta_n = \theta_c = 1.8$. The plots in panels **b.** and **c.** display the corresponding population density functions of tumour cells (n) and CTLs (c) of the individual-based model (solid, coloured lines) and of the continuum model (dashed, black lines) at the end of simulations (*i.e.* at $t = t_f = 100$). Initial conditions (2.42) and (2.43) with $a = 1$ and $A = 5$ were used to carry out numerical simulations. Analogous results were obtained when using different values of the parameter A (results not shown). The results from the individual-based model correspond to the average over five realisations of the underlying random walk and the related variance is displayed by the coloured areas surrounding the curves.

2.7 Discussion, conclusions and research perspectives

Discussion and conclusions We developed an individual-based model for the coevolutionary dynamics between tumour cells and CD8+ cytotoxic T lymphocytes that takes into account the selectivity of antigen-specific immunity. We formally derived the deterministic continuum counterpart of such an individual-based model, and we integrated the results of numerical simulations of the two models with the results of steady-state and linear-stability analyses of the continuum model equations.

The results presented in this study shed light on the way in which different parameters shape the coevolutionary dynamics between tumour cells and CD8+ cytotoxic T lymphocytes. In particular, we demonstrated that, *ceteris paribus*, higher values of the TCR-tumour antigen binding affinity (i.e. the parameter γ in the model) promote the eradication of tumour cells by CTLs, while lower values facilitate the coexistence between tumour cells and CTLs. Specifically, progressively reducing the TCR-tumour antigen binding affinity brings about the emergence of: *hot tumour-like scenarios*, which are characterised by a large number of *in situ* CTLs and a low number of tumour cells, and thus represent a more fertile ground for anticancer therapeutic intervention; *altered tumour-like scenarios*, which reflect the intrinsic ability of the immune system to effectively mount a CTL-mediated immune response and the ability of tumour cells to partially escape such a response; *cold tumour-like scenarios*, which are characterised by an insufficient number of *in situ* CTLs and are invariably associated with poor prognosis [70]. This classification of tumours is also supported by experimental works showing that *in situ* immune reaction might be the strongest parameter influencing clinical outcome, regardless of the local tumour extension and its spread to lymph nodes [164, 72, 71]. Moreover, our findings support the idea that TCR-tumour antigen binding affinity may be a good intervention target for immunotherapy that aims to turn cold or altered tumours into hot ones by enhancing CTL response. In this regard, our findings are in agreement with the conclusions of previous experimental articles indicating that a strong binding affinity of T cells to tumour antigens may play a key role in the overall immune response to the disease [83].In particular, in altered tumours, increasing antigenicity, via the removal of co-inhibitory signals and/or the supply of co-stimulatory signals [71, 220], may enhance *in situ* CTLs activity, and has proven to be effective in the treatment of advanced-stage melanoma [222], renal cell carcinoma [156] and non-small cell lung cancer [98]. In cold tumours, a proposed approach to overcome the lack of a pre-existing immune response consists in combining a priming therapy that boosts CTL responses with the removal of co-inhibitory signals through approaches such as immune checkpoint [70]. The therapeutic success achieved by combining immune checkpoint therapy with chemotherapy in metastatic NSCLC has demonstrated the potential strength of this dual approach [74].

Moreover, the results presented here indicate that the affinity range of TCRs (i.e. the parameter η in the model), the selectivity of clonal competition amongst tumour cells (i.e. the inverse of the parameter θ_C in the model) and the selectivity of self-regulation mechanisms acting on CD8+ cytotoxic T lymphocytes (i.e. the inverse of the parameter θ_T in the model) play a pivotal role in the formation of patterns of phenotypic coevolution, which create the substrate for the emergence of less regular cell phenotype distributions with multiple peaks. Such patterns are underpinned by some form of immunoediting whereby the population of CTLs evolves and continuously adapts its receptor repertoire in order to recognise and effectively eliminate tumour cells and, in turn, the antigen-specific selective pressure exerted by CTLs leads to the selection of those tumour clones that are able to evade immune recognition [60]. The adaptability of tumour cells and CTLs and the selective pressure they mutually exert on each other during cancer development are emerging as crucial factors in determining cancer evolutionary trajectories. This has been shown in the context of chronic lymphocytic leukemia [177] and other cancer types,

as reviewed in [82]. Our results offer also a theoretical basis for the development of anti-cancer therapy aiming at engineering TCRs so as to shape their affinity for cancer targets [23, 47, 129, 229] and adaptive therapy aiming at altering intratumour clonal competition [79, 218], in order to control the coevolutionary dynamics between tumour cells and CD8+ cytotoxic T lymphocytes. In this respect, one of the best known treatment based on engineering specific TCRs is based on CAR-T cells [216], which confer CTLs the ability to target specific antigens. It has been demonstrated that this therapeutic strategy has several potential advantages over conventional therapies, including specificity, rapidity, high success rate and long-lasting effects [111, 86].

The good agreement between the results of numerical simulations of the individual-based and continuum models, along with the quantitative information given by (2.23) and (2.25) and the precise conditions given by (2.34) and (2.41), testifies to the robustness of the biological insight gained in this work. We also showed that possible differences between cell dynamics produced by the individual-based and continuum models can emerge under parameter settings that correspond to less regular cell phenotype distributions and more pronounced demographic stochasticity. In fact, these cause a reduction in the quality of the approximations employed in the formal derivation of the deterministic continuum model from the individual-based model (cf. Appendix B.1). This demonstrates the importance of integrating individual-based and continuum approaches when considering mathematical models for tumour-immune competition.

Research perspectives From a mathematical point of view, we plan to carry out a systematic investigation of the conditions on the affinity range of TCRs that may lead to the emergence of oscillations in cell numbers observed in the numerical simulations presented in this work. Moreover, from a modelling point of view, our individual-based modelling framework for the coevolutionary dynamics between tumour cells and CD8+ cytotoxic T lymphocytes, along with the formal derivation of the corresponding continuum model, can be developed further in several ways. For instance, a myriad of immunosuppressive strategies, the so-called immune checkpoints, help tumour cells acquiring features that enable them to evade immune detection, which may ultimately induce the exhaustion of CTLs in the tumour micro-environment, which impairs the immune response. The modelling approach presented here does not capture this aspect. However, exhaustion mechanisms could be incorporated into the individual-based model by, for example, allowing CTLs to enter a suppressed state (i.e. CTLs would become exhausted and thus would no longer able to eliminate tumour cells). In the continuum model, this would result in the presence of an additional loss term in the IDE $(2.13)_2$ along with a third equation for the dynamics of exhausted CTLs. Another track to follow to further enrich our model would be to include a spatial structure, for instance by embedding the tumour cells in the geometry of a solid tumour, and to take explicitly into account the effect of both spatial and antigen-specific interactions between tumour cells and CTLs, as similarly done in [113, 140, 139]. Including a spatial structure would make it possible, *inter alia*, to introduce a more precise definition of the immune score that incorporates the level of CTL infiltration. Furthermore, at this stage, the mathematical representation of the phenotypic state of tumour cells and CTLs employed in our modelling framework is rather abstract. This might make it difficult to carry out precise quantitative comparisons between the results of numerical simulations and experimental data. This limitation could be overcome by employing a mathematical representation of tumour antigens and TCRs similar to the one that we proposed in [127], whereby a discrete set of tumour antigens that can be recognised by a unique repertoire of TCRs is considered. Finally, it would be interesting to incorporate explicitly into the model the effects of immunotherapeutic agents or other therapeutic agents. These are all lines of research that we will be pursuing in the future.

Chapter 3

A mathematical model to study the impact of intra-tumour heterogeneity on anti-tumour T cell immune response

3.1 Motivation

In the previous chapter we have developed a discrete model, and formally derived its continuum counterparts, of tumour-immune competition to describe the interactions between cytotoxic T lymphocytes (CTLs) and tumour cells. In the model, we considered that tumour cells and CTLs were structured by a variable representing a parameterisation of the antigen expression profiles and a parameterisation of the target antigens of T-cell receptors.

For the sake of simplicity, in this first work we did not consider spatial aspects of tumour-immune interaction dynamics. Moreover, we considered that the tumour cell population was characterized by the same antigen expression profile, which could eventually be recognized by every CTL. However, solid tumours can be characterized by different antigen profiles and different levels of antigen presentation by the major histocompatibility complex 1 (MHC-I), possibly preventing their recognition by CTLs. These aspects, as well as spatial dynamics between tumour cells and CTLs (such as cell spatial growth and movement, spatial heterogeneity within the tumour), can affect the efficacy of immune action and the outcomes of immune response. In particular, intra-tumour heterogeneity (ITH) has a strong impact on the efficacy of the immune response against solid tumours. The number of sub-populations of cancer cells expressing different antigens and the percentage of immunogenic cells (*i.e.* tumour cells that are effectively targeted by immune cells) in a tumour are both expressions of ITH.

In this chapter, we aim to capture these two expressions of ITH using mathematical modelling techniques. As mentioned in Section 1.3.1, stochastic discrete models, such as individual-based models, are appropriate modelling approaches for addressing the role of diversity in cell populations and also within each individual cell. Therefore, we develop a spatially explicit stochastic individual-based model of the interaction dynamics between tumour cells and CTLs, which makes it possible to dissect out the specific impact of these two expressions of ITH on anti-tumour immune response.

The originality of this model lies in the characterisation of antigen presentation levels by tumour cells, which drive the influx of CTLs in the tumour micro-environment and their movement towards tumour cells. As explained in 1.2.2, by 'level of antigen presentation' we refer to different mechanisms that may affect the recognition of antigens by antigen presenting cells, the activation of CTLs, and the efficacy of immune action. The characterization of antigen presentation levels allows us to include different level of immunogenicity in the tumour and to consider two different subtypes of tumour cells, that is: immunogenic cells (*i.e.* tumour cells that are effectively targeted by CTLs) and non-immunogenic cells (*i.e.* tumour cells that are poorly targeted by CTLs). In our model, the effectiveness of the anti-tumour immune response is directly linked to the level of presentation of tumour antigens.

The set-up of numerical simulations of the model is defined so as to mimic scenarios considered in previous experimental studies. Moreover, the ability of the model to qualitatively reproduce experimental observations of successful and unsuccessful immune surveillance is demonstrated. First, the results of numerical simulations of this model indicate that the presence of a larger number of sub-populations of tumour cells that express different antigens is associated with a reduced ability of CTLs to mount an effective anti-tumour immune response. Secondly, the presence of a larger percentage of tumour cells that are not effectively targeted by CTLs may reduce the effectiveness of anti-tumour immunity. Ultimately, the mathematical model presented in this chapter may provide a framework to help biologists and clinicians to better understand the mechanisms that are responsible for the emergence of different outcomes of immunotherapy.

This study is a joint work in collaboration with:

- Shensi Shen, Institute of Thoracic Oncology, West China Hospital, Sichuan University, Chengdu, China.

The model described in this chapter and the results shown have been published in E. L., Tommaso Lorenzi, Shensi Shen, Luis Almeida, Chloe Audebert, *A mathematical model to study the impact of intra-tumour heterogeneity on anti-tumour CD8+ T cell immune response*, Journal of Theoretical Biology, 2022.

3.2 Background

3.2.1 Biological background

Cytotoxic T lymphocytes (CTLs) are capable of detecting and eliminating tumour cells by recognising cancer-associated antigens expressed by tumour cells. The effectiveness of the immune response depends on the level of presentation of such antigens by the major histocompatibility complex 1 (MHC-I) [45, 151]. In particular, CTLs express T cell receptors (TCRs) and, once activated, they migrate via chemotaxis in response to concentration gradients of chemical signals towards the tumour cells expressing the matching antigens [153]. The influx and movement of CTLs are dictated by the spatial distribution of tumour antigens and by the level of chemokines in the tumour micro-environment [20]. Upon intratumoural infiltration, CTLs can trigger tumour cell death by direct interaction with tumour cells, releasing cytotoxic factors (*i.e.* granzime B, interferon gamma) [117].

Oncogenic mutation-driven cancers harbor neoantigens that can be recognized by CTL receptors [93]. A high mutational burden and neoantigen load in tumours have been associated with an enhanced response to immunotherapy [36, 84, 97, 182, 190, 211]. However, it has recently been reported that many of these neoantigens arise from sub-clonal branching mutations and could potentially increase intratumour heterogeneity (ITH) [149, 150, 180]. These tumours are characterised by clonal antigens (presented by all tumour cells), and sub-clonal antigens (presented only

by sub-populations of tumour cells). Moreover, such sub-clonal antigens may be associated with decreased level of antigen presentation by the MHC-I, leading to a weaker antigen-specific CTL response [80]. In contrast, more homogeneous tumours express few clonal antigens in all tumour cells and appear to have a better response to immunotherapy across a wide range of tumour types [65, 150]. Furthermore, CTLs activated against clonal antigens are more commonly found at the tumour site than CTLs reactive to sub-clonal antigens [150]. These findings suggest that ITH may strongly affect the effectiveness of the anti-tumour immune response.

3.2.2 The mathematical model

In light of these considerations, we present a spatial stochastic individual-based model of tumour-immune interaction dynamics that can be used to explore the effect of ITH on immune surveillance. There is a variety of individual-based model approaches (*e.g.*, cellular automata, Cellular Potts models, hybrid discrete/continuous models). In our study, we used a Cellular Potts model and the CompuCell3D open-source simulation environment [107]. The originality of this model lies in the characterisation of antigen presentation levels by tumour cells, which drive the influx of CTLs in the tumour micro-environment and their movement towards tumour cells. In our model, the effectiveness of the anti-tumour immune response is directly linked to the level of presentation of tumour antigens. In addition, the model takes into account biological phenomena that are driven by stochastic aspects of the interaction dynamics between tumour cells and CTLs.

The effect of ITH on immune surveillance is investigated at two different levels through computational simulations of this model. First, we explore the outcomes of the immune response considering different number of sub-populations of cancer cells constituting the tumour. Then, we asses the efficiency of the immune response by varying the immunogenicity of tumour cells. We study the impact of these two characteristics on tumour progression independently and together, assessing their influence on anti-tumour immunity in a controlled manner.

3.2.3 Structure of the chapter

The chapter is organised as follows. In Section 3.3, we present the individual-based model and the mathematical description of each biological process included in the model. Section 3.4 summarises the set-up of computational simulations and presents some preliminary results of computational simulations. Full details of model implementation and model parametrisation are provided in Appendix A and Appendix C.1, respectively. In Section 2.6.2 we present the main computational results and we discuss them in view of previous biological works. Finally, Section 3.6 concludes the chapter and provides a brief overview of possible research perspectives.

3.3 Model and methods

We consider two cell types in our model: tumour cells, characterised by an antigen profile and a level of antigen presentation, and antigen-specific CTLs. To describe the interactions occurring between the two cell types we use an on-lattice individual-based model posed on a 2D spatial domain partitioned into square elements of side Δx. In our model, this domain biologically represents the tumour micro-environment. At each time step of length Δt, the states of the cells are updated according to the probabilistic and deterministic rules described below.

In the remainder of this section, we first present the modelling framework in a general setting, along with the underlying biological hypotheses and assumptions. Then, we detail how

each biological mechanism is mathematically described. A detailed description of the computational implementation of the model, which relies on a Cellular Potts approach, can be found in Appendix A.

3.3.1 Modelling framework

To include different level of immunogenicity in the tumour, two different subtypes of tumour cells are considered: immunogenic cells (*i.e.* tumour cells that are effectively targeted by CTLs) and non-immunogenic cells (*i.e.* tumour cells that are poorly targeted by CTLs). On the one hand, we define immunogenic cells as cells expressing one or more clonal antigens, considered as immunodominant, and presented at a normal level by the MHC-I. On the other hand, we assume that non-immunogenic cells have experienced, through mutations, a deterioration of their level of antigen presentation, and have acquired new antigens. These new antigens are presented only by a subset of tumour cells, and will be denoted as sub-clonal antigens [150]. Therefore, we define non-immunogenic cells as cells expressing clonal and sub-clonal antigens, both presented at a low level by the MHC-I. The system is initially composed of tumour cells only, which grow and proliferate through mitosis. Tumour cells secrete different chemoattractants that trigger the influx of specific CTLs into the domain. When they arrive in the domain, CTLs move via chemotaxis towards tumour cells expressing the matching antigens and, upon contact, try to eliminate them.

The modelling strategies used to reproduce these dynamics are described in detail in the following subsections, and are also schematically illustrated with an example in Figure 3.1 and Figure 3.2.

Dynamics of tumour cells

Antigen expression We let $N_T(t)$ denote the number of tumour cells in the system at time $t = h\Delta t$, with $h \in \mathbb{N}_0$, and we label each cell by an index $n = 1, \dots, N_T(t)$. We let each tumour cell express one or more antigens, and we characterise the antigen profile of the tumour by means of a vector

$$A = (a_1, \dots, a_f), \quad a_1, \dots, a_f \in \mathbb{N}, \tag{3.1}$$

where a_i denotes an antigen and f is the total number of antigens expressed by the tumour [see Figure 3.1**(a)**]. Using phylogenetic tree representations [see Figure 3.1**(b)-(c)**], we define each antigen $a_i \in A$, $i = 1, \dots, f$, of the tumour as clonal if it belongs to the trunk of the phylogenetic tree, or sub-clonal if it belongs to one of the branches of the phylogenetic tree. We let A_C and A_{SC} denote the sets of clonal and the sub-clonal antigens, whereby:

$$A_C, A_{SC} \subset A, \quad A_C \cup A_{SC} = A \quad \text{and} \quad A_C \cap A_{SC} = \emptyset. \tag{3.2}$$

Then, based on the phylogenetic tree representation, we divide the tumour in f different sub-populations of tumour cells labelled by the last antigen $a_i \in A$ acquired [see Figure 3.1**(d)**]. Following this notation, in this model, cells in the same sub-population express the same set of antigens [see Figure 3.1(a, b, d)]. Moreover, if $a_i \in A_C$, cells in the sub-population labelled by the antigen a_i express only clonal antigens, whereas if $a_i \in A_{SC}$, cells in the sub-population labelled by the antigen a_i express both clonal and sub-clonal antigens. Therefore, we define cells in sub-populations labelled by a clonal antigen $a_i \in A_C$ as immunogenic cells, whereas cells in sub-populations labelled by a sub-clonal antigen $a_i \in A_{SC}$ are defined as non-immunogenic cells.

Antigen presentation by MHC-I We incorporate antigen presentation into our model by letting each tumour cell present its antigens at a certain level. There can be high variability in each antigen's presentation between patients with the same type of tumour and even within tumour cell samples from the same patient [8, 150]. Therefore, for the n^{th} tumour cell, we characterise the level of presentation of each one of its antigens $a_i \in A$ by the normalized variable

$$l^n_{a_i} \in [0, 1] \tag{3.3}$$

whereby the value $l^n_{a_i} = 0$ corresponds to a tumour cell that lost the expression of the antigen a_i, while $l^n_{a_i} = 1$ corresponds to a tumour cell presenting the antigen a_i at the highest level.

To capture the idea that immunogenic cells present their antigens at a higher level than non-immunogenic cells, we introduce the discrete sets

$$L_I = \{\mathrm{m}_I, \ldots, \mathrm{M}_I\} \subset [0, 1] \text{ and } L_{NI} = \{\mathrm{m}_{NI}, \ldots, \mathrm{M}_{NI}\} \subset [0, 1], \text{ with } \mathrm{M}_{NI} < \mathrm{M}_I. \tag{3.4}$$

They characterise the range of different values that can be taken by the variable $l^n_{a_i}$ [see Figure 3.1**(d)**]. In particular, if the n^{th} tumour cell is an immunogenic cell, it presents each antigen a_i at a normal level $l^n_{a_i} \in L_I$, whereas if the n^{th} tumour cell is a non-immunogenic cell, all of its antigens a_i are presented at a low level $l^n_{a_i} \in L_{NI}$.

Tumour cell growth and division At each time-step, we let tumour cells grow at a random rate drawn from a uniform distribution; the parameters of the bounds of the uniform distribution are chosen to match the mean duration of a tumour cell cycle length. Mitosis occurs when a tumour cell grows to a critical size and then divides along a randomly orientated axis. Upon division at the time t, the n^{th} tumour cell is replaced by two cells [see Figure 3.1**(e)**], one labelled by the parent index n and the other one labelled by the index $N_T(t) + 1$. The daughter cell will inherit most of the properties of the parent cell, including the antigens expressed by the parent cell, so the fact that the cell is immunogenic or not [see Figure 3.1**(e)**]. For each antigen a_i expressed by the daughter cell, a random level of antigen presentation $l^{N_T(t)+1}_{a_i}$ will be chosen. This level of antigen presentation can then be different from the one of the parent cell. Another property not inherited by the daughter cell is the intrinsic lifespan of the cell, which is randomly drawn from a uniform distribution. In this model, we do not take into account the appearance of new antigens due to the occurrence of mutations.

Tumour cell death If a tumour cell exhausts its lifespan (which is drawn when the cell is created), it dies (*i.e.* it undergoes apoptosis) at the end of the time-step and it is removed from the domain. A tumour cell can also die due to intra-tumour competition, with a rate proportional to the total number of tumour cells, or because of the cytotoxic action of CTLs. More details about tumour cell death due to the cytotoxic action of CTLs will be given in Section 3.3.1.

Secretion of chemoattractants We let tumour cells at the border of the tumour (the region where cytokines and immune cells are more abundant [20]) secrete different chemoattractants for each expressed antigen $a_i \in A$. The secretion of a chemoattractant by a tumour cell expressing antigen a_i is proportional to the level of presentation of such antigen a_i. Therefore, we model the chemoattractant secretion rate $s^n_{a_i}$ by the n^{th} tumour cell expressing antigen a_i using the following definition:

$$s^n_{a_i} := C_1\, l^n_{a_i}, \tag{3.5}$$

where $C_1 \in \mathbb{R}^+$ is a scaling factor of units $\frac{[mol]}{[time]\,[space]}$, where $[mol]$, $[time]$ and $[space]$ denote respectively the number of chemoattractant molecules and the units of time and of the size of a

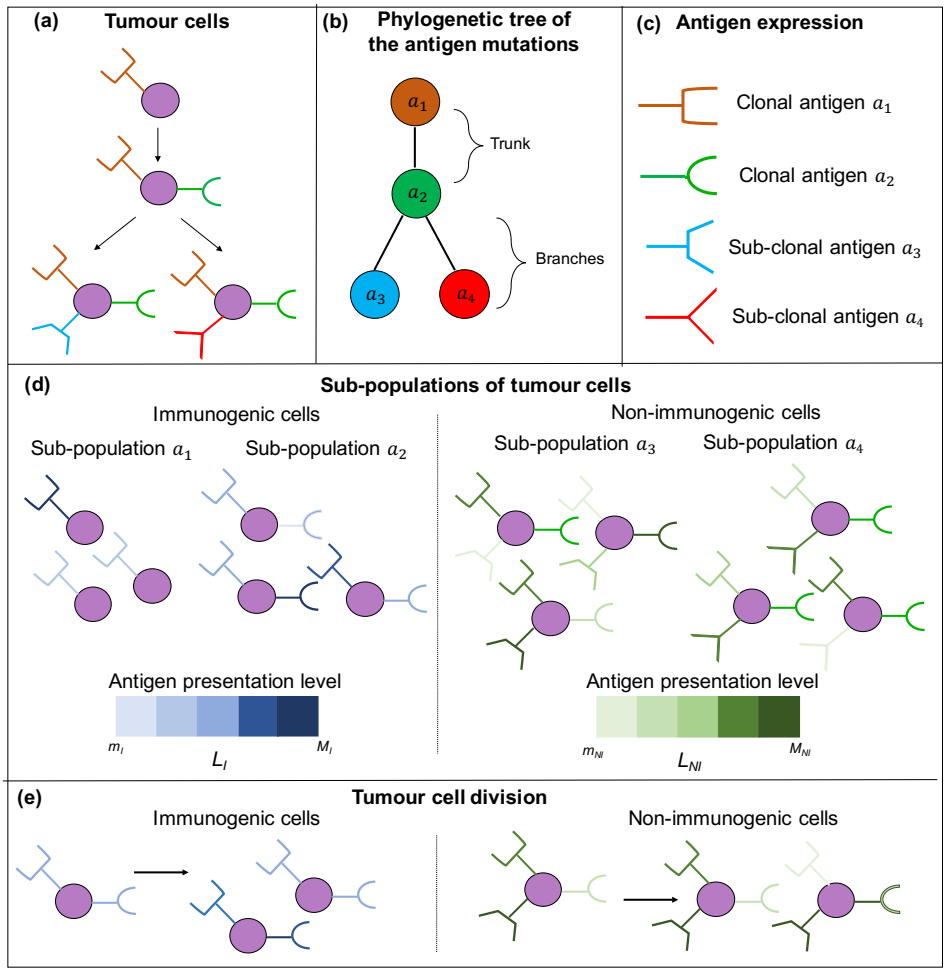

Figure 3.1: **Schematic representation of the modelling assumptions for tumour cells.** **(a)** Purple circles represent tumour cells. In this example, the antigen profile of the tumour is characterised by 4 different antigens, each one represented by a specific color and shape. **(b)** Phylogenetic tree illustrating the mutations leading to the different antigens expressed by tumour cells. The clonal and sub-clonal antigens are represented as the phylogenetic tree trunk and branches, respectively. **(c)** In this example, 4 antigens are expressed by the tumour, each one characterised by a different color and shape. Based on the phylogenetic tree **(b)**, we denote a_1 and a_2 as clonal antigens, whereas a_3 and a_4 are denoted as sub-clonal antigens. **(d)** The tumour is divided in 4 sub-populations of tumour cells, labelled by the last antigen acquired by each cell. Here, the color of each antigen represents its level of antigen presentation. Cells in the sub-populations labelled by the antigens a_1 and a_2 express only clonal antigens and are defined as immunogenic cells. They present their antigens at a normal level, with values chosen from the discrete set $L_I = \{\mathrm{m}_I, \ldots, \mathrm{M}_I\}$. Cells in the sub-populations labelled by the antigens a_3 and a_4 express clonal and sub-clonal antigens and are defined as non-immunogenic cells. They present all their antigens at a low level, with values chosen from the discrete set $L_{NI} = \{\mathrm{m}_{NI}, \ldots, \mathrm{M}_{NI}\}$. **(e)** A tumour cell divides when it reaches a certain target volume. An immunogenic (respectively non-immunogenic) cell divide in two immunogenic (respectively non-immunogenic) cells. The daughter cell has the same antigens of the parent cell, but with a new random level of antigen presentation.

grid site, and $l^n_{a_i}$ is the level of presentation of antigen a_i by the n^{th} tumour cell.

The total amount of chemoattractant secreted by tumour cells expressing antigen a_i induces the arrival of CTLs specific to antigen a_i into the domain. More details about the mathematical modelling of the different chemoattractant dynamics will be discussed in Section 3.3.1.

Dynamics of CTLs

Influx of CTLs Following [87], to model the tumour vessels that allow the arrival of CTLs in the tumour micro-environment, we generate a set of points in the domain. In order not to rely on a detailed angioarchitecture, we generate 5 entry points, equidistant from each other and from the centre of the domain. At each time step, a CTL specific to antigen $a_i \in A$ can be supplied to the domain from one of the 5 entry points, provided that the entry point is not occupied by other cells. The probability $0 < p(t) \leqslant 1$ of influx of a CTL specific to antigen a_i into the domain is proportional to the total amount $S^{tot}_{a_i}(t)$ of chemoattractant associated to antigen a_i secreted at time t. Therefore, we define $p(t)$ as

$$p(t) := C_2\, S^{tot}_{a_i}(t),$$

with $C_2 \in \mathbb{R}^+$ a scaling factor of units $\frac{[time]}{[mol]}$.

Since the secretion of chemoattractants by tumour cells is proportional to the level of antigen presentation (see Eq. (3.5)), the total amount of chemoattractants secreted by non-immunogenic cells is lower than the total amount of chemoattractants secreted by immunogenic cells. Therefore, the influx of CTLs targeted to sub-clonal antigens, which are expressed only by non-immunogenic cells, is lower than the influx of CTLs targeted to clonal antigens.

TCR expression and CTL death We denote by $N_C(t)$ the number of CTLs in the system at time t, and we label each of them by an index $m = 1, ..., N_C(t)$. Every CTL has a unique TCR [see Figure 3.2**(a)**], and we suppose that each TCR is specific to a unique tumour antigen [see Figure 3.2**(b)**]. When the m^{th} CTL with a TCR targeted against antigen $a_i \in A$ arrives into the domain it undergoes chemotactic movement towards tumour cells expressing the matching antigen a_i.

CTL division occurs mostly in the lymph nodes [55] and cells then move to the tumour site. CTLs can also proliferate at the tumour site but this is not the main site of proliferation. We thus neglect the effects of CTL proliferation at the tumour site and consider only the effects of proliferation outside the spatial domain of the model, leading to a varying influx of CTLs. A CTL undergoes apoptosis when it reaches the end of its intrinsic lifespan, which is drawn from a uniform distribution upon its arrival in the domain.

Elimination of tumour cells by CTLs Upon contact, CTLs can interact only with tumour cells expressing the matching antigen [see Figure 3.2**(c)**], and can induce their death, on the condition that the matching antigen is presented at a sufficiently high level. If a CTL is in contact with more than one tumour cell expressing the matching antigen, it will try to eliminate the one presenting the antigen at the highest level. In particular, when the m^{th} CTL interacts with the n^{th} tumour cell expressing the matching antigen a_i, we let the tumour cell be removed from the system, provided that

$$\mu\, l^n_{a_i} > (1 - r). \tag{3.6}$$

Here μ is a random variable drawn from the standard uniform distribution, $l^n_{a_i}$ is the level of presentation of antigen a_i by the n^{th} tumour cell and $0 < r \leqslant 1$ is the intrinsic TCR-recognition probability, which we suppose to be equal for every CTL. If the tumour cell satisfies the conditions

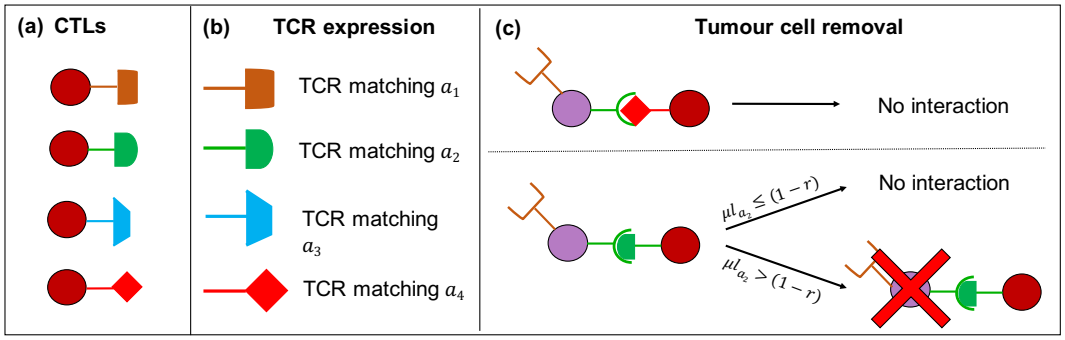

Figure 3.2: **Schematic representation of the modelling assumptions for CTLs and their interaction with tumour cells. (a)** Red circles represent CTLs, which express a unique TCR. **(b)** TCR are represented with different shapes and colors. Each TCR is able to recognize a particular tumour antigen. In the model, the number of TCRs is equal to the number of expressed tumour antigens. **(c)** Purple circles represent tumour cells. CTLs can eliminate tumour cells, upon contact, under certain conditions. A tumour cell is eliminated if it presents the antigen matching the CTL receptor at a sufficiently high level. In this example, a tumour cell expressing antigen a_1 and a_2 cannot be eliminated by a CTL with TCR matching antigen a_4. On the other hand, the same tumour cell may be eliminated by a CTL expressing the TCR matching antigen a_2, under a condition on the level l_{a_2} of presentation of such antigen a_2. The parameter r is the intrinsic TCR-recognition probability and μ is a random variable drawn from a standard uniform distribution.

to be eliminated, it undergoes apoptosis. The parameter r determines the range of tumour cells the CTL population can interact with: large values of r represent a CTL population able to eliminate tumour cells presenting their antigens at a low level, whereas low values of r model the scenario where the CTLs can only eliminate tumour cells presenting their antigens at a high level. Tumour cell elimination by CTLs takes approximately 6 hours to be completed *in vitro* [30] and *in vivo* [24]. Accordingly, we require that an elimination event keeps a CTL engaged for 6 hours and only after this time the CTL can eliminate again [113]. If the condition (3.6) is not satisfied, the CTL is not engaged and can try, in the next time step, to eliminate again a tumour cell.

Chemoattractant field

As mentioned earlier, we let the n^{th} tumour cell at the border of the tumour secrete a different chemoattractant for each antigen a_i that it expresses. Denoting by ϕ_{a_i} the concentration of the chemoattractant secreted by tumour cells expressing antigen a_i, we let the dynamic of ϕ_{a_i} be described by the following reaction-diffusion equation:

$$\frac{\partial \phi_{a_i}}{\partial t} = D\Delta\phi_{a_i} - \gamma\phi_{a_i} + \sum_{n \in N_{BT}(t)} s^n_{a_i}, \quad a_i \in A. \tag{3.7}$$

In Eq. (3.7), D is the diffusion constant and γ is the rate of natural decay; these two parameters are assumed to have the same value for each chemoattractant. On the other hand, we recall that the secretion rate $s^n_{a_i}$ is specific to the n^{th} tumour cell, because it is proportional to the level of presentation of antigen a_i by the tumour cell (see Eq. (3.5)). $N_{BT}(t)$ denotes the set of tumour cells in contact with the surrounding medium at time t.

We add to Eq. (3.7) zero-flux boundary conditions and an initial concentration ϕ_a^{init} which is set to be zero everywhere in the domain but at the border of the tumour.

3.4 Numerical simulations and preliminary results

3.4.1 Set-up of simulations

For numerical simulations of our individual-based model, we use a Cellular Potts approach on a 2D spatial grid with a total of 400×400 lattice sites. Simulations were developed and run using the software CompuCell3D [107] on a standard workstation (Intel i7 Processor, 4 cores, 16 GB RAM, macOS 11.2.2), with one time-step chosen to be $\Delta t = 1$ min. The computational implementation of Cellular Potts models is described in Appendix A, while full details of the model parametrisation are provided in Appendix C.1. Files to run a simulation example with Compucell3D software [107] are available at: https://plmlab.math.cnrs.fr/audebert/cc3dmodeltumourcd8.

At the initial time point of the simulation, a certain number of tumour cells are already present in the domain, while CTLs arrive only when the simulation starts. At the beginning of simulations there is a total of 400 tumour cells, tightly packed in a circular configuration positioned at the centre of the domain, reproducing the geometry of a solid tumour.

All quantities we present in this section and in Section 3.5 are obtained by averaging over the results of 10 simulations, with parameter values kept constant and equal to those listed in Table C.1 and Table C.2. Unless otherwise explicitly stated, we carry out numerical simulations for 28800 time-steps, corresponding to 20 days.

The next two subsections describe two preliminary computational results of our model which will be used to guide the simulations leading to the main results presented in Section 3.5.

3.4.2 Baseline scenario: tumour development in the absence of CTLs

We first establish a baseline scenario where tumour cells grow, divide and die via the modelling rules described in Section 3.3.1, in the absence of CTLs. For this case, we carry out numerical simulations for 36000 time-steps, corresponding to 25 days. Figure 3.3 shows the growth over time of the number of tumour cells. The growth of the tumour cell number is of logistic type, as expected by the rules that govern tumour cell death. Logistic growth has been used by a number of authors to model the temporal evolution of the size of solid tumours [58, 118, 123]. The carrying capacity, *i.e.* the saturation value reached by the number of tumour cells due to intra-population competition, is numerically estimated to be of about 1100 cells.

In the following subsections, we explore the immune response to tumours characterised by different degrees of ITH. Each simulation is carried out by keeping all parameter values fixed (and equal to this baseline scenario) and changing only the initial compositions of the different tumours.

3.4.3 Tumours with larger number of sub-populations of cancer cells lead to lower immune response efficacy

In a recent *in vivo* study in mice, the volume of UVB irradiated tumours after 20 days is found to be linked to the number of sub-populations of cancer cells constituting each inoculated tumour [223]. In our next simulations, we attempt to verify that our model reproduces such phenomenon, exploring the outcomes of immune response to 7 different tumours characterised by an increasing number of sub-populations of tumour cells. At this preliminary stage, we simplify our model. We consider that each tumour consists of the same type of cells, and we do not

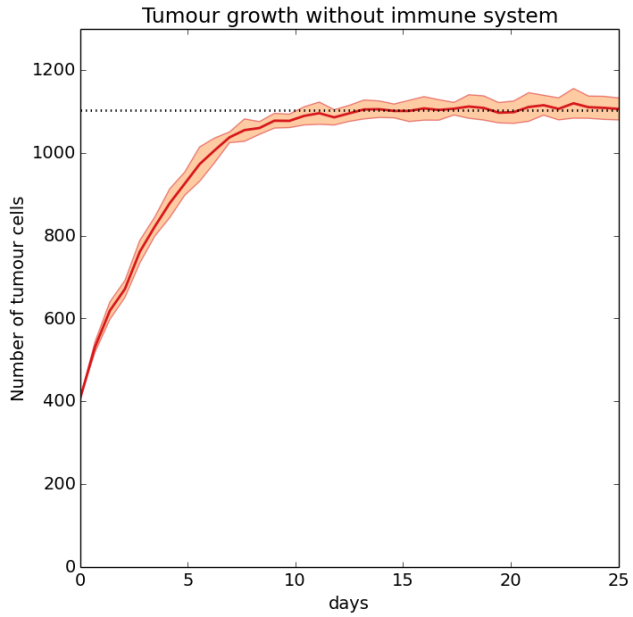

Figure 3.3: **Baseline scenario: tumour development in the absence of CTLs.** Time evolution of the tumour cell number in the absence of CTLs. The shaded area indicates +/− standard deviation between 10 simulations. The black dotted line highlights a numerical estimation of the tumour cell carrying capacity.

differentiate between immunogenic and non-immunogenic cells. In particular, here we let each sub-population of tumour cells be characterised by cells expressing a single antigen. This antigen is presented at a random level, chosen uniformly from the discrete set $L = \left\{\frac{1}{6}, \frac{2}{6}, \frac{3}{6}, \frac{4}{6}, \frac{5}{6}, 1\right\}$. In this way, tumour cells that express the same antigen belong to the same sub-population.

The plots in Figure 3.4**(a)-(g)** display the time evolution of the tumour cell number of 7 tumours that comprise 1 to 7 different sub-populations of cancer cells. Plot in Figure 3.4**(h)** displays the corresponding number of tumour cells and CTLs remaining at the end of simulations (after 20 days) for the 7 tumours. For tumours constituted of 1 or 2 sub-populations of cancer cells, none or very few tumour cells remain after 20 days [see Figure 3.4**(a)-(b)**]. When 3 sub-populations of cancer cells constitute the tumour, the number of tumour cells over time tends to stay constant and slightly above its initial value [see Figure 3.4**(c)**]. Finally, for tumours initially constituted of more than 3 sub-populations, the number of tumour cells after 20 days is more than twice the initial value. In addition, the final number of tumour cells increases as we increase the number of sub-populations of cancer cells constituting the tumour from 1 to 6. For tumours with 6 and 7 sub-populations, the final number of tumour cells is similar and is about 1000 cells [see Figure 3.4**(f)-(g)**]. These results support the idea that the anti-tumour immune action is efficient only when the tumour is constituted of 1 or 2 sub-populations of tumour cells. Moreover, up to a certain point, the increase of the number of sub-populations of tumour cells results in a weaker immune response. Finally, increasing the number of sub-populations of tumour cells beyond 6 does not appear to change the effect of the immune response. Comparing the dynamics of the two last tumours (with 6 and 7 sub-populations of tumour cells) to the baseline scenario

of Section 3.4.2, we see that the immune response is almost inefficient, as it is not able to really limit the growth of the two tumours.

Our computational results are in agreement with experimental results presented in [223]. In this study, the induction of UVB-derived tumour, which lead to an increase in the number of sub-populations of cancer cells, results in aggressive tumours with reduced anti-tumour immune activity. However, when different single-cell-clone derived tumours (characterised by a unique sub-population of tumour cells) are considered, the immune system is able to effectively eradicate them.

Figure 3.4**(h)** also shows that, when the tumour is constituted of more than 3 sub-populations of tumour cells, the total number of CTLs at the end of simulations remain almost constant in the different tumours (around 200 cells). A consequence of this is that the average size of each specific CTL sub-population decreases as we consider tumours with increased number of sub-populations of tumour cells. This leads to a less efficient anti-tumour immune response. As highlighted in [223], these computational results also suggest that increasing the number of sub-populations of tumour cells reduce the exposition of each antigen to the "front-line", thus making more difficult for immune cells to detect them. The resulting outcome is a reduced influx of specific CTLs in the tumour micro-environment and a weaker anti-tumour immune response.

3.4.4 Initial composition of two tumours inspired by biological studies

In the previous subsections we investigated simple cases of tumour growth with and without the action of the immune system. We will now explore further the effect of ITH on immune surveillance considering two tumours inspired by biological studies, in order to effectively capture more layers of biological complexity. For the two tumours we consider different initial antigenic compositions, corresponding to different degrees of ITH. In particular, following the experiments presented in [223], we dissect out two characteristics of ITH: the number of sub-populations of cancer cells constituting a tumour and the percentage of immunogenic and non-immunogenic cells within it. With our model, we wish to investigate the effect of these two expressions of ITH on tumour aggressiveness independently and together, evaluating their influence on anti-tumour immunity in a controlled manner. To this end, first we generate two tumours with different number of sub-populations of cancer cells. Following the experiments presented in [223] and the results of Section 3.4.3, we consider, respectively, tumours with 3 and 7 sub-populations of cancer cells. For simplicity, we denote the first tumour as *tumour-3a* and the second one as *tumour-7a*. The antigenic composition of the two tumours and their corresponding phylogenetic tree representation are inspired by experiments presented in [223]. More details about the two tumours are given in the next paragraphs. Next, for each tumour we consider different initial percentages of immunogenic and non-immunogenic cells. When different sub-populations of immunogenic (or non-immunogenic) cells are considered, the total percentage of immunogenic (or non-immunogenic) cells is equally distributed in each sub-population. This enables us to decouple antigen heterogeneity and antigen immunogenicity, and study their influence on tumour aggressiveness in a causal, systematic manner.

Tumour-3a The first tumour we consider expresses three different antigens, one of which is clonal and the other two are sub-clonal (see Figure 3.5**(a)**). With the notation introduced in Section 3.3.1, we denote respectively by

$$A = \{4, 5, 7\}, \quad A_C = \{5\} \quad \text{and} \quad A_{SC} = \{4, 7\} \tag{3.8}$$

the antigen profile of the tumour, the clonal antigens and the sub-clonal antigens.

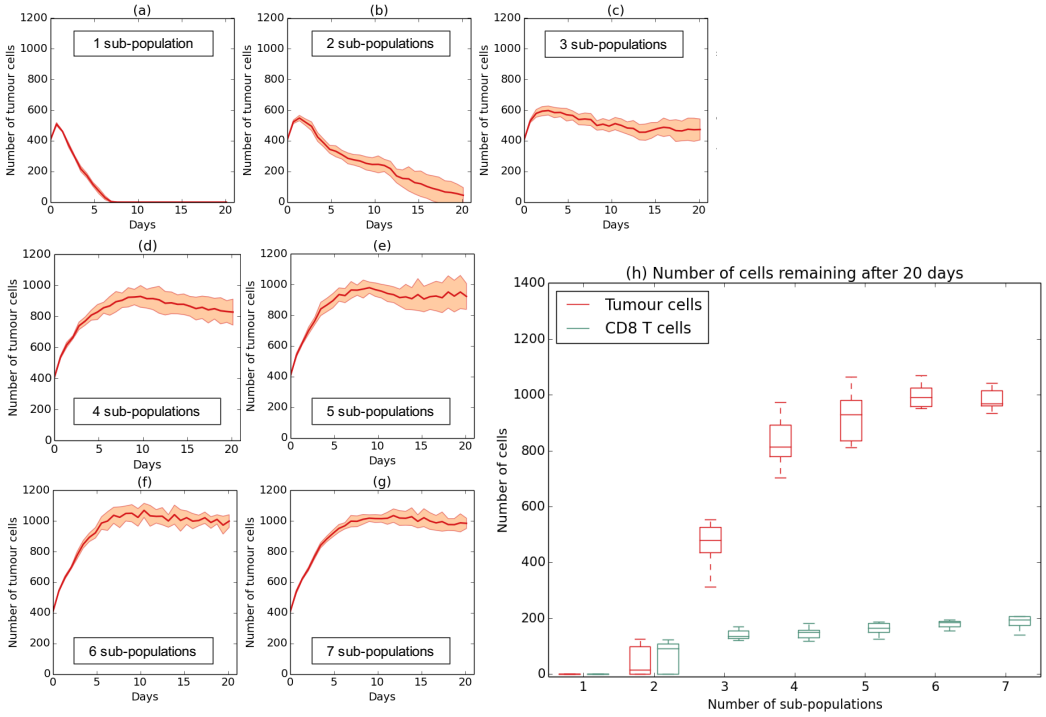

Figure 3.4: **Tumours with larger number of sub-populations of cancer cells lead to lower immune response efficacy.** Plots in panel **(a)-(g)** display the time evolution of the tumour cell number for tumours characterised by increasing numbers of sub-populations. Shaded areas indicate +/− standard deviation between 10 simulations. Plot in panel **(h)** displays the corresponding number of tumour cells (in red) and CTLs (in green) remaining after 20 days (28800 time-steps) for the different initial tumour compositions. The cell numbers presented here were obtained as the average over 10 simulations and the error bars display the related standard deviation.

Based on the phylogenetic tree representation of Figure 3.5**(a)**, we divide *tumour-3a* in 3 sub-populations of tumour cells labelled by the last antigen acquired by each cell. Cells in the sub-population labelled by antigen 5 carry only this antigen, while cells in sub-populations labelled by antigens 4 and 7 express, respectively, antigens 5 and 4 or antigens 5 and 7.

As cells in the sub-population labelled by antigen 5 are immunogenic, their level of antigen presentation by the MHC-I is assumed to be normal and randomly chosen from the discrete set L_I, which is defined as

$$L_I = \left\{ \frac{1}{6}, \frac{2}{6}, \frac{3}{6}, \frac{4}{6}, \frac{5}{6}, 1 \right\}. \tag{3.9}$$

On the other hand, as cells in sub-populations labelled by antigens 4 and 7 are non-immunogenic, their level of antigen presentation by the MHC-I is deteriorated and, therefore, randomly chosen from the discrete set L_{NI}, which is defined as

$$L_{NI} = \left\{ \frac{5}{100}, \frac{10}{100}, \frac{15}{100}, \frac{20}{100}, \frac{25}{100}, \frac{30}{100} \right\}. \tag{3.10}$$

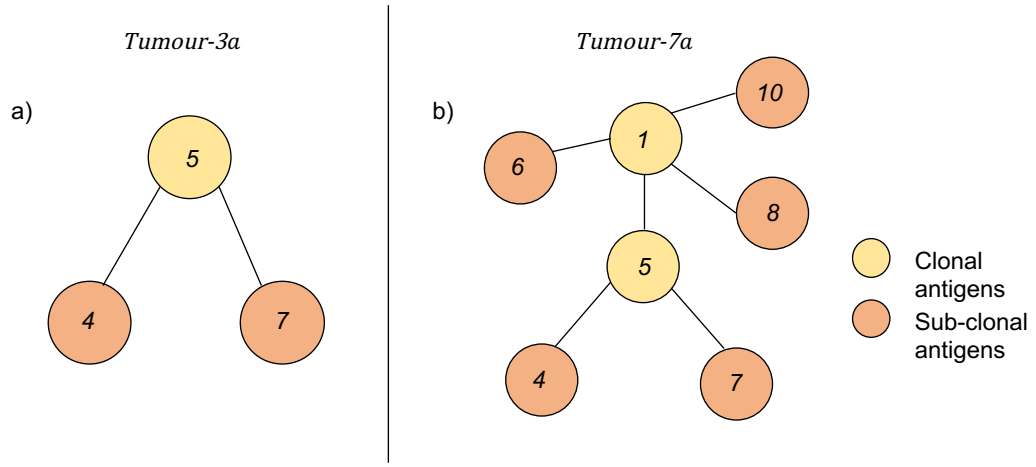

Figure 3.5: **Phylogenetic tree representations of the antigens considered for the two tumours. (a)** *Tumour-3a* expresses three antigens. Antigen 5 is the only clonal antigen (in yellow) and antigens 4 and 7 are two sub-clonal antigens (in orange). As a results, *tumour-3a* is composed of 3 sub-populations of tumour cells. **(b)** *Tumour-7a* expresses seven antigens. Antigens 1 and 5 are clonal antigens (in yellow) and antigens 4, 6, 7, 8 and 10 are sub-clonal antigens (in orange). Hence, *tumour-7a* is composed of 7 sub-populations of tumour cells. The phylogenetic tree representations of the two tumours are inspired by experiments presented in [223].

Tumour-7a The second tumour expresses seven different antigens, two of which are clonal and five are sub-clonal (see Figure 3.5**(b)**). We denote respectively by

$$A = \{1, 4, 5, 6, 7, 8, 10\}, \quad A_C = \{1, 5\} \quad \text{and} \quad A_{SC} = \{4, 6, 7, 8, 10\} \tag{3.11}$$

the antigen profile of the tumour, the clonal antigens and the sub-clonal antigens.

Based on the phylogenetic tree representation of Figure 3.5**(b)**, we divide *tumour-7a* in 7 sub-populations of tumour cells. Cells in sub-populations labelled by antigens 1 and 5 are immunogenic, and present their antigens at a level randomly chosen from set L_I, which is defined in (3.9). On the other hand, cells in sub-populations labelled by antigens 4, 6, 7, 8 and 10 are non-immunogenic, and present all their antigens at a lower level randomly chosen from set L_{NI}, which is defined in (3.10).

In the next Section, we investigate the effects of CTL response to different tumours characterised by different levels of ITH. The obtained dynamics are compared with the baseline scenario. In the next simulations, we consider different compositions of the initial tumour, while the other parameters are kept constant to the values listed in Table C.1 and Table C.2. The values of the parameters are chosen so as to qualitatively reproduce essential aspects of the experimental results obtained in [223].

3.5 Main results

3.5.1 Large number of sub-populations of cancer cells constituting a tumour reduces the effectiveness of the immune response

To investigate how the immune response is affected by different degrees of heterogeneity, we start by comparing two situations in which the initial tumours are characterised by different number of sub-populations of tumour cells. We consider as initial conditions *tumour-3a*, with 3 different sub-populations of tumour cells, and *tumour-7a*, with 7 different sub-populations of tumour cells, defined as in Section 3.4.4. For each tumour, we consider the same initial percentage of immunogenic and non-immunogenic cells, corresponding to 75% of immunogenic cells and 25% of non-immunogenic cells. Note that these two tumours are different from those considered in the results presented in Section 3.4.3. In fact, in *tumour-3a* and *tumour-7a* cells can express clonal and sub-clonal antigens and, therefore, be either of immunogenic or non-immunogenic type. On the other hand, in the results presented in Section 3.4.3, each tumour cell presents a unique antigen, which is shared by all the cells in the same sub-population of tumour cells. The situation considered here provides a more faithful representation of biological complexity, as a tumour cell can express more than one antigen presented at different levels.

Figure 3.6**(a)-(c)** show the time evolution of the total number of tumour cells, along with the corresponding time evolution of immunogenic and non-immunogenic cell number. Figures 3.6**(d)-(f)** also display the spatial cell distributions observed at different times of two simulations. As shown by Figure 3.6**(a)**, the two tumours have similar dynamics from the beginning of simulations until day 10, with an initial increase of the cell number followed by a steep decrease. After day 10, in *tumour-3a*, the number of tumour cells continues to decrease until it reaches a low, almost constant level. Figure 3.6**(b)-(c)**, along with the corresponding panel of Figure 3.6**(f)**, show that, at the end of simulations, all the immunogenic cells are eliminated by the CTLs, and only few non-immunogenic cells remain in the system. On the other hand, for *tumour-7a*, after day 10 the tumour cell number increases steadily over time. This dynamic leads to a final tumour size similar to the initial one. Moreover, as shown by Figure 3.6**(b)**, the number of immunogenic cells tends to decrease over time, whereas the number of non-immunogenic cells, after being initially kept under control by immune cells, increases steeply (*cf.* Figure 3.6**(c)**). The related panels of Figure 3.6**(d)-(f)** show the progressive colonisation of the tumour by non-immunogenic cells.

Due to the relatively large standard deviation observed in the *tumour-7a* results, we run 100 realisations of this simulation (see Figure C.1 in C.2), in order to check the robustness of our results. Comparing Figures 3.6 and C.1, we observe a qualitative similar behaviour (*i.e.* similar mean and standard deviation), confirming the reliability of the *tumour-7a* results presented in Figure 3.6. As shown by Figure 3.6, we observe a larger variability in the simulation of *tumour-7a* than in the one of *tumour-3a*. This variability is probably due to the larger number of antigens that are present in *tumour-7a*. This result indicates that the number of antigens can be an important source of variability in the model.

Comparing these results with the baseline scenario of Section 3.4.2, for both tumours we clearly see the effects of the action of immune cells on tumour growth, which is no longer simply logistic and saturating to carrying capacity. However, the effectiveness of the immune response depends on the tumour considered. For *tumour-3a*, the immune response is efficient and almost eliminates all tumour cells. On the other hand, for *tumour-7a*, the higher heterogeneity leads to a less effective immune response and the tumour eventually grows again. These results suggest that, even if characterised by equal percentages of immunogenic and non-immunogenic cells, tumours with a larger number of sub-populations of tumour cells, which express a wider spectrum of antigens, are more aggressive. This was already suggested by the results presented in Section

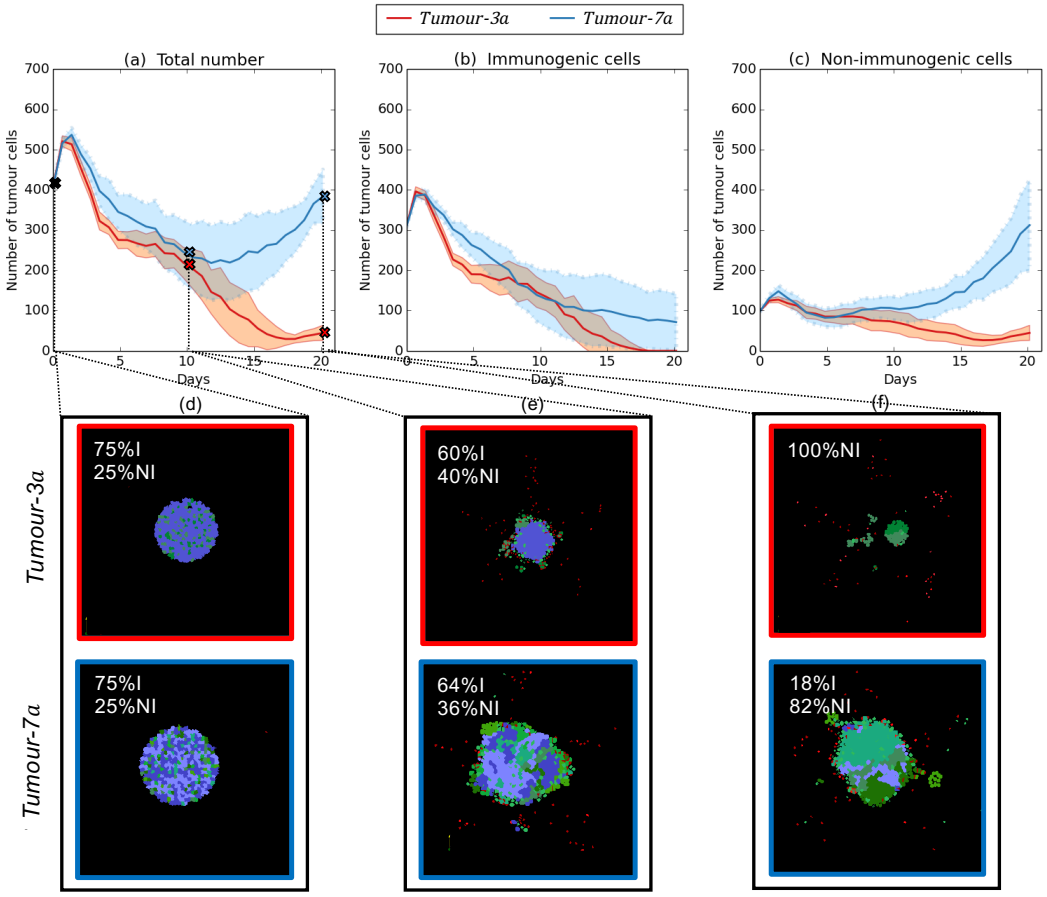

Figure 3.6: **The number of sub-populations constituting a tumour impacts on the effectiveness of the immune response.** Plots in panels **(a)-(c)** display the time evolution of the total tumour cell number, and the corresponding evolution of the number of immunogenic cells and non-immunogenic cells for *tumour-3a* (in red) and *tumour-7a* (in blue). Shaded areas indicate +/− standard deviation between 10 simulations. For these simulations, an equal initial percentage of 75% of immunogenic cells and 25% of non-immunogenic cells was considered. Insets in panels **(d)-(f)** display an example of the spatial distribution of cells for *tumour-3a* (first row) and *tumour-7a* (second row) at different times of the simulation. Purple cells are immunogenic cells, green cells are non-immunogenic cells and red cells are CTLs.

3.4.3. Moreover, even with all tumour cells presenting clonal antigens (it was not the case in Section 3.4.3) the CTLs are not able to control the growth of the tumour. This again indicates that the number of sub-populations and antigens in a tumour have an impact on the effectiveness of the immune response.

The outcomes of our model indicate that in *tumour-3a* the presence of a low number of antigens leads to a better immune detection, enhancing the ability of the immune system to eliminate the tumour. In both tumours the immune system rapidly targets and eliminates immunogenic cells, giving a competitive advantage to non-immunogenic cells. In fact, we initially observe a reduction in the number of tumour cells. However, in *tumour-7a*, as more sub-populations

of tumour cells are present, non-immunogenic cells have a better chance of escaping immune surveillance. The outcome is a weaker anti-tumour immune response. Overall, our results are in agreement with the recent hypothesis presented in [223] that, because of increased antigenic variability, the relative expression of each antigen is weaker in tumours composed of a larger number of sub-populations of tumour cells. In particular, clonal antigens undergo "dilution" within the tumour, and, therefore, the chance for CTLs to identify immunogenic cells is reduced. This leads to a diminished ability of CTLs to mount a sufficient cytotoxic response.

3.5.2 Different initial percentages of immunogenic and non-immunogenic cells can cause variations in anti-tumour immune response

The results discussed in the previous subsection illustrate how the effectiveness of the immune response can decreases in tumours with larger number of sub-populations of tumour cells. We investigate the effects of ITH further, focusing on the role of the percentage of immunogenic and non-immunogenic cells. We fix the number of sub-populations of tumour cells considering only *tumour-3a*, and vary the initial percentage of immunogenic and non-immunogenic cells.

The plot in Figure 3.7 displays the number of tumour cells remaining at the end of simulations (after 20 days), for different initial percentages of immunogenic and non-immunogenic cells. For low percentages of non-immunogenic cells ($\leqslant 25\%$), none or very few tumour cells survive after 20 days. On the contrary, for tumours initially composed of more than 50% of non-immunogenic cells, the number of tumour cells after 20 days is larger than the initial one. In addition, the final number of cells increases as we increase the initial percentage of non-immunogenic cells. These results suggest that the anti-tumour immune action is efficient only when the percentage of non-immunogenic cells is low compared to the percentage of immunogenic cells. Moreover, the larger the percentage of non-immunogenic cells, the weaker the immune response is.

Compared to the baseline scenario of Section 3.4.2, we see the effects of the immune system on tumour growth. In fact, for each scenario the number of cells at the end of simulations is lower than the tumour carrying capacity shown in Figure 3.3. However, for larger percentages of non-immunogenic cells, the immune response is not efficient enough to reduce the initial tumour size.

Taken together, our results qualitatively reproduce key findings of experiments performed in *in vivo* syngeneic mice tumour models [80]. The results presented in [80] indicate that a non-effective immune response may occur when the percentage of immunogenic cells in the tumour is low. Our computational results provide an explanation for such emergent behaviour. Since sub-clonal antigens are presented at a low level by the MHC-I, non-immunogenic cells trigger a poor CTL response. Thus, tumours characterised by a major percentage of non-immunogenic cells result in a weaker overall immune response. Furthermore, the experimental results presented in [80] put forward the idea that the threshold percentage of immunogenic cells that is required to trigger an antigen-specific CTL response may vary depending on the antigens. In order to address this point, such a feature could be implemented in the model, for example by considering antigen presentation levels or chemotactic responses specific to each antigen.

The role of the immunogenic cell percentage within the tumour is further analysed as we observe a gap between the results obtained considering 25% and 50% of non-immunogenic cells (see Figure 3.7). This is investigated by performing simulations considering percentages of non-immunogenic cells between these two values. Figure 3.8 displays the time evolution of the number of tumour cells for 10 different realisations of the same simulation, considering the same initial condition with 33% of non-immunogenic cells and 67% of immunogenic cells. In this case, we carried out numerical simulations for 38800 time-steps (corresponding to 27 days).

Under this choice of the initial condition, we observe a large variability in the tumour-immune

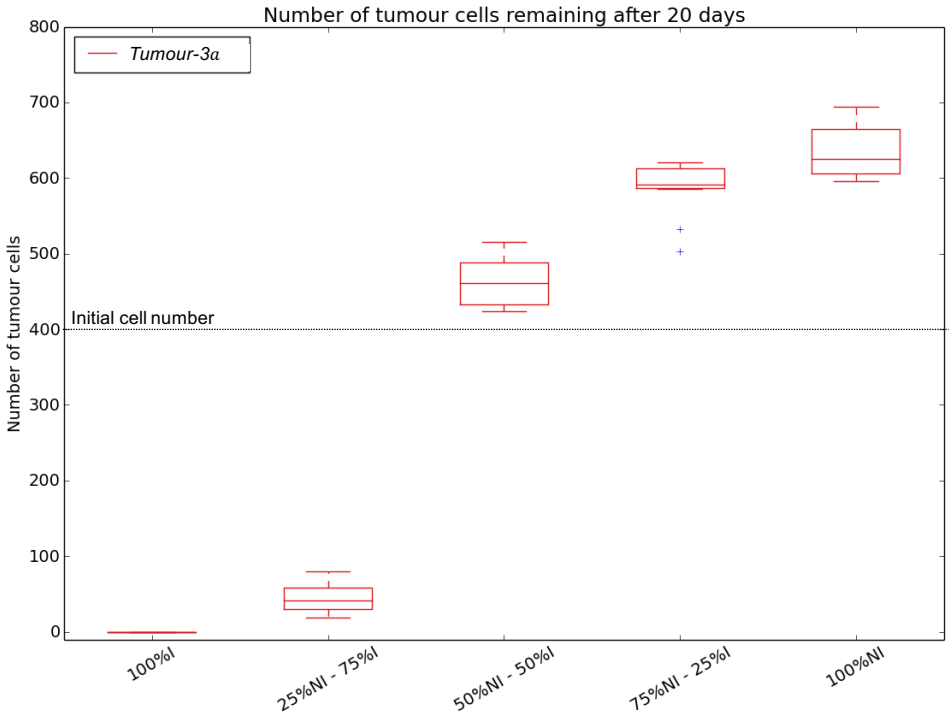

Figure 3.7: **Different initial percentages of immunogenic and non-immunogenic cells can cause variations in the immune response to tumour cells.** Plot displaying the number of tumour cells remaining after 20 days (28800 time-steps) for different initial percentages of immunogenic and non-immunogenic cells. For these simulations, only *tumour-3a* was considered. The tumour cell numbers presented here were obtained as the average over 10 simulations and the error bars display the related standard deviation. The black dotted line highlights the number of tumour cell at the initial time of the simulations.

cell dynamics, which does not lead to a clear emergent behaviour. In particular, Figure 3.8**(a)** shows that, in some simulations, the number of tumour cells decreases over time and only few cells remain at the end of the simulations. In other cases, after an initial phase between day 0 and day 10 where CTLs keep under control the growth of the tumour, the number of tumour cells eventually increases and the resulting final number of tumour cells is larger than the initial one. This is also illustrated by Figure 3.8**(b)**, which displays a sample of the spatial cell distributions at different time of two simulations. In particular, here we show that, starting from the same initial condition, we obtain two different outcomes: in one case immune clearance occurs and tumour cells are almost entirely eliminated by the immune system; in the other case tumour cells escape immune surveillance. When immune escape occurs, in the example proposed in Figure 3.8**(b)** at day 14, immunogenic cells are surrounded by non-immunogenic cells, which hamper immune detection. This leads to a decreased influx of CTLs in the tumour micro-environment and results in a weaker immune response.

These results suggest that the stochasticity which is present in cell dynamics may affect the outcomes of immune action. These results may partially explain the outcomes of earlier experimental research [38, 116], which found that responses of patients with similar tumours can vary

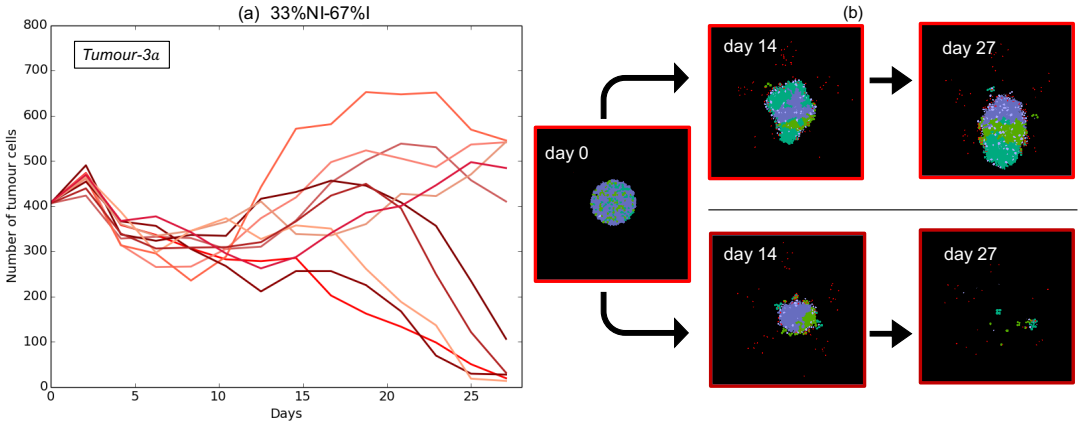

Figure 3.8: **Stochasticity in cell dynamics may affect the outcomes of immune action.** Plot in panel **(a)** displays the time evolution of the tumour cell number for an initial percentage of 33% of non-immunogenic cells and 67% of immunogenic cells for 10 runs of simulations. Each line corresponds to a unique realisation of our model. For these simulations, only *tumour-3a* was considered. The insets in panel **(b)** show an example of the observed spatial distributions of cells corresponding to different times of two simulations.

considerably. In this regard, the use of mathematical models for identification and understanding of immune escape mechanisms in individual tumour could help advancing personalized tumour treatment.

3.5.3 Both the number of sub-populations of cancer cells constituting a tumour and the percentage of immunogenic and non-immunogenic cells affect the effectiveness of the immune response

So far, we have investigated with our model the effects of ITH on immune response by varying independently the number of sub-populations of cancer cells constituting a tumour and the percentage of immunogenic and non-immunogenic cells. Now, we study their combined effect in mediating tumour growth. We consider as initial conditions *tumour-3a* and *tumour-7a*, characterised by different numbers of sub-populations of tumour cells, and for different initial percentages of immunogenic and non-immunogenic cells.

Figure 3.9 displays the time evolution of the total number of cells for different initial tumour compositions, and compares the number of immunogenic and non-immunogenic cells at the end of simulations with respect to the initial one. As shown by Figure 3.9**(a1)**, the immune system is able to completely eradicate the tumour only when it is initially composed of 100% of immunogenic cells, independently of the number of sub-populations of tumour cells. When the initial tumour is made of 25% of non-immunogenic cells, Figure 3.9**(b1)** show that the two tumours have different dynamics. In particular, as already observed in the results presented in Section 3.5.1, the number of cells in *tumour-3a* decreases over time until the end of the simulations, while the number of cells in *tumour-7a*, after an initial decrease, steadily increases until the end of the simulations. Finally, when tumours are initially composed of more than 50% of non-immunogenic cells, similarly to the baseline scenario of Section 3.4.2, they follow a logistic growth, except for an initial decrease shown by Figure 3.9**(c1)**. For both tumours, the tumour

cell number eventually saturates at a certain value (see Figure 3.9**(c1)-(e1)**). In these cases, the saturation value of the number of tumour cells is larger than the initial tumour cell number. Moreover, the saturation value attained increases as we increase the level of heterogeneity of the tumour (respectively, the number of sub-populations of tumour cells and the percentage of non-immunogenic cells). Such results indicate that in these cases CTLs are present in the tumour micro-environment but do not produce an effective immune response. Persistent antigen presentation has been proven to cause continuous TCR stimulation that could directly induce CTL dysfunction and exhaustion [226, 231]. The model presented in this work does not include this aspect, but it could be easily extended to do so.

The outcomes of our model recapitulate the main results of in *in vivo* clonal mixing experiments in mice models presented in [223], who studied the combined effect of these two characteristics of ITH in mediating tumour growth and eradication. Wolf and collaborators have demonstrated that tumours with increased number of clones and large genetic diversity are more aggressive. In our model, the number of clones can be linked to the number of sub-populations of tumour cells, while genetic diversity may be linked to the immunogenicity of the tumour. Moreover, our findings are in agreement with an experimental work indicating that patients whose tumours are highly heterogeneous have increased levels of relapse after an initial response to immunotherapy and worse survival expectations than patients with more homogeneous tumours [150].

We next analyse the evolution over time of immunogenic and non-immunogenic cells. When tumours are initially composed of 25% of non-immunogenic cells, Figure 3.9**(b2)** shows that the two tumours evolve in different ways. While the number of non-immunogenic cells is considerably reduced in *tumour-3a*, the final number of non-immunogenic cells increases up to four times its initial number in *tumour-7a*. On the other hand, when tumours are initially composed of more than 50% of non-immunogenic cells, independently of the tumour considered, we observe a similar trend in the evolution of immunogenic and non-immunogenic cells (see Figure 3.9**(c2)-(e2)**). In particular, for both tumour types, the number of immunogenic cells tends to remain stable or decreases slightly. On the other hand, the number of non-immunogenic cells increases and grows to up to twice its initial value.

These results suggest that, beyond a certain non-immunogenic cell percentage threshold, the immune system becomes inefficient in both tumour types independently of the number of sub-populations of tumour cells. Moreover, they suggest that the selective pressure of the immune response can lead to more aggressive tumours, characterised by larger percentages of non-immunogenic cells. In this regard, our results follow the same behaviour of previous experimental works demonstrating that, under cancer therapeutics (*e.g.* chemotherapy or radiotherapy), the population of tumour cells is exposed to the selective stress induced by the treatment [90, 106, 206]. Therefore, more resistanCTLs acquire a competitive advantage over more sensitive cells and induce a weaker response to treatment in the long run. The resulting outcome is a more aggressive tumour, which may ultimately grow again [161].

3.6 Discussion, conclusions and research perspectives

3.6.1 Discussion and conclusions

The number of sub-populations of cancer cells constituting a tumour and the percentage of immunogenic and non-immunogenic cells within it are two major components of ITH, and play a key role in the immune response against solid tumours. Mathematical models make possible to asses the influence of these two components of ITH on anti-tumour immunity in a controlled manner.

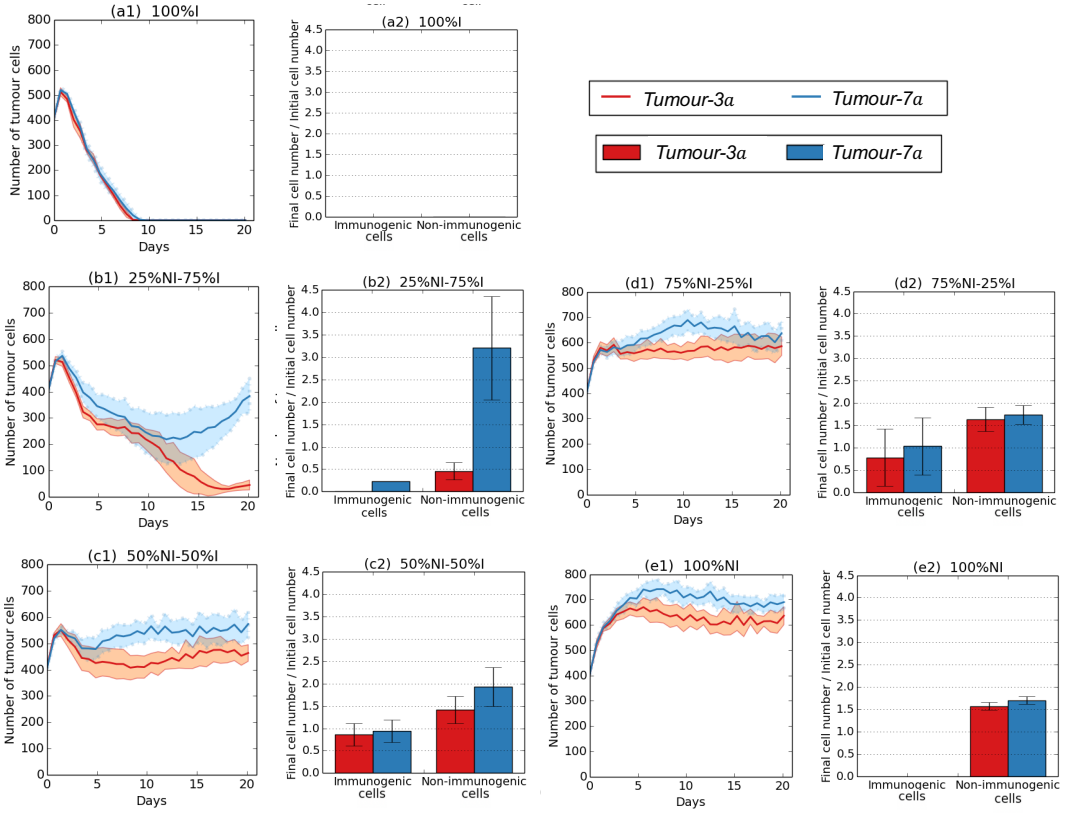

Figure 3.9: **Both the number of sub-populations of cancer cells constituting a tumour and the percentage of non-immunogenic cells affect the effectiveness of the immune response.** Plots in panel **(a1)-(e1)** display the time evolution of the tumour cell number for *tumour-3a* (in red) and *tumour-7a* (in blue). In both tumours, from **(a1)** to **(e1)** the initial percentage of non-immunogenic cells is increased. Shaded areas indicate $+/-$ standard deviation between 10 simulations. Plots in panel **(a2)-(e2)** display the corresponding average number of immunogenic and non-immunogenic cells at the end of simulations with respect to the initial one. The error lines represent the standard deviation between 10 simulations.

In this chapter, we have presented a spatially explicit stochastic individual-based model of the interaction dynamics between CTLs and tumour cells, and we have investigated how ITH affects the anti-tumour immune response.

Our numerical results show that the number of sub-populations of cancer cells constituting a tumour can have a crucial impact upon the outcome of the immune response (*cf.* Figures 3.4 and 3.6). In the scenario of tumours characterised by a low number of sub-populations of cancer cells, immune clearance can occur. Conversely, tumours composed of a larger number of sub-populations of cancer cells may be able to escape immune recognition and ultimately grow again. Our results suggest that increasing the number of sub-populations of cancer cells reduces the exposition of each antigen to the "front-line", thus making more difficult for the immune cells to detect them (*cf.* Figure 3.4). Moreover, when tumours expressing clonal and sub-clonal antigens are considered, our results demonstrate that, in more heterogeneous tumours, tumour cells could

have a better chance of escaping immune surveillance. This outcome may be explained by the fact that clonal antigens undergo "dilution" within the tumour relative to other antigens, diminishing the ability of CTLs to mount a sufficient cytotoxic response (*cf.* Figure 3.6).

The outcomes of our model support the idea that varying the initial percentage of immunogenic and non-immunogenic cells leads to variations on the effectiveness of the immune response and results in distinct scenarios, from immune clearance of the tumour to immune escape (*cf.* Figure 3.7). We have also observed that for certain intermediate percentages of immunogenic and non-immunogenic cells, stochasticity in cell dynamics plays an important role, and can lead both scenarios close to tumour eradication and to scenarios where a large number of tumour cells persists over time (*cf.* Figure 3.8).

We have also studied the effects of ITH on anti-tumour immune response by varying both the number of sub-populations of cancer cells and the initial percentage of immunogenic and non-immunogenic cells (*cf.* Figure 3.9). For equal percentage of immunogenic and non-immunogenic cells, tumours with increased number of sub-populations of cancer cells are more aggressive than tumours with lower number of sub-populations of cancer cells. However, beyond a certain threshold value of the percentage of non-immunogenic cells, the immune system becomes inefficient against both types of tumours, independently of the number of sub-populations of cancer cells. In addition, we found that increasing initial percentages of non-immunogenic cells always led to a less effective CTL response. When the tumours are not eradicated, the final percentage of non-immunogenic cells is larger than the initial one. This suggests that the immune system may act as a bottleneck which selects and eliminates immunogenic cells, thus allowing the tumours to escape immune regulation.

In summary, our findings demonstrate the importance of ITH as a possible predictor of the outcome of immune action. Our results support the idea that patients with tumours bearing few clonal antigens are expected to be more likely to exhibit a durable benefit from immune response than patients with heterogeneous tumours characterised by many different sub-clonal antigens [150]. On the other hand, our results disbelieve the fact that highly heterogeneous tumours, characterised by the expression of many different antigens, can enhance the efficacy of immune response. In fact, our results indicate that excessive antigen heterogeneity may, conversely, actively impair anti-tumour CTL immune response. This is also supported by a recent clinical work which found that excessive mutagenesis, directed to enhance the tumour mutational burden, may decrease the efficacy of immunotherapy [223].

3.6.2 Research perspectives

The current version of our model can be developed further in several ways. We could incorporate extended aspects of the tumour micro-environment, such as the expression of immunosuppressive factors (*e.g.* PD1 or CTLA4), which affect the effectiveness of anti-tumour immune response. In fact, these inhibitory factors induce the exhaustion of CTLs in the tumour micro-environment impairing the immune response [109, 219]. The inclusion of CTL exhaustion caused by inhibitory factors could give further explanations for other mechanisms of immune escape. The exhaustion mechanism could be included in the model by, for example, altering the value of the parameter governing the efficiency of the CTL population in eliminating tumour cells.

The spatial dimension and the flexibility of our model would also allow for the study of the spatial distribution of CTLs within the tumour and the role of immune infiltration on the tumour dynamics [70]. Moreover, by posing the model on a 3D domain, a deeper understanding of the spatial dynamics of tumour-immune interactions could be achieved.

All results we have reported on were obtained by averaging over the results of 10 realisations, in order to present in a synthetic way the outcomes of our model which includes inherent

stochastic variations. When the standard deviation between these 10 realisations was relatively small, we presented the results of these realisations along with the mean and the standard deviation. This is the case of the results displayed in Figures 3.3, 3.4, 3.7, 3.9 and part of Figure 3.6. When the standard deviation was relatively large, we presented the results of each realisation individually (*cf.* Figure 3.8). This allowed us to investigate the different emerging behaviours of our stochastic model. Moreover, in order to check the robustness of the results, for one simulation that had a relatively large standard deviation (*tumour-7a* in Figure 3.6), we reported on the results of 100 realisations of this simulation (*cf.* Figure C.1). We observed that the overall dynamics of the 100-realisation case were qualitatively similar to those of the 10-realisation case. Consistency analysis would be another option to establish the number of replicate runs needed to obtain a desired level of numerical robustness. This could be performed using, for example, the tool presented in [4].

We managed to estimate some parameters of the model (see Table (C.1) and Table (C.2)) from the literature and define them on the basis on precise biological assumptions. However, there are some parameters (*e.g* r, C_1, C_2 and the parameters related to the chemoattractants) whose values were simply chosen with an exploratory aim and to qualitatively reproduce essential aspects of the experimental results obtained in [223]. In order to minimise the impact of this limitation on the conclusions of our study, we carried out simulations by keeping all parameter values fixed and changing only the initial composition of the tumours, and then comparing the simulation results so obtained.

Finally, from a modelling point of view, although more tailored to capture fine details of the dynamics of single cells, individual-based models are not amenable to analytical studies, which may support a more in-depth theoretical understanding of the application problems under study. For this reason, in future work we plan to derive a continuum model from a simplified version of our individual-based model by using mean filed methods similar to those employed in [13, 40, 166].

In its present form, our modelling framework qualitatively reproduces scenarios of successful and unsuccessful immune surveillance reported in experimental studies [80, 150] and [223]. However, at this stage, the model has not been calibrated using any particular type of data. Hence, it cannot be employed to generate predictions that can directly be used in the clinic. By fitting its parameters to a specific type of clinical data, our model could, in principle, be used to assess different levels of ITH as potential biomarkers for comparing and predicting outcomes in tumour immunotherapy treatments. Integrating the model with tumour biopsies from patients could offer insight into potential outcomes of treatments. Finally, our model may be a promising tool to explore therapeutic strategies designed to decrease tumour heterogeneity and improve the overall anti-tumour immune response.

Chapter 4

A hybrid discrete-continuum modelling approach to explore the impact of T cell infiltration on anti-tumour immune response

4.1 Motivation

Individual-based models track the dynamics of single cells, thus permitting the representation of single cell-scale mechanisms, and account for possible stochastic fluctuations in single-cell biophysical properties. However, they can be computationally time consuming and do not allow for analysis to be completed on the model. Considering the continuum counterpart of our stochastic discrete individual-based model developed in Chapter 3 would allow us to carry out numerical simulations that require computational times smaller than those required by the numerical exploration of the individual-based model.

In the mathematical model developed in Chapter 3, cells grow, die and interact, and we characterized antigen presentation levels by tumour cells, which drive the influx of CTLs in the tumour micro-environment and their movement toward tumour cells. In our study, we used a Cellular Potts model and the CompuCell3D open-source simulation environment. Due to the complexity of the modelling approach used in the previous chapter, the derivation of a continuum version of this model would be potentially challenging. The derivation of a continuum description from Cellular Potts model has been studied in [2, 3, 137]. These works of increasing complexity studied, both in 1D and 2D, the continuous limit of Cellular Potts models describing the motion of an homogeneous cell population in a medium and in the presence of an external field with contact cell-cell interactions. Moreover, in [137] the finite size of cells in the Cellular Potts model was taken into account, using exclusion volume principle (meaning that two cells can not occupy the same volume). However, these models did not consider many of the biological aspects included in the modelling framework developed in Chapter 3, such as cell growth and mitosis, cell death, interactions between cells of different types, etc. Therefore, these methods may not be applicable for deriving the continuum counterpart of our stochastic discrete individual-based model developed in Chapter 3.

Therefore, in this chapter we start by considering a simpler model of tumour-immune inter-

actions. In this work, we present a spatial hybrid discrete-continuum modelling framework for the interaction dynamics between tumour cells and CTLs. Building on the modelling strategies developed in the previous chapter, in this framework, a stochastic individual-based model for the dynamics of tumour cells and CTLs is coupled with a balance equation for the concentration of a chemoattractant, which dictates the movement of CTLs towards the tumour. In order to take into account possible alterations in the infiltration capabilities of CTLs within the tumour, we let the probability of CTL movement be modulated by a decaying function of the densities of tumour cells and CTLs

We formally derive the deterministic continuum counterpart of this model, which is given by a coupled system that comprises an integro-differential equation for the density of tumour cells, a partial differential equation for the density of CTLs, and a partial differential equation for the concentration of chemokines.

We report on computational results of the hybrid model and show that there is an excellent quantitative agreement between them and numerical solutions of the corresponding continuum model. These results shed light on the mechanisms that underlie the emergence of different levels of infiltration of CTLs into the tumour and elucidate how CTL infiltration shapes anti-tumour immune response. Moreover, exploiting the computational efficiency of the continuum model, we carry out extensive numerical simulations to investigate the impact of CTL infiltration on the response of tumour cells to different types of anti-cancer immunotherapy.

The model described in this chapter and the results shown have been published in Luis Almeida, Chloe Audebert, E. L. and Tommaso Lorenzi, *A hybrid discrete-continuum modelling approach to explore the impact of T-cell infiltration on anti-tumour immune response*, Bulletin of mathematical biology, 2022.

4.2 Background

4.2.1 Biological background

Experimental and clinical evidence indicates that the immune system plays a critical role in the prevention and eradication of tumours, by detecting immunogenic tumour cells through mutational or abnormally expressed genes and mounting an adaptive immune response [45]. In an efficient immune response, cytotoxic T lymphocytes (CTLs), are activated in secondary lymphoid organs draining the tumour site. Then, these CTLs migrate to the tumour micro-environment (TME) in an attempt to eliminate the tumour [20, 153].

However, a myriad of immunosuppressive strategies, the so-called immune checkpoints, help tumour cells acquiring features that allow them to evade immune detection, which may ultimately result in tumour escape. One important route towards this escape is created as tumour cells hijack the regulatory pathways of the immune system to suppress its functionality [178]. The programmed cell death protein-1 (PD1) and its ligand PD-L1 are amongst these inhibitory pathways [95, 105]. Under protracted immune stress, PD-L1 expression can be induced on tumour cells, leading to CTL exhaustion and resistance to anti-tumour immune action in many cancers, such as melanoma [193, 221] and non-small cell lung cancer (NSCLC) [150]. Moreover, the engagement of various oncogenic pathways results in the expression of cytokines and chemokines that mediate the exclusion of CTLs from the TME [114] or, alternatively, the repression of factors that facilitate CTL trafficking and infiltration into the tumour [193]. In this context, the design of immune checkpoint therapies which target regulatory pathways in CTLs to enhance anti-tumour immune responses may be beneficial to the treatment of multiple types of cancer [95, 114, 181].

The observation that type, density and location of immune cells within the tumour may be associated with prognosis in different types of cancer led to the development of the 'immunoscore' as a prognostic marker in cancer patients [10, 70, 72, 71]. The immunoscore provides a score that increases with the density of CD8+ and CD3+ CTLs both in the centre and at the margin of the tumour. In this vein, a new immune-based, rather than a cancer-based, classification of tumours that relies on the immunoscore has been proposed in [72], where the authors have classified tumours in four categories. The "hot" category comprises tumours which are highly infiltrated by CTLs and thus have a high immunoscore. The category "altered-immunosuppressed" is for tumours with a small amount of infiltrated CTLs. Tumours in the "altered-excluded" category are characterised by two different regions: their margin is T cell-infiltrated while the centre is not. Tumours in these two categories have an intermediate immunoscore. Finally, "cold" tumours have a low immunoscore and are often associated with a poor response to immunotherapies, since CTLs are absent both in the centre of the tumour and at its margin.

4.2.2 The mathematical model

In this chapter, we develop a spatial hybrid discrete-continuum model for the interaction dynamics between tumour cells and CTLs. In this framework, a stochastic individual-based model tracking the dynamics of single tumour cells and CTLs is coupled with a balance equation for the concentration of chemokines (*e.g.* CXCL9/10) which are secreted by tumour cells and drive the chemotactic movement of CTLs towards the tumour [70, 88].

In this model, cell dynamics are governed by a set of rules that result in a discrete-time branching random walk on a regular lattice [104]. Using methods similar to those we have previously employed in [6, 26, 138], we formally derive the deterministic continuum counterpart of the hybrid model, which is given by a coupled system that comprises an IDE for the density of tumour cells, a PDE for the density of CTLs, and a PDE for the concentration of chemokines. We report on computational results of the hybrid model and show that there is an excellent quantitative agreement between them and numerical solutions of the corresponding continuum model. These results shed light on the mechanisms that underlie the emergence of different levels of infiltration of CTLs into the tumour and elucidate how CTL infiltration shapes anti-tumour immune response. Moreover, exploiting the computational efficiency of the continuum model, we carry out extensive numerical simulations to investigate the impact of CTL infiltration on the response of tumour cells to different types of anti-cancer immunotherapy.

4.2.3 Structure of the chapter

The chapter is organised as follows. In Section 4.3, the hybrid discrete-continuum model is introduced. In Section 4.4, the deterministic continuum counterpart of this model is presented (a formal derivation is provided in Appendix D.1). In Section 4.5, computational results of the hybrid model are discussed and integrated with numerical solutions of the continuum model. In Section 4.6, biological implications of the main findings of this study are summarised and directions for future research are outlined.

4.3 Hybrid discrete-continuum model

In our model, each cell is seen as an agent that occupies a position on a lattice, while the concentration of chemokines, to which we will refer as "chemoattractant" in the remainder of the chapter, is described by a discrete, non-negative function. Each tumour cell can proliferate or die at certain rates. In the vein of [14, 127, 139], here we focus on tumours in the early stages

of development (*i.e.* small pre-angiogenic tumours) and, therefore, we neglect the effects of the movement of tumour-cell. As similarly done in [14], we let the chemoattractant be secreted by tumour cells and undergo both natural decay and linear diffusion. CTLs enter the spatial domain where the tumour is located through blood vessels at a rate that is proportional to the total amount of chemoattractant. Upon entering the domain, CTLs undergo undirected, random movement and chemotactic movement towards regions of higher concentration of the chemoattractant (*i.e.* cells migrate towards the tumour), and exert a cytotoxic action against tumour cells.

For ease of presentation, we let the cells and the chemoattractant be distributed across a d-dimensional domain Ω, with $d = 1$ or $d = 2$. In particular, we consider the case where the spatial domain is represented by the set $\Omega := [0, \ell]^d$, with $\ell \in \mathbb{R}_+^*$, where $\mathbb{R}_+^*$ is the set of positive real numbers not including zero. The position of the cells and the molecules of chemoattractant at time $t \in \mathbb{R}_+$ is modelled by the variable $x \in [0, \ell]$ when $d = 1$ and by the vector $\mathbf{x} = (x, y) \in [0, \ell]^2$ when $d = 2$.

We discretise the time variable t as $t_k = k\tau$ with $k \in \mathbb{N}_0$ and the space variables x and y as $x_i = i\chi$ and $y_j = j\chi$, with $(i, j) \in [0, \mathcal{N}]^2 \subset \mathbb{N}_0^2$, where $\tau \in \mathbb{R}_+^*$ and $\chi \in \mathbb{R}_+^*$ are the time- and space-step, respectively, and $\mathcal{N} := 1 + \lceil \frac{\ell}{\chi} \rceil$, where $\lceil \cdot \rceil$ denotes the ceiling function. Here, $\mathbb{N}_0$ is the set of natural numbers including zero. Throughout this section we use the notation $\mathbf{i} \equiv i$ and $\mathbf{x_i} \equiv x_i$ when $d = 1$, and $\mathbf{i} \equiv (i, j)$ and $\mathbf{x_i} \equiv (x_i, y_j)$ when $d = 2$.

We denote by $n_{\mathbf{i}}^k$ the density of tumour cells, which is defined as the number of tumour cells at position $\mathbf{x_i}$ and at time t_k, $N_{\mathbf{i}}^k \in \mathbb{N}_0$, divided by the size of a lattice site, that is

$$n_{\mathbf{i}}^k \equiv n(\mathbf{x_i}, t_k) := \frac{N_{\mathbf{i}}^k}{\chi^d}. \tag{4.1}$$

Furthermore, we denote by $c_{\mathbf{i}}^k$ the density of CTLs, which is defined as the number of CTLs at position $\mathbf{x_i}$ and at time t_k, $C_{\mathbf{i}}^k \in \mathbb{N}_0$, divided by the size of a lattice site, that is

$$c_{\mathbf{i}}^k \equiv c(\mathbf{x_i}, t_k) := \frac{C_{\mathbf{i}}^k}{\chi^d}. \tag{4.2}$$

Finally, the concentration of chemoattractant on the lattice site $\mathbf{i}$ and at time-step k is modelled by the discrete, non-negative function $\phi_{\mathbf{i}}^k \equiv \phi(\mathbf{x_i}, t_k)$.

In the mathematical framework of our model, the quantity

$$I^k \equiv I(t_k) := \frac{|\Omega_\mathrm{c}|}{|\Omega_\mathrm{tum}|} I_{\Omega_\mathrm{c}}(t_k) + \frac{|\Omega_\mathrm{m}|}{|\Omega_\mathrm{tum}|} I_{\Omega_\mathrm{m}}(t_k) \tag{4.3}$$

provides a possible simplified measure of the immunoscore I at time t_k. In (4.3), $I_{\Omega_\mathrm{c}} \in \mathbb{N}_0$ is the number of CTLs within the set $\Omega_\mathrm{c} \subset \Omega$ defined as the 'centre of the tumour', $I_{\Omega_\mathrm{m}} \in \mathbb{N}_0$ is the number of CTLs within the set $\Omega_\mathrm{m} \subset \Omega$ defined as the 'margin of the tumour', and $\Omega_\mathrm{tum} = \Omega_\mathrm{c} \cup \Omega_\mathrm{m}$ is the whole region occupied by the tumour. Here, $|(\cdot)|$ is the measure of the set $(\cdot)$. Given the initial distribution of tumour cells, we define (*cf.* Fig 4.1)

$$\Omega_c := \{\mathbf{x_i} \in \Omega : \|\mathbf{x_i} - \mathbf{x_{cm}}\|_d < R\} \quad \text{and} \quad I_{\Omega_\mathrm{c}}(t_k) := \sum_{\mathbf{i}} c_{\mathbf{i}}^k \, \chi^d \, \mathbb{1}_{\Omega_c}(\mathbf{x_i}) \tag{4.4}$$

while

$$\Omega_m := \Omega_\mathrm{tum} \setminus \Omega_c \quad \text{and} \quad I_{\Omega_\mathrm{m}}(t_k) := \sum_{\mathbf{i}} c_{\mathbf{i}}^k \, \chi^d \, \mathbb{1}_{\Omega_m}(\mathbf{x_i}). \tag{4.5}$$

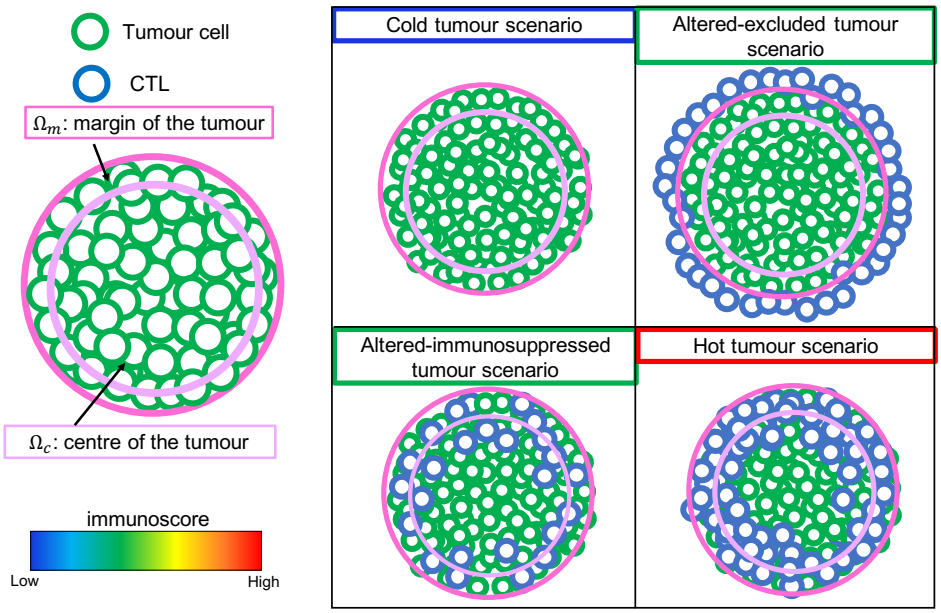

Figure 4.1: **Schematics describing the classification of cold, altered-excluded, altered-immunosuppressed and hot tumour scenarios based on the immunoscore.** In the mathematical framework of our model we classify different tumour scenarios depending on the value of the immunoscore at the end of numerical simulations, *i.e.* the quantity defined via (4.7). The immunoscore is here defined as a weighted sum of the number of CTLs in the centre of the tumour and the number of CTLs in the margin of the tumour. In more detail, following [70], scenarios for which the value of the immunoscore is low will be classified as 'cold tumour scenarios'; scenarios with an intermediate value of the immunoscore will be classified as 'altered tumour scenarios', which will then be further classified as 'altered-immunosuppressed tumour scenarios' or 'altered-excluded tumour scenarios' based on the distribution of CTLs in the centre and at the margin of the tumour; finally, scenarios characterised by a high value of the immunoscore will be classified as 'hot tumour scenarios'.

Here, $\mathbf{x_{cm}} \in \Omega$ is the initial centre of mass of the tumour, which is computed as

$$\mathbf{x_{cm}} = \frac{1}{\rho_n^0} \sum_{\mathbf{i}} n_{\mathbf{i}}^0 \chi^d \mathbf{x_i}, \tag{4.6}$$

where ρ_n^0 is the initial number of tumour cells. Moreover, $\mathbb{1}_{\Omega_m}$ and $\mathbb{1}_{\Omega_c}$ are the indicator functions of the sets Ω_m and Ω_c, respectively. Note that, in the definition of sets Ω_c and Ω_m, we are supposing that the radius R is fixed and, therefore, the two sets do not change over time. This is coherent with the fact that, as mentioned earlier, tumour-cell movement is neglected.

Abstracting from the 'immunoscore'-based classification of tumours recalled in Section 4.2.1, throughout the chapter we will classify different tumour scenarios depending on the value of I at the end of numerical simulations, *i.e.* the quantity

$$I^f \equiv I(t_f) = \frac{|\Omega_\mathrm{c}|}{|\Omega_\mathrm{tum}|} I_{\Omega_\mathrm{c}}(t_f) + \frac{|\Omega_\mathrm{m}|}{|\Omega_\mathrm{tum}|} I_{\Omega_\mathrm{m}}(t_f). \tag{4.7}$$

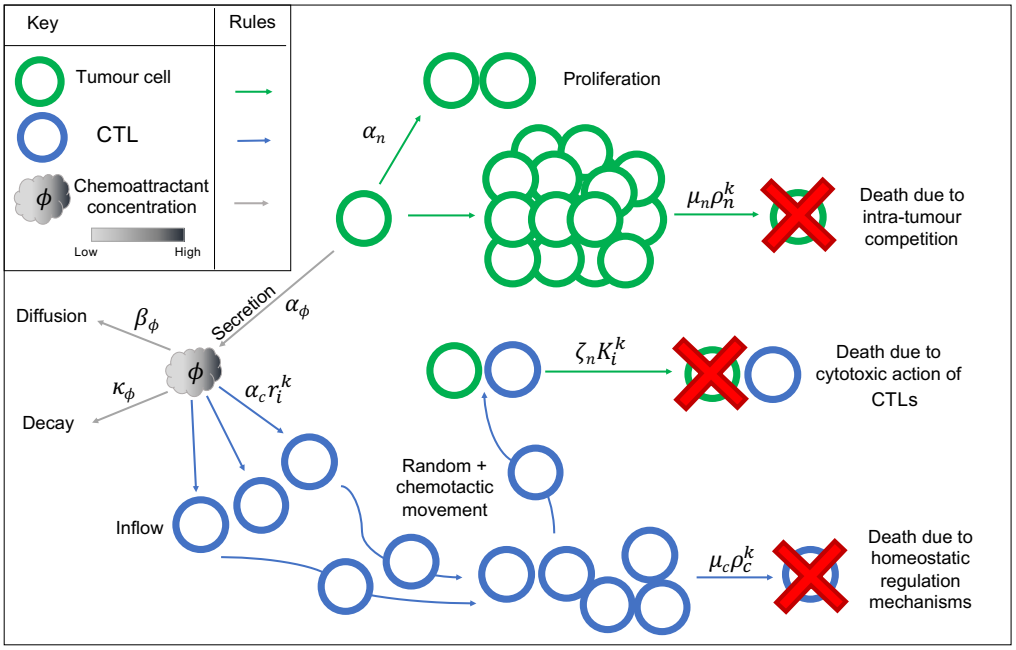

Figure 4.2: **Schematics summarising the mechanisms and processes included in the hybrid discrete-continuum model.** The governing rules for the dynamics of tumour cells are here represented by green solid arrows, the rules for the dynamics of CTLs are represented by blue solid arrows, and the processed underlying the dynamics of the chemoattractant are represented by grey solid arrows. At each time-step t_k, tumour cells divide at rate α_n, die due to intra-tumour competition at rate $\mu_n\rho_n^k$ or die due to the cytotoxic action of CTLs at rate $\zeta_n K_i^k$. The quantities ρ_n^k and K_i^k are, respectively, defined via (4.9) and (4.11). Tumour cells also secrete the chemoattractant at rate α_ϕ. The chemoattractant diffuses through the domain at rate β_ϕ and decays at rate κ_ϕ. CTLs enter the domain at position x_i at rate $\alpha_c r_i^k$, with r_i^k defined via (4.17). CTLs change their position through a combination of undirected, random movement and chemotactic movement in response to the chemoattractant secreted by tumour cells, while tumour cell movement is neglected. Finally, CTLs die due to homeostatic regulation mechanisms at rate $\mu_c\rho_c^k$, with ρ_c^k defined via (4.20).

In particular, scenarios for which the value of I^f is low will be classified as 'cold tumour scenarios'; scenarios with an intermediate value of I^f will be classified as 'altered tumour scenarios', which will then be further classified as 'altered-immunosuppressed tumour scenarios' or 'altered-excluded tumour scenarios' based on the distribution of CTLs at the centre and margin of the tumour; finally, scenarios characterised by a high value of I^f will be classified as 'hot tumour scenarios'. This tumour classification is illustrated by the schematics presented in Fig. 4.1.

The strategies used to model the dynamics of the cells and the chemoattractant when $d = 1$ are described in detail in the following subsections, and are also schematically illustrated in Fig. 4.2. Analogous strategies are used in the case where $d = 2$.

4.3.1 Dynamics of tumour cells

We consider a scenario where tumour cells proliferate (*i.e.* undergo cell division) and die due to intra-tumour competition as well as to the cytotoxic action of CTLs. We assume that a dividing tumour cell is replaced by two identical cells that are placed on the same lattice site as their parent, while a dying cell is removed from the system.

Tumour cell proliferation and death induced by intra-tumour competition

At every time-step k, we allow tumour cells to undergo cell division with probability

$$\tau\alpha_n > 0, \tag{4.8}$$

where $\alpha_n \in \mathbb{R}_+^*$ represents the rate of tumour cell proliferation.

In order to capture the effect of cell death induced by intra-tumour competition, we let tumour cells die at a rate proportional to their number, which is defined as

$$\rho_n^k \equiv \rho_n(t_k) := \sum_i n_i^k \, \chi, \tag{4.9}$$

with constant of proportionality $\mu_n \in \mathbb{R}_+^*$. Hence, between the time-step k and the time-step $k+1$, we let a tumour cell die due to intra-tumour competition with probability

$$\tau \, \mu_n \rho_n^k \geqslant 0. \tag{4.10}$$

Notice that we are implicitly assuming that the time-step τ is sufficiently small that the quantities defined via (4.8) and (4.10) are between 0 and 1.

Cytotoxic action of CTLs against tumour cells

When CTLs are sufficiently close to a tumour cell, they release cytotoxic substances which eventually lead to the death of the tumour cell [20]. Therefore, building on the modelling strategies proposed in [14], we let a tumour cell die due to the cytotoxic action of CTLs at a rate proportional to the number of CTLs in a sufficiently close neighbourhood of the tumour cell. This mimics the fact that CTLs can interact with a tumour cell up to a certain distance, and that beyond such a distance the tumour cell can no longer be induced to death. Hence, we introduce $K_i^k \in \mathbb{N}_0$ which models, at each time-step t_k, the number of CTLs that can exert a cytotoxic action against a tumour cell at position x_i. In particular, we define K_i^k as

$$K_i^k \equiv K(x_i, t_k) := \sum_p \eta(x_i, x_p; \theta) c_p^k \, \chi. \tag{4.11}$$

The function η is defined as follow

$$\eta(x, z; \theta) := \begin{cases} 1 & \text{if} \quad |x - z| \leqslant \theta \\ 0 & \text{if} \quad |x - z| > \theta \end{cases} \qquad \text{for } (x, z; \theta) \in \Omega \times \Omega \times (0, |\Omega|], \tag{4.12}$$

where $|\Omega|$ denotes the size of the set Ω (*i.e.* $|\Omega| = \ell$ if $\Omega := [0, \ell]$). The quantity K_i^k defined via (4.11) and (4.12) represents the number of CTLs at positions x_p at a distance smaller than or equal to θ from x_i. The parameter $0 < \theta \leqslant |\Omega|$ regulates the maximum radius of interaction between a tumour cell at position x_i and the CTLs in its neighbourhood. Therefore, we define

the probability of death of tumour cells at position x_i and time t_k due to the cytotoxic action of CTLs as

$$\tau\zeta_n K_i^k \geqslant 0. \tag{4.13}$$

The parameter $\zeta_n \in \mathbb{R}_+^*$ is linked to the level of efficiency of CTLs at eliminating tumour cells: lower values of ζ_n correspond to scenarios in which this cytotoxic action of CTLs is less effective, due for example to a higher expression of PD1/PD-L1 inhibitory receptors on the surface of CTLs/tumour cells [95, 105].

Remark 2. Note that (4.8), (4.10) and (4.13) implicitly require the time-step τ to be sufficiently small that $\tau\alpha_n + \tau\left(\mu_n\rho_n^k + \zeta_n K_i^k\right)$ is less than or equal to 1.

4.3.2 Dynamics of the chemoattractant

We denote by ϕ_i^k the concentration of chemoattractant at position x_i and at time t_k. The dynamic of ϕ_i^k is governed by the following discrete balance equation

$$\phi_i^{k+1} = \phi_i^k + \tau\beta_\phi(\mathcal{L}\phi^k)_i + \tau\alpha_\phi n_i^k - \tau\kappa_\phi\phi_i^k, \quad (i,k) \in [1, \mathcal{N}-1] \times \mathbb{N}, \tag{4.14}$$

subject to discrete zero-flux boundary conditions, *i.e.*

$$\phi_0^k = \phi_1^k \text{ and } \phi_{\mathcal{N}}^k = \phi_{\mathcal{N}-1}^k, \quad k \in \mathbb{N}. \tag{4.15}$$

In the balance equation (4.14), $\mathcal{L}$ is the second-order central difference operator on the lattice $\{x_i\}_i$, *i.e.*

$$(\mathcal{L}\phi^k)_i = \frac{1}{\chi^2}\left(\phi_{i+1}^k + \phi_{i-1}^k - 2\phi_i^k\right) \tag{4.16}$$

Moreover, the parameter $\beta_\phi \in \mathbb{R}_+^*$ is the diffusion coefficient of the chemoattractant and $\kappa_\phi \in \mathbb{R}_+^*$ is the rate at which the chemoattractant undergoes natural decay. Finally, the parameter $\alpha_\phi \in \mathbb{R}_+^*$ represents the per capita production rate of the chemoattractant by tumour cells. The balance equation (4.14) is simply a standard discretisation of a reaction-diffusion equation of the type that is commonly used to describe the dynamics of molecular species, see for example [141]. Moreover, we will assume that

$$0 < \phi_i^k \leqslant \phi_{\max} \quad \forall\, (i,k) \in [0, \mathcal{N}] \times \mathbb{N}_0$$

for some maximal concentrations $\phi_{\max} \in \mathbb{R}_+^*$ (see comments below definition (4.25)).

4.3.3 Dynamics of CTLs

Following [87], we consider a scenario where CTLs are recruited from different sources corresponding to blood vessels that are located in the tissue surrounding the tumour. CTLs can change their position according to a combination of undirected, random movement and chemotactic movement, which are seen as independent processes. Finally, CTLs can die at a certain rate due to homeostatic regulation mechanisms, and dying cells are removed from the system. This results in the following rules for the dynamics of CTLs.

Inflow and death of T cells

We let $\omega \subset \Omega$ be the set of points in the tissue surrounding the tumour that are occupied by blood vessels, through which new T cells can enter the domain. Since we do not consider the

formation of new blood vessels, we assume that ω is given and does not change in time. We denote by r_i^k the term controlling the inflow of T cells from blood vessels, which is defined as

$$r_i^k \equiv r(x_i, t_k) := \phi_{tot}^k \mathbb{1}_\omega(x_i), \tag{4.17}$$

where $\mathbb{1}_\omega$ is the indicator function of the set ω and ϕ_{tot}^k is the total amount of chemoattractant at time t_k, that is,

$$\phi_{tot}^k \equiv \phi_{tot}(t_k) := \sum_i \phi_i^k \, \chi. \tag{4.18}$$

We then let the influx rate of T cells from blood vessels at position x_i and time t_k be proportional to r_i^k with constant of proportionality $\alpha_c \in \mathbb{R}_+^*$. Hence, between the time-step k and the time-step $k+1$, we let a density of T cells equal to

$$\tau \alpha_c r_i^k \geqslant 0 \tag{4.19}$$

enter a blood vessel at position x_i. Finally, we let T cells die due to homeostatic regulation mechanisms. In analogy with the case of tumour cells, we suppose the rate of death of T cells to be proportional to the number of T cells

$$\rho_c^k \equiv \rho_c(t_k) := \sum_i c_i^k \, \chi, \tag{4.20}$$

with constant of proportionality $\mu_c \in \mathbb{R}_+^*$. Therefore, between the time-step k and the time-step $k+1$, we let a T cell die with probability

$$\tau \mu_c \rho_c^k \geqslant 0. \tag{4.21}$$

Remark 3. Note that (4.21) implicitly requires the time-step τ to be sufficiently small that the corresponding quantity is less than or equal to 1.

Chemotactic movement of CTLs

We now turn to modelling the chemotactic movement of CTLs (i.e. the movement of CTLs up the gradient of the chemoattractant ϕ_i^k). Building on [26], chemotactic movement is here modelled as a biased random walk whereby the movement probabilities depend on the difference between the concentration of chemoattractant at the site occupied by a CTL and the concentration of chemoattractant at the neighbouring sites. To take into account possible reduction in cell motility at high cell densities [165, 189, 225], we incorporate into the model volume-filling effects [167], whereby CTL movement is allowed only to site locations x_i where the total cell density $w_i^k := n_i^k + c_i^k$ is smaller than a threshold value $w_{max} \in \mathbb{R}_+^*$, which corresponds to a cell tight-packing state. Therefore, we modulate the movement probabilities of CTLs by a monotonically decreasing function of the total cell density at the neighbouring sites. Specifically, as similarly done in [217], we define this function as

$$\psi(w_i^k) := \begin{cases} 1 - \dfrac{w_i^k}{w_{max}}, & 0 \leqslant w_i^k \leqslant w_{max}, \\ 0, & \text{otherwise.} \end{cases} \tag{4.22}$$

Hence, for a CTL on the lattice site x_i and at time step t_k, we define:

1. the probability of moving to the lattice site x_{i-1} (*i.e.* the probability of moving left) via

chemotaxis as

$$q_{Li}^k := \nu\,\psi(w_{i-1}^k)\Big(\frac{\phi_{i-1}^k - \phi_i^k}{2\phi_{\max}}\Big)_+ \quad \text{for} \quad i \in [1,\mathcal{N}] \quad \text{and} \quad q_{L0}^k = 0 \tag{4.23}$$

where $(\cdot)_+$ denotes the positive part of $(\cdot)$;

2. the probability of moving to the lattice site x_{i+1} (*i.e.* the probability of moving right) via chemotaxis as

$$q_{Ri}^k := \nu\,\psi(w_{i+1}^k)\Big(\frac{\phi_{i+1}^k - \phi_i^k}{2\phi_{\max}}\Big)_+ \quad \text{for} \quad i \in [0,\mathcal{N}-1] \quad \text{and} \quad q_{R\mathcal{N}}^k = 0; \tag{4.24}$$

3. and the probability of not undergoing chemotactic movement as

$$1 - q_{Li}^k - q_{Ri}^k \quad \text{for} \quad i \in [0,\mathcal{N}]. \tag{4.25}$$

Here, the parameter $\nu \in \mathbb{R}_+$, with $0 \leqslant \nu \leqslant 1$, is directly proportional to the chemotactic sensitivity of CTLs. Moreover, the parameter $\phi_{\max} > 0$ is directly proportional to the maximal value that can be attained by the concentration of chemoattractant. In particular, on the basis of the considerations drawn in [26], we define $\phi_{\max}$ as

$$\phi_{\max} := \max\Big(\max_i \phi_i^0, A\,w_{\max}\Big),$$

where $w_{\max}$ is given by (4.22) and $A > 0$ is a scaling factor that ensures unit consistency. Dividing by $\phi_{\max}$ ensures that the values of the quotients in (4.23)-(4.25) are all between 0 and 1.

Undirected, random movement of CTLs

To model the effect of undirected, random movement, we allow CTLs to update their position according to a random walk with movement probability $\lambda \in \mathbb{R}_+^*$, where $0 < \lambda \leqslant 1$. In particular, we assume that a CTL on the lattice site x_i can move via undirected, random movement into either the lattice site x_{i-1} or the lattice site x_{i+1} with probability $\dfrac{\lambda}{2}$. As similarly done in the case of chemotactic movement, in order to capture a possible reduction in CTL motility at higher cell densities [165, 189, 225], we modulate the movement probability by a decreasing function of the density of tumour cells and CTLs at the neighbouring sites. In particular, for a CTL on the lattice site i and at the time-step k, recalling the notation $w_i^k := n_i^k + c_i^k$ for the total cell density and definition (4.22) of the modulating function $\psi(w_i^k)$, we define:

1. the probability of moving to the lattice site $i-1$ via undirected, random movement as

$$T_{Li}^k := \frac{\lambda}{2}\,\psi(w_{i-1}^k) \quad \text{for} \quad i \in [1,\mathcal{N}] \quad \text{and} \quad T_{L0}^k = 0; \tag{4.26}$$

2. the probability of moving to the lattice site $i+1$ via undirected, random movement as

$$T_{Ri}^k := \frac{\lambda}{2}\,\psi(w_{i+1}^k) \quad \text{for} \quad i \in [0,\mathcal{N}-1] \quad \text{and} \quad T_{R\mathcal{N}}^k = 0; \tag{4.27}$$

3. and the probability of not undergoing undirected, random movement as

$$1 - T_{Li}^k - T_{Ri}^k \quad \text{for} \quad i \in [0,\mathcal{N}]. \tag{4.28}$$

4.4 Corresponding continuum model

Letting the time-step $\tau \to 0$ and the space-step $\chi \to 0$ in such a way that

$$\frac{\lambda \chi^2}{2d\,\tau} \to \beta_c \in \mathbb{R}_*^+ \quad \text{and} \quad \frac{\nu \chi^2}{2d\,\phi_{\max}\,\tau} \to \gamma_c \in \mathbb{R}_*^+, \tag{4.29}$$

using the formal method employed in [6, 26, 138], it is possible to formally show (see Appendix D.1) that the deterministic continuum counterpart of the hybrid model described in Section 4.3 comprises the following coupled IDE-PDE-PDE system for the density of tumour cells $n(\mathbf{x},t)$, the density of CTLs $c(\mathbf{x},t)$ and the chemoattractant concentration $\phi(\mathbf{x},t)$

$$\begin{cases} \partial_t n = \alpha_n n - \mu_n \rho_n(t)\, n - \zeta_n K(\mathbf{x},t) n \\ \\ \partial_t c - \nabla \cdot \Big[\beta_c \psi(w) \nabla c - \gamma_c \psi(w) c \nabla \phi - \beta_c c \psi'(w) \nabla w \Big] = -\mu_c \rho_c(t) c + \alpha_c r(\mathbf{x},t) \\ \\ \partial_t \phi - \beta_\phi \Delta \phi = \alpha_\phi n - \kappa_\phi \phi \\ \\ w(\mathbf{x},t) := n(\mathbf{x},t) + c(\mathbf{x},t), \end{cases} \tag{4.30}$$

where the IDE $(4.30)_1$ is posed on $\Omega \times \mathbb{R}_+^*$, while the PDEs $(4.30)_2$ and $(4.30)_3$ are posed on $\Omega \setminus \partial\Omega \times \mathbb{R}_+^*$ and are subject to zero-flux boundary conditions on $\partial\Omega$. The IDE-PDE-PDE system (4.30) is complemented with the following definitions

$$K(\mathbf{x},t) := \int_\Omega \eta(\mathbf{x},\mathbf{x}';\theta) c(\mathbf{x}',t)\,\mathrm{d}\mathbf{x}', \quad r(\mathbf{x},t) := \phi_{tot}(t) \mathbb{1}_\omega(\mathbf{x})$$

$$\rho_n(t) := \int_\Omega n(\mathbf{x},t)\,\mathrm{d}\mathbf{x}, \quad \rho_c(t) := \int_\Omega c(\mathbf{x},t)\,\mathrm{d}\mathbf{x}, \quad \phi_{tot}(t) := \int_\Omega \phi(\mathbf{x},t)\,\mathrm{d}\mathbf{x}.$$

In system (4.30), $\beta_c \in \mathbb{R}_+^*$ defined via (4.29) is the diffusion coefficient (*i.e.* the motility) of CTLs, while $\gamma_c \in \mathbb{R}_+$ defined via (4.29) is the chemotactic sensitivity of CTLs to the chemoattractant.

4.5 Numerical simulations

In this section, we report on computational results of the hybrid discrete-continuum model along with numerical solutions of the corresponding continuum model given by the IDE-PDE-PDE system (4.30). First, we establish a baseline scenario in which the level of efficiency of CTLs at eliminating tumour cells (*i.e.* the parameter ζ_n) is sufficiently high so as to lead to tumour eradication. Then, we reduce the level of CTL efficiency in order to avoid tumour eradication, and we explore the mechanisms that underlie the emergence of different levels of infiltration of CTLs into the tumour, which correspond to cold, altered-immunosuppressed, altered-excluded and hot tumour scenarios. In particular, we carry out sensitivity analysis to two parameters that we expect to play a key role in determining the spatial distribution of CTLs: the secretion rate of chemoattractant by tumour cells (*i.e.* the parameter α_ϕ) and the threshold value of the total cell density above which CTL movement is impaired (*i.e.* the parameter $w_{\max}$ in definition (4.22)). Finally, we investigate the impact of CTL infiltration on the response of tumour cells to different types of anti-cancer immunotherapy.

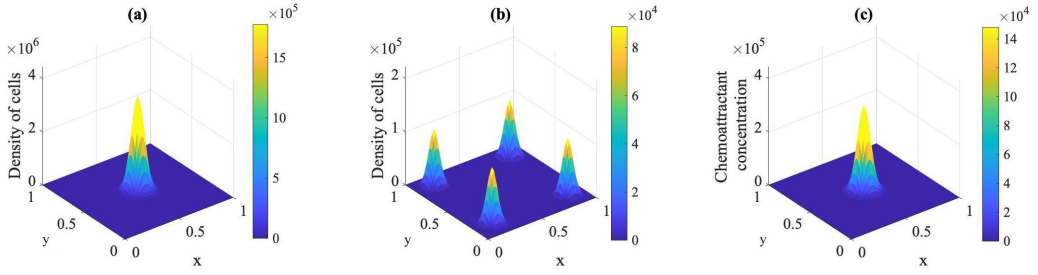

Figure 4.3: **Initial conditions.** Plots of the density of tumour cells $n(x, y, t)$ (panel **(a)**), the density of CTLs $c(x, y, t)$ (panel **(b)**), and the chemoattractant concentration $\phi(x, y, t)$ (panel **(c)**) at the initial time of the simulations (*i.e.* at $t = 0$) for the continuum model. Analogous initial conditions are used for the hybrid model.

4.5.1 Set-up of numerical simulations

The hybrid and continuum models are parameterised using parameter values retrieved from the literature, wherever possible. The full list of parameter values and related references are provided in Table 4.1. For the numerical simulations we report on, we use the 2D spatial domain $\Omega := [0, 1]^2$. Under the parameter choice of Table 4.1, this is equivalent to considering a square region of a 2D cross-section of a tumour tissue of area $1\, cm^2$. Furthermore, to carry out numerical simulations of the hybrid model, we use the space-step $\chi = 0.016$ *cm* and the time-step $\tau = 1 \times 10^{-4}$ *days*. Finally, unless otherwise specified, we choose the final time $t_f = 15$ *days*. All simulations are performed in MATLAB [146].

Initial conditions and blood vessel distribution Fig. 4.3 displays the initial conditions chosen to carry out numerical simulations. In particular, for the hybrid model we have

$$n_{ij}^0 = 800 \exp[-200(i\chi - x_{11}^*)^2 - 200(j\chi - y_{11}^*)^2], \tag{4.31}$$

$$c_{ij}^0 = 60 \sum_{p=1}^{4} \exp[-300(i\chi - x_{2p}^*)^2 - 300(j\chi - y_{2p}^*)^2], \tag{4.32}$$

and

$$\phi_{ij}^0 = 90 \exp[-200(i\chi - x_{11}^*)^2 - 200(j\chi - y_{11}^*)^2], \tag{4.33}$$

with $(x_{11}^*, y_{11}^*) = (0.5, 0.5)$, $(x_{21}^*, y_{21}^*) = (0.26, 0.74)$, $(x_{22}^*, y_{22}^*) = (0.26, 0.26)$, $(x_{23}^*, y_{23}^*) = (0.74, 0.74)$ and $(x_{24}^*, y_{24}^*) = (0.74, 0.26)$. The points where CTLs are initially concentrated are the points where blood vessels are assumed to be located, that is, the set ω in (4.17) is defined as

$$\omega := \{(x_{21}^*, y_{21}^*), (x_{22}^*, y_{22}^*), (x_{23}^*, y_{23}^*), (x_{24}^*, y_{24}^*)\}.$$

Similarly, for the continuum model we have

$$n(x, y, 0) = 800 \exp[-200(x - x_{11}^*)^2 - 200(y - y_{11}^*)^2], \tag{4.34}$$

$$c(x, y, 0) = 60 \sum_{p=1}^{4} \exp[-300(x - x_{2p}^*)^2 - 300(y - y_{2p}^*)^2], \tag{4.35}$$

and

$$\phi(x, y, 0) = 90 \exp[-200(x - x_{11}^*)^2 - 200(y - y_{11}^*)^2]. \tag{4.36}$$

A description of the algorithmic rules that underlie computational simulations of the hybrid model is provided in Appendix D.2.1, while the methods employed to numerically solve the IDE-PDE-PDE system (4.30), subject to suitable initial conditions and no-flux boundary conditions, are detailed in Appendix D.2.2.

Given the initial conditions of the two models, we compute the coordinates of the centre of mass of the tumour $(x_{cm}^*, y_{cm}^*) = (0.5, 0.5)$, and we define the set Ω_c (*i.e.* the 'centre of the tumour') via definition (4.4) as

$$\Omega_c := \left\{ \mathbf{x_i} \equiv (x_i, y_j) \in [0,1]^2 : \sqrt{(x_i - x_{cm}^*)^2 + (y_j - y_{cm}^*)^2} < 0.144 \right\}.$$

The set Ω_c corresponds to approximately 65% of the region initially occupied by the tumour and, therefore, the set $\Omega_m = \Omega \setminus \Omega_c$ (*i.e.* the 'margin of the tumour') comprises the remaining 35% of the tumour region.

Parameter values Unless otherwise specified, we use the parameter values listed in Table 4.1. Here, the value of the parameter α_n is consistent with previous measurement and estimation studies on the dynamics of tumour cells [43], where the authors calculated the estimated proliferation rate of a tumour cell using the average duplication time of melanoma cells. The values of the diffusion coefficient β_ϕ and decay rate κ_ϕ of the chemoattractant correspond to those used in [44, 148]. Moreover, the range of values of the secretion rate α_ϕ is consistent with those used in [14]. To explore a wide range of biological situations corresponding to different degrees of immune infiltration, we use an arbitrary range of values for the parameter $w_{\max}$. Finally, the values of the parameters λ and ν correspond to values of β_c and γ_c that are consistent with those reported in [148] and [14], respectively. Given the values of the parameters β_c and γ_c chosen to carry out numerical simulations of the continuum model, the following definitions are used for the hybrid model

$$\lambda := \beta_c \frac{4\tau}{\chi^2} \quad \text{and} \quad \nu := \gamma_c \frac{4\phi_{\max}\tau}{\chi^2}$$

so that conditions (4.29) are met.

4.5.2 Baseline scenario corresponding to tumour eradication

As mentioned earlier, we first establish a baseline scenario where the parameter ζ_n is high enough so that CTLs are able to eradicate the tumour. The plots in Fig. 4.4 and Fig. 4.5 summarise the results of simulations of the hybrid and continuum models obtained under this scenario.

After initial growth, the number of tumour cells decreases steadily over time until tumour cells are completely eliminated (*cf.* Fig. 4.4). The chemoattractant produced by tumour cells triggers the inflow of CTLs through blood vessels and the movement of CTLs towards the tumour (*cf.* Fig. 4.5). Since the value of ζ_n is sufficiently large, once CTLs are close enough to tumour cells they start eliminating them until eradication (*cf.* Fig. 4.5). When the number of tumour cells decreases, the total amount of chemoattractant decays as well, thus triggering a reduction in the inflow of CTLs, which initiates a decrease in the number of CTLs (*cf.* Fig. 4.4).

Both Fig. 4.4 and Fig. 4.5 indicate that there is an excellent quantitative agreement between numerical solutions of the continuum model (4.30) and the results of numerical simulations of the hybrid model.

Table 4.1: Model parameters and related values used in numerical simulations.

Phenotype	Description	Value & Units	Reference
Domain	Space-step in the x and y direction	$\chi = 0.016\ cm$	
	Time-step	$\tau = 10^{-4}\ (days)$	
	Final time	$t_f = 15\ (days)$	
Tumour cells	Cell density at position $\mathbf{x}$	$n(\mathbf{x}, t) \geqslant 0\ (cells/cm^2)$	
	Initial number	$\rho_n(0) = 45228\ (cells)$	
	Proliferation rate	$\alpha_n = 1.5\ (1/day)$	[43]
	Rate of death due to competition between tumour cells	$\mu_n = 1.25 \times 10^{-5}\ (1/day/cell)$	
	Level of efficiency of CTLs	$\zeta_n \in [0.001, 1]\ (1/day/cell)$	
	Radius of interaction between tumour cells and CTLs	$\theta = 3 \times 0.016\ (cm)$	
CTLs	Cell density at position $\mathbf{x}$	$c(\mathbf{x}, t) \geqslant 0\ (cells/cm^2)$	
	Initial number	$\rho_c(0) = 8960\ (cells)$	
	inflow rate	$\alpha_c = 6\ (cell/cm^2/day/mol)$	
	Chemotactic sensitivity (hybrid model)	$\nu = \gamma_c \frac{4\phi_{\max}\tau}{\chi^2}$	
	Chemotactic coefficient (continuum model)	$\gamma_c = 10\ (cm^2/day/mol)$	[14]
	Random movement prob. (hybrid model)	$\lambda = \beta_c \frac{4\tau}{\chi^2}$	
	Diffusion coefficient (continuum model)	$\beta_c = 1 \times 10^{-3}\ (cm^2/day)$	[148]
	Total cell density above which CTL movement is impaired	$w_{\max} = [0.74 \times 10^5, 8.88 \times 10^5]$ $(cells/cm^2)$	
	Rate of death due to competition between CTLs	$\mu_c = 6 \times 10^{-6}\ (1/day/cell)$	
Chemoattr.	Concentration at position $\mathbf{x}$	$\phi(\mathbf{x}, t) \geqslant 0\ (mol/cm^2)$	
	Total amount	$\phi_{tot}(t) \geqslant 0\ (mol)$	
	Diffusion coefficient	$\beta_\phi = 10^{-1}\ (cm^2/day)$	[148]
	Secretion rate	$\alpha_\phi \in [0.001, 1.5](mol/cell/day)$	[14]
	Decay rate	$\kappa_\phi = 2\ (1/day)$	[44]
	Maximal concentration	$\phi_{\max} = A w_{\max}$, with $A = 1$	

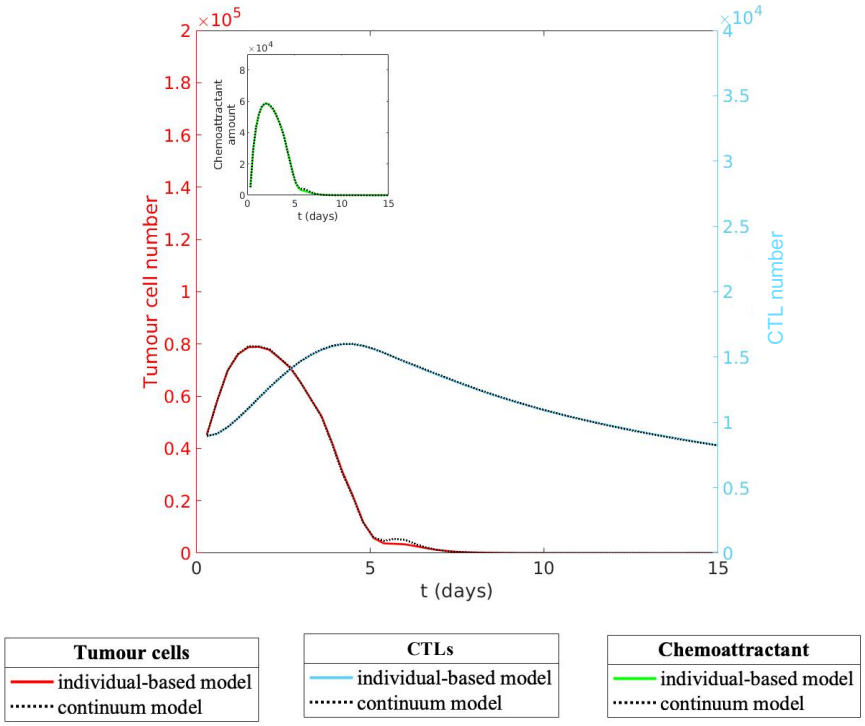

Figure 4.4: **Baseline scenario: evolution of the numbers of tumour cells and CTLs, and the total amount of chemoattractant**. Plots of the time evolution of the number of tumour cells $\rho_n(t)$, the number of CTLs $\rho_c(t)$, and the total amount of chemoattractant $\phi_{tot}(t)$ (in the inset) of the hybrid model (solid, coloured lines) and the continuum model (dotted, black lines) for a choice of parameters that results in the eradication of the tumour. Here, $\zeta_n = 0.004$ and all the other parameters are as in Table 4.1 with $\alpha_\phi = 1.5$ and $w_{\max} = 2.96 \times 10^5$. The results from the hybrid model correspond to the average over three simulations and the related variance is displayed by the coloured areas surrounding the curves.

4.5.3 Emergence of hot, altered and cold tumour scenarios

We now consider a lower value of the parameter ζ_n in order to explore biological scenarios in which the cytotoxic action of CTLs is less effective, for example due to high expression of PD1/PD-L1 inhibitory receptors on the surface of CTLs/tumour cells. As mentioned earlier, we wish to investigate how the spatial distribution of CTLs within the tumour varies depending on the value of the parameters α_ϕ and $w_{\max}$. Therefore, we perform numerical simulations holding all parameters constant but considering different combinations of α_ϕ and $w_{\max}$. For each pair of values considered, we stored the resulting dynamics of the densities of tumour cells and CTLs along with the dynamics of the corresponding cell numbers, and the final value of the immunoscore computed via (4.7). The results obtained are summarised by the heat maps in Fig. 4.6 and the plots in Figs. 4.7-4.11.

Low immunoscore and emergence of cold tumour scenarios As shown by the blue regions on the left side of the two heat maps of Fig. 4.6, for sufficiently small values of α_ϕ,

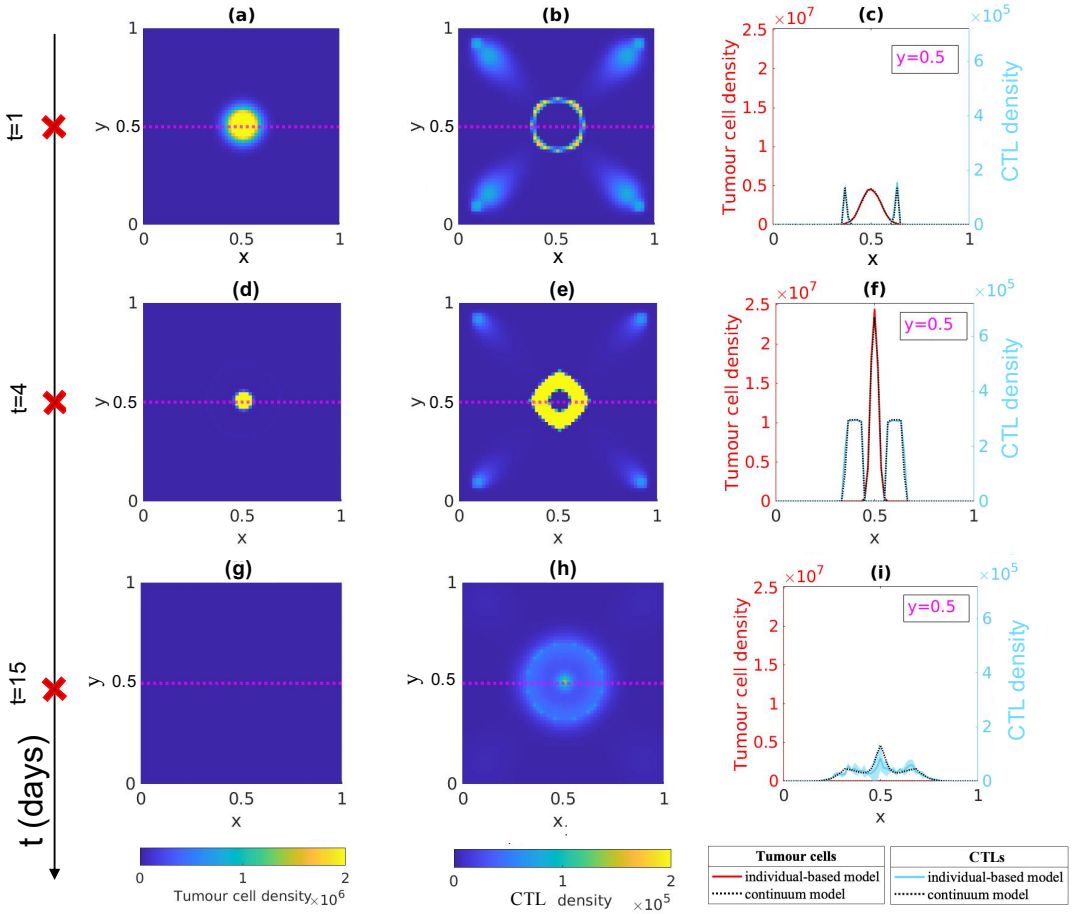

Figure 4.5: **Baseline scenario: evolution of the spatial distributions of cells over time**. Panels **(a)-(d)-(g)** display the plots of the density of tumour cells $n(x, y, t)$ and panels **(b)-(e)-(h)** display the plots of the density of CTLs $c(x, y, t)$ of the continuum model at three successive time instants – *i.e.* $t = 1$, $t = 4$, and $t = 15$. The pink dashed lines highlight the 1D cross-section corresponding to $y = 0.5$. Panels **(c)-(f)-(i)** display the corresponding side on view plot of the densities of tumour cells $n(x, y, t)$ and CTLs $c(x, y, t)$ of the hybrid model (solid, coloured lines) and continuum model (dotted, black lines) (*i.e.* at $y = 0.5$ and $t = 1$, $t = 4$, and $t = 15$). Here, $\zeta_n = 0.004$ and all the other parameters are as in Table 4.1 with $\alpha_\phi = 1.5$ and $w_{\max} = 2.96 \times 10^5$. The results from the hybrid model correspond to the average over three simulations and the related variance is displayed by the coloured areas surrounding the curves.

the immunoscore is relatively low independently of the value of $w_{\max}$. This is due to the small concentration of chemoattractant present in the domain, which poses limitations to the inflow and movement of CTLs towards the tumour. Hence, in the framework of our model, this parameter range corresponds to the emergence of cold tumour scenarios.

Sample dynamics of the numbers and densities of tumour cells and CTLs for the values of α_ϕ and $w_{\max}$ corresponding to the dotted pink square **1** in Fig. 4.6 are displayed in the plots in Fig. 4.7**(a)** and Fig. 4.8. As shown by Fig. 4.7**(a)**, for sufficiently small values of α_ϕ, the total

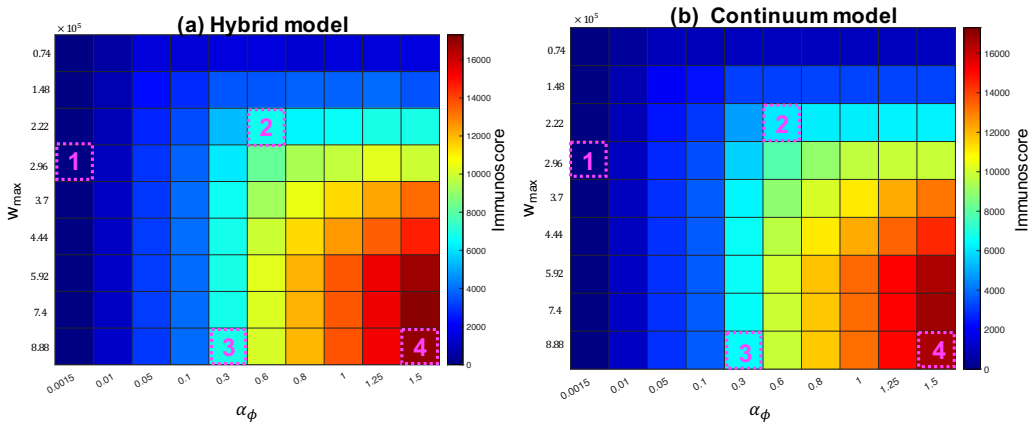

Figure 4.6: **Immunoscore**. The heat map in panel **(a)** displays the value of the immunoscore computed via (4.7) at the end of numerical simulations of the hybrid model for different combinations of α_ϕ and $w_{\max}$. For each given value of α_ϕ and $w_{\max}$, the values of the other parameters are as in Table 4.1, with $\zeta_n = 0.00012$. This heat map matches with the corresponding heat map obtained for the continuum model, which is displayed in panel **(b)**. Sample dynamics of the numbers and densities of tumour cells and CTLs for the values of parameters α_ϕ and $w_{\max}$ corresponding to the dotted pink squares **1-4** are displayed in the plots of Fig. 4.7 and Figs. 4.8-4.11, respectively.

amount of chemoattractant in the domain is too small to trigger a sufficiently high inflow of CTLs that can compensate for the loss caused by CTL death. As a result, the number of CTLs decreases over time. Moreover, there is a shallow gradient of the chemoattractant, which results in a slow movement of CTLs towards the tumour. Therefore, as shown by Fig. 4.8**(b)-(c)**, at the end of simulations, the density of CTLs around the tumour is almost zero and CTLs are still very much concentrated in the proximity of the blood vessels (*i.e.* their entry points).

Intermediate immunoscore and emergence of altered tumour scenarios The light blue regions of the heat maps of Fig. 4.6 indicate that there are two possible parameter ranges giving rise to an intermediate immunoscore. The first one corresponds to intermediate values of α_ϕ along with intermediate to large values of $w_{\max}$, while the second one corresponds to larger values of α_ϕ along with small values of $w_{\max}$. In the framework of our model, altered tumour scenarios emergence under these two parameter ranges.

Sample dynamics of the numbers and densities of tumour cells and CTLs for the values of α_ϕ and $w_{\max}$ corresponding to the dotted pink squares **2** and **3** in Fig. 4.6 are displayed in the plots in Fig. 4.7**(b)-(c)**, Fig. 4.9 and Fig. 4.10. The results of Fig. 4.7**(b)-(c)** show that increasing the value of α_ϕ leads to a progressive increase in the total amount of chemoattractant. This in turn increases the inflow of CTLs and facilitates their movement towards the tumour. The spatial distribution of CTLs within the tumour varies depending on the value of $w_{\max}$. Fig. 4.9 shows that smaller values of $w_{\max}$ lead to an accumulation of CTLs at the margin of the tumour, which corresponds to an altered-excluded tumour scenario. On the other hand, larger values of $w_{\max}$ promote the infiltration of CTLs into the tumour and lead to an altered-immunosuppressed tumour scenario (see Fig. 4.10).

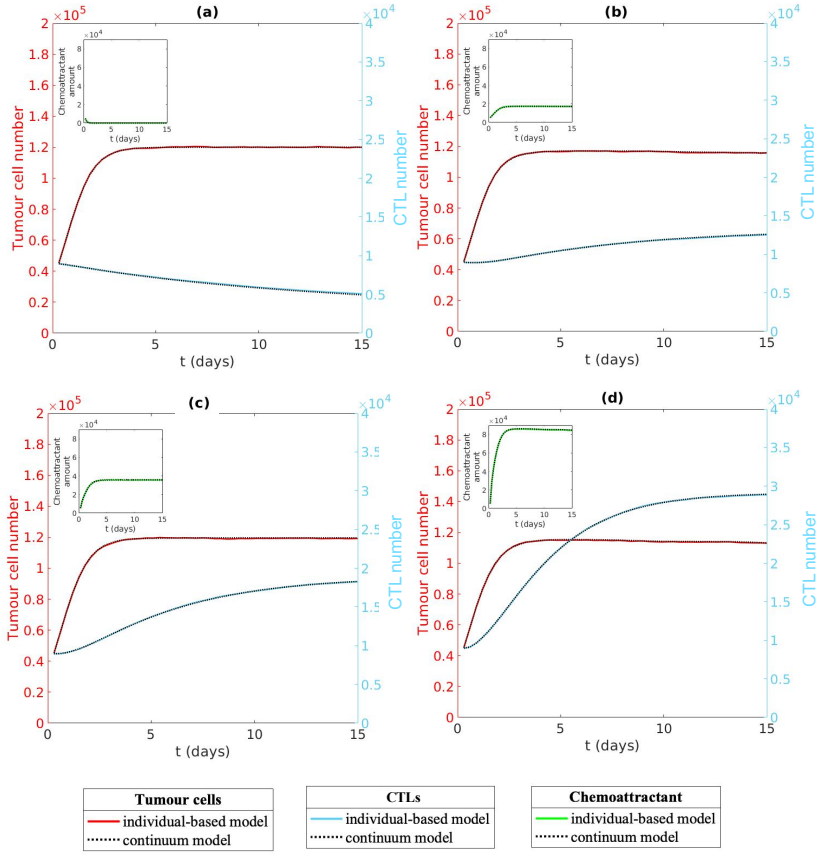

Figure 4.7: **Sample dynamics of the numbers of tumour cells and CTLs in hot, altered-immunosuppressed, altered-excluded and cold tumour scenarios.** Time evolution of the number of tumour cells $\rho_n(t)$, the number of CTLs $\rho_c(t)$, and the total amount of chemoattractant $\phi_{tot}(t)$ (in the insets) of the hybrid model (solid, coloured lines) and the continuum model (dotted, black lines) for values of α_ϕ and $w_{\max}$ corresponding to the dotted pink squares **1-4** of Fig. 4.6. Sufficiently low values of α_ϕ lead to the emergence of cold tumour scenarios (panel **(a)**); intermediate values of α_ϕ and sufficiently high values of $w_{\max}$ lead to the emergence of altered-immunosuppressed tumour scenarios (panel **(b)**); intermediate values of α_ϕ and sufficiently small values of $w_{\max}$ lead to the emergence of altered-excluded tumour scenarios (panel **(c)**); and sufficiently high values of α_ϕ and $w_{\max}$ lead to the emergence of hot tumour scenarios (panel **(d)**). To obtain these results, we used the values of the parameters α_ϕ and $w_{\max}$ corresponding to the dotted pink squares **1** (panel **(a)**), **3** (panel **(b)**), **2** (panel **(c)**), and **4** (panel **(d)**) of Fig. 4.6. All the other parameters are as in Table 4.1, with $\zeta_n = 0.00012$. The results from the hybrid model correspond to the average over three simulations and the related variance is displayed by the coloured areas surrounding the curves.

High immunoscore and emergence of hot tumour scenarios Finally, as shown by the red regions on the bottom-right side of Fig. 4.6, for large values of α_ϕ and $w_{\max}$, the value of the immunoscore is relatively high. In the framework of our model, this parameter range corresponds to the emergence of hot tumour scenarios.

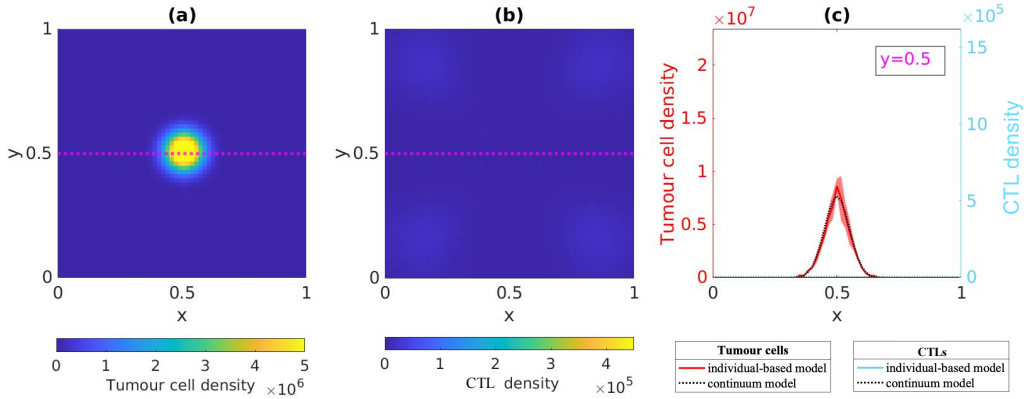

Figure 4.8: **Sample spatial distributions of cells in cold tumour scenarios**. Panels **(a)** and **(b)** display, respectively, the densities of tumour cells $n(x, y, t)$ and CTLs $c(x, y, t)$ of the continuum model at the end of numerical simulations (*i.e.* at $t = 15$) for a choice of parameters that results in the emergence of a cold tumour scenario (*cf.* dotted pink square **1** in Fig. 4.6). The pink dashed line highlights the 1D cross-section corresponding to $y = 0.5$. Panel **(c)** displays the corresponding side on view plot of the densities of tumour cells $n(x, y, t)$ and CTLs $c(x, y, t)$ of the hybrid model (solid, coloured lines) and continuum model (dotted, black lines) (*i.e.* at $y = 0.5$ and $t = 15$). Here, $\zeta_n = 0.00012$, $\alpha_\phi = 0.0015$, $w_{\max} = 2.96 \times 10^5$, and all the other parameters are as in Table 4.1. The results from the hybrid model correspond to the average over three simulations and the related variance is displayed by the coloured areas surrounding the curves.

Sample dynamics of the numbers and densities of tumour cells and CTLs for the values of α_ϕ and $w_{\max}$ corresponding to the dotted pink square **4** in Fig. 4.6 are displayed in the plots in Fig. 4.7**(d)** and Fig. 4.11. When α_ϕ is high enough, the larger amount of chemoattractant promotes the inflow of a larger number of CTLs (see Fig. 4.7**(d)**). Moreover, Fig. 4.11 shows that, similarly to the altered-immunosuppressed tumour scenario, larger values of $w_{\max}$ facilitate the infiltration of CTLs into the tumour. As the number of infiltrated CTLs is larger, the immune action is more efficient than in the previous scenarios, and leads to a slightly decreased number of tumour cells.

Remark 4. Although the specific colours of the regions of the heat maps in Fig. 4.6 can vary according to the values of the other parameters of the model, the behaviours of the spatial distributions of CTLs and tumour cells in the case of hot, altered-immunosuppressed, altered-excluded and cold tumour scenarios remain qualitatively similar to those shown in Figs. 4.8-4.11. Moreover, the heat maps in Fig. 4.6, as well as the plots in Fig. 4.7 and Figs. 4.8**(c)**-4.11**(c)** demonstrate that there is an excellent agreement between numerical simulations of the hybrid and continuum models. This testifies to the robustness of the computational results presented here and the biological insight that they provide.

4.5.4 Immunotheraphy effects

The results presented in the previous subsection summarise how scenarios corresponding to different levels of CTL infiltration into the tumour can emerge under different combinations of the

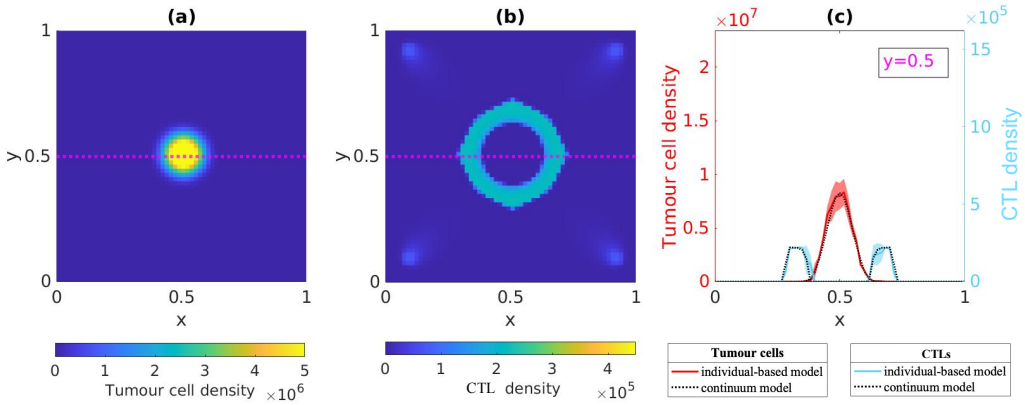

Figure 4.9: **Sample spatial distributions of cells in altered-excluded tumour scenarios**. Panels **(a)** and **(b)** display, respectively, the densities of tumour cells $n(x, y, t)$ and CTLs $c(x, y, t)$ of the continuum model at the end of numerical simulations (*i.e.* at $t = 15$) for a choice of parameters that results in the emergence of a altered-excluded tumour scenario (*cf.* dotted pink square **2** in Fig. 4.6). The pink dashed line highlights the 1D cross-section corresponding to $y = 0.5$. Panel **(c)** displays the corresponding side on view plot of the densities of tumour cells $n(x, y, t)$ and CTLs $c(x, y, t)$ of the hybrid model (solid, coloured lines) and continuum model (dotted, black lines) (*i.e.* at $y = 0.5$ and $t = 15$). Here, $\zeta_n = 0.00012$, $\alpha_\phi = 0.15$, $w_{\max} = 2.22 \times 10^5$, and all the other parameters are as in Table 4.1. The results from the hybrid model correspond to the average over three simulations and the related variance is displayed by the coloured areas surrounding the curves.

values of the parameters α_ϕ and $w_{\max}$. We now investigate possible outcomes of immunotheraphy in these different scenarios.

In order to do this, we consider the same parameter settings used for the numerical simulations of Fig. 4.6, but now we allow the level of efficiency of CTLs at eliminating tumour cells to be higher (*i.e.* we increase the value of ζ_n). This corresponds to a biological scenario in which the tumour is treated with anti-PD1 monotherapy, which restores immune efficacy [204]. We also investigate the effects of coupling anti-PD1 therapy with two other therapies. First we explore the effects of anti-PD1 therapy in combination with another immune checkpoint therapy, *i.e.* the anti CTLA-4 therapy [211]. To do so, we perform numerical simulations defining all parameters as in the case of the anti-PD1 therapy but increasing the rate of inflow of CTLs through blood vessels (*i.e.* the value of the parameter α_c). Then, we explore the effects of combining anti-PD1 therapy with chemotherapy, which inhibits tumour cell division, inflames the TME with tumour antigens, and boosts the activation of CTLs [70]. To do so, we perform numerical simulations defining all parameters as in the scenario of the anti-PD1 therapy but decreasing the proliferation rate of tumour cells (*i.e.* the value of the parameter α_n) and increasing the rate of inflow of CTLs through blood vessels (*i.e.* the value of the parameter α_c). The results obtained are displayed in Fig. 4.12, which shows a comparison between the numbers of tumour cells at the end of numerical simulation in the scenario "without treatment" (*i.e.* with the parameter values considered in Section 4.5.3) and the three aforementioned scenarios in which the effects of different therapeutic protocols are considered.

Exploiting the excellent agreement between the results of numerical simulations of the hybrid

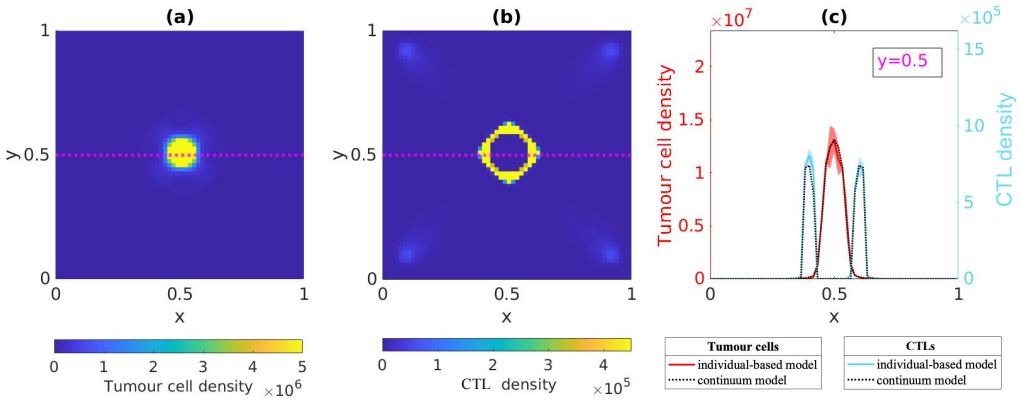

Figure 4.10: **Sample spatial distributions of cells in altered-immunosuppressed tumour scenarios**. Panels **(a)** and **(b)** display, respectively, the densities of tumour cells $n(x, y, t)$ and CTLs $c(x, y, t)$ of the continuum model at the end of numerical simulations (*i.e.* at $t = 15$) for a choice of parameters that results in the emergence of a altered-immunosuppressed tumour scenario (*cf.* dotted pink square **3** in Fig. 4.6). The pink dashed line highlights the 1D cross-section corresponding to $y = 0.5$. Panel **(c)** displays the corresponding side on view plot of the densities of tumour cells $n(x, y, t)$ and CTLs $c(x, y, t)$ of the hybrid model (solid, coloured lines) and continuum model (dotted, black lines) (*i.e.* at $y = 0.5$ and $t = 15$). Here, $\zeta_n = 0.00012$, $\alpha_\phi = 0.15$, $w_{\max} = 8.88 \times 10^5$, and all the other parameters are as in Table 4.1. The results from the hybrid model correspond to the average over three simulations and the related variance is displayed by the coloured areas surrounding the curves.

and continuum models presented in the previous subsections, here we carry out the numerical simulations of the continuum model only, since they require computational times much smaller than those required by the numerical exploration of the corresponding hybrid model. Moreover, to obtain these results, we carried out numerical simulations only for 10 days, *i.e.* $t_f = 10$.

Anti-PD1 monotherapy Fig. 4.12**(b)** displays the number of tumour cells at the end of numerical simulations of the continuum model for parameter settings corresponding to anti-PD1 monotherapy (*i.e.* when only the value of ζ_n in increased). Comparing these results with those displayed in Fig. 4.12**(a)**, we see that, in general, for the same values of parameters α_ϕ and $w_{\max}$, increasing the value of ζ_n leads to a decrease in the numbers of tumour cells at the end of simulations. However, when the value of α_ϕ is too small (*i.e.* in cold tumour scenarios) or when the value of $w_{\max}$ is too small (*i.e.* in altered-excluded tumour scenarios), increasing ζ_n has no benefit on the action of CTLs against tumour cells. Finally, when the values of α_ϕ and $w_{\max}$ are sufficiently large (*i.e.* in hot tumour scenarios) anti-PD1 monotherapy is more effective.

Anti-PD1-CTLA4 dual therapy Fig. 4.12**(c)** displays the number of tumour cells at the end of numerical simulations of the continuum model for parameter settings corresponding to anti-PD1-CTLA4 dual therapy (*i.e.* when both the value of ζ_n and the value of α_c are increased). Comparing these results with those displayed in Fig. 4.12**(b)**, we see that increasing the value of α_c along with the value of ζ_n improves immune efficacy only when the values of α_ϕ and $w_{\max}$ are large enough (*i.e.* in hot tumour scenarios). Moreover, for intermediate values of α_ϕ (*i.e.*

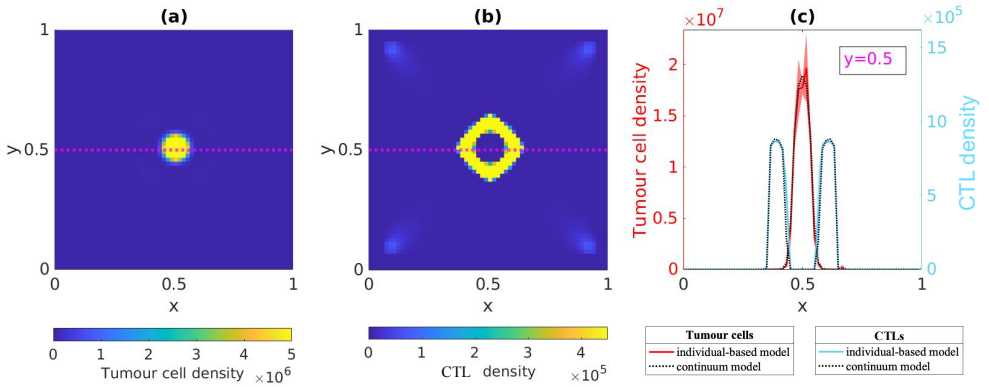

Figure 4.11: **Sample spatial distributions of cells in hot tumour scenarios**. Panels **(a)** and **(b)** display, respectively, the density of tumour cells $n(x, y, t)$ and CTLs $c(x, y, t)$ of the continuum model at the end of numerical simulations (*i.e.* at $t = 15$) for a choice of parameters that results in the emergence of a hot tumour scenario (*cf.* dotted pink square **4** in Fig. 4.6). The pink dashed line highlights the 1D cross-section corresponding to $y = 0.5$. Panel **(c)** displays the corresponding side on view plot of the densities of tumour cells $n(x, y, t)$ and CTLs $c(x, y, t)$ of the hybrid model (solid, coloured lines) and continuum model (dotted, black lines) (*i.e.* at $y = 0.5$ and $t = 15$). Here, $\zeta_n = 0.00012$, $\alpha_\phi = 1.5$, $w_{\max} = 8.88 \times 10^5$, and all the other parameters are as in Table 4.1. The results from the hybrid model correspond to the average over three simulations and the related variance is displayed by the coloured areas surrounding the curves.

in altered-immunosuppressed tumour scenarios), increasing the value of α_c slightly decreases the number of tumour cells at the end of simulations. Finally, when the values of α_ϕ or $w_{\max}$ are too small, increasing α_c has no benefit on the action of CTLs against tumour cells.

Chemotherapy combined with anti-PD1 therapy Fig. 4.12**(d)** displays the number of tumour cells at the end of numerical simulations of the continuum model for parameter settings corresponding to chemotherapy in combination with anti-PD1 therapy (*i.e.* when the value of α_n is decreased and the values of ζ_n and α_c are increased). Compared to the other heat maps of Fig. 4.12, these results show that the number of tumour cells decreases even for small values of α_ϕ or $w_{\max}$. Moreover, when the values of α_ϕ or $w_{\max}$ are small (*i.e.* in cold and altered-excluded tumour scenarios), the numbers of tumour cells at the end of simulations are similar. On the other hand, from intermediate to large values of α_ϕ and $w_{\max}$, the numbers of tumour cells at the end of simulation decrease as the values of these two parameters increase. As expected, the larger the values of α_ϕ and $w_{\max}$ (*i.e.* the "hotter" the tumour scenario considered), the more effective the combined action of chemotherapy and anti-PD1 therapy.

4.6 Discussion, conclusions and research perspectives

4.6.1 Discussion and conclusions

In this chapter, we have developed a hybrid discrete-continuum modelling framework for the interactions between tumour cells and cytotoxic T lymphocytes, which explicitly takes into ac-

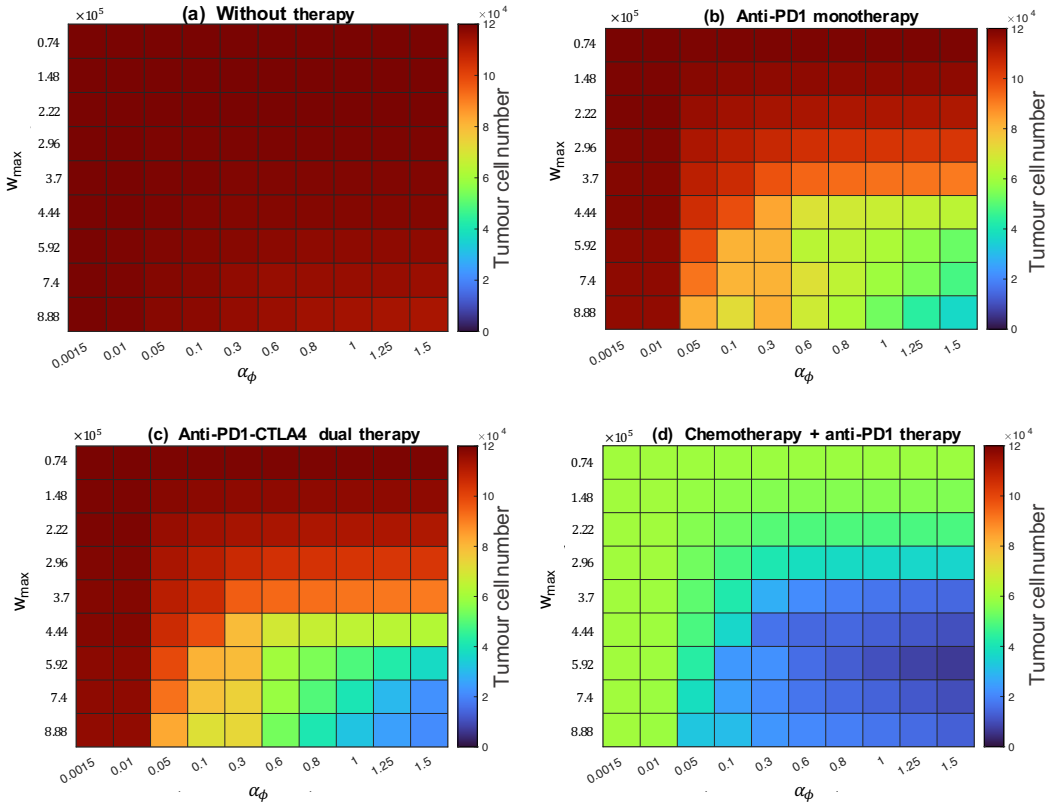

Figure 4.12: **Immunotherapy effects**. Comparison between the numbers of tumour cells $\rho_n(t)$ at the end of simulations (*i.e.* at $t = 10$) of the continuum model for different values of α_ϕ and $w_{\max}$ without therapy (panel **(a)**) and when the effects of different immunotherapies are incorporated by considering different values of the parameters ζ_n, α_c and α_n (panel **(b)-(d)**. In panel **(a)**, $\zeta_n = 0.00012$ and the values of the other parameters are as in Table 4.1. In panel **(b)**, $\zeta_n = 0.001$ and the values of the other parameters are as in Table 4.1. In panel **(c)**, $\zeta_n = 0.001$, $\alpha_c = 12$ and the values of the other parameters are as in Table 4.1. In panel **(d)**, $\zeta_n = 0.001$, $\alpha_c = 12$, $\alpha_n = 0.75$ and the values of the other parameters are as in Table 4.1.

count the spatial dynamics leading to infiltration of CTLs into the tumour. We used a discrete mass-balance equation for the evolution of a chemoattractant, which drives the movement of CTLs towards the tumour, while cell dynamics were described by stochastic individual-based models. From our hybrid model, a continuum model comprising a PDE for the CTL density, an IDE for the tumour cell density and a PDE for the concentration of chemoattractant has been formally derived. Through comparison of both models we found that the results of computational simulations of the hybrid model faithfully mirror the qualitative properties of the solutions to the corresponding continuum model. The results of computational simulations of the hybrid model, which are in excellent agreement with numerical solutions of the continuum model, shed light on the way in which different parameters affect the spatial distribution of CTLs within the tumour and allow us to assess the impact of CTL infiltration on the immune response against tumours.

The results that we have presented demonstrate that the level of efficiency of CTLs at eliminating tumour cells (*i.e.* the parameter ζ_n) plays a key role in tumour-immune competition. In fact, when the value of ζ_n is large enough, our results indicate that tumour eradication can occur, while lower values of ζ_n may result in tumour cell survival. This is consistent with experimental and clinical data which point to a key role of immune check-points in immunosuppressing CTL responses. In fact, the presence of immunosuppressive components in the TME, such as PD-1 and/or PD-L1 inhibitory receptors, decreases the efficiency of CTLs at eliminating tumour cells, and can ultimately result in tumour escape [102, 208].

Moreover, our numerical results indicate that when tumour eradication does not occur (*i.e.* when the value of ζ_n is sufficiently small), the secretion rate of the chemoattractant by tumour cells (*i.e.* the parameter α_ϕ) and the threshold value of the total cell density above which CTL movement is impaired (*i.e.* the parameter $w_{\max}$) have a strong impact on the level of infiltration of CTLs into the tumour, and different combinations of the values of these parameters bring about the emergence of four immune-based tumour scenarios. Hot tumour scenarios emerge for high values of α_ϕ and $w_{\max}$, and are characterised by a large number of CTLs in the centre of the tumour. By displaying a high degree of CTL infiltration, these tumours provide a fertile ground for immune checkpoint therapies. Altered tumour scenarios emerge for intermediate values of α_ϕ, and reflect the intrinsic ability of the immune system to effectively mount a CTL -mediated immune response and the ability of tumour cells to partially escape such a response. This can either be due to an insufficient number of infiltrated CTLs (the immunosuppressed tumour scenarios, which emerge for intermediate to large values of $w_{\max}$) or to the presence of physical barriers that hinder CTL infiltration (the excluded tumour scenarios, which emerge for small values of $w_{\max}$). Finally, cold tumour scenarios emerge for sufficiently small values of α_ϕ and $w_{\max}$. These tumours are characterised by an insufficient number of CTLs both in the centre of the tumour and at its margin, and are invariably associated with poor prognosis.

We also explored how the outcomes of different immunotherapy protocols can vary in these four immune-based tumour scenarios. In particular, our results suggest that increasing the level of efficiency of CTLs (*i.e.* the value of the parameter ζ_n), which is associated to the effects of anti-PD1 monotherapy, is not sufficient for treating all types of tumour scenarios, and it is particularly ineffective in altered-excluded and cold tumour scenarios. This finding is coherent with experimental observations indicating that anti-PD1 monotherapy is effective only in the context of hot or altered-immunosuppressed tumours, as a certain number of CTLs is already infiltrated into the tumour [70].

Moreover, the results of our model indicate that, in these two categories of tumours, increasing both the level of efficiency of CTLs and their rate of inflow (*i.e.* the value of the parameters ζ_n and α_c), which are associated with the combined effects of anti-PD1 and anti-CTLA4 therapy, may lead to a better therapeutic outcome. This conclusion is also supported by experimental work showing that anti-PD1-CTLA4 dual therapy may be successful in treating advanced-stage melanoma [222], renal-cell carcinoma [156] and non-small-cell lung cancer (NSCLC) [98], resulting in regulatory approval. However, our results suggest that prognosis in altered-excluded and cold tumour scenarios may not benefit from the combined effects of these two immune checkpoint inhibitors. Nevertheless, our results indicate that therapeutic strategies promoting the infiltration of CTLs could turn altered-excluded tumours into altered-immunosuppressed or hot tumours, helping to decrease the resistance of tumours to the combination of anti-PD1 and anti-CTLA4 therapy. This finding is coherent with experimental observations suggesting that a synergistic effect can be achieved by combining anti-angiogenic therapies, which act on vascular abnormalities facilitating CTL infiltration, with immune checkpoint therapies [203].

Finally, the outputs of our model suggest that increasing both the level of efficiency of CTLs and their rate of inflow (*i.e.* the values of the parameters ζ_n and α_c) and decreasing the pro-

liferation rate of tumour cells (*i.e.* the parameter α_n), which may represent the combination of anti-PD1 therapy with chemotherapy, a stronger immune response may be induced. In fact, a proposed approach to overcome the lack of a pre-existing immune response consists in combining a priming therapy that enhances CTL responses (such as chemotherapy) with the removal of co-inhibitory signals (through approaches such as immune checkpoint therapies) [70]. For example, the success of the combination of anti-PD-1 therapy with chemotherapy in metastatic NSCLC has demonstrated the strength of this dual approach [73].

4.6.2 Research perspectives

We conclude with an outlook on possible extensions of the present work. While here we focused on the role of the secretion rate of the chemoattractant by tumour cells and the threshold value of the total cell density above which T cell movement is impaired, it would be interesting to investigate how other model parameters (*e.g.* the chemotactic sensitivity of T cells) may affect the level of infiltration of T cells into the tumour. Carrying out a more extensive exploration of the model parameter space would ultimately allow more robust biological conclusions to be drawn.

Moreover, our hybrid modelling framework for the spatial dynamics of tumour cells and cytotoxic T cells, along with the formal derivation of the corresponding continuum model, can be developed further in several ways. For instance, a key factor of the immune response is that T cells express a unique repertoire of T cell receptors (TCRs) [45], and are capable of detecting and eliminating tumour cells by recognising specific cancer-associated antigens. The model presented here does not include this aspect, but it could easily be extended to do so by introducing, for instance, a variable representing the antigens expressed by tumour cells and the TCR expressed by T cells. This would make it possible to take explicitly into account the effects of both spatial and antigen-specific interactions between tumour cells and T cells, as similarly done in [113, 127, 140, 139], and then study the effects of antigen presentation or intra-tumour heterogeneity on immune surveillance.

Only a simplified representation of the action of different types of immunotherapy was considered in this work, but it would be important to carry out a more detailed study of the impact of T-cell infiltration on the dynamics of tumour cells under different immunotherapeutic protocols. In particular, by using optimal control methods for the continuum model, we could investigate the best delivery schedule of therapeutic agents (*i.e.* the best delivery times and dosages) that make it possible to minimise the number of tumour cells at the end of the treatment and achieve the best therapeutic outcomes [108]. These are all lines of research that we will be pursuing in the near future.

Chapter 5

Integrating the model with data: a discrete model to investigate the effect of psychological stress on immune infiltration

5.1 Motivation

In the previous chapters, we have developed discrete and continuum models of tumour-immune interactions that attempt to describe different aspects of the anti-tumour immune response. The different models have been parametrised using parameter values obtained from published works wherever possible and aim to investigate, or qualitatively reproduce, observed cell behaviours. However, at this stage, these models have not been calibrated using any particular type of data. Hence, they cannot be employed to generate predictions that can directly be used in the clinic.

Motivated by experimental observations in co-culture between breast cancer spheroids and activated immune cells, which reproduce *in vivo* behaviours as described in [99], in this chapter we explore a simple setting to study the effect of psychological stress on immune infiltration. In comparison to the models developed in the previous chapters, the mathematical framework presented here is developed in collaboration with the biologists who designed and conducted the *in vitro* experiment presented in [99]. Compared to *in vivo* studies, which are performed on a whole living organism, *in vitro* experiments are performed in a controlled environment, allowing for a more detailed analysis and examination of biological effects. For this reason, mathematical models can more easily be calibrated on *in vitro* studies, in order to reproduce the specific *in vitro* experiment.

To study the effects of stress on immune infiltration, we use a mathematical model based on a simplified version of the one developed in Chapter 3, and we calibrate it to qualitatively reproduce, *in silico*, the experimental results obtained in [99]. In this experimental study, the authors found that the introduction of cortisol in the co-culture resulted in a decrease in immune cell infiltration into cancer spheroids, a decrease in the levels of the pro-inflammatory cytokine IFN-γ and an increase in the levels of the anti-inflammatory cytokine IL-10. In our model, we assume that stress replaces the role of cortisol in the experiment, and investigate which mechanisms are most likely to be affected by stress and impact immune infiltration. Using a

method similar to the one employed in [99], we define a score to quantify the effects of stress on immune infiltration in a controlled manner. The results of numerical simulations of this model are able to qualitatively reproduce the results of *in vitro* experiments presented in [99], and demonstrate the importance of including the effect of different factors when exploring the role played by psychological stress on immune infiltration.

This study is a joint work in collaboration with:

- Melanie S. Flint, School of Pharmacy and Biomolecular sciences, University of Brighton, Centre for Stress and Age-related Diseases, Moulsecoomb, Brighton, BN2, 4GJ, UK,
- Chandrasekhar Venkataraman, School of Mathematical and Physical Sciences, University of Sussex, Department of Mathematics, Falmer, Brighton, BN1 9QH, UK,

both authors of [99].

This chapter contains preliminary results from an ongoing work.

5.2 Background

5.2.1 Biological background

The ability of psychological stress to induce immune suppression is widely recognised, but the mechanisms underlying the effects of stress on the adaptive immune system during tumour progression are not completely understood.

There has been increasing interest in detailing the mechanistic role that psychological stress may play in the context of initiation, progression, metastasis and recurrence of cancer. In particular, it has been reported that stress positively influences carcinogenesis through mechanisms that promote proliferation, angiogenesis and metastasis, as well as mechanisms that protect tumour cells from apoptosis [124, 160]. In addition to the direct effect on tumour cell biology, the negative role played by stress on the immune system has also been documented. Using a pre-clinical mouse model, in [27] the authors showed that stress has a negative impact on T cell numbers and activation, as evidenced by a decrease in CD8+ and CD3+CD69+ T cells. The administration of beta-blockers made it possible to reverse the negative effect of stress on the adaptive immune system and slowed down tumour progression.

In the study that motivated our work [99], the authors developed a co-culture *in vitro* model to test the effects of the stress hormone cortisol, with a particular emphasis in exploring its role on immune cell infiltration. Prior to testing the effect of cortisol on the *in vitro* co-culture model, the authors verified that this model was able to reproduce the outcomes of a 66CL4 syngeneic *in vivo* mouse model. Using two independent image analysis algorithms, they successfully quantified the effects of cortisol on immune infiltration, which was interpreted as the number of immune cells within the tumour spheroid boundary. The results from the *in vitro* co-culture model, as well as the *in vivo* experiments, showed that cortisol decreases immune infiltration. In this respect, the outcomes obtained in [99] recapitulate the conclusions of [27], which also report that stress negatively affects immune infiltration into tumours.

The mixture of cytokines that is produced in the tumour microenvironment has an important role in tumour progression [57]. Pro-inflammatory cytokines that are released in response to infection can inhibit tumour development and progression. Alternatively, tumour cells can produce anti-inflammatory cytokines that promote growth, attenuate apoptosis and facilitate invasion and metastasis. In stressed conditions, the production of pro- and anti-inflammatory cytokines can be altered. For example, in [27], the authors found that stress increased the levels

of inhibitory cytokines, such as the pro-tumourigenic chemokine CXCL10 and granzyme B, contributing to suppression of anti-tumour immune response. In [99], the results from the analysis of IFN-γ and IL-10 demonstrated that stress decreased the levels of IFN-γ and increased the levels of IL-10. IFN-γ is a pro-inflammatory cytokine that stimulates immune response, such as T cell trafficking in the tumour-microenvironment and infiltration [33, 183], whereas IL-10 is an anti-inflammatory cytokine that inhibits immune response, such as T cell proliferation [5, 46].

From a biological and medical perspective, it is difficult to investigate the connection between stress, immune infiltration and the underlying molecular and cellular processes. The challenge is to integrate theoretical and empirical knowledge to better understand the mechanisms and factors that contribute to failure of the anti-tumour immune response. In this context, mathematical models provide useful tools towards identifying dependencies between different phenomena and how these may affect the efficacy of the immune response.

5.2.2 The mathematical model

In light of these considerations, and motivated by the results presented in [99], in this chapter we develop a spatial stochastic individual-based model of the interaction dynamics between tumour cells and cytotoxic T lymphocytes (CTLs), to explore the role played by psychological stress in immune infiltration. In particular, our goal is to investigate which mechanisms are most likely to be influenced by psychological stress and impact immune infiltration. The individual-based model considered here is based on a modified and simplified version of the Cellular Potts model developed in Chapter 3. In the *in vitro* experiment only one tumour cell line is used. Therefore, compared to the model presented in Chapter 3, here we are not interested in intra-tumour heterogeneity, and we do not incorporate antigen expression in the model.

In [99], the authors found that cortisol decreased the levels of the pro-inflammatory cytokine IFN-γ and increased the levels of the anti-inflammatory cytokine IL-10. Therefore, to explore which mechanisms are influenced by psychological stress, in our model we take into account the effects that these two cytokines may have on immune response. On the one hand, the effect of INF-γ is taken into account by letting tumour cells at the border of the tumour (the region where cytokines and immune cells are more abundant in the tumour-microenvironment) secrete a chemoattractant, which drives the movement of CTLs towards the tumour. Moreover, we let INF-γ also affect the capability of CTLs to infiltrate through tumour cells. On the other hand, the effect of IL-10 is taken into account by modulating the growth rate of CTLs, which directly affects their proliferation rate.

In this work, we explore different scenarios. We suppose that in normal conditions the levels of IFN-γ are high, the levels of IL-10 are low, and CTLs are able to infiltrate into the tumour. In stressed conditions however, we suppose that the levels of IFN-γ decrease, the levels of IL-10 increase, and CTL infiltration is reduced. By varying the secretion rate of the chemoattractant, the capability of CTL to infiltrate through tumour cells and the growth rate of CTLs, we study the impact of stress on immune infiltration. Finally, using a method similar to the one employed in [99], we define a score to quantify the effects of stress on immune infiltration in a controlled manner.

5.2.3 Structure of the chapter

The chapter is organised as follows. In Section 5.3, we describe the *in vitro* experiments and the main experimental observations that motivated our modelling assumption. The model developed in collaboration with the biologists is described in Section 5.4. The set-up of computational simulations is summarised in Section 5.5, where some preliminary results of computational sim-

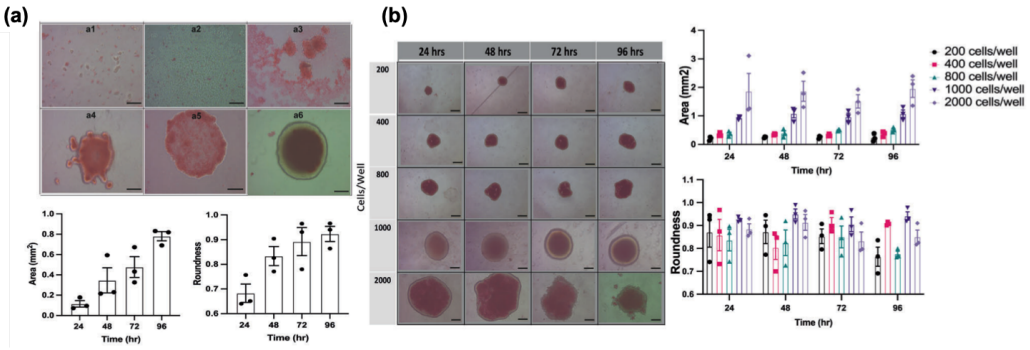

Figure 5.1: **Morphology, seeding density and viability of spheroids.** Panel **(a)** displays the visual stages of spheroid generation using ultra-low attachment plates of the murine triple negative breast cancer 66CL4 cell line, from 0 to 96 h. Panel **(b)** displays representative phase contrast microscope images of spheroids seeded from different number of cells ranging from 200 to 2000 over 4 days after full spheroid generation and growth. The highest level of uniformity in shape (roundness) and size was observed in the spheroids seeded from 1000 cells/well.
Figure is taken from [99], under Creative Commons licence http://creativecommons.org/licenses/by/4.0/.

ulations are also presented. Full details of model implementation and model parametrisation are provided in Appendix A and Appendix E, respectively. In Section 5.6, we present the main computational results and we discuss them in view of the biological results obtained in [99]. Finally, we conclude the chapter and provide some research perspectives in Section 5.7.

5.3 Description of the experiments

To address the question of the role played by stress in T cell infiltration, we took advantage of a recently developed 3D co-culture *in vitro* model between cancer spheroids and activated immune cells (splenocytes). This model explored the effect of the gluco-corticoid stress hormone, cortisol on 66CL4 co-culture between cancer spheroids and activated immune cells. We now describe the different steps that have been followed to develop the co-culture model and the main experimental observations that motivated the development of our mathematical model.

From day -7 to day 0: growth of the spheroids In order to establish the co-culture, tumour spheroids from a murine triple negative 66CL4 breast cancer cell line were generated using ultra low attachment round bottom flasks. It took 4 days for the spheroids to fully form [see Figure 5.1**(a)**]. Then, spheroids were grown for 7 days (*i.e.* from day -7 to day 0), during which their area and roundness increased over time. At day 0, both cell lines were seeded at different densities. The seeding density with the largest area and roundness, and with the least variation over 4 days, was chosen [see Figure 5.1**(b)**]. This was done to allow the changes in the spheroids to be attributed to the infiltration of immune cells and not to the spheroids themselves.

Day 0: introduction of splenocytes At day 0, immune cells (splenocytes), containing activated T cells, were co-cultured with 66CL4 spheroids. At the initial time of the co-culture

there were 5 times as many T cells as tumour cells at time -7. Spheroids and splenocytes were later co-cultured, imaged daily using confocal microscopy, and split into 7 groups. Group-**1** contained spheroids only and group-**2** comprised spheroids and splenocytes. The other 5 groups were treated daily with corticosterone (cortisol). Group-**3** contained spheroids, splenocytes and cortisol. Groups-**4-5-6** contained spheroids, splenocytes and 3 different glucocorticoid receptor antagonists. Group-**7** contained spheroids and cortisol. Spheroids from each group were treated daily for 4 days (*i.e.* from day 0 to day 4), and the media was saved for further analysis.

Implementation of two independent trafficking indexes to measure infiltration levels To test whether cortisol decreased immune infiltration in the co-culture model, the co-culture of each group was imaged daily for 4 days (*i.e.* from day 0 to day 4) using confocal microscopy. Two trafficking indexes were developed by the authors and applied every day to quantify immune infiltration levels. Both approaches sought to measure immune cell infiltration into the spheroid, which was interpreted as the number of immune cells into the tumour spheroid boundary.

The first trafficking index, which the authors refer to as *segmentation-based trafficking index* (TIS), relies on a two-step approach. In the first step, the tumour boundary is identified using image segmentation techniques. Alongside this, in the second step, connected regions of high red channel intensity (which correspond to the presence of immune cells) are segmented. The TIS is a dimensionless number computed as the sum over each pixel that is in both the segmented regions (*i.e.* in regions with both tumour and immune cells) of the red channel intensity divided by the green channel intensity (which characterize the presence of only tumour cells). The TIS is the largest in pixels within the tumour (and segmented immune cell regions) at which the red channel intensity is high, and the green channel intensity is low, respectively. In fact, these pixels unambiguously correspond to immune cells within the tumour, indicating successful trafficking.

The second alternative independent algorithm to measure trafficking, which the authors refer to as *K-means classification-based trafficking index* (TIC), does not involve segmentation, and is based on a k-means classifier. The assumption underlying the classification is that the red and green levels of a pixel in a given image characterise the cell type that occupies the region, respectively immune and tumour cells. The TIC is also a two-step approach in which first a machine learning algorithm is used to classify each pixel in the image into different groups obtaining four classes, background, tumour cell, immune cell or colour saturated. The identification of the colour saturated class allows for the exclusion of pixels that cannot be quantified appropriately, since the colour saturation hinders any comparison between the red and green levels. The TIC is then based on the number of pixels classified as immune cells that are completely surrounded by pixels classified as tumour cells. The resulting statistics yields a number in the interval $[0, 1]$.

From day 0 to day 4: investigation of the effects of cortisol on immune infiltration For 4 days (*i.e.* from day 0 to day 4), the co-culture in each group was imaged, and the TIS and TIC trafficking indexes described above were applied on the images.

The authors found that, compared to the group with untreated spheroids and splenocytes only (*i.e.* group-**2**), the introduction of cortisol significantly decreased immune cell infiltration in the spheroids in group-**3** [see Figure 5.2**(a)-(d)**]. Moreover, the 3 glucocorticoid receptor antagonists, respectively introduced in groups-**4-5-6**, reversed the effects of cortisol and significantly increased immune infiltration in spheroids compared to the group of cells treated with cortisol (*i.e.* group-**3** - results not shown). The results also showed that cortisol did not affect spheroid area and did not alter their roundness [see Figure 5.2**(e)-(f)**]. Finally, the authors measured the concentration of two cytokines in the co-culture media, namely: the pro-inflammatory cytokine INF-γ and the anti-inflammatory cytokine IL-10. They found that cortisol significantly decreased the levels of INF-γ and significantly increased the levels of IL-10 [see Figure 5.2**(g)-(h)**].

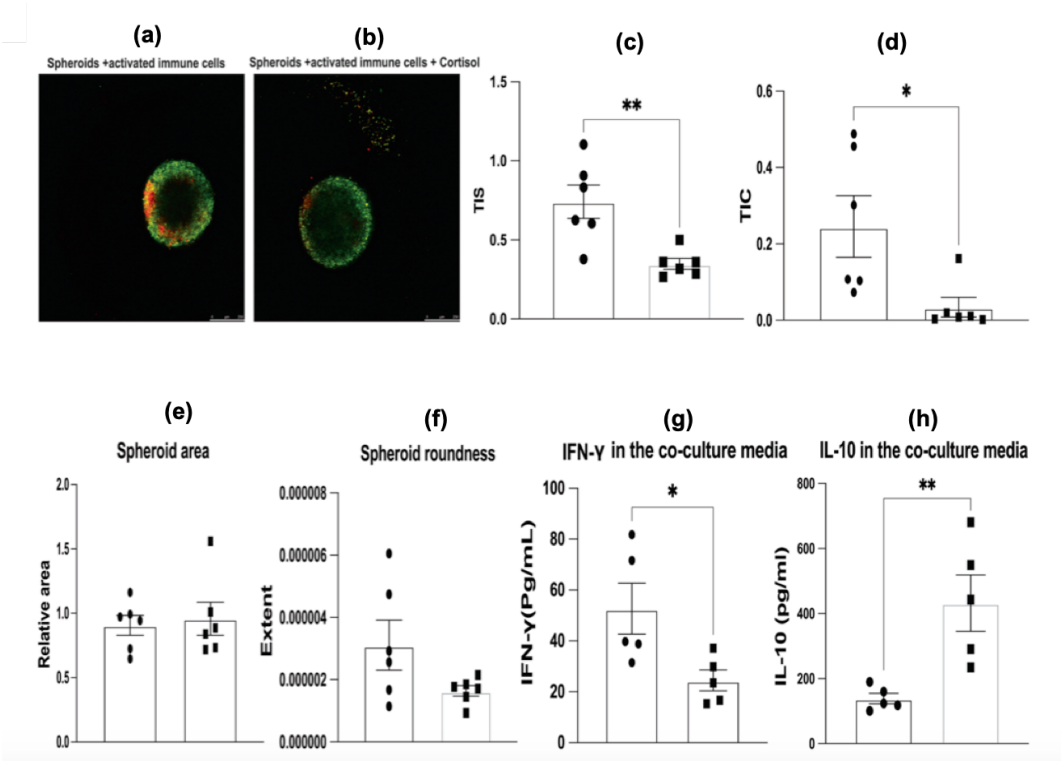

Figure 5.2: **Cortisol decreases immune cell infiltration into 66CL4 spheroids.** Panels **(a)**-**(b)** display representative confocal images of the co-culture for the groups of spheroids + activated immune cells (panel **(a)**) and spheroids + activated immune cells + cortisol (panel **(b)**). Green represents spheroids and red represents splenocytes. The scale bar represents 250 μm. Histograms in panels **(c)**-**(d)** display the value of immune infiltration measured using the *segmentation-based algorithm* (TIS) and the *k-means classification-based method* (TIC) for the groups of spheroids + activated immune cells (left hand-side histogram) and spheroids + activated immune cells + cortisol (right hand-side histogram). Histograms in panels **(c)**-**(d)** display the 66CL4 spheroid area and roundness for the two groups. Cortisol does not affect 66CL4 spheroid area and roundness. Histograms in panels **(g)**-**(h)** display the levels of INF-γ and IL-10 in the co-culture media for the two groups. Cortisol significantly decreases the levels of INF-γ and increases the levels of IL-10.
Figure is taken from [99], under Creative Commons licence http://creativecommons.org/licenses/by/4.0/.

5.4 Modelling framework

Building upon our previous model developed in Chapter 3, to reproduce the *in vitro* results of the co-culture between cancer spheroids and activated splenocytes, we consider two cell types: tumour cells and cytotoxic T lymphocytes (CTLs). We use a Cellular Potts approach and the CompuCell3D open-source [107] simulation environment to describe the interactions between these two cell types.

The choice of a Cellular Potts model is of particular interest in this context, since interactions

between neighboring cells in Cellular Potts models have an effective energy, which characterises the strength of cell-cell adhesion [107] (see Appendix A for a detailed description of the implementation of Cellular Potts models). Therefore, in our model, the effective energy between cells can directly affect the capability of CTLs to infiltrate through tumour cells. In particular, small values of the energy at the interface between tumour cells and CTLs correspond to a high adhesivity between the two cells types and, therefore, lead to scenarios in which CTLs display a high capability to infiltrate through tumour cells. On the other hand, large values of the energy at the interface between tumour cells and CTLs correspond to a low adhesivity between the two cells types and, therefore, lead to scenarios in which CTLs will tend to accumulate at the margin of the tumour, without infiltrating it. From here on, we use the term "tumour cell-CTL adhesion strength" (TC-CTL adhesion strength) to refer to the parameter associated with the energy at the interface between tumour cells and CTLs and regulating CTL infiltration. With this notation, we will assume that high values of the TC-CTL adhesion strength facilitate the infiltration of CTLs through tumour cells, while low values of this parameter lead the CTLs to accumulate at the margin of the tumour, without infiltrating it.

Our model is posed on a 2D spatial domain partitioned into square elements of side Δx. In our modelling framework, this domain biologically represents the media in which the co-culture is analysed. At each time step of length Δt, the states of the cells are updated according to the probabilistic and deterministic rules described below.

From day -7 to day 0: growth of tumour cells We let $N_T(t)$ denote the number of tumour cells in the system at time $t = h\Delta t$, with $h \in \mathbb{N}_0$, and we label each cell by an index $n = 1, \ldots, N_T(t)$. Motivated by the experiments described in Section 5.3, at the initial time point of the simulation (corresponding to day -7 of the experiments described in Section 5.3), a certain number of tumour cells is already present in the domain. Tumour cells are tightly packed in a circular configuration positioned at the centre of the domain, reproducing a 2D cross-section of the geometry of the spheroids.

At each time-step, we let tumour cells grow at a certain rate drawn from a uniform distribution; the parameters of the bounds of the uniform distribution are chosen to match the mean duration of the spheroids cycle length. Mitosis occurs when a tumour cell grows to a critical size and then divides. We refer the reader to Chapter 3 for a detailed description of cell division modelling strategy.

A tumour cell can die due to intra-tumour competition, at a rate proportional to the total number of tumour cells. This modelling rule allows us to obtain a logistic growth in the number of tumour cells.

Day 0: introduction of CTLs We denote by $N_C(t)$ the number of CTLs in the system at time t, and we label each of them by an index $m = 1, ..., N_C(t)$. At day 0 of our simulations, a certain number of CTLs is randomly distributed across the spatial domain. To match the experiments, the number of CTLs introduced in the domain at day 0 corresponds to 5 times the number of tumour cells introduced at day -7. Once in the domain, we let CTLs grow, divide by mitosis and die due to intra-population competition with rules similar to those used for tumour cells. If a CTL exhausts its lifespan (which is drawn when the cell is created), it dies (*i.e.* it undergoes apoptosis) at the end of the time-step and it is removed from the domain.

Tumour cells at the border of the tumour secrete a chemoattractant (which models the effects of INF-γ) that triggers the movement of CTLs towards tumour cells. Denoting by ϕ the concentration of the chemoattractant secreted by tumour cells, we let the dynamic of ϕ be

described by the following reaction-diffusion equation:

$$\frac{\partial \phi}{\partial t} = D\Delta\phi - \gamma\phi + \alpha \sum_{n \in N_{TB}(t)} \delta_{n \in N_{TB}(t)}. \tag{5.1}$$

In Eq. (5.1), D is the diffusion rate of the chemoattractant, γ is the rate of natural decay and α is the secretion rate. Moreover, $\delta_{n \in N_{TB}(t)} = 1$ if $n \in N_{TB}(t)$, and $\delta_{n \in N_{TB}(t)} = 0$ otherwise, where $N_{TB}(t)$ denotes the set of tumour cells contact with the surrounding medium at time t. This function allows to take into account the fact that only the tumour cells at the border of the tumour secrete the chemoattractant.

Once in the domain, CTLs move up the gradient of the chemoattractant in direction of tumour cells. The chemotaxis of CTLs towards the tumour is modulated by a parameter λ_{chem}, which determines the strength and direction of chemotaxis (see Appendix A for a detailed description of the implementation of Cellular Potts models).

Implementation of our algorithm to measure infiltration levels In a similar way as the authors of [99] developed two trafficking indexes to measure the level of infiltration of splenocytes into the spheroids, in our work we define an 'infiltration score'. This score allows us to quantify the level of CTL infiltration into the tumour and is defined in a numerically equivalent way of the TIC algorithm developed in [99]. In fact, we define the infiltration score as the number of CTLs surrounded by tumour cells, divided by the number of tumour cells and CTLs surrounded by tumour cells, and can be written as

$$I(t) := \sum_{n=1}^{N_T(t)} \sum_{m=1}^{N_C(t)} \frac{\delta_{m \in N_{CS}(t)}}{\delta_{m \in N_{CS}(t)} + \delta_{n \in N_{TS}(t)}}. \tag{5.2}$$

In Eq. (5.2), functions $\delta_{m \in N_{CS}(t)}$ and $\delta_{n \in N_{TS}(t)}$ are defined in a similar way of function $\delta_{n \in N_{TB}(t)}$ in Eq. (5.1). Here, these functions allow to respectively count the number of CTLs in set $N_{CS}(t)$, and the number of tumour cells in set $N_{TS}(t)$, where $N_{CS}(t)$ and $N_{TS}(t)$ respectively denote the sets of CTLs and tumour cells surrounded by tumour cells at time t. This computation gives a number in the interval $[0, 1]$.

From day 0 to day 4: investigation of the effects of stress on immune infiltration Between day 0 and day 4, CTLs grow and divide, move via chemotaxis towards the tumour and infiltrate it.

Accordingly to the experiments, CTLs are activated against the tumour cells. Therefore, we suppose that upon contact, CTLs can induce tumour cell death with a certain probability. We refer to this probability as the "immune success rate". If the tumour cell satisfies the conditions to be eliminated, it undergoes apoptosis. Building on the same modelling framework developed in Chapter 3, we require that an elimination event keeps a CTL engaged for 6 hours and only after this time the CTL can eliminate again.

Figure 5.3 describes the strategies adopted in our model to study the effects of stress on immune infiltration and qualitatively reproduce the experimental results obtained in [99]. In this study, to test whether stress decreased infiltration levels in the co-culture model, cortisol was added to the co-culture and the outcomes were compared to those obtained for the group of spheroids and activated splenocytes only. Cortisol significantly decreased the levels of INF-γ in the co-culture media and significantly increased the levels of IL-10 (*cf.* step **(1)** of Figure 5.3). In our model, we explore the way in which immune infiltration is affected by three parameters

which can be associated to the effects of cortisol in the co-culture. Such parameters are: the secretion rate of the chemoattractant, the TC-CTL adhesion strength and the growth rate of CTLs. The first two parameters are associated to the role played by INF-γ in the co-culture model, while the last one is associated to the role played by IL-10 (*cf.* step **(2)** of Figure 5.3). Varying these parameters affects both the number of CTLs at the end of the simulation, as well as their movement towards and within the tumour. In this work, we explore different scenarios. We suppose that in normal conditions (*i.e.* in our control scenario) the levels of IFN-γ are high, the levels of IL-10 are low, and CTLs are able to infiltrate into the tumour. In stressed conditions however, we suppose that the levels of IFN-γ decrease, the levels of IL-10 increase, and CTL infiltration is reduced. By considering a range of values of the three aforementioned parameters, we study their impact on tumour-immune dynamics independently and together, assessing their influence on immune infiltration in a controlled manner (*cf.* step **(3)** of Figure 5.3).

5.5 Numerical simulations and preliminary results

5.5.1 Set-up of simulations

For numerical simulations of our individual-based model, we use a Cellular Potts approach on a 2D spatial grid with a total of 400×400 lattice sites. Simulations were developed and run using the software CompuCell3D [107] on a standard workstation (Intel i7 Processor, 4 cores, 16 GB RAM, macOS 11.2.2). The computational implementation of Cellular Potts models is described in Appendix A, while full details of the model parametrisation are provided in Appendix E.

At the initial time point of the simulation (*i.e.* at day -7 of the experiments), a small number of tumour cells is placed in the domain. Tumour cells proliferate for 7 days (*i.e.* from day -7 to day 0) and CTLs are introduced in the domain at day 0.

All quantities we present in this section and in Section 5.6 are obtained by averaging over the results of 5 simulations, with parameter values equal to those listed in Table E.1 and Table E.2. First we let tumour cells grow in absence of CTLs for 11 days, carrying out numerical simulation for 33000 time-steps. Then we introduce CTLs, and we let them interact with tumour cells for 4 days, carrying out numerical simulation for 1200 time-steps.

In the next two subsections, two preliminary computational results of our model are presented, which will be used to guide the simulations leading to the main results presented in Section 5.6.

5.5.2 Tumour development in the absence of CTLs

We first establish a preliminary scenario where tumour cells grow, divide and die via the modelling rules described in Section 5.4, in the absence of CTLs. For this case, we carry out numerical simulations for 33000 time-steps, corresponding to 11 days (*i.e.* from day -7 to day 4 of the experiments). Figure 5.4**(a)** shows the growth over time of the number of tumour cells. Figure 5.4**(b)** also displays an example of the spatial cell distribution observed at different times of one simulation. As shown by Figure 5.4**(a)**, the number of tumour cells increases from day -7 to day 0. At day 0, the number of tumour cells reaches its carrying capacity, *i.e.* the saturation value attained due to intra-population competition. Therefore, from day 0 to day 4, the number of tumour cells remains stable around the value of carrying capacity. These results qualitatively reproduce the growth of the spheroids obtained in the experiments described in Section 5.3.

In the following subsection, we establish a control scenario in which CTLs are introduced into the domain and interact with tumour cells in non-stressed conditions. These simulations are performed by keeping the values of the parameters related to tumour cells fixed (and equal to this preliminary scenario) and by setting the initial number of tumour cells at its carrying

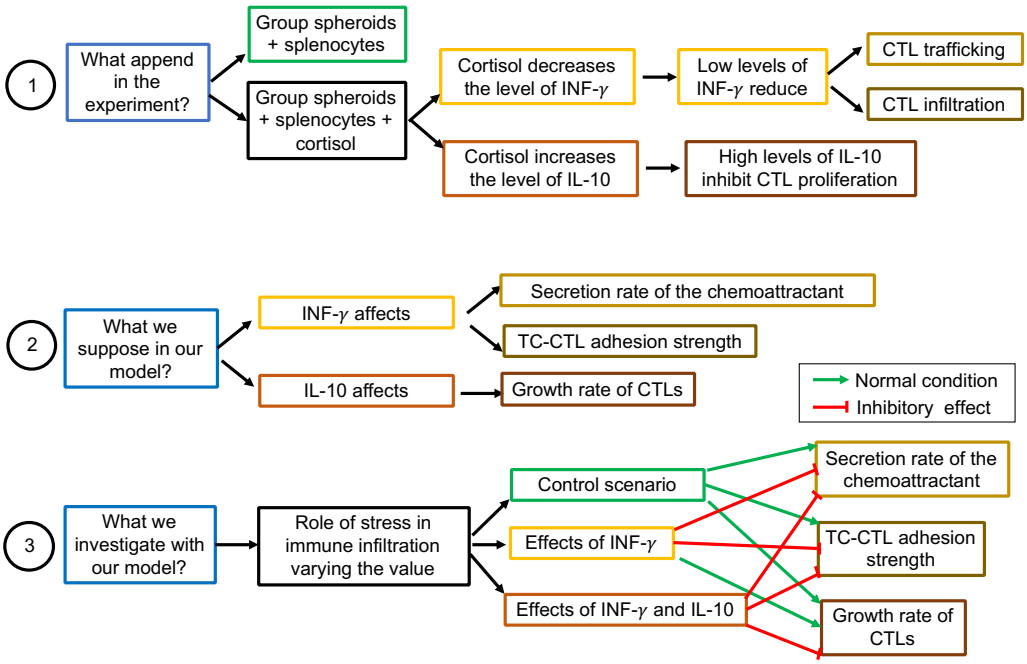

Figure 5.3: **Modelling strategies.** Step **(1)**: in [99], to test whether stress decreased infiltration levels in the co-culture model, they compared the outcomes obtained between the group of spheroids and splenocytes only and the one of spheroids, splenocytes and cortisol. Cortisol significantly decreased the levels of INF-γ and significantly increased the levels of IL-10. IFN-γ is a pro-inflammatory cytokine that stimulates immune response, such as T cell trafficking in the tumour-microenvironment and infiltration, whereas IL-10 is an anti-inflammatory cytokine that inhibits immune response, such as T cell proliferation. Step **(2)**: in our model, we explore the way in which immune infiltration is affected by three parameters which can be associated to the effects of cortisol in the co-culture. Such parameters are: the secretion rate of the chemoattractant, the TC-CTL adhesion strength and the growth rate of CTLs. The first two parameters are associated to the role played by INF-γ in the co-culture model, while the last one is associated to the role played by IL-10. Step **(3)**: in this work, we explore different scenarios. We suppose that in normal conditions (*i.e.* in our control scenario) the levels of IFN-γ are high, the levels of IL-10 are low, and CTLs are able to infiltrate into the tumour. In stressed conditions however, we suppose that the levels of IFN-γ decrease, the levels of IL-10 increase, and CTL infiltration is reduced. By considering a range of values of the three aforementioned parameters, we study their impact on tumour-immune dynamics independently and together, assessing their influence on immune infiltration in a controlled manner.

capacity. The number of CTLs introduced in the domain at day 0 corresponds to 5 times the number of tumour cells introduced at day -7, and the values of the parameters related to CTLs are chosen so as to qualitatively reproduce the experimental results obtained by [99].

5.5.3 Control scenario: immune infiltration in non-stressed conditions

In the experimental results obtained by [99], in absence of cortisol, splenocytes are able to infiltrate the spheroids. Moreover, the levels of INF-γ measured in the co-culture are high,

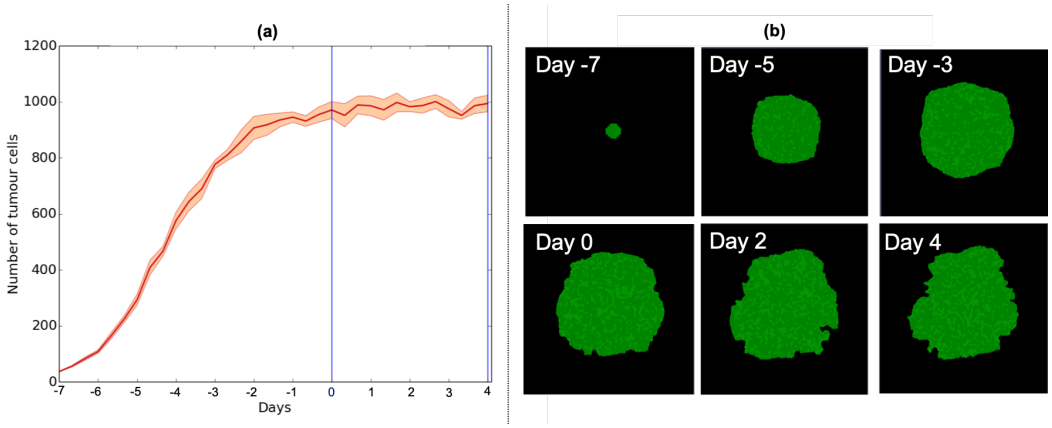

Figure 5.4: **Tumour development in the absence of CTLs.** Panel **(a)** displays the time evolution of the tumour cell number in the absence of CTLs. The shaded area indicates +/− standard deviation between 5 simulations. Insets in panel **(b)** display an example of the spatial distribution of tumour cells at different times of the simulation.

while the levels of IL-10 are low. In our next simulations, we attempt to verify that our model reproduces such phenomenon, exploring the infiltration of CTLs into the tumour over 4 days. For these simulations we assume that the levels of INF-γ are high and, therefore, we let tumour cells secrete the chemoattractant at a high rate. Moreover, we assume that CTLs display a high capability to infiltrate through tumour cells and, therefore, we consider a high value for the TC-CTL adhesion strength. Finally, we assume that the levels of IL-10 are low and, therefore, we let CTLs grow at their normal rate. For now, we simplify our model. We consider that when CTLs are in contact with tumour cells, they are not able to eliminate tumour cells (*i.e.* the immune success rate is equal to 0). We will consider that CTLs induce tumour cell death with an immune success rate greater than 0 in Section 5.6.3. These assumptions establish our control scenario.

Insets in Figure 5.5**(a)** display an example of the spatial distribution of tumour cells and CTLs at different times of the simulation for a choice of parameters that results in the infiltration of CTLs into the tumour. Plots in Figure 5.5**(b)**-**(c)** respectively display the corresponding average value of the infiltration score, computed via (5.2), and the time evolution of the numbers of tumour cells and CTLs. As shown by Figure 5.5**(a)**, as soon as CTLs are introduced in the domain, they rapidly move towards the tumour and infiltrate it. Figure 5.5**(b)** shows that the infiltration score increases over time, but its value tends to saturate between day 3 and day 4. Moreover, the mean value of the infiltration score obtained at day 4 of our simulations is similar to the mean value of the TIC algorithm obtained in [99], when cortisol was not introduced in the co-culture (*cf.* Figure 5.2**(d)**). Finally, as shown by Figure 5.5**(c)**, and as expected by the rules that govern tumour cell and CTL growth and death, over time the number of tumour cells tends to stay constant around the value of carrying capacity, while the number of CTLs increases until it reaches a saturation value. This result demonstrates that the changes in the tumour surface must be attributed to the infiltration of CTLs into the tumour and not to the growth of the tumour.

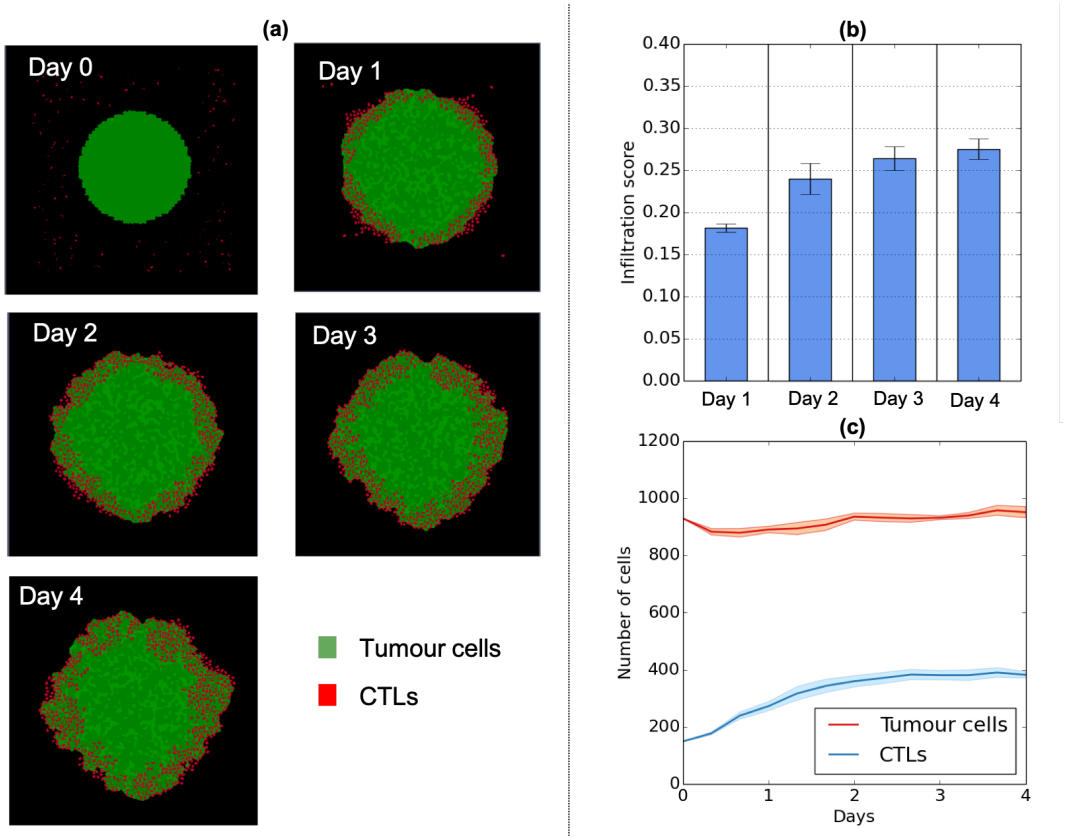

Figure 5.5: **Control scenario: immune infiltration in non-stressed conditions.** Insets in panel **(a)** display an example of the spatial distribution of tumour cells and CTLs at different times of the simulation for a choice of parameters that results in the infiltration of CTLs into the tumour. Plot in panel **(b)** displays the corresponding average value of the infiltration score, computed via (5.2), at different times of the simulation. The error lines represent the standard deviation between 5 simulations. Plot in panel **(c)** displays the corresponding time evolution of the numbers of tumour cells and CTLs. The shaded area indicates +/− standard deviation between 5 simulations.

5.5.4 Investigation of the effects of stress on immune infiltration

In the two previous subsections we investigated preliminary scenarios of tumour development and tumour-immune interaction in absence of stress. We will now explore the effects of stress on immune infiltration. In particular, following the experimental results presented in [99], we study the impact that two cytokines may have on immune infiltration, that is: INF-γ and IL-10. In [99], the authors demonstrated that, under stress, the levels of INF-γ in the co-culture media decreased, while the levels of IL-10 increased. With our model, we wish to investigate the effect of these two cytokines on tumour-immune dynamics independently and together, evaluating their influence on immune infiltration in a controlled manner. To this end, first we investigate the effects of stress by decreasing the secretion rate of the chemoattractant, which may be associated with a decrease in the levels of INF-γ in the experiments. To consider a wide range of biological situations corresponding to different degrees of immune infiltration, for each scenario considered

we also explore different values of the TC-CTL adhesion strength. Next, for each scenario considered, we decrease the growth rate of CTLs. This parameter slows down the proliferation rate of CTLs and, therefore, may be associated with increased levels of IL-10 in the experiments.

In the next section, we investigate the effects of stress on immune infiltration. The obtained dynamics are compared to the control scenario. In the next simulations, we vary the values of the secretion rate of the chemoattractant, the TC-CTL adhesion strength, and the growth rate of CTLs, while the other parameters are kept constant to the values listed in Table E.1 and Table E.2. The values of the parameters are chosen so as to qualitatively reproduce essential aspects of the experimental results obtained by [99]. For each scenario, we compute the infiltration score via (5.2), and compare it with the infiltration score obtained in the control scenario.

5.6 Main results

5.6.1 Decreasing the secretion rate of the chemoattractant and the TC-CTL adhesion strength reduces the infiltration of CTLs into the tumour

To investigate how immune infiltration is affected by the levels of INF-γ in the domain, we start by comparing our control scenario with different scenarios in which the secretion rate of the chemoattractant is progressively decreased. For each scenario considered, we also vary the value of the TC-CTL adhesion strength.

Figure 5.6**(a)** displays the average value of the infiltration score at different times of the simulation, for different combined values of the secretion rate of the chemoattractant and the TC-CTL adhesion strength. In particular, Figure 5.6**(a)** shows that both parameters affect the infiltration of CTLs into the tumour, as the infiltration score decreases as soon as the TC-CTL adhesion strength or the secretion rate of the chemoattractant decrease. In addition, when the TC-CTL adhesion strength is sufficiently high, decreasing the secretion rate of the chemoattractant considerably reduces the infiltration score. On the other hand, when low values of the TC-CTL adhesion strength are considered, decreasing the secretion rate of the chemoattractant does not have an impact on the infiltration score, as its value is already small. These results suggest that the secretion rate of the chemoattractant has an impact on T cell infiltration only when CTLs display a sufficiently high capability to infiltrate through tumour cells. On the other hand, if CTLs have a low capability to infiltrate through tumour cells, independently on the dynamics of the chemoattractant, they will not be able infiltrate into the tumour.

We next analyse the spatial cell distributions observed at the end of simulations (*i.e.* at day 4 of the experiments). Figure 5.6**(c)**-**(d)** show an example of the final spatial distributions of tumour cells and CTLs for two decreasing values of the TC-CTL adhesion strength, whereas Figure 5.6**(e)**-**(f)** show similar plots for two decreasing values of the secretion rate of the chemoattractant. These plots are compared to the one displayed in Figure 5.6**(b)**, which shows the final spatial distributions of tumour cells and CTLs obtained in the control scenario. In particular, Figure 5.6**(b)**-**(d)** show that decreasing the TC-CTL adhesion strength leads to a scenario in which CTLs accumulate around the tumour, because the secretion rate of the chemoattractant is high, but they do not infiltrate into it. On the other hand, Figure 5.6**(b)**-**(e)**-**(f)** show that decreasing the secretion rate of the chemoattractant leads to a scenario in which CTLs away from the tumour are not sensitive to the gradient of the chemoattractant and, therefore, do not move towards the tumour.

Taken together, our results qualitatively reproduce key findings of the experimental results presented in [99]. The results presented in [99] indicate that cortisol decreased the levels of

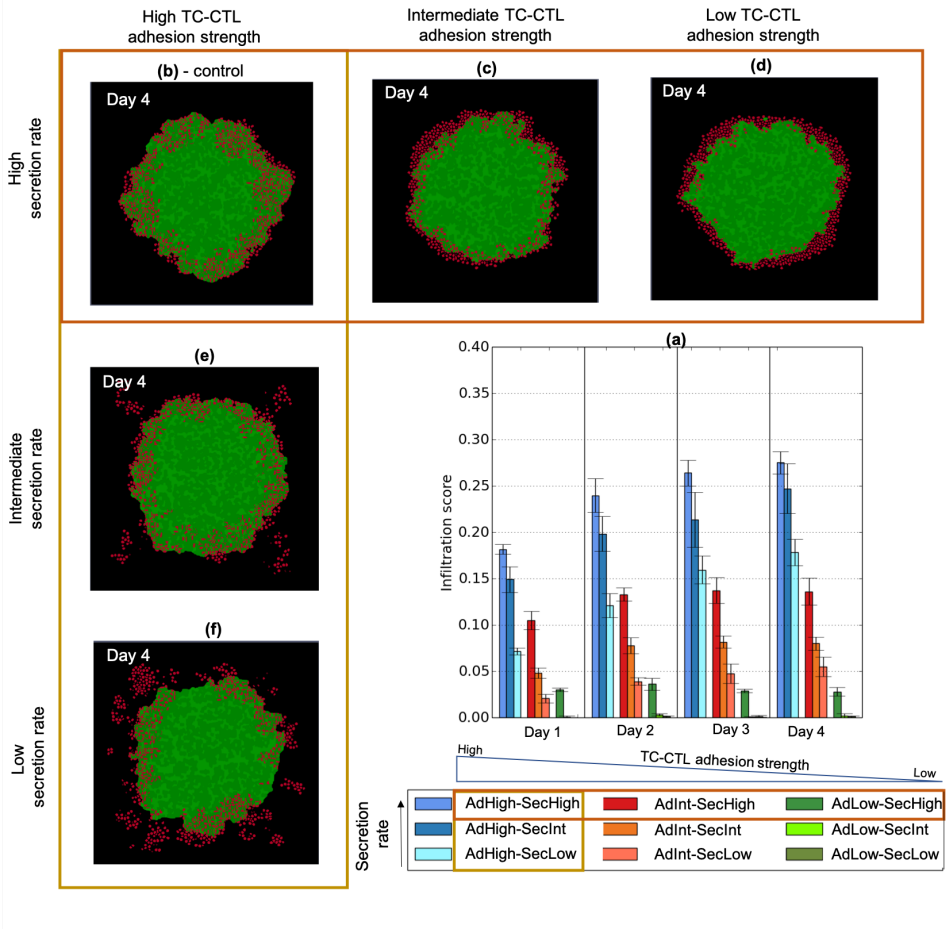

Figure 5.6: **Decreasing the secretion rate of the chemoattractant and the TC-CTL adhesion strength reduce the infiltration of CTLs into the tumour.** Plot in panel **(a)** displays the average value of the infiltration score, computed via (5.2), for different combined values of the secretion rate of the chemoattractant and the TC-CTL adhesion strength, at different times of the simulation. The error lines represent the standard deviation between 5 simulations. Inset in panel **(b)** displays an example of the spatial distribution of tumour cells and CTLs at the end of numerical simulations for the parameter values considered in the control scenario. Insets in panels **(c)**-**(d)** display similar plots for 2 decreasing values of the TC-CTL adhesion strength. Insets in panels **(e)**-**(f)** display similar plots for 2 decreasing values of the secretion rate of the chemoattractant.

INF-γ and decreased immune infiltration. Our computational results provide an explanation for such emergent behaviour. Since INF-γ may affect both T cell movement and infiltration, decreasing the levels of INF-γ inhibit CTL ability to migrate towards the tumour and their ability to infiltration into it.

5.6.2 Decreasing the growth rate of CTLs decreases the number of infiltrated CTLs

The results discussed in the previous subsection illustrate how the infiltration of CTLs into the tumour is affected by the levels of INF-γ in the domain. We further investigate the effects of stress, exploring the role played by IL-10 on immune infiltration. Therefore, for these simulations, we consider the same parameter values used in the previous subsection, and decrease the value of the growth rate of CTLs.

Figures 5.7**(a)**-**(b)** compare the infiltration score obtained when the effects of IL-10 are not considered (*i.e.* we consider a normal value for the growth rate of CTLs), with those obtained when the effects of IL-10 are considered (*i.e.* the value of the growth rate of CTLs is decreased). Figures 5.7**(c)**-**(d)** also compare the number of tumour cells and CTLs at the end of numerical simulations (*i.e.* at day 4 of the experiments) for the two scenarios considered. Comparing the results of Figure 5.7**(a)** with those displayed in Figure 5.7**(b)**, we see that, similarly to the results of the previous paragraph, decreasing the growth rate of CTLs decreases the infiltration score only when the TC-CTL adhesion strength is high. Moreover, for intermediate values of the TC-CTL adhesion strength, decreasing the growth rate of CTLs slightly decreases the infiltration score. Finally, when the TC-CTL adhesion strength is low, decreasing the growth rate of CTLs does not have an impact on the infiltration score, as its value is already small. As shown by Figures 5.7**(c)**-**(d)**, decreasing the growth rate of CTLs leads to a decreased number of CTLs at the end of simulations. However, as CTLs are not able to eliminate tumour cells, the final number of tumour cells remains similar in the two scenarios.

The outcomes of our model indicate that increasing the levels of IL-10 may inhibit the proliferation rate of CTLs, which in turn diminish the number of CTLs in the domain. When the levels of INF-γ are high and CTLs display a high capability to infiltrate trough tumour cells, we observe a reduction in the number of infiltrated CTLs (*i.e.* value of the infiltration score decreases). On the other hand, if the levels of INF-γ are low and CTLs have a low capability to infiltrate through tumour cells, increasing the levels of IL-10 does not affect the infiltration score, as the number of infiltrated CTLs is already low. Therefore, our computational results suggest that IL-10 decreases immune infiltration only when the levels of INF-γ are high and CTLs display a high capability to infiltrate trough tumour cells.

5.6.3 Increasing the immune success rate has an impact on the infiltration score only when the TC-CTL adhesion strength is high

So far, we have investigated with our model the effects of stress on immune infiltration in a framework in which CTLs are not able to eliminate tumour cells (*i.e.* the value of the immune success rate is equal to 0). Now, we investigate tumour-immune dynamics and the effects of stress on immune infiltration in the scenario in which CTLs can eliminate tumour cells with a small probability (*i.e.* the value of the immune success rate is slightly greater then 0).

Figures 5.8**(a)**-**(b)** compare the infiltration score obtained with the parameter values considered in Section 5.6.1, with the infiltration score obtained when the same parameter values are considered and CTLs can eliminate tumour cells with a small probability (*i.e.* we only increase the value of the immune success rate). Figures 5.8**(c)**-**(d)** show a comparison between the number of tumour cells and CTLs at the end of simulations (corresponding to day 4 of the experiments) for the two scenarios considered. Comparing the results of Figure 5.8**(a)** with those displayed in Figure 5.8**(b)**, we see that, when the TC-CTL adhesion strength is high, increasing the value of the immune success rate decreases the infiltration score. This is probably due to the fact that, when CTLs can infiltrate through tumour cells, they are more likely to come into con-

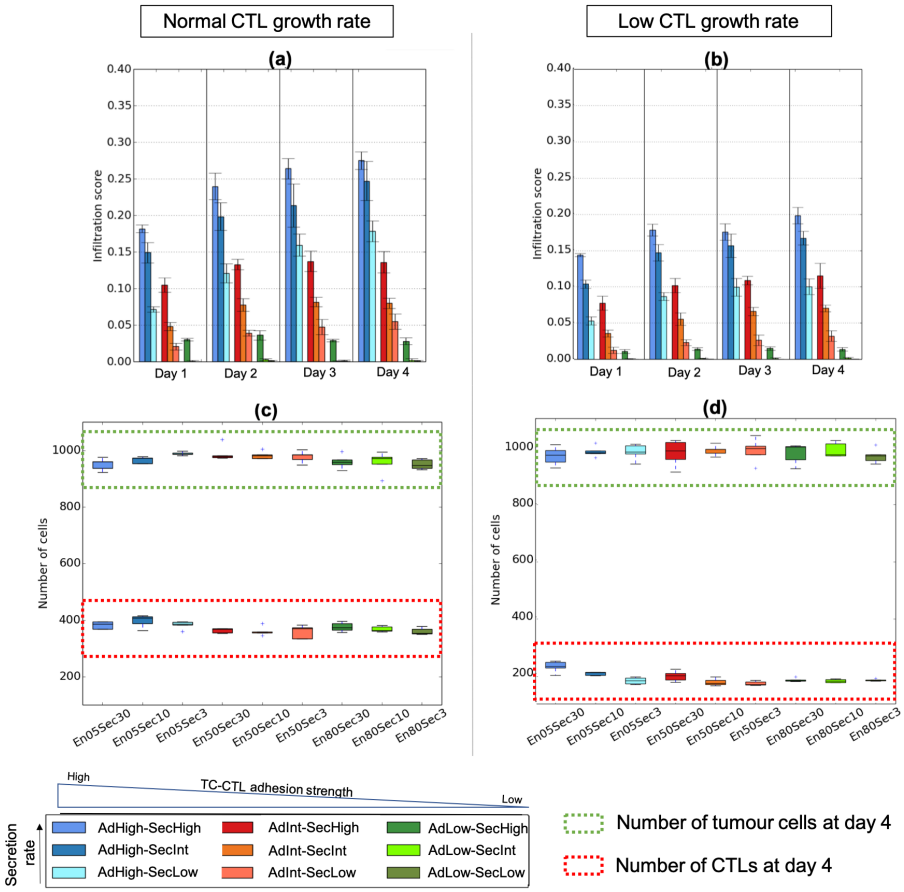

Figure 5.7: **Decreasing the growth rate of CTLs decreases the number of infiltrated CTLs.** Plots in panels **(a)**-**(b)** display the average value of the infiltration score, computed via (5.2), for different combined values of the secretion rate of the chemoattractant and the TC-CTL adhesion strength, and at different times of the simulation. In panel **(a)** CTLs grow at their normal rate, while their growth rate is decreased in panel **(b)**. The error lines represent the standard deviation between 5 simulations. Plots in panels **(c)**-**(d)** display the corresponding number of tumour cells and CTLs at the end of simulations (corresponding to day 4 of the experiments).

tact with tumour cells, increasing the chance of CTLs to eliminate them. Dead tumour cell are cleared from the domain. This in turn diminishes the number of CTLs surrounded by tumour cells, decreasing also the infiltration score. However, when the TC-CTL adhesion strength is low, increasing the value of the immune success rate does not have an impact on the infiltration score. In fact, in this scenario CTLs accumulate around the tumour, decreasing their probability to come into contact with tumour cells. This decreases their likelihood of eliminate tumour cells. Analogous considerations hold for the case in which also lower rates of the growth rate of CTLs are considered (results not shown).

As shown by Figures 5.8**(c)**-**(d)**, increasing the value of the immune success rate leads to a

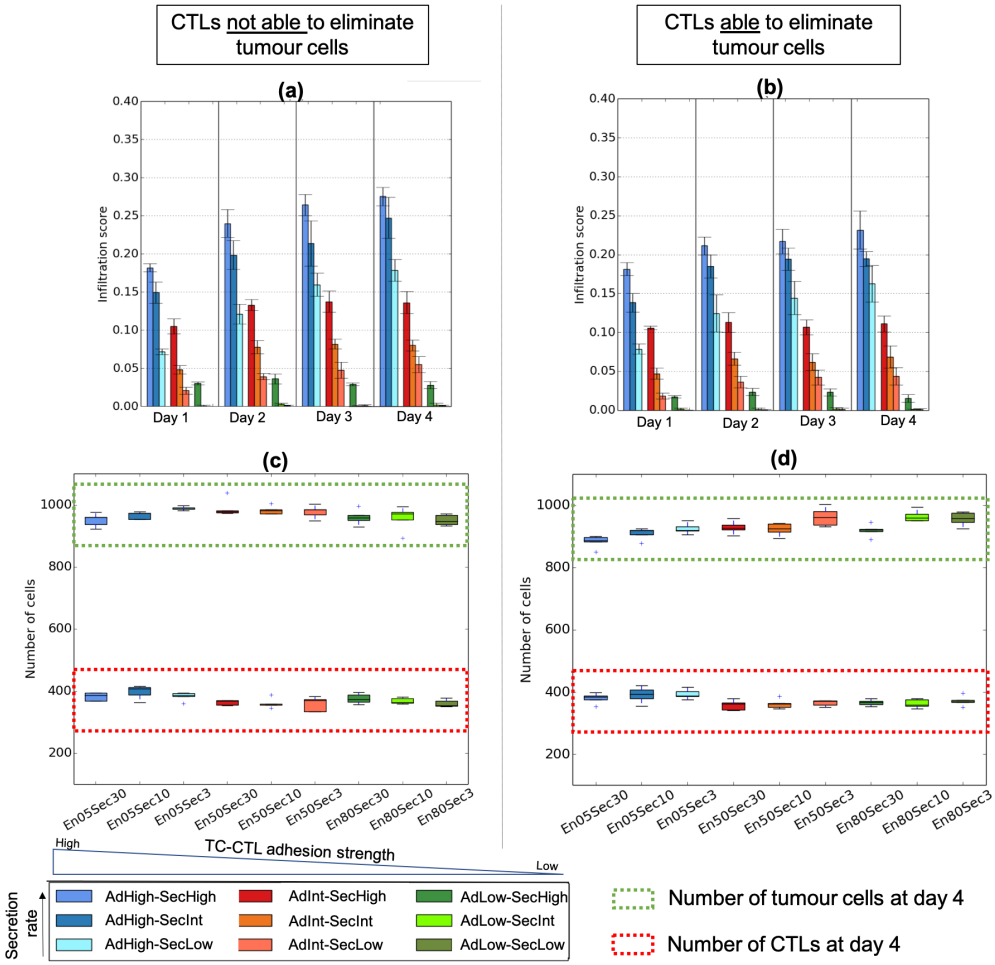

Figure 5.8: **Increasing the immune success rate has an impact on the infiltration score only when the TC-CTL adhesion strength is high.** Plot in panel **(a)** displays the average value of the infiltration score, computed via (5.2), for different combined values of the secretion rate of the chemoattractant and the TC-CTL adhesion strength, and at different times of the simulation. The error lines represent the standard deviation between 5 simulations. Inset in panel **(b)** displays an example of the spatial distribution of tumour cells and CTLs at the end of numerical simulations for the parameter values considered in our control scenario. Plots in panels (c)-(d) display the corresponding number of tumour cells and CTLs at the end of simulations (corresponding to day 4 of the experiments).

slightly decreased number of tumour cells at the end of simulations only when sufficiently high values of the TC-CTL adhesion strength and the secretion rate of chemoattractant are considered. On the other hand, for intermediate and low values of these two parameters, increasing the value of the immune success rate does not have an impact on the final number of tumour cells. Finally, independently from the value of the two parameters, the number of CTLs at the end of simulations remains similar in both scenarios.

5.7 Discussion, conclusions and research perspectives

5.7.1 Discussion and conclusions

In this chapter, we have presented a spatially explicit stochastic individual-based model of the interaction dynamics between CTLs and tumour cells to study the effects of physiological stress on immune infiltration. Building on the *in-vitro* experiments presented in [99], we have investigated, *in silico*, the way in which two cytokines, namely INF-γ and IL-10 can impact on the infiltration of CTLs into the tumour. We explored different scenarios: first we supposed that, in normal conditions, the levels of IFN-γ were high, the levels of IL-10 were low and CTLs had a high capability to infiltrate through tumour cells. Then we supposed that, in stressed conditions, the levels of IFN-γ decreased, the levels of IL-10 increased and CTLs had a lower capability to infiltrate through tumour cells. By varying the secretion rate of the chemoattractant, the growth rate of CTLs and the TC-CTL adhesion strength, we studied the impact of stress on immune infiltration. Building an infiltration score on the basis of the TIC algorithm developed in [99], we quantified the effects of stress on immune infiltration in a controlled manner.

First, our numerical results are able to qualitatively reproduce the growth of the spheroids prior the introduction of activated immune cells (*cf.* Figure 5.4). The growth of the number of tumour cells is of logistic type, so that when CTLs are introduced, changes in the tumour surface can be attributed to the infiltration of CTLs. Then, we have established our control scenario. In the experimental results obtained by [99], in absence of cortisol, splenocytes were able to infiltrate the spheroids. Our numerical results indicate that when the values of the secretion rate of the chemoattractant, the TC-CTL adhesion strength and the growth rate of CTLs are high, CTLs are able to infiltrate into the tumour (*cf.* Figure 5.5).

We then have investigated the effects of stress on immune infiltration. First, the outcomes of our model support the idea that decreasing the secretion rate of the chemoattractant and the TC-CTL adhesion strength, which are associated to a decrease in the levels of INF-γ, reduces the infiltration of CTLs into the tumour (*cf.* Figure 5.6). Our results also suggest that the secretion rate of the chemoattractant is more likely to have an impact on T cell infiltration when CTLs display a sufficiently high capability to infiltrate through tumour cells. We have also studied the effects of stress on immune infiltration by decreasing the growth rate of CTLs, which is associated to an increase in the levels of IL-10 (*cf.* Figure 5.7). Decreasing the growth rate of CTLs decreases the number of CTLs in the domain. This significantly decreases the infiltration score only when the TC-CTL adhesion strength is high. Conversely, when the TC-CTL adhesion strength is low, decreasing the growth rate of CTLs does not have an impact on the infiltration score, as its value is already small. Finally, we have investigated the outcomes of our model by letting CTLs eliminate tumour cells with a small probability (*i.e.* we increase the value of the immune success rate) (*cf.* Figure 5.8). In the scenario in which CTLs are able to infiltrate into the tumour, increasing the value of the immune success rate decreases the infiltration score, as tumour cells in contact with CTLs are eliminated. This in turn leads to a slightly decreased number of tumour cells at the end of simulations. However, when the CTL infiltration level is low, increasing the value of the immune success rate does not have an impact on the infiltration score, nor does it decrease the final number of tumour cells.

In summary, our findings demonstrate the importance of including the effect of different factors when exploring the role of stress on immune infiltration. Our results support the idea that a high infiltration score can be obtained only when the secretion rate of the chemoattractant and the TC-CTL adhesion strength are high, provided that the growth of CTLs is not inhibited. On the other hand, our results suggest that decreasing the value of these parameters can decrease immune infiltration in different ways. For example, our results indicate that the parameter

having the strongest impact on immune infiltration is the TC-CTL adhesion strength, which is associated with the capability of CTLs to infiltrate through tumour cells. When the TC-CTL adhesion strength is low, independently of the value of the secretion rate of the chemoattractant and the growth rate of CTLs, we obtain a low infiltration score. On the other hand, when the TC-CTL adhesion strength is high, varying the value of the other two parameters has a greater impact on immune infiltration, and leads to a different scenarios with different infiltration scores.

5.7.2 Research perspectives

In the future, better quantitative comparison with experiments will allow for systematic choice of parameters and validation of the mechanisms we propose here. From a biological point of view, a natural sequel of this work consists in studying the effects of therapeutic strategies which counteract the effects of stress. In fact, in [99], the authors found that the administration of glucocorticoid receptor antagonists reversed the effects of cortisol and significantly increased the immune infiltration in 66CL4 spheroids compared to those cells treated with cortisol. Finally, the effects of changing the spatial domain from 2D to 3D would need to be considered. It is probable that the change of dimension would alter the time it takes to run simulations of our mathematical model. However, in this way, a more realistic scenario, closer to the 3D co-culture model, could be explored.

Chapter 6

Conclusion and perspectives

The past decade's technological advances have led to the development of immunotherapies, which differ from conventional anti-cancer therapies by targeting tumour-immune cell interactions in order to enhance the effectiveness of the anti-tumour immune response. However, these interactions are based on complex mechanisms that make it difficult to design treatments to effectively boost the immune response. For this reason, mathematical models are useful tools for reproducing and predicting the spatio-temporal dynamics of interactions between tumour cells and immune cells, in order to test the potential of new therapeutic techniques in a flexible and affordable way.

Throughout this thesis, a series of mathematical models have been proposed to study different mechanisms involved in tumour-immune interactions, with the goal of investigating the biological settings which allow for the clearance or the escape of the tumour.

We began this thesis by describing the key biological processes and mechanisms governing the interactions between malignant tumour cells and immune cells, focussing on the role of one particular type of immune cells: the cytotoxic T lymphocytes (CTLs). CTLs are the main actors of the anti-tumour immune response, as they can actively target and destroy tumour cells. Along with a description of the immune response to tumours, we described processes that allow tumour cells to evade the immune response and some immunotherapy techniques developed and used to restore an effective immune action.

Mathematical models for tumour-immune interactions have become increasingly popular over the past few decades and are used as a tool to aid in the understanding of the mechanisms of tumour escape. We provided a short review of the existing mathematical models of tumour-immune interactions and their applications, with a focus on discrete stochastic individual-based models, deterministic continuum models and hybrid discrete-continuum models.

Following this background chapter, we provided the main body of this work. This thesis was organized in four chapters. Each chapter focussed on a mathematical model considering a specific aspect involved in the interactions between tumour cells and CTLs. In particular, these models have been developed to investigate:
(1) the coevolutionary dynamics between CTLs and tumour cells in a well mixed system;
(2) the impact of intra-tumour heterogeneity (ITH) on anti-tumour CTL immune response;
(3) the role of CTL infiltration on anti-tumour immune response;
(4) the effect of psychological stress on immune infiltration.

To investigate these problems, different methods of mathematical modelling have been developed, which allowed to include different layers of biological complexity and different aspects of tumour-immune interactions. In particular, the mathematical models proposed in this thesis were formulated as:

(A) discrete stochastic individual-based models, which relied on an explicit representation of individual cells in space and time, tracking and updating their internal states according to a predefined set of biological and biophysical rules. The development of these models allowed to represent stochasticity and heterogeneity in the interaction dynamics between tumour cells and CTLs;
(B) deterministic continuum models, which were not formulated on the basis of phenomenological arguments, which can hinder a precise mathematical description of crucial biological and biophysical aspects, but have been formally derived from the discrete models through suitable asymptotic methods. The continuum models were formulated as systems of nonlinear and nonlocal IDEs and PDEs, and provided a mean-field representation of the underlying cellular dynamics. Through linear stability analysis, we identified possible conditions on the model parameters leading to different dynamics of one continuum model, gaining a more in-depth theoretical understanding of the system under consideration.

Numerical simulations, relying on parameter values drawn from the extant literature, have been employed for *in silico* investigations of the underlying biological aspect, to qualitatively test the model assumptions against empirical observations. When the continuum model was derived from the discrete model, an excellent quantitative agreement between numerical simulations of the two models was obtained. Moreover:
(A) we developed our own computational code to carry out computational simulations of two discrete individual-based models, in order to have a deeper understanding and control over the dynamic produced. For the computational implementation of the two other individual-based models, instead, we took advantage of the Cellular Potts modelling approach, and simulations were run using the CompuCell3D open-source simulation environment. This software demonstrated to be a very useful tool when modelling tumour-immune interaction dynamics, due to the easy inclusion of precise biological aspects (such as cell adhesion, cell growth and mitosis, motility, competition for space, etc);
(B) appropriate numerical schemes were used for the numerical simulations of the continuum models, which prevented the emergence of spurious oscillations. Moreover, the computational efficiency of the continuum model with respect to its discrete counterpart has been exploited, to carry out extensive numerical simulations to investigate particular hypothesis.

In agreement with biological studies, the results obtained have shed light on:
(1) the way in which different parameters shape the coevolutionary dynamics between tumour cells and CTLs and induce the formation of patterns of phenotypic coevolution;
(2) the specific impact of different expressions of ITH on immune surveillance, highlighting the importance of ITH as a possible predictor of the outcome of immune action;
(3) the mechanisms that underlie the emergence of different levels of infiltration of CTLs into the tumour, and their impact on the response to different types of anti-cancer immunotherapy;
(4) the way in which a simple mathematical model can qualitatively reproduce an *in vitro* experiment, and demonstrate the importance of including the effect of different factors when exploring the impact of physiological stress on immune infiltration into tumours.

Each chapter of this thesis was ended with a specific discussion of the model and research perspectives. Below we discuss global potential future directions and perspectives.

Optimisation of anti-tumour treatments An important objective in oncology is the improvement of anti-tumour therapies and their combinations, with the goal of increasing the overall treatment efficacy. One option to achieve this goal is optimization of the schedule of drug administration or performing other medical actions. A key advantage of mathematical models is that they can be amenable to an analysis of their control (optimization and optimal control). Let us note that optimization and optimal control methods can be applied mainly to deterministic,

both ODE and PDE models, having in mind that therapeutic optimization may resort to these methods. Optimization of an anti-tumour treatment usually implies determining what should be the best schedule, *i.e.* dose distribution and timing, for a treatment that affects both tumour cells and healthy (usually fast renewing) cells. Of course, from the point of view of clinical use, the goal is to achieve the best therapeutic results with the fewest possible side effects to healthy cells.

Optimal control theory is applied in a huge number of studies of different natures and has also become popular in mathematical oncology (see [122] for a review on examples of therapeutic problems in oncology and how they have been addressed theoretically).

In Chapter 4 we investigated the effects of immunotherapeutic protocols only when they were delivered at the initial time of simulations and treatment effect was constant in time. Therefore, it would be interesting to include in our models the effects of different types of therapies and to apply optimal control methods. This would allow to determine the best delivery schedule of different therapeutic agents that would achieve the best therapeutic outcome, minimising the number of tumour cells at the end of the treatment with the least possible side effects to healthy cells.

Data availability and model vadility One of the goals of mathematical modelling in oncology is to provide personalized predictions by taking into account patient-specific data. In clinical practice, cancer patients undergo several examinations such as blood sample analysis, clinical imaging (e.g. CT, MRI), biopsy sampling, etc. However, such clinical data are provided for very limited time-points. There are different reasons for that, *e.g.* the fact that data collection is restricted to the clinical presentation of the patient, the cost, the availability of the equipments, the side effects of the exams, etc. Moreover, the mechanistic connection between these data is elusive, and the way to connect all these variables in a single model can be complex. Therefore, many of these data sets are left out from the model development process. Moreover, even having all the required mechanistic knowledge to develop an appropriate model, this latter would involve a huge number of parameters, making the model untractable mathematically. In combination with the lack of clinical data with sufficient temporal resolution and specificity, the goal of personalized model calibration would have been a 'mission impossible'. Under this constraint, delivering personalized predictions becomes a difficult task.

However, the obsession for data fitting should not be the main driver for model development. One should keep in mind that the purpose of a model is to answer a specific question and that its domain of applicability and validity is always restricted. It is important to point out that the complexity of cancer makes it impossible to accurately model all aspects which allow it to escape immune surveillance. In this thesis, we aimed at showing that mathematical models are an excellent tool to describe underlying dynamics of tumour-immune interaction, and may elucidate some important biological actions that govern it. The models developed in the different chapters proved very useful in giving some insights into different mechanisms that allow the tumour to escape immune surveillance, as well as into some therapeutic aspects, to understand why and how therapeutic combinations can lead to the clearance or the escape of the tumour.

In 1976, George Box, a British statistician, wrote the famous line, "*All models are wrong, some are useful.*" His point was that we should focus more on whether something can be applied to everyday life in a useful manner rather than debating endlessly if an answer is correct in all cases. Therefore, regardless of being right or wrong, mathematical models for tumour-immune interactions can be very useful, and can open up new avenues and stimulate new experimental or theoretical researches.

The importance of interdisciplinary research In this thesis, we have developed different models of tumour-immune interactions which try to better understand some mechanisms that are responsible for immune escape. During the development of the different models, fruitful discussions with biologists and immunologists helped us to construct reasonable modelling assumptions, and to test them on interesting biological problems. The different models may provide possible insight to design immunotherapy strategies which effectively improve the effectiveness of the overall anti-tumour immune response. However, it is of paramount importance that more experimental clinical data is used when developing and implementing these models to try and enrich and validate the results.

More effort should be made to try to find a common language between mathematicians and medical workers, as well as to find the right balance between the rigor of mathematical models and the level of uncertainty prevailing in the clinical environment. Collaborations between biologists, clinicians and mathematicians can ensure that models are more in-depth and can increase the success of research on the development of new cancer therapies. Nevertheless, confronted with the undoubtable successes met in the last 50 years in clinical oncology, encountering more and more limitations as new treatments emerge, oncologists together with evolutionary biologists, immunologists, physicists and mathematicians, have begun to lower barriers between their disciplines. This trend of interdisciplinary research has recently reached even up to philosophers [17] who have thus emerged as a community of "philosophers of cancer".

Interdisciplinary work has become more common in cancer research, and mathematical modelling has already led to several predictions, as well as to the discovery of some important biological actions that govern tumour dynamics, with a hope to develop better treatments to extend the host's life, or to eradicate the cancer completely.

Appendix A

Cellular Potts models and Compucell3D

The individual-based models developed in Chapter 3 and Chapter 5 have been numerically solved using the multicellular modelling environment CompuCell3D [107]. This software is an open source solver, which uses a Cellular Potts model [89] (also known as CPM, or Glazier-Graner-Hogeweg model). The system is written in the programming language C++, but allows users to create new models in a user-friendly manner in the XML and Python languages. The software runs on Windows, Mac and Linux platforms without change of model specification.

CompuCell3D models have a range of different uses within mathematical biology, allowing rapid and compact specification of cells, diffusing fields and biochemical networks, all of this in two or three dimensions.

A.1 Lattice configuration

Each Cellular Potts model is made up of generalized objects, a description of their behaviours and appropriate initial conditions. The objects in each model are comprised of regular lattice sites, called pixels in 2D and voxels in 3D. The most fundamental object is a generalized cell, which may represent a biological cell, a subcellular compartment, a cluster of cells, or a piece of non-cellular material or surrounding medium [107]. Each generalized cell has an associated list of attributes, *e.g.* cell type, surface area and volume. The index of the cell occupying cell-lattice site i is uniquely defined as $\sigma(i)$ and the type of the cell is referred to as $\tau(\sigma(i))$. Here, i is a vector of integer occupying pixel i. Either increasing or decreasing the number of pixels a cell contains can change its volume and surface. For example, in the model we developed in Chapter 3, to characterise the different sub-populations of cancer cells, we define as many types of tumour cells as sub-populations of cancer cells. Moreover, CTLs have as many types as TCRs considered for the simulation, which corresponds also to the number of antigens considered.

Interaction descriptions and dynamics between cells are modelled by means of the system's effective energy. This determines many characteristics such as cell size, shape, motility, adhesion strength and the reaction to gradients of chemotactic fields. The effective energy define a way to produce a desired set of biological and physiological cell behaviors and does not represent the physical energy of the cells. The user defines the parameters for the effective energy for each cell type and these parameters determine the characteristics of each cell. During a simulation, each cell will attempt to extend its boundaries, through a series of index-copy attempts, known as

"flip", in order to minimise the effective energy. If the index-copy attempt is successful the cell will increase in volume by a lattice site and the neighbouring cell will decrease in volume. The success of the index copy attempt is dependent upon a Boltzmann acceptance function which takes into account the change in energy. Once all of the boundary pixels in the simulation have performed an index-copy attempt, a Monte Carlo Step (MCS) has been completed.

In addition to generalized cells, CompuCell3D can also adequately model nutrients, chemical gradients or the extra cellular matrix by using a field component. Fields evolve due to secretion, absorption, diffusion, reaction and decay according to appropriate PDEs. Generalised-cell behaviors are affected by extracellular chemical fields and subcellular networks (*e.g.* changes in cell target volume due to chemical absorption, chemotaxis in response to a field gradient or cell differentiation based on the internal state of a genetic network). Auxiliary ODE equations are used to describe cell interactions with fields, such as absorption, and secretion, and state changes within the cells, such as mitosis and cell death. Figure A.1 shows how a lattice configuration evolves to minimize the total energy of the system.

A.2 Effective energy

The effective energy is the basis for operation of all Cellular Potts Models, including CompuCell3D, because it determines the behavior of the interactions between generalized cells. The energy is described in two ways: boundary energy or constraints. The most important boundary energy components of the effective energy equations governs the adhesion of cells. Adhesion is defined by the boundary energy $J(\tau(\sigma_i), \tau(\sigma_j))$, which describe the contact energy per unit area between the two cells (σ_i, σ_j) of types ($\tau(\sigma_i), \tau(\sigma_j)$). This is calculated by the sum over all neighbouring pixels i and j that form the boundary between two cells:

$$H_{boundary} = \sum_{i,j \text{ neighbours}} J(\tau(\sigma_i), \tau(\sigma_j))(1 - \delta(\sigma_i, \sigma_j)) \tag{A.1}$$

The delta function restricts the boundary energy contribution to cell-cell interfaces. $J(\tau(\sigma_i), \tau(\sigma_j))$ is defined as a matrix indexed by the cell types. Higher boundary energies between cells result in greater repulsion between cells and lower boundary energies imply a greater adhesion between cells.

As said before, the second way of using the effective energy in a model is by means of constraints on cell behaviour. Constraints are written in a general elastic form and are represented by:

$$H_{constrain} = \lambda(value - target\ value)^2 \tag{A.2}$$

As we can see, if $value = target\ value$, the constraint is satisfied and, therefore, the energy is zero. This condition is known as the equilibrium condition. Since CompuCell3D tries to minimise the effective energy in a simulation the constraint will be driven to the equilibrium condition. However, as the nature of the simulations is stochastic, the condition does not always have to be met and it is possible that two or more constraints conflict with each other so that they are only able to be partially met, resulting in random fluctuations. Parameter λ, a positive real number known as the spring constraint, determines how far the value can deviate from the target. Large values of λ will result in a larger effective energy change, essentially preventing a index-copy attempt, whereas small values allow for greater deviation from the equilibrium condition.

The most common employment of constraint energies for biological cells in CompuCell3D is to restrict the size of a cell to a given target value. This is done through two constraints: the

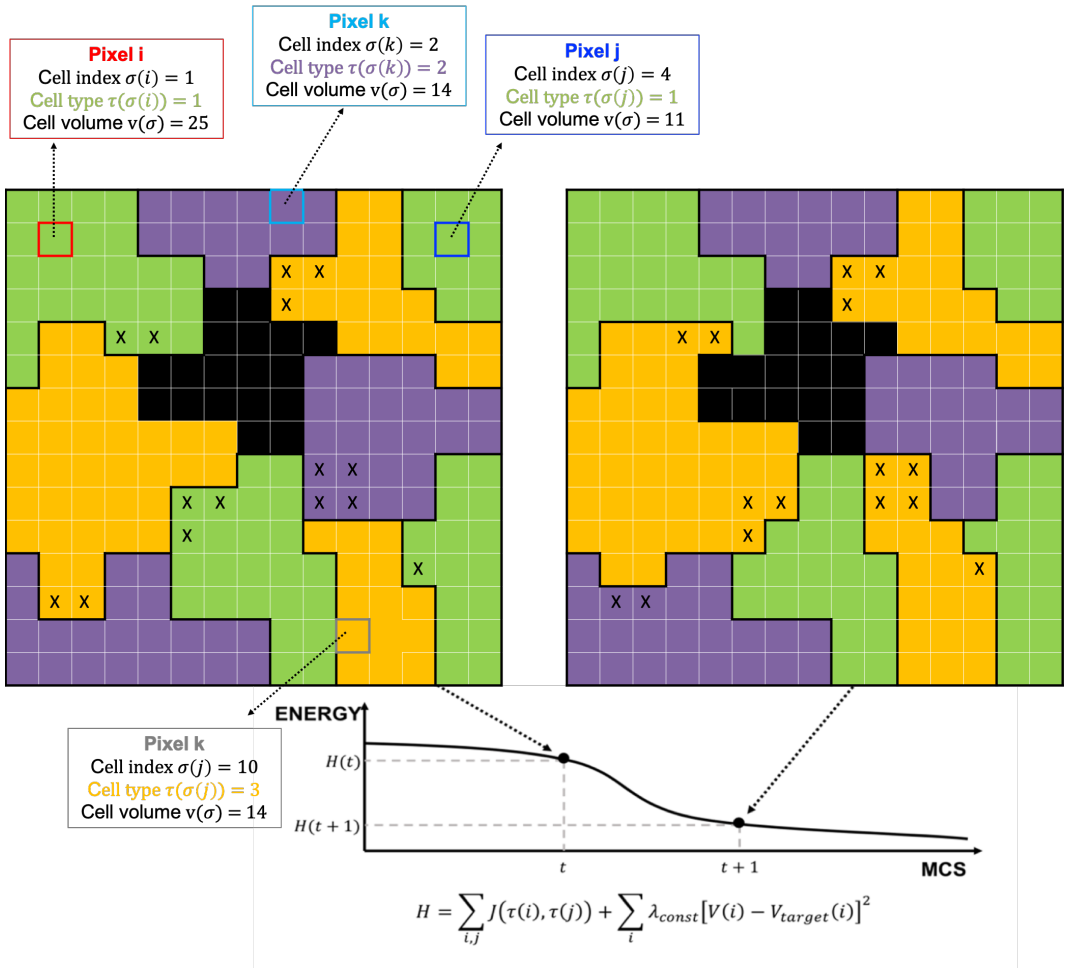

Figure A.1: **Cellular Potts Model lattice configuration and effective energy.** Schematic representation of evolution of a lattice configuration of a Cellular Potts Model. In this example, 10 different cells uniquely identified by their index σ are grouped in three different types $\tau(\sigma)$) (green - type 1, purple - type 2, yellow - type 3), and occupy multiple pixels, which define their volume $v(\sigma)$. The medium is represented by the black pixels. The biological characteristics of each cell are contained in each pixel belonging to the cell and are expressed as constraints in the effective energy that encodes the dynamics of the systems. The lattice evolves by changes in the identity of each pixel that minimize the energy of the system. In this example 15 "flips" have been accepted. Adapted from [11].

volume and the surface area. The volume constraint energy for each cell σ is defined as:

$$H_{vol} = \sum_{\sigma} \left[\lambda_{vol}(\sigma)(v(\sigma) - V_t(\sigma))^2\right] \tag{A.3}$$

where $\lambda_{vol}(\sigma)$ is the inverse compressibility of the cell, $v(\sigma)$ is the number of pixels in the cell and $V_t(\sigma)$ is the cell's target volume in pixels. The volume constraint define $P = -2\lambda_{vol}(v(\sigma) -$

$V_t(\sigma)$) as the pressure inside the cell. When $v < V_t$ the cell has positive internal pressure, which encourages it to expand, and when $v > V_t$ the cell has negative internal pressure, which encourages it to shrink. The amplitudes of fluctuations of the cell's volume about is target volume are controlled by the value of parameter $\lambda_{vol}(\sigma)$.

In similar fashion the surface area constraint is given by:

$$H_{surf} = \sum_{\sigma} \left[\lambda_{surf}(\sigma)(s(\sigma) - S_t(\sigma))^2\right] \tag{A.4}$$

where $s(\sigma)$ is the surface area of the cell σ, $S_t(\sigma)$ is the cell's target surface area and $\lambda_{surf}(\sigma)$ is its inverse membrane compressibility. By combining together the boundary energy in Equation (A.1) and volume constraints in Equation (A.3), the basic GGH effective energy is modelled by:

$$H = \sum_{i,j} J(\tau(\sigma_i), \tau(\sigma_j))(1 - \delta(\sigma_i, \sigma_j)) + \sum_{\sigma} \left[\lambda_{vol}(\sigma)(v(\sigma) - V_t(\sigma))^2\right] \tag{A.5}$$

A.3 A Monte Carlo Step

Time is measured in CompuCell3D simulations by Monte Carlo Steps (MCS), which indicate when every pixel on the lattice has made an index-copy attempt to a neighbouring pixel. To begin an index-copy attempt, the algorithm randomly selects a lattice site to be a target pixel i, and a neighbouring lattice site to be a source pixel i'. An attempt will then be made to switch the target pixel to the same generalised cell as the source pixel, thereby increasing the volume of the source cell and decreasing the volume of the target cell. If the source and target pixels belong to the same cell (*i.e.* $\sigma(i) = \sigma(i')$), they do not need to attempt a flip and thus the effective energy will not be calculated.

If different generalized cells occupy these pixels, the algorithm sets $\sigma(i) = \sigma(i'))$ with probability $P(\sigma(i)) \rightarrow \sigma(i')$, given by the Boltzmann acceptance function [152]:

$$P(\sigma(i)) \rightarrow \sigma(i') = \begin{cases} 1 & : \quad \Delta H \leq 0 \\ \exp^{\frac{\Delta H}{T_m}} & : \quad \Delta H > 0 \end{cases} \tag{A.6}$$

where ΔH is the change in effective energy if the copy occurs and T_m determines the amplitude of cell membrane fluctuations and the effective cell random motility. For an index-copy attempt, this probability means that if the change in effective energy is less than or equal to zero then the attempt will be successful. On the other hand, if the resulting change in effective energy is greater than zero the attempt may still be successful with the probability $\exp^{\frac{\Delta H}{T_m}}$. For biological simulations, the parameters ΔH and T_m allow for a conversion between the number of MCS and experimental time. The conversion depends on the average values of $\frac{\Delta H}{T_m}$. In practice, in simulations, high values of the ratio $\frac{\Delta H}{T_m}$ results in rigid, barely- or non-motile cells and little cell rearrangement. For low $\frac{\Delta H}{T_m}$, large fluctuations allow a high degree of cell random motility and rearrangement.

A.4 Subcellular dynamics and chemotaxis

In addition to generalized cells, Compucell3D simulations may contain other objects such as chemical fields and subcellular networks as well as auxiliary equations to describe events at the cellular level like cell growth, division and rule-based differentiation. These chemical fields and

subcellular networks evolve due to secretion, absorption, diffusion, reaction and decay according to appropriate PDEs and affect generalized-cell behaviors by modifying the effective energy.

A cellular behaviour easy to simulate with Compucell3D is chemotaxis, defined as the cell motion induced by a presence of a chemical. In a simulation, chemotaxis is obtained biasing a cell's motion up or down a field gradient by changing the calculated effective-energy change used in the acceptance function. For a field $\phi(i)$:

$$\Delta H_{chem} = -\lambda_{chem}(\phi(i) - \phi(i')) \tag{A.7}$$

where $\phi(i)$ is the chemical field at the index-copy target pixel i, $\phi(i')$ the field at the index-copy source pixel i', and λ_{chem} the strength and direction of chemotaxis. If $\lambda_{chem} > 0$ and $\phi(i) > \phi(i')$, then ΔH_{chem} is negative, increasing the probability of accepting the index copy. The net effect is that the cell moves up the field gradient with a velocity $\sim \lambda_{chem}\nabla\phi$. If $\lambda_{chem} < 0$ is negative, the opposite occurs, and the cell will move down the field gradient.

The change in concentration of the chemical field ϕ is obtained by solving a reaction-diffusion equation of the following general form:

$$\frac{\partial\phi}{\partial t} = D\nabla^2\phi - \gamma\phi + S \tag{A.8}$$

where D, γ and S denote the diffusion constant, decay constant and secretion rates of the field, respectively. These three parameters may vary with position and cell-lattice configuration, and thus be a function of cell σ and pixel i.

Appendix B

Appendix for Chapter 2

B.1 Formal derivation of the continuum model

Using a method analogous to that employed in [13, 40, 194], we show that the PDE-IDE system (2.13) can be formally derived as the appropriate continuum limit of the individual-based model presented in Chapter 2.

Substituting definitions (2.9) of P_n^b and P_n^q into the difference equation $(2.11)_1$ for n_i^k and definitions (2.10) of P_c^b and P_c^q into the difference equation $(2.11)_2$ for c_j^k yields

$$\begin{cases} n_i^{k+1} = \left[1 + \tau\,\alpha_n - \tau\,\left(\mu_n\,K_{n_i}^k + \zeta_n\,\gamma\,J_{n_i}^k\right)\right]\left[\dfrac{\lambda_n}{2}\left(n_{i+1}^k + n_{i-1}^k\right) + (1-\lambda_n)\,n_i^k\right], \\ \\ c_j^{k+1} = \left[1 + \tau\,\left(\alpha_c + \zeta_c\,\gamma\,J_{n_i}^k\right) - \tau\,\mu_c\,K_{c_j}^k\right]\,c_j^k, \end{cases} \tag{B.1}$$

where $n_i^k \equiv n(x_i, t_k)$ with $(x_i, t_k) \in \mathcal{I} \times (0, t_f]$ and $c_j^k \equiv c(y_j, t_k)$ with $(y_j, t_k) \in \overline{\mathcal{I}} \times (0, t_f]$. Using the fact that the following relations hold for τ and χ sufficiently small

$$t_k \approx t, \quad t_{k+1} \approx t + \tau, \quad x_i \approx x, \quad x_{i\pm1} \approx x \pm \chi, \quad y_j \approx y,$$

$$n_i^k \approx n(x,t), \quad n_i^{k+1} \approx n(x, t+\tau), \quad n_{i\pm1}^k \approx n(x \pm \chi, t), \quad \rho_n^k \approx \rho_n(t) := \int_{\mathcal{I}} n(x,t)\,\mathrm{d}x,$$

$$J_{n_i}^k \approx J_n(x,t) := \int_{\mathcal{I}} g(x,y;\eta)\,c(y,t)\,\mathrm{d}y, \quad K_{n_i}^k \approx K_n(x,t) := \int_{\mathcal{I}} g(x,z;\theta_n)\,n(z,t)\,\mathrm{d}z,$$

$$c_j^k \approx c(y,t), \quad c_j^{k+1} \approx c(y, t+\tau), \quad \rho_c^k \approx \rho_c(t) := \int_{\mathcal{I}} c(y,t)\,\mathrm{d}y,$$

$$J_{c_j}^k \approx J_c(y,t) := \int_{\mathcal{I}} g(y,x;\eta)\,n(x,t)\,\mathrm{d}x, \quad K_{c_j}^k \approx K_c(y,t) := \int_{\mathcal{I}} g(y,z;\theta_c)\,c(z,t)\,\mathrm{d}z,$$

where the function g is defined via (2.6), the system of equations (B.1) can be formally rewritten

in the approximate form

$$\begin{cases} n(x,t+\tau) = \Big[1+\tau\, R_n(K_n(x,t),J_n(x,t))\Big]\times \\ \qquad\qquad\qquad\qquad \times \left[\dfrac{\lambda_n}{2}\,(n(x+\chi,t)+n(x-\chi,t))+(1-\lambda_n)\,n(x,t)\right], \\ \\ c(y,t+\tau) = \Big[1+\tau\, R_c(K_c(y,t),J_c(y,t))\Big]\, c(y,t), \end{cases} \tag{B.2}$$

where $x \in \mathcal{I}$, $y \in \overline{\mathcal{I}}$ and $t \in (0,t_f]$. Here,

$$R_n(K_n,J_n) := \alpha_n - \Big(\mu_n\, K_n + \zeta_n\, \gamma\, J_n\Big), \quad R_c(K_c,J_c) := \Big(\alpha_c + \zeta_c\, \gamma\, J_c\Big) - \mu_c\, K_c. \tag{B.3}$$

If the function $n(x,t)$ is twice continuously differentiable with respect to the variable x, for χ sufficiently small we can use the Taylor expansions

$$n(x\pm\chi,t) = n(x,t) \pm \chi\partial_x n(x,t) + \frac{\chi^2}{2}\partial^2_{xx} n(x,t) + h.o.t.\ . \tag{B.4}$$

Substituting the Taylor expansions (B.4) into equation $(B.2)_1$ for $n(x,t+\tau)$, after a little algebra we find

$$\begin{cases} \dfrac{n(x,t+\tau)-n(x,t)}{\tau} - \dfrac{\lambda_n\chi^2}{2\tau}\partial^2_{xx} n(x,t) = R_n(K_n(x,t),J_n(x,t))\, n(x,t) + \\ \qquad\qquad\qquad\qquad + \dfrac{\lambda_n\chi^2}{2}\, R_n(K_n(x,t),J_n(x,t))\, \partial^2_{xx} n(x,t) + h.o.t.\,, \\ \\ \dfrac{c(y,t+\tau)-c(y,t)}{\tau} = R_c(K_c(y,t),J_c(y,t))\, c(y,t). \end{cases}$$

If, in addition, the functions $n(x,t)$ and $c(y,t)$ are continuously differentiable with respect to the variable t, letting $\tau \to 0$ and $\chi \to 0$ in such a way that condition (2.12) is met, from the latter system of equations we formally obtain

$$\begin{cases} \partial_t n(x,t) - \beta_n \partial^2_{xx} n(x,t) = R_n(K_n,J_n)\, n(x,t), \quad (x,t) \in \mathcal{I}\times(0,t_f], \\ \\ \partial_t c(y,t) = R_c(K_c,J_c)\, c(y,t), \quad (y,t) \in \overline{\mathcal{I}}\times(0,t_f]. \end{cases}$$

Substituting definitions (B.3) of $R_n(K_n,J_n)$ and $R_c(K_c,J_c)$ into the above system of equations gives the PDE-IDE system (2.13). Finally, the no-flux boundary conditions (2.14) follow from the fact that the attempted phenotypic variation of a tumour cell is aborted if it requires moving into a phenotypic state that does not belong to the interval $\overline{\mathcal{I}}$.

B.2 Details of numerical simulations of the continuum model

To construct numerical solutions of the PDE-IDE system (2.13) subject both to the no-flux boundary conditions (2.14) and to the initial condition (2.43), we use a uniform discretisation of step $\Delta x = 0.0013$ of the interval $\overline{\mathcal{I}} = [-L,L]$ as the computational domain of the independent variables x and y, and a uniform discretisation of step $\Delta t = 0.05$ of the time interval $(0,t_f]$.

We construct numerical solutions of the non-local PDE $(2.13)_1$ for n using a time-splitting approach, which is based on the idea of decomposing the original problem into simpler subproblems that are then sequentially solved at each time-step using an explicit Euler method with step Δt. This leads to the following time-dicretisation of the PDE-IDE system (2.13) subject to the Neumann boundary conditions (2.14):

$$\begin{cases} n^{k+\frac{1}{2}}(x) = n^k(x) + \Delta t\, R_n(K_n^k(x), J_n^k(x))\, n^k(x), \quad x \in [-L, L], \\ \\ n^{k+1}(x) = n^{k+\frac{1}{2}}(x) + \Delta t\, \beta_n\, \partial_{xx}^2 n^{k+\frac{1}{2}}(x), \quad x \in (-L, L), \\ \\ \partial_x n^{k+1}(x) = 0, \quad x \in \{-L, L\} \\ \\ c^{k+1}(y) = c^k(y) + \Delta t\, R_c(K_c^k(y), J_c^k(y))\, c^k(y), \quad y \in [-L, L], \end{cases} \tag{B.5}$$

where

$$R_n(K_n^k, J_n^k) := \alpha_n - \mu_n K_n^k - \zeta_n \gamma J_n^k, \quad R_c(K_c^k, J_c^k) := \alpha_c - \mu_c K_c^k - \zeta_c \gamma J_c^k.$$

The system of equations (B.5) is numerically solved using a three-point finite difference explicit scheme for the diffusion term [128] and an implicit-explicit finite difference scheme for the remaining terms [131, 135], which leads to the following system of equations

$$\begin{cases} n_i^{k+\frac{1}{2}} = n_i^k \dfrac{1 + \Delta t\, R_n(K_{n_i}^k, J_{n_i}^k)_+}{1 + \Delta t\, R_n(K_{n_i}^k, J_{n_i}^k)_-}, \quad x_i \in [-L, L], \\ \\ n_i^{k+1} = n_i^{k+\frac{1}{2}} + \beta_n \Delta t \dfrac{n_{i+1}^{k+\frac{1}{2}} - 2n_i^{k+\frac{1}{2}} + n_{i-1}^{k+\frac{1}{2}}}{\Delta x^2}, \quad x_i \in (-L, L), \\ \\ n_i^{k+1} = n_{i-1}^{k+1}, \quad x_i \in \{-L, L\}, \\ \\ c_j^{k+1} = c_j^k \dfrac{1 + \Delta t\, R_c(K_{c_j}^k, J_{c_j}^k)_+}{1 + \Delta t\, R_c(K_{c_j}^k, J_{c_j}^k)_-}, \quad y_j \in [-L, L]. \end{cases}$$

Here, $R_n(\cdot,\cdot)_+$ and $R_c(\cdot,\cdot)_+$ are the positive parts of $R_n(\cdot,\cdot)$ and $R_c(\cdot,\cdot)$, while $R_n(\cdot,\cdot)_-$ and $R_c(\cdot,\cdot)_-$ are the negative parts of $R_n(\cdot,\cdot)$ and $R_c(\cdot,\cdot)$. Moreover,

$$K_{n_i}^k = \sum_h g(x_i, x_h; \theta_n)\, n_h^k\, \Delta x, \qquad K_{c_j}^k = \sum_h g(y_j, y_h; \theta_c)\, c_h^k\, \Delta x$$

and

$$J_{n_i}^k = \sum_j g(x_i, y_j; \eta)\, c_j^k\, \Delta x, \qquad J_{c_j}^k = \sum_i g(y_j, x_i; \eta)\, n_i^k\, \Delta x.$$

Given the values of the parameter τ, χ and λ_n of the individual-based model, the value of the parameter β_n is defined so that condition (2.12) is met. The other parameter values are chosen to be coherent with those used to carry out numerical simulations of the individual-based model, which are specified in the main body of Chapter 2.

B.3 Supplementary figures

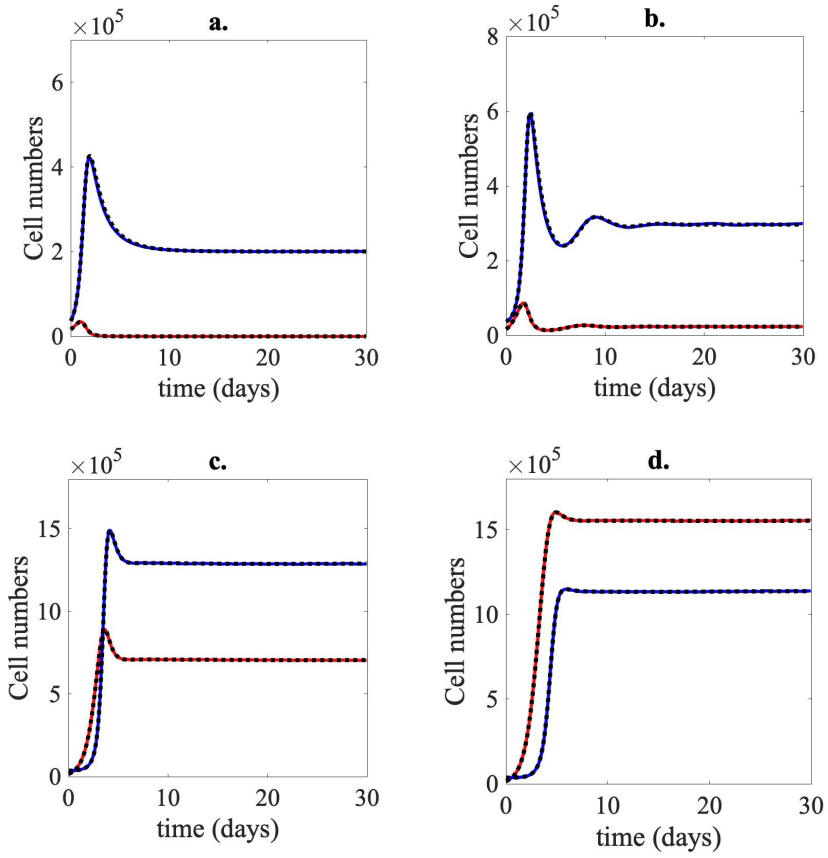

Figure B.1: **Eradication of tumour cells and emergence of hot tumour-like, altered tumour-like and cold tumour-like scenarios: the case where** $a > 0$**.** Panel **a.** displays the plots of the time evolution of the total number of tumour cells (ρ_n) and CTLs (ρ_c) of the individual-based model (solid, coloured lines) and the continuum model (dashed, black lines) when γ is high enough that condition (2.34) is satisfied (i.e. condition (2.24) does not hold). Here, $\alpha_c = 0.5$ and all the other parameters are as in Table 2.1 with $\gamma = 3.5$, $\eta = 1.8$ and $\theta_n = \theta_c = 1.8$. Panels **b.-d.** display similar plots for sufficiently large, intermediate and sufficiently small values of γ that satisfy condition (2.24) – i.e. $\gamma = 2$ (panel **b.**), $\gamma = 0.3$ (panel **c.**) and $\gamma = 0.12$ (panel **d.**). All the other parameters are as in Table 2.1 with $\eta = 1.8$ and $\theta_n = \theta_c = 1.8$. Initial conditions (2.42) and (2.43) with $a = 1$ and $A = 5$ were used to carry out numerical simulations. Analogous results were obtained when using different values of the parameter A (results not shown). The results from the individual-based model correspond to the average over two realisations of the underlying random walk and the related variance is displayed by the coloured areas surrounding the curves.

Appendix C

Appendix for Chapter 3

C.1 Model parameters

The individual-based model developed in Chapter 3 is parametrised using parameter values obtained from published biological data wherever possible. We use a 2D squared spatial domain with 400×400 lattice sites (pixels). We assume that a pixel of the domain corresponds to $3 \times 3\ \mu m^2$. As the CTL diameter is estimated to be between 10 μm and 12 μm [75, 87], the initial size of a CTL is 4×4 pixels. A tumour cell diameter is estimated to be about 20 μm [43], therefore we assume that each newly divided tumour cell is made of 5×5 pixels. In addition, the maximum CTL migration speed measured in the simulation is around 10 pixels/100 MCS. Therefore, using the CTL migration measurements *in vivo* ($2-25\ \mu m/min$, see [153]), we choose 1 MCS $\sim$ 1 minute as a time scale. The parameters for the Cellular Potts model are listed in Table C.1, while all the other parameters with their related references are listed in Table C.2.

We now provide a discussion on how some of the parameters of the Cellular Potts model were chosen. Interactions between neighboring pixels in the Cellular Potts model have an effective energy, J (as it appears in Equation (A.5)), which characterises the strength of cell-cell adhesion (see Table C.1). A larger J means that more energy is associated with the interface between two cells, which is less energetically favourable, corresponding to weaker adhesivity. It can be observed that J_{CT} and J_{TT} are lower than J_{CC}. We make the assumption that tumour cells stay in contact to compactly create the tumour mass and that when a CTL enters in contact with a tumour cell then strongly binds to it. When they migrate in the domain to search for tumour cells, CTLs are not in contact with each other.

Files to run a simulation example with Compucell3D software are available at: https://plmlab.math.cnrs.fr/audebert/cc3dmodeltumourcd8.

C.2 Supplementary figures

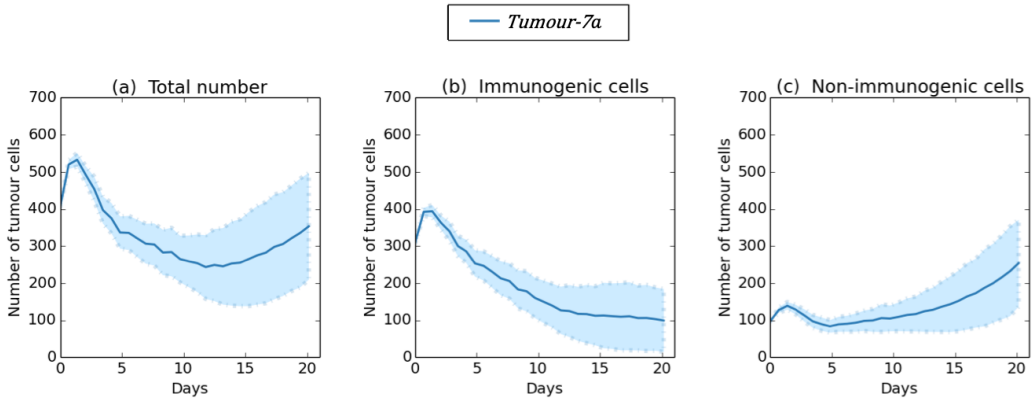

Figure C.1: **The overall dynamics between 100 realisations of the same simulation are qualitatively similar to those between 10 realisations.** Plots in panels **(a)-(c)** display the time evolution of the total tumour cell number, and the corresponding evolution of the number of immunogenic cells and non-immunogenic cells for *tumour-7a*. Shaded areas indicate +/− standard deviation between 100 simulations. For these simulations, the same initial conditions used for *tumour-7a* in Figure 3.6 were used. The parameter values are kept constant and equal to those listed in Table C.1 and Table C.2.

Table C.1: Parameter values used to implement the Cellular Potts model. Energies, temperature and constrains are dimensionless parameters.

Phenotype	Symbol	Description	Value	Reference
Domain	$\Delta x, \Delta y$	Domain spacing in the x or y direction	1 Pixel $= 3 \times 3\ \mu m^2$	
	Δt	Time-step	1 MCS = 1 min	
	t_f	Final time	20 $(days)$	
CC3D	J_{MT}	Contact energy tumour cells-medium	50	
	J_{MC}	Contact energy CTLs-medium	50	
	J_{CT}	Contact energy CTLs-tumour cells	20	
	J_{TT}	Contact energy tumour cells-tumour cells	110	
	J_{CC}	Contact energy CTLs-CTLs	1000	
	d_T	Tumour cell diameter	20-40 (μm)	[87]
	d_C	CTL diameter	12 (μm)	[75]
	λ_{area}	Tumour cell and CTL area constrain	10	
	λ_{per}	Tumour cell and CTL perimeter constrain	10	
	T_m	Fluctuation amplitude parameter	10	
	λ_{chem}	Strength and direction of chemotaxis	50	

Table C.2: Parameter values used in numerical simulations.

Phenotype	Description	Value	Reference
Tumour	Initial number	$N_T(0) = 400$	
	Index identifier	$n = 1, \ldots, N_T(t)$	
	Lifespan	$\mathcal{U}_{[3,7]}$ $(days)$	[87]
	Growth rate	$\mathcal{U}_{[0.015,0.02]}$ $(pixel/min)$	[87]
	Mean cycle time	24 $(hours)$	[87]
	Rate of death due to competition between tumour cells	3.8×10^{-7} $(1/min)$	
	Antigen profile	$A = (a_1, \ldots, a_f)$	
	Clonal antigen profile	$A_C \subset A$	
	Sub-clonal antigen profile	$A_{SC} \subset A$	
	Range of value of antigen presentation for clonal cells	$L_I = \left\{\frac{1}{6}, \frac{2}{6}, \frac{3}{6}, \frac{4}{6}, \frac{5}{6}, 1\right\}$	
	Range of value of antigen presentation for sub-clonal cells	$L_{NI} = \left\{\frac{5}{100}, \frac{10}{100}, \frac{15}{100}, \frac{20}{100}, \frac{25}{100}, \frac{30}{100}\right\}$	
	Antigen	$a_i \in A$	
	Level of presentation of antigen a_i of tumour cell n	$l^n_{a_i} \in [0, 1]$	
CTLs	Total number at time t	$N_C(t) \geqslant 0$	
	Index identifier	$m = 1, \ldots, N_C(t)$	
	Influx rate	$p(t) = C_1 \times S^{tot}_a(t)$ $C_1 = 2 \times 10^{-5}$ (min/mol)	
	Lifespan	$\mathcal{U}_{[2.5,3.5]}$ $(days)$	[87]
	Migration speed	2 - 25 $(\mu m/min)$	[75]
	Engagement time	6 $(hours)$	[43]
	TCR-recognition probability	$r = 0.901$	
Chemoattractant	Concentration	$\phi_{a_i} \geqslant 0$ $(mol/pixel)$	
	Total amount secreted	$S^{tot}_{a_i} \geqslant 0$ (mol/min)	
	Diffusion	$D = 7 \times 10^{-1}$ $(pixel^2/min)$	
	Secretion	$s^n_{a_i} = C_2 \times l^n_a$ $(mol/min/pixel)$ $C_2 = 10$ $(mol/min/pixel)$	
	Decay	$\gamma = 3 \times 10^{-4}$ $(1/min)$	
	Initial concentration	$\phi^{init}_{a_i} = 0.5(280 - \sqrt{(x-200)^2 + (y-200)^2})$	

Appendix D

Appendix for Chapter 4

D.1 Formal derivation of the continuum model

Building on the methods employed in [26], we carry out a formal derivation of the deterministic continuum model given by the IDE-PDE-PDE system (4.30) for $d = 1$. Similar methods can be used in the case where $d = 2$.

D.1.1 Formal derivation of the IDE for the density of tumour cells $n(x,t)$

In the case where tumour cell dynamics are governed by the rules described in Sections 4.3.1 and 4.3.1, considering $(i,k) \in [0,\mathcal{N}] \times \mathbb{N}_0$, between time-steps k and $k+1$ the principle of mass balance gives the following difference equation for the tumour cell density n_i^k:

$$n_i^{k+1} = \left[2\,\tau\alpha_n + 1 - \tau(\alpha_n + \zeta_n K_i^k + \mu_n \rho_n^k\right] n_i^k. \tag{D.1}$$

Using the fact that the following relations hold for τ and χ sufficiently small

$$t_k \approx t, \quad t_{k+1} \approx t + \tau, \quad x_i \approx x, \quad x_{i\pm1} \approx x \pm \chi, \tag{D.2}$$

$$n_i^k \approx n(x,t), \quad n_i^{k+1} \approx n(x,t+\tau), \quad c_i^k \approx c(x,t), \tag{D.3}$$

$$\rho_n^k \approx \rho_n(t) := \int_\Omega n(x,t)\,\mathrm{d}x, \quad K_i^k \approx K(x,t) := \int_\Omega \eta(x,x';\theta)c(x',t)\,\mathrm{d}x', \tag{D.4}$$

where the function η is defined via (4.12), equation (D.1) can be formally rewritten in the approximate form

$$n(x,t+\tau) - n(x,t) = \tau\left(\alpha_n - \zeta_n K(x,t) - \mu_n \rho_n(t)\right) n(x,t). \tag{D.5}$$

If, in addiction, the function $n(x,t)$ is continuously differentiable with respect to the variable t, starting from equation (D.5), and letting the time-step $\tau \to 0$, one formally obtains the following IDE for the tumour cell density $n(x,t)$:

$$\partial_t n(x,t) = \alpha_n n(x,t) - \mu_n \rho_n(t)\, n(x,t) - \zeta_n K(x,t) n(x,t) \quad (x,t) \in \Omega \times \mathbb{R}_+^*.$$

D.1.2 Formal derivation of the PDE for the density of CTLs $c(x,t)$

The formal derivation of the PDE for the density of CTLs $c(x,t)$ is built on the methods employed in [26]. In the case where T cell dynamics are governed by the rules described in Section 4.3.3, considering $(i,k) \in [1, \mathcal{N}-1] \times \mathbb{N}_0$, between time-steps k and $k+1$ the principle of mass balance gives the following difference equation for the CTLdensity c_i^k:

$$\begin{aligned} c_i^{k+1} &= c_i^k(1-\tau\,\mu_c\rho_c^k) + \tau\,\alpha_c r_i^k \\ &+ \frac{\lambda}{2}\psi(w_i^k)\Big(c_{i+1}^k + c_{i-1}^k\Big) \\ &- \frac{\lambda}{2}\Big(\psi(w_{i-1}^k) + \psi(w_{i+1}^k)\Big)c_i^k \\ &+ \frac{\nu}{2\phi_{\max}}\psi(w_i^k)\Big[\Big(\phi_i^k - \phi_{i-1}^k\Big)_+ c_{i-1}^k\Big] \\ &+ \frac{\nu}{2\phi_{\max}}\psi(w_i^k)\Big[\Big(\phi_i^k - \phi_{i+1}^k)\Big)_+ c_{i+1}^k\Big] \\ &- \frac{\nu}{2\phi_{\max}}\psi(w_{i+1}^k)\Big[\Big(\phi_{i+1}^k - \phi_i^k\Big)_+ c_i^k\Big] \\ &- \frac{\nu}{2\phi_{\max}}\psi(w_{i-1}^k)\Big[\Big(\phi_{i-1}^k - \phi_i^k\Big)_+ c_i^k\Big]. \end{aligned} \tag{D.6}$$

Using the fact that relations (D.2)-(D.4) and the following relations

$$c_i^k \approx c(x,t), \quad c_{i\pm1}^k \approx c(x\pm\chi), \quad \rho_c^k \approx \rho_c(t) := \int_\Omega c(x,t)\,\mathrm{d}x,$$

$$\phi_i^k \approx \phi(x,t), \quad \phi_i^{k+1} \approx \phi(x,t+\tau), \quad \phi_{i\pm1}^k \approx \phi(x\pm\chi),$$

$$w_i^k \approx w(x,t), \text{ with } w(x,t) := n(x,t) + c(x,t), \quad w_{i\pm1}^k \approx w(x\pm\chi),$$

$$r_i^k \approx r(x,t) := \phi_{tot}(t)\mathbb{1}_\omega(x), \text{ with } \phi_{tot}(t) := \int_\Omega \phi(x,t)\,\mathrm{d}x$$

hold for τ and χ sufficiently small, equation (D.6) can be formally rewritten in the approximate form

$$\begin{aligned} c(x,t+\tau) &= c(x,t)(1-\tau\,\mu_c\rho_c(t)) + \tau\,\alpha_c r(x,t) \\ &+ \frac{\lambda}{2}\psi(w(x,t))\Big(c(x+\chi,t) + c(x-\chi,t)\Big) \\ &- \frac{\lambda}{2}\Big(\psi(w(x-\chi,t)) + \psi(w(x+\chi,t))\Big)c(x,t) \\ &+ \frac{\nu}{2\phi_{\max}}\psi(w(x,t))\Big[\Big(\phi(x,t) - \phi(x-\chi,t)\Big)_+ c(x-\chi,t)\Big] \\ &+ \frac{\nu}{2\phi_{\max}}\psi(w(x,t))\Big[\Big(\phi(x,t) - \phi(x+\chi,t)\Big)_+ c(x+\chi,t)\Big] \\ &- \frac{\nu}{2\phi_{\max}}\psi(w(x+\chi,t))\Big[\Big(\phi(x+\chi,t) - \phi(x,t)\Big)_+ c(x,t)\Big] \\ &- \frac{\nu}{2\phi_{\max}}\psi(w(x-\chi,t))\Big[\Big(\phi(x-\chi,t) - \phi(x,t)\Big)_+ c(x,t)\Big]. \end{aligned}$$

If the function $\psi(w(x,t))$ is twice continuously differentiable and the functions $c(x,t)$ and $\phi(x,t)$ are twice continuously differentiable with respect to the variable x, for χ sufficiently small

we can use their Taylor expansions

$$\psi(w(x \pm \chi, t)) = \psi \pm \chi \partial_x \psi + \frac{\chi^2}{2} \partial_{xx} \psi + \mathcal{O}(\chi^3),$$

where

$$\psi \equiv \psi(w),\ \partial_x \psi = \psi'(w) \partial_x w,\ \partial_{xx} \psi = \psi''(w) \Big(\partial_x w \Big)^2 + \psi'(w) \partial_{xx} w$$

and

$$c(x \pm \chi, t) = c \pm \chi \partial_x c + \frac{\chi^2}{2} \partial_{xx} c + \mathcal{O}(\chi^3), \quad \phi(x \pm \chi, t) = \phi \pm \chi \partial_x \phi + \frac{\chi^2}{2} \partial_{xx} c + \mathcal{O}(\chi^3).$$

Therefore, after a little algebra we obtain

$$\psi \Big(c(x + \chi, t) + c(x - \chi, t) \Big) - \Big(\psi(w(x - \chi, t)) + \psi(w(x + \chi, t)) \Big) c = \chi^2 (\partial_{xx} c \psi - c \partial_{xx} \psi)$$

$$\Big(\phi(x, t) - \phi(x - \chi, t) \Big)_+ c(x - \chi, t) = \Big(\chi \partial_x \phi(x, t) - \frac{\chi^2}{2} \partial_{xx} \phi(x, t) \Big)_+ [c(x, t) - \chi \partial_x c(x, t)],$$

$$\Big(\phi(x, t) - \phi(x + \chi, t) \Big)_+ c(x + \chi, t) = \Big(- \chi \partial_x \phi(x, t) - \frac{\chi^2}{2} \partial_{xx} \phi(x, t) \Big)_+ [c(x, t) + \chi \partial_x c(x, t)],$$

$$\Big(\phi(x - \chi, t) - \phi(x, t) \Big)_+ c(x, t) = \Big(- \chi \partial_x \phi(x, t) + \frac{\chi^2}{2} \partial_{xx} \phi(x, t) \Big)_+ c(x, t)$$

and

$$\Big(\phi(x + \chi, t) - \phi(x, t) \Big)_+ c(x, t) = \Big(\chi \partial_x \phi(x, t) + \frac{\chi^2}{2} \partial_{xx} \phi(x, t) \Big)_+ c(x, t)$$

We compute

$$\begin{aligned} \partial_{xx} c \psi(w) - c \partial_{xx} \psi(w) &= \partial_x \Big[\psi(w) \partial_x c \Big] - \partial_x \Big[c \psi'(w) \partial_x w \Big] \\ &= \partial_x \Big[(\psi(w) - c \psi'(w)) \partial_x c - c \psi'(w)) \partial_x n \Big], \end{aligned} \tag{D.7}$$

and using the elementary property $(a)_+ - (-a)_+ = a$ for $a \in \mathbb{R}$ we also obtain

$$\begin{aligned} -\psi c \Big(\Big(\partial_{xx} \phi \Big)_+ - \Big(- \partial_{xx} \phi \Big)_+ \Big) - \psi \partial_x c \Big(\Big(\partial_x \phi \Big)_+ - \Big(- \partial_x \phi \Big)_+ \Big) \\ + \partial_x \psi c \Big(\Big(- \partial_x \phi \Big)_+ - \Big(\partial_x \phi \Big)_+ \Big) = - \partial_x \Big[\psi c \partial_x \phi \Big]. \end{aligned} \tag{D.8}$$

Substituting the computation into Equation (D.6), letting $\tau \to 0$ and $\chi \to 0$ in such a way that

$$\frac{\lambda}{2} \frac{\chi^2}{\tau} \to \beta_c \in \mathbb{R}_*^+ \quad \text{and} \quad \frac{\nu}{2 \phi_{\max}} \frac{\chi^2}{\tau} \to \gamma_c \in \mathbb{R}_*^+,$$

after a little algebra, considering $(x, t) \in \Omega \setminus \partial\Omega \times \mathbb{R}_+^*$, we find

$$\partial_t c - \partial_x \Big[\beta_c \psi(w) \partial_x c - \gamma_c \psi(w) c \partial_x \phi - \beta_c c \psi'(w) \partial_x w \Big] = - \mu_c \rho_c(t) c + \alpha_c r$$

where ψ is given by (4.22) and $w := n + c$.

Moreover, zero-flux boundary conditions easily follow from the fact that T-cell moves that require moving out of the spatial domain are not allowed.

D.1.3 Formal derivation of the balance equation for the concentration of chemoattractant $\phi(x,t)$

In the case where the chemoattractant dynamics are governed by the rules described in Section 4.3.2, using the same methods employed in [26], considering $(i,k) \in [1, \mathcal{N}-1] \times \mathbb{N}_0$ and assuming that relations (D.2)-(D.4) and relations (D.1.2)-(D.1.2) hold for τ, χ sufficiently small, the difference Equation (4.14) can be formally rewritten in the approximate form

$$\frac{\phi(x,t+\tau)-\phi(x,t)}{\tau} = \beta_\phi \frac{\phi(x-\chi,t)+\phi(x+\chi,t)-2\phi(x,t)}{\chi^2} + \alpha_\phi n(x,t) - \kappa_\phi \phi(x,t) \tag{D.9}$$

If the function ϕ is continuously differentiable with respect to the variable t and twice differentiable with respect to the variable x, letting $\tau, \chi \to 0$ in the above equation gives

$$\partial_t \phi(x,t) - \beta_\phi \partial_{xx} \phi(x,t) = \alpha_\phi n(x,t) - \kappa_\phi \phi(x,t) \tag{D.10}$$

which is the balance equation for the chemoattractant concentration ϕ posed on $\Omega \times \mathbb{R}_+^*$. We complement Equation (D.10) with zero flux boundary conditions.

D.2 Details of numerical simulations

The numerical simulations of our hybrid and continuum models are carried out on a two-dimensional domain and are performed in MATLAB.

D.2.1 Details of numerical simulations of the hybrid model

The flowchart in Fig. D.1 illustrates the general computational procedure to carry out simulations of the hybrid model in a one-dimensional setting, while the flowchart in Fig. D.2 provides further details of the computational procedure to simulate cell dynamics in a one-dimensional setting. Analogous strategies are used in a two-dimensional setting. All random numbers mentioned in Fig. D.2 are real numbers drawn from the standard uniform distribution on the interval $(0,1)$, which in our case are obtained using the built-in MATLAB function RAND.

As summarised by Fig. D.2, at each time-step τ, each CTLundergoes a three-phase process: Phase A) undirected, random movement according to the probabilities defined via (4.26) and (4.27); Phase B) chemotaxis according to the probabilities defined via (4.23) and (4.24); Phase C) inflow and death according to the probabilities defined via equations (4.17) and (4.21). We let then each tumour cell proliferate with the probability defined via (4.8), die due to intra-tumour competition with the probability defined via (4.10), or die due to immune action with the probability defined via (4.13). Finally, the tumour cell density at every lattice site is computed via (4.1) and inserted into (4.14) in order to update the concentration of the chemoattractant.

In a two-dimensional setting, the positions of the single CTLs are updated following a procedure analogous to that explained in Fig. D.1 and Fig. D.2, with the only difference being that the CTLs are allowed to move up and down as well. Moreover, the concentration of the chemoattractant is updated through the two-dimensional analogue of (4.14), where the operator $\mathcal{L}$ is defined as the finite-difference Laplacian on a two-dimensional regular lattice of step χ and the tumour and T cell densities are respectively computed via (4.1) and (4.2).

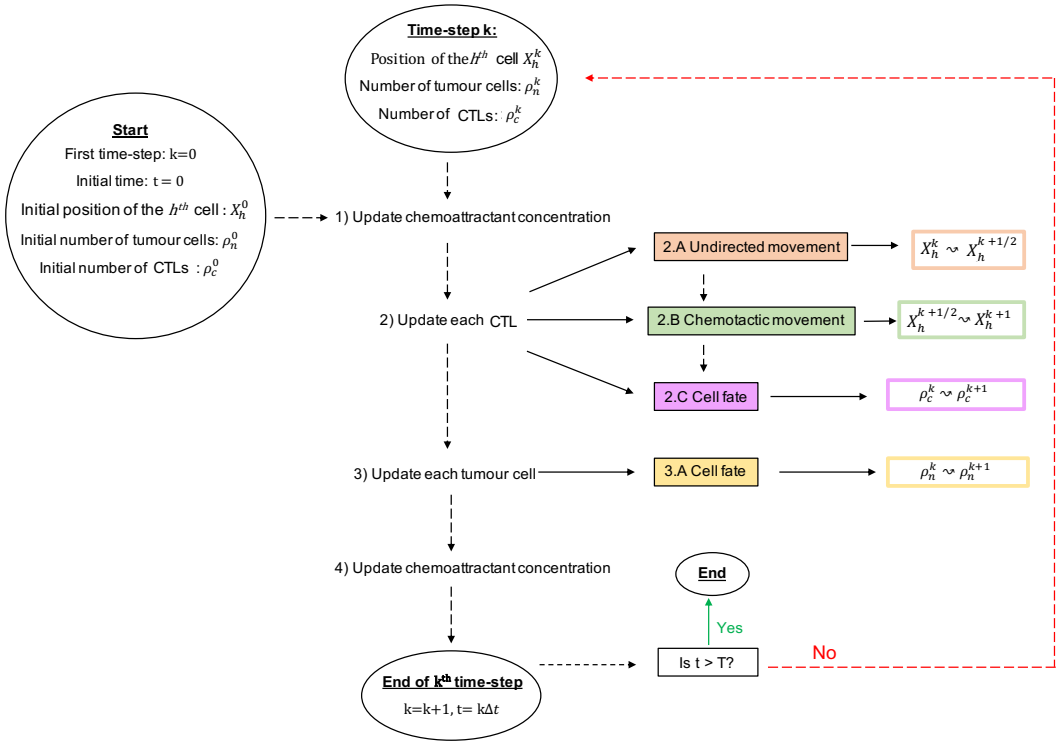

Figure D.1: Flowchart illustrating the computational procedure to simulate the hybrid model in a one-dimensional setting. A detailed summary of steps 2) and 3) is provided by the flowchart in Fig. D.2. A similar procedure is used in a two-dimensional setting.

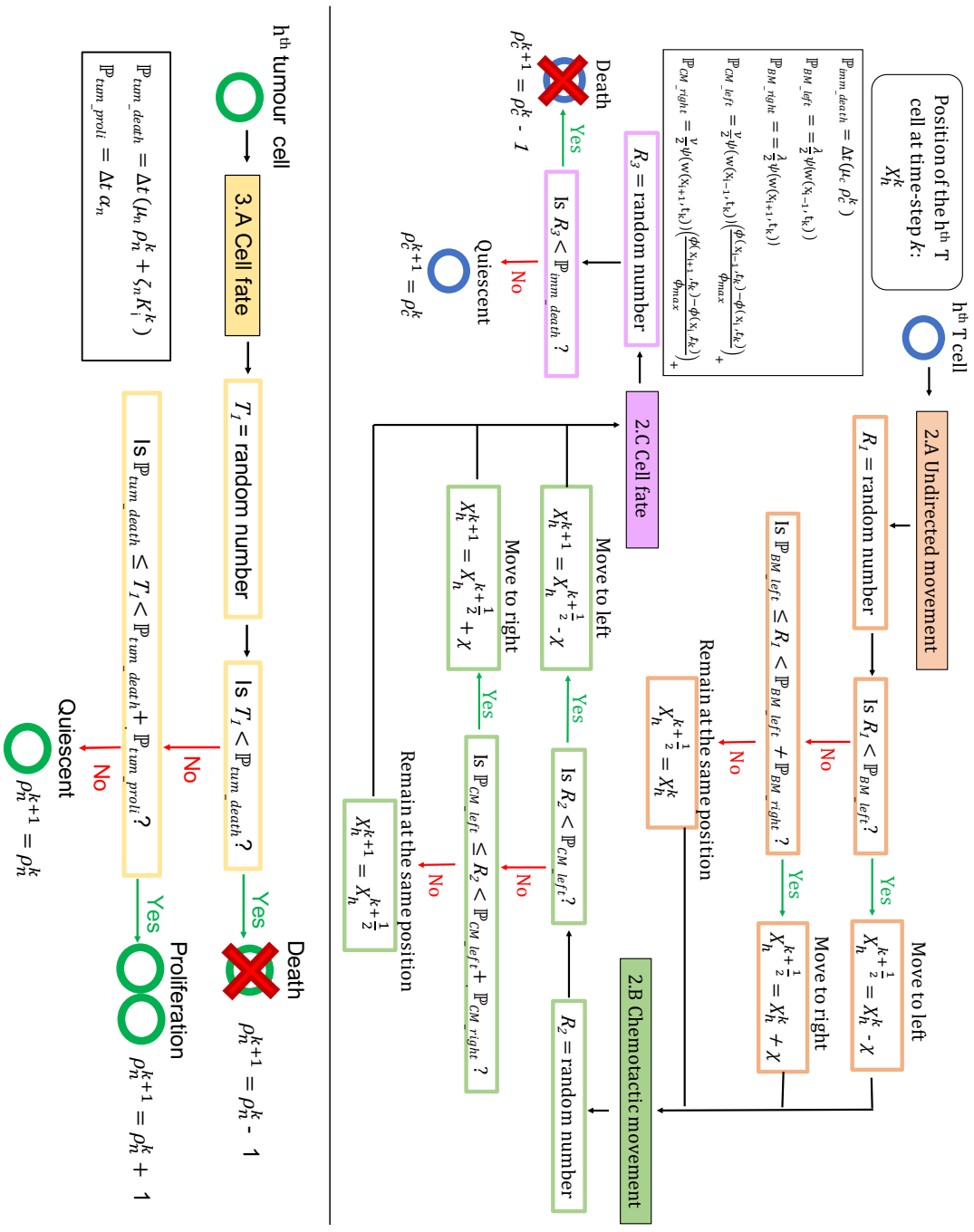

Figure D.2: Flowchart illustrating the detailed computational procedure followed to update the positions of every CTL, as well as the fate of each tumour cell and CTL in 1D. Analogous strategies are then used in a two-dimensional domain.

D.2.2 Details of numerical simulations of the continuum model

To construct numerical solutions of the IDE-PDE-PDE system (4.30), we use a uniform discretisation consisting of $N^2 = 3721$ points of the square $\Omega := [0,1]^2$ as the computational domain of the independent variable $\mathbf{x} \equiv (x,y)$ (*i.e.* $(x_i, y_j) = (i\Delta x, j\Delta x)$ with $\Delta x = 0.016$ and $i,j = 0,\dots,N$) Moreover, we choose the time step $\Delta t = 1 \times 10^{-4}$, and we perform numerical simulations for 15×10^4 time-steps (*i.e.* the final time of simulations is $t_f = 15$).
The method for constructing numerical solutions of the IDE-PDE-PDE system (4.30) is based on a finite difference scheme whereby the discretised dependent variables are

$$n^k_{i,j} := n(x_i, y_j, t_k), \quad c^k_{i,j} := c(x_i, y_j, t_k) \quad \text{and} \quad \phi^k_{i,j} := \phi(x_i, y_j, t_k).$$

We solve numerically the IDE $(4.30)_1$ for n and the PDE $(4.30)_3$ for ϕ using the following schemes

$$\frac{n^{k+1}_{i,j} - n^k_{i,j}}{\Delta t} = \left(\alpha_n - \mu_n \rho^k_n - \zeta_n K^k_{i,j}\right) n^k_{i,j} \quad i,j = 0,\dots,N,$$

and

$$\begin{aligned}\frac{\phi^{k+1}_{i,j} - \phi^k_{i,j}}{\Delta t} =& \beta_\phi \frac{\phi^k_{i-1,j} + \phi^k_{i+1,j} - 2\phi^k_{i,j}}{(\Delta x)^2} + \beta_\phi \frac{\phi^k_{i,j-1} + \phi^k_{i,j+1} - 2\phi^k_{i,j}}{(\Delta x)^2} \\ &+ \alpha_\phi n^k_{i,j} - \kappa_\phi \phi^k_{i,j}, \quad i,j = 1,\dots,N-1,\end{aligned}$$

and impose zero-flux boundary conditions for ϕ by letting

$$\phi^{k+1}_{0,j} = \phi^{k+1}_{1,j} \quad \text{and} \quad \phi^{k+1}_{N,j} = \phi^{k+1}_{N-1,j}, \quad j = 0,\dots,N$$

$$\phi^{k+1}_{i,0} = \phi^{k+1}_{i,1} \quad \text{and} \quad \phi^{k+1}_{i,N} = \phi^{k+1}_{i,N-1}, \quad i = 0,\dots,N$$

Moreover, we solve numerically the PDE $(4.30)_2$ for c using the following explicit scheme, which is the same as the one used in [26],

$$\frac{c^{k+1}_{i,j} - c^k_{i,j}}{\Delta t} - \frac{F^k_{i+\frac{1}{2},j} + F^k_{i-\frac{1}{2},j}}{\Delta x} - \frac{F^k_{i,j+\frac{1}{2}} + F^k_{i,j-\frac{1}{2}}}{\Delta x} = r(\phi^k_{i,j}) - \mu_c \rho^k_c c^k_{i,j}$$

for $i,j = 0,\dots,N$, where

$$\begin{aligned}F^k_{i+\frac{1}{2},j} :=& \beta_c \psi(w^k_{i+\frac{1}{2},j}) \frac{c^k_{i+1,j} - c^k_{i,j}}{\Delta x} - \beta_c c^k_{i+\frac{1}{2},j} \psi'(w^k_{i+\frac{1}{2},j}) \frac{w^k_{i+1,j} - w^k_{i,j}}{\Delta x} \\ &- b^{k,+}_{i+\frac{1}{2},j} c^k_{i,j} \psi(w^k_{i+1,j}) + b^{k,-}_{i+\frac{1}{2},j} c^k_{i+1,j} \psi(w^k_{i,j}), \quad i = 0,\dots N-1,\ j = 0,\dots N,\end{aligned}$$

$$\begin{aligned}F^k_{i,j+\frac{1}{2}} :=& \beta_c \psi(w^k_{i,j+\frac{1}{2}}) \frac{c^k_{i,j+1} - c^k_{i,j}}{\Delta x} - \beta_c c^k_{i,j+\frac{1}{2}} \psi'(w^k_{i,j+\frac{1}{2}}) \frac{w^k_{i,j+1} - w^k_{i,j}}{\Delta x} \\ &- b^{k,+}_{i,j+\frac{1}{2}} c^k_{i,j} \psi(w^k_{i,j+1}) + b^{k,-}_{i,j+\frac{1}{2}} c^{k+1}_{i,j+1} \psi(w^k_{i,j}), \qquad i = 0,\dots N,\ j = 0,\dots N-1,\end{aligned}$$

with

$$w^k_{i+\frac{1}{2},j} := \frac{w^k_{i+1,j} + w^k_{i,j}}{2}, \qquad w^k_{i,j+\frac{1}{2}} := \frac{w^k_{i,j+1} + w^k_{i,j}}{2},$$

$$c^k_{i+\frac{1}{2},j} := \frac{c^k_{i+1,j} + c^k_{i,j}}{2}, \qquad c^k_{i,j+\frac{1}{2}} := \frac{c^k_{i,j+1} + c^k_{i,j}}{2},$$

$$b^k_{i+\frac{1}{2},j} := \gamma_c \frac{\phi^k_{i+1,j} - \phi^k_{i,j}}{\Delta x},\ b^{k,+}_{i+\frac{1}{2},j} = \max\left(0, b^k_{i+\frac{1}{2},j}\right),\ b^{k,-}_{i+\frac{1}{2},j} = \max\left(0, -b^k_{i+\frac{1}{2},j}\right)$$

and

$$b^k_{i,j+\frac{1}{2}} := \gamma_c \frac{\phi^k_{i,j+1} - \phi^k_{i,j}}{\Delta x},\ b^{k,+}_{i,j+\frac{1}{2}} = \max\left(0, b^k_{i,j+\frac{1}{2}}\right),\ b^{k,-}_{i,j+\frac{1}{2}} = \max\left(0, -b^k_{i,j+\frac{1}{2}}\right)$$

The discrete fluxes $F^k_{i-\frac{1}{2},j}$ for $i = 1, \ldots, N$, $j = 0, \ldots, N$ and $F^k_{i,j-\frac{1}{2}}$ for $i = 0, \ldots, N$, $j = 1, \ldots, N$ are defined in an analogous way, and we impose zero-flux boundary conditions by using the definitions

$$F^k_{0-\frac{1}{2},j} := 0 \quad \text{and} \quad F^k_{N+\frac{1}{2},j} := 0, \quad \text{for} \quad j = 0, \ldots, N,$$

$$F^k_{i,0-\frac{1}{2}} := 0 \quad \text{and} \quad F^k_{i,N+\frac{1}{2}} := 0, \quad \text{for} \quad i = 0, \ldots, N.$$

Appendix E

Appendix for Chapter 5

The individual-based model developed in Chapter 5 is based on a simplified version of the mathematical model developed in Chapter 3, which has been calibrated to qualitatively reproduce the experimental results presented in [99]. We refer the reader to Appendix C.1 for a description of the parameterisation of the original model. We describe here the way in which additional components of the model were calibrated using the parameter values reported in tables E.1 and E.2, to reproduce the qualitative behaviour of the experimental results presented in [99].

The value of the rate of death due to competition between tumour cells is chosen so that the number of tumour cells reaches its carrying capacity after 7 days of proliferation. The number of CTLs introduced in the domain at day 0 corresponds to 5 times the number of tumour cells introduced at day -7. The value of the rate of death due to competition between CTLs is chosen so that the value of our infiltration score computed at the end of simulations in the control scenario is similar to the value of the TIC algorithm obtained at day 4 in [99] when cortisol was not introduced in the co-culture.

The ratio between the energy at the interface between tumour cells and CTLs and the energy at the interface between tumour cells (*i.e.* the values of parameters J_{CT} and J_{TT} in Equation (A.5)) allow us to consider a wide range of biological scenarios corresponding to different degrees of immune infiltration. In particular, if the value of J_{CT} is lower than the one J_{TT} then CTLs infiltrate through tumour cells, whereas if the value of J_{CT} is larger than the one of J_{TT} then CTLs accumulate at the margin of the tumour, without infiltrating it. Therefore, to obtain different degrees of immune infiltration, we fix the value of J_{TT} and we vary the value of J_{CT}. In the control scenario we suppose that CTLs have a high capability of infiltrate through tumour cells. Therefore we suppose that J_{CT} is lower than J_{TT}. In stressed conditions however, we suppose that CTLs have a lower capability to infiltrate through tumour cells. Therefore, we increase the value of J_{CT} to a value equal to or greater than the one chosen for J_{TT}.

E.1 Model parameters

Table E.1: Parameter values used to implement the Cellular Potts model. Energies, temperature and constrains are dimensionless parameters.

Phenotype	Symbol	Description	Value	Reference
Domain	$\Delta x, \Delta y$	Domain spacing in the x or y direction	1 Pixel $= 3 \times 3\ \mu m^2$	
	Δt	Time-step	1 MCS = 2.1 min	
	t_f	Final time	4 $(days)$	
CC3D	J_{MT}	Contact energy tumour cells-medium	50	
	J_{MC}	Contact energy CTLs-medium	50	
	J_{CT}	Contact energy CTLs-tumour cells	5 or 50 or 95	
	J_{TT}	Contact energy tumour cells-tumour cells	50	
	J_{CC}	Contact energy CTLs-CTLs	1000	
	d_T	Tumour cell diameter	20-40 (μm)	[87]
	d_C	CTL diameter	12 (μm)	[75]
	λ_{area}	Tumour cell and CTL area constrain	10	
	λ_{per}	Tumour cell and CTL perimeter constrain	10	
	T_m	Fluctuation amplitude parameter	10	
	λ_{chem}	Strength and direction of chemotaxis	50	

Table E.2: Parameter values used in numerical simulations.

Phenotype	Description	Value	Reference
Tumour	Initial number	$N_T(0) = 36$	
	Index identifier	$n = 1, \ldots, N_T(t)$	
	Lifespan	$\mathcal{U}_{[3,7]}$ $(days)$	[87]
	Growth rate	$\mathcal{U}_{[0.015,0.019]}$ $(pixel/MCS)$	[99]
	Mean cycle time	12 $(hours)$	[99]
	Rate of death due to competition between tumour cells	4.6×10^{-6} $(1/MCS)$	estimated
CTLs	Initial number	$N_C(0) = 150$	
	Index identifier	$m = 1, \ldots, N_C(t)$	
	Growth rate	$\mathcal{U}_{[0.0038,0.0042]}$ $(pixel/MCS)$	[99]
	Mean cycle time	6-8 $(hours)$	[87]
	Rate of death due to competition between CTLs	1.2×10^{-5} $(1/MCS)$	estimated
	Lifespan	$\mathcal{U}_{[2.5,3.5]}$ $(days)$	[87]
	Engagement time	6 $(hours)$	[43]
	Killing probability	0 or 0.00005	
Chemoattr.	Concentration	$\phi \geqslant 0$ $(mol/pixel)$	
	Diffusion	$D = 7 \times 2 \times 10^{-5}$ $(pixel^2/MCS)$	
	Secretion	$\alpha = 30$ or 10 or 3 $(mol/MCS/pixel)$	
	Decay	$\gamma = 7 \times 10^{-4}$ $(1/MCS)$	
	Initial concentration	$\phi^{init} = 0.5(280 - \sqrt{(x-200)^2 + (y-200)^2})$	

Bibliography

[1] G. Aguadé-Gorgorió and R. Solé. "Tumour neoantigen heterogeneity thresholds provide a time window for combination immunotherapy". In: *J. R. Soc. Interface* 17.171 (2020), p. 20200736.

[2] M. Alber, N. Chen, T. Glimm, and P. M. Lushnikov. "Multiscale dynamics of biological cells with chemotactic interactions: from a discrete stochastic model to a continuous description". In: *Phys. Rev. E* 73.5 (2006), p. 051901.

[3] M. Alber, N. Chen, P. M. Lushnikov, and S. A. Newman. "Continuous macroscopic limit of a discrete stochastic model for interaction of living cells". In: *Phys. Rev. Lett.* 99.16 (2007), p. 168102.

[4] K. Alden, M. Read, J. Timmis, P. S. Andrews, H. Veiga-Fernandes, and M. Coles. "Spartan: a comprehensive tool for understanding uncertainty in simulations of biological systems". In: *PLoS Comput. Biol.* 9.2 (2013), e1002916.

[5] S. S. Alhakeem et al. "Chronic lymphocytic Leukemia–Derived IL-10 suppresses antitumor immunity". In: *J. Immunol.* 200.12 (2018), pp. 4180–4189.

[6] L. Almeida, C. Audebert, E. Leschiera, and T. Lorenzi. "Discrete and continuum models for the coevolutionary dynamics between CD8+ cytotoxic T lymphocytes and tumour cells". In: *arXiv preprint arXiv:2109.09568* (2021).

[7] L. Almeida, G. Estrada-Rodriguez, L. Oliver, D. Peurichard, A. Poulain, and F. Vallette. "Treatment-induced shrinking of tumour aggregates: A nonlinear volume-filling chemotactic approach". In: *J. Math. Biol.* 83.3 (2021), pp. 1–41.

[8] V. Anagnostou et al. "Evolution of neoantigen landscape during immune checkpoint blockade in non–small cell lung cancer". In: *Cancer Discov.* 7.3 (2017), pp. 264–276.

[9] A. Anderson and K. Rejniak. *Single-cell-based models in biology and medicine*. Springer Science & Business Media, 2007.

[10] H. Angell and J. Galon. "From the immune contexture to the Immunoscore: the role of prognostic and predictive immune markers in cancer". In: *Curr. Opin. Immunol.* 25.2 (2013), pp. 261–267.

[11] J. O. Aponte-Serrano. "Multicellular Multiscale Spatial Modeling of the Immune Response to Pathogens and Cancer". PhD thesis. Indiana University, 2021.

[12] J. C. Arciero, T. L. Jackson, and D. E. Kirschner. "A mathematical model of tumor-immune evasion and siRNA treatment". In: *Discrete Contin. Dyn. Syst. - B* 4.1 (2004), p. 39.

[13] A. Ardaševa, A. R. A. Anderson, R. A. Gatenby, H. M. Byrne, P. K. Maini, and T. Lorenzi. "Comparative study between discrete and continuum models for the evolution of competing phenotype-structured cell populations in dynamical environments". In: *Phys. Rev. E* 102.4 (2020), p. 042404.

[14] K. Atsou, F. Anjuère, V. M Braud, and T. Goudon. "A size and space structured model describing interactions of tumor cells with immune cells reveals cancer persistent equilibrium states in tumorigenesis". In: *J. Theor. Biol.* 490 (2020), p. 110163.

[15] V. P. Balachandran et al. "Identification of unique neoantigen qualities in long-term survivors of pancreatic cancer". In: *Nature* 551.7681 (2017), pp. 512–516.

[16] G. L. Beatty and E. K. Moon. "Chimeric antigen receptor T cells are vulnerable to immunosuppressive mechanisms present within the tumor microenvironment". In: *Oncoimmunology* 3.11 (2014), e970027.

[17] M. Bertolaso. *Philosophy of cancer*. Springer, 2016.

[18] A. Besse, G. D. Clapp, S. Bernard, F. E. Nicolini, D. Levy, and T. Lepoutre. "Stability analysis of a model of interaction between the immune system and cancer cells in chronic myelogenous leukemia". In: *Bull. Math. Biol.* 80.5 (2018), pp. 1084–1110.

[19] J. N. Blattman, R. Antia, D. J. D. Sourdive, X. Wang, S. M. Kaech, K. Murali-Krishna, J. D. Altman, and R. Ahmed. "Estimating the precursor frequency of naive antigen-specific CD8 T cells". In: *J. Exp. Med.* 195.5 (2002), pp. 657–664.

[20] A. Boissonnas, L. Fetler, I. S. Zeelenberg, S. Hugues, and S. Amigorena. "In vivo imaging of cytotoxic T cell infiltration and elimination of a solid tumor". In: *J. Exp. Med.* 204.2 (2007), pp. 345–356.

[21] T. Boon, J. C. Cerottini, B. Van den Eynde, P. van der Bruggen, and A. Van Pel. "Tumor antigens recognized by T lymphocytes". In: *Annu. Rev. Immunol.* 12.1 (1994), pp. 337–365.

[22] T. Boon, P. G. Coulie, B. Van den Eynde, and P. van der Bruggen. "Human T cell responses against melanoma". In: *Annu. Rev. Immunol.* 24 (2006), pp. 175–208.

[23] E. C. Border, J. P. Sanderson, T. Weissensteiner, A. B. Gerry, and N. J. Pumphrey. "Affinity-enhanced T-cell receptors for adoptive T-cell therapy targeting MAGE-A10: strategy for selection of an optimal candidate". In: *Oncoimmunology* 8.2 (2019), e1532759.

[24] B. Breart, F. Lemaítre, S. Celli, and P. Bousso. "Two-photon imaging of intratumoral CD8+ T cell cytotoxic activity during adoptive T cell therapy in mice". In: *J. Clin. Investig.* 118.4 (2008), pp. 1390–1397.

[25] D. Bruni, H. K. Angell, and J. Galon. "The immune contexture and Immunoscore in cancer prognosis and therapeutic efficacy". In: *Nat. Rev. Cancer* 20.11 (2020), pp. 662–680.

[26] F. Bubba, T. Lorenzi, and F. R. Macfarlane. "From a discrete model of chemotaxis with volume-filling to a generalized Patlak–Keller–Segel model". In: *Proc. R. Soc. A: Math. Phys. Eng. Sci.* 476.2237 (2020), p. 20190871.

[27] R. A. Budiu et al. "Restraint and social isolation stressors differentially regulate adaptive immunity and tumor angiogenesis in a breast cancer mouse model". In: *Cancer Clin. Oncol.* 6.1 (2017), p. 12.

[28] H. Byrne and Di. Drasdo. "Individual-based and continuum models of growing cell populations: a comparison". In: *J. Math. Biol.* 58.4 (2009), pp. 657–687.

[29] M. Campoli and S. Ferrone. "HLA antigen changes in malignant cells: epigenetic mechanisms and biologic significance". In: *Oncogene* 27.45 (2008), pp. 5869–5885.

[30] I. Caramalho, M. Faroudi, E. Padovan, S. Müller, and S. Valitutti. "Visualizing CTL/melanoma cell interactions: multiple hits must be delivered for tumour cell annihilation". In: *J. Cell. Mol. Med.* 13.9b (2009), pp. 3834–3846.

[31] N. Carelle, E. Piotto, A. Bellanger, J. Germanaud, A. Thuillier, and D. Khayat. "Changing patient perceptions of the side effects of cancer chemotherapy". In: *Cancer* 95.1 (2002), pp. 155–163.

[32] F. Castiglione and B. Piccoli. "Optimal control in a model of dendritic cell transfection cancer immunotherapy". In: *Bull. Math. Biol.* 68.2 (2006), pp. 255–274.

[33] F. Castro, A. P. Cardoso, R. M. Gonçalves, K. Serre, and M. J. Oliveira. "Interferon-gamma at the crossroads of tumor immune surveillance or evasion". In: *Front. Immunol.* 9 (2018), p. 847.

[34] C. Cattani, A. Ciancio, and A. d'Onofrio. "Metamodeling the learning–hiding competition between tumours and the immune system: a kinematic approach". In: *Math. Comput. Model.* 52.1 (2010), pp. 62–69.

[35] N. Champagnat, R. Ferrière, and S. Méléard. "From individual stochastic processes to macroscopic models in adaptive evolution". In: *Stochastic Models* 24.sup1 (2008), pp. 2–44.

[36] T. A. Chan, M. Yarchoan, E. Jaffee, C. Swanton, S. A. Quezada, A. Stenzinger, and S. Peters. "Development of tumor mutation burden as an immunotherapy biomarker: utility for the oncology clinic". In: *Ann. Oncol.* 30.1 (2019), pp. 44–56.

[37] D. D. Chaplin. "Overview of the immune response". In: *J. Allergy Clin. Immunol.* 125.2 (2010), S3–S23.

[38] D. S. Chen and I. Mellman. "Elements of cancer immunity and the cancer–immune set point". In: *Nature* 541.7637 (2017), pp. 321–330.

[39] D. S. Chen and I. Mellman. "Oncology meets immunology: the cancer-immunity cycle". In: *Immunity* 39.1 (2013), pp. 1–10.

[40] R. H. Chisholm, T. Lorenzi, L. Desvillettes, and B. D. Hughes. "Evolutionary dynamics of phenotype-structured populations: from individual-level mechanisms to population-level consequences". In: *Z. Angew. Math. Phys.* 67.4 (2016), p. 100.

[41] Heyrim Cho and Doron Levy. "Modeling the chemotherapy-induced selection of drug-resistant traits during tumor growth". In: *Journal of theoretical biology* 436 (2018), pp. 120–134.

[42] Heyrim Cho and Doron Levy. "Modeling the dynamics of heterogeneity of solid tumors in response to chemotherapy". In: *Bull. Math. Biol.* 79.12 (2017), pp. 2986–3012.

[43] C. Christophe, S. Müller, M. Rodrigues, A. E. Petit, P. Cattiaux, L. Dupré, S. Gadat, and S. Valitutti. "A biased competition theory of cytotoxic T lymphocyte interaction with tumor nodules". In: *PLoS ONE* 10.3 (2015), e0120053.

[44] A. K. Cooper and P. S. Kim. "A Cellular Automata and a Partial Differential Equation Model of Tumor–Immune Dynamics and Chemotaxis". In: *Mathematical Models of Tumor-Immune System Dynamics*. Ed. by Amina Eladdadi, Peter Kim, and Dann Mallet. New York, NY: Springer New York, 2014, pp. 21–46.

[45] P. G. Coulie, B. J. Van Den Eynde, P. Van Der Bruggen, and T. Boon. "Tumour antigens recognized by T lymphocytes: at the core of cancer immunotherapy". In: *Nat. Rev. Cancer* 14.2 (2014), pp. 135–146.

[46] K. N. Couper, D. G. Blount, and E. M. Riley. "IL-10: the master regulator of immunity to infection". In: *J. Immunol.* 180.9 (2008), pp. 5771–5777.

[47] R. M. Crean et al. "Molecular Rules Underpinning Enhanced Affinity Binding of Human T Cell Receptors Engineered for Immunotherapy". In: *Mol. Ther. Oncolytics* 18 (2020), pp. 443–456.

[48] A. d'Onofrio. "A general framework for modeling tumor-immune system competition and immunotherapy: Mathematical analysis and biomedical inferences". In: *Phys. D: Nonlinear Phenom.* 208.3-4 (2005), pp. 220–235.

[49] P. Darvin, S. M. Toor, V. Sasidharan Nair, and E. Elkord. "Immune checkpoint inhibitors: recent progress and potential biomarkers". In: *Exp. Mol. Med.* 50.12 (2018), pp. 1–11.

[50] A. R. David and M. R. Zimmerman. "Cancer: an old disease, a new disease or something in between?" In: *Nat. Rev. Cancer* 10.10 (2010), pp. 728–733.

[51] T. S. Deisboeck, Z. Wang, P. Macklin, and V. Cristini. "Multiscale cancer modeling". In: *Annu. Rev. Biomed. Eng.* 13 (2011), pp. 127–155.

[52] M. Delitala, U. Dianzani, T. Lorenzi, and M. Melensi. "A mathematical model for immune and autoimmune response mediated by T-cells". In: *Comput. Math. Appl.* 66.6 (2013), pp. 1010–1023.

[53] M. Delitala and T. Lorenzi. "Evolutionary branching patterns in predator-prey structured populations". In: *Discrete Contin. Dyn. Syst. Ser. B* 18.9 (2013), p. 2267.

[54] M. Delitala and T. Lorenzi. "Recognition and learning in a mathematical model for immune response against cancer." In: *Discrete Contin. Dyn. Syst. Ser. B* 18.4 (2013).

[55] P. J. Delves and I. M. Roitt. "The immune system". In: *N. Engl. J. Med.* 343.1 (2000), pp. 37–49.

[56] W. Doerfler and P. Böhm. *DNA methylation: development, genetic disease and cancer.* Vol. 310. Springer Science & Business Media, 2006.

[57] G. Dranoff. "Cytokines in cancer pathogenesis and cancer therapy". In: *Nat. Rev. Cancer* 4.1 (2004), pp. 11–22.

[58] D. Drasdo and S. Höhme. "Individual-based approaches to birth and death in avascu1ar tumors". In: *Math. Comput. Model.* 37.11 (2003), pp. 1163–1175.

[59] P. Duesberg, R. Stindl, and R. Hehlmann. "Explaining the high mutation rates of cancer cells to drug and multidrug resistance by chromosome reassortments that are catalyzed by aneuploidy". In: *Proc. Natl. Acad. Sci. U.S.A.* 97.26 (2000), pp. 14295–14300.

[60] G. P. Dunn, A. T. Bruce, H. Ikeda, L. J. Old, and R. D. Schreiber. "Cancer immunoediting: from immunosurveillance to tumor escape". In: *Nat. Immunol.* 3.11 (2002), pp. 991–998.

[61] R. Eftimie, J. L. Bramson, and D. J. D. Earn. "Interactions between the immune system and cancer: a brief review of non-spatial mathematical models". In: *Bull. Math. Biol.* 73.1 (2011), pp. 2–32.

[62] L. M. Ellis and I. J. Fidler. "Angiogenesis and metastasis". In: *Eur. J. Cancer.* 32.14 (1996), pp. 2451–2460.

[63] P. M. Enriquez-Navas et al. "Exploiting evolutionary principles to prolong tumor control in preclinical models of breast cancer". In: *Sci. Transl. Med.* 8.327 (2016), 327ra24–327ra24.

[64] G. I. Evan and K. H. Vousden. "Proliferation, cell cycle and apoptosis in cancer". In: *Nature* 411.6835 (2001), pp. 342–348.

[65] F. L. Fennemann, I. J. M. de Vries, C. G. Figdor, and M. Verdoes. "Attacking tumors from all sides: Personalized multiplex vaccines to tackle intratumor heterogeneity". In: *Front. immunol.* 10 (2019), p. 824.

[66] A. D. Fesnak, C. H. June, and B. L. Levine. "Engineered T cells: the promise and challenges of cancer immunotherapy". In: *Nat. Rev. Cancer* 16.9 (2016), pp. 566–581.

[67] U. Foryś, J. Waniewski, and P. Zhivkov. "Anti-tumor immunity and tumor anti-immunity in a mathematical model of tumor immunotherapy". In: *J. Biol. Syst.* 14.01 (2006), pp. 13–30.

[68] K. Franciszkiewicz, A. Boissonnas, M. Boutet, C. Combadiere, and F. Mami-Chouaib. "Role of Chemokines and Chemokine Receptors in Shaping the Effector Phase of the Antitumor Immune Response". In: *Cancer Res.* 72.24 (2012), pp. 6325–6332.

[69] F. Frascoli, P. S. Kim, B. D. Hughes, and K. A. Landman. "A Dynamical Model of Tumour Immunotherapy". In: *Math. Biosci.* 253 (2014), pp. 50–62.

[70] J. Galon and D. Bruni. "Approaches to treat immune hot, altered and cold tumours with combination immunotherapies". In: *Nat. Rev. Drug Discov.* 18.3 (2019), pp. 197–218.

[71] J. Galon et al. "Immunoscore and Immunoprofiling in cancer: an update from the melanoma and immunotherapy bridge 2015". In: *J. Transl. Med.* 14.273 (2016).

[72] J. Galon et al. "Type, density, and location of immune cells within human colorectal tumors predict clinical outcome". In: *Science* 313.5795 (2006), pp. 1960–1964.

[73] L. Gandhi et al. "Pembrolizumab plus chemotherapy in metastatic non–small-cell lung cancer". In: *N. Engl. J. Med.* 378.22 (2018), pp. 2078–2092.

[74] Leena Gandhi et al. "Pembrolizumab plus chemotherapy in metastatic non–small-cell lung cancer". In: *New England journal of medicine* 378.22 (2018), pp. 2078–2092.

[75] X. Gao, C. Arpin, J. Marvel, S. A. Prokopiou, O. Gandrillon, and F. Crauste. "IL-2 sensitivity and exogenous IL-2 concentration gradient tune the productive contact duration of CD8+ T cell-APC: a multiscale modeling study". In: *BMC Syst. Biol.* 10.1 (2016), p. 77.

[76] F. Garrido, N. Aptsiauri, E. M. Doorduijn, A. M. G. Lora, and T. Van Hall. "The urgent need to recover MHC class I in cancers for effective immunotherapy". In: *Curr. Opin. Immunol.* 39 (2016), pp. 44–51.

[77] F. Garrido, T. Cabrera, and N. Aptsiauri. ""Hard" and "soft" lesions underlying the HLA class I alterations in cancer cells: implications for immunotherapy". In: *Int. J. Cancer Res.* 127.2 (2010), pp. 249–256.

[78] K. R. Garrod, H. D. Moreau, Z. Garcia, F. Lemaitre, I. Bouvier, M. L. Albert, and P. Bousso. "Dissecting T cell contraction in vivo using a genetically encoded reporter of apoptosis". In: *Cell Rep.* 2.5 (2012), pp. 1438–1447.

[79] R. A. Gatenby, A. S. Silva, R. J. Gillies, and B. R. Frieden. "Adaptive therapy". In: *Cancer Res.* 69.11 (2009), pp. 4894–4903.

[80] R. S. Gejman, A. Y. Chang, H. F. Jones, K. DiKun, A. A. Hakimi, A. Schietinger, and D. A. Scheinberg. "Rejection of immunogenic tumor clones is limited by clonal fraction". In: *Elife* 7 (2018), e41090.

[81] S. Génieys, V. Volpert, and P. Auger. "Adaptive dynamics: modelling Darwin's divergence principle". In: *C. R. Biol.* 329.11 (2006), pp. 876–879.

[82] Jason T George and Herbert Levine. "Implications of tumor–immune coevolution on cancer evasion and optimized immunotherapy". In: *Trends in Cancer* 7.4 (2021), pp. 373–383.

[83] Ulrike Gerdemann et al. "Cytotoxic T lymphocytes simultaneously targeting multiple tumor-associated antigens to treat EBV negative lymphoma". In: *Molecular therapy* 19.12 (2011), pp. 2258–2268.

[84] G. Germano et al. "Inactivation of DNA repair triggers neoantigen generation and impairs tumour growth". In: *Nature* 552.7683 (2017), pp. 116–120.

[85] A. Ghaffarizadeh, R. Heiland, S. H. Friedman, S. M Mumenthaler, and P. Macklin. "PhysiCell: an open source physics-based cell simulator for 3-D multicellular systems". In: *PLoS Comput. Biol.* 14.2 (2018), e1005991.

[86] Diogo Gomes-Silva and Carlos A Ramos. "Cancer immunotherapy using CAR-T cells: from the research bench to the assembly line". In: *Biotechnology journal* 13.2 (2018), p. 1700097.

[87] C. Gong, O. Milberg, B. Wang, P. Vicini, R. Narwal, L. Roskos, and A. S. Popel. "A computational multiscale agent-based model for simulating spatio-temporal tumour immune response to PD1 and PDL1 inhibition". In: *J. R. Soc. Interface* 14.134 (2017), p. 20170320.

[88] A. V. Gorbachev, Hi. Kobayashi, D. Kudo, Ch. S. Tannenbaum, J. H. Finke, Su. Shu, J. M. Farber, and R. L. Fairchild. "CXC chemokine ligand 9/monokine induced by IFN-γ production by tumor cells is critical for T cell-mediated suppression of cutaneous tumors". In: *J. Immunol.* 178.4 (2007), pp. 2278–2286.

[89] F. Graner and J. A. Glazier. "Simulation of biological cell sorting using a two-dimensional extended Potts model". In: *Phys. Rev. Lett.* 69.13 (1992), p. 2013.

[90] M. Greaves and C. C. Maley. "Clonal evolution in cancer". In: *Nature* 481.7381 (2012), pp. 306–313.

[91] A. L Grilo and A. Mantalaris. "The increasingly human and profitable monoclonal antibody market". In: *Trends Biotechnol.* 37.1 (2019), pp. 9–16.

[92] G. Gross and Z. Eshhar. "Therapeutic potential of T cell chimeric antigen receptors (CARs) in cancer treatment: counteracting off-tumor toxicities for safe CAR T cell therapy". In: *Annu. Rev. Pharmacol. Toxicol.* 56 (2016), pp. 59–83.

[93] M. M. Gubin et al. "Checkpoint blockade cancer immunotherapy targets tumour-specific mutant antigens". In: *Nature* 515.7528 (2014), pp. 577–581.

[94] D. Hanahan and R. A. Weinberg. "Hallmarks of cancer: the next generation". In: *Cell* 144.5 (2011), pp. 646–674.

[95] P. S. Hegde, V. Karanikas, and S. Evers. "The where, the when, and the how of immune monitoring for cancer immunotherapies in the era of checkpoint inhibition". In: *Clinical Cancer Res.* 22.8 (2016), pp. 1865–1874.

[96] M. D. Hellmann, C. F. Friedman, and J. D. Wolchok. "Combinatorial cancer immunotherapies". In: *Adv. Immunol.* 130 (2016), pp. 251–277.

[97] M. D. Hellmann et al. "Genomic features of response to combination immunotherapy in patients with advanced non-small-cell lung cancer". In: *Cancer Cell* 33.5 (2018), pp. 843–852.

[98] M. D. Hellmann et al. "Nivolumab plus ipilimumab in lung cancer with a high tumor mutational burden". In: *N. Eng. J. Med.* 378.22 (2018), pp. 2093–2104.

[99] G. Al-Hity et al. "An integrated framework for quantifying immune-tumour interactions in a 3D co-culture model". In: *Commun. Biol.* 4.1 (2021), pp. 1–12.

[100] S. Hoehme and D. Drasdo. "A cell-based simulation software for multi-cellular systems". In: *Bioinformatics* 26.20 (2010), pp. 2641–2642.

[101] X. Hu, G. Ke, and S. R.-J. Jang. "Modeling pancreatic cancer dynamics with immunotherapy". In: *Bull. Math. Biol.* 81.6 (2019), pp. 1885–1915.

[102] A. C. Huang et al. "T-cell invigoration to tumour burden ratio associated with anti-PD-1 response". In: *Nature* 545.7652 (2017), p. 60.

[103] S. Huang. "Genetic and non-genetic instability in tumor progression: link between the fitness landscape and the epigenetic landscape of cancer cells". In: *Cancer Metastasis Rev.* 32.3-4 (2013), pp. 423–448.

[104] B. D. Hughes. *Random walks and random environments: random walks*. Vol. 1. Oxford University Press, 1995.

[105] Y. Iwai, M. Ishida, Y. Tanaka, T. Okazaki, T. Honjo, and N. Minato. "Involvement of PD-L1 on tumor cells in the escape from host immune system and tumor immunotherapy by PD-L1 blockade". In: *Proc. Natl. Acad. Sci. U.S.A.* 99.19 (2002), pp. 12293–12297.

[106] Y. Iwasa, M. A. Nowak, and F. Michor. "Evolution of resistance during clonal expansion". In: *Genetics* 172.4 (2006), pp. 2557–2566.

[107] J. A Izaguirre et al. "CompuCell, a multi-model framework for simulation of morphogenesis". In: *Bioinformatics* 20.7 (2004), pp. 1129–1137.

[108] A. M. Jarrett, D. Faghihi, D. A Hormuth, E. A.B. F. Lima, J. Virostko, G. Biros, D. Patt, and T.s E. Yankeelov. "Optimal control theory for personalized therapeutic regimens in oncology: Background, history, challenges, and opportunities". In: *J. Clin. Med.* 9.5 (2020), p. 1314.

[109] Y. Jiang, Y. Li, and B. Zhu. "T-cell exhaustion in the tumor microenvironment". In: *Cell Death & Disease* 6.6 (2015), e1792–e1792.

[110] S. T. Johnston, M. J. Simpson, and R. E. Baker. "Modelling the movement of interacting cell populations: a moment dynamics approach". In: *J. Theor. Biol.* 370 (2015), pp. 81–92.

[111] Carl H June, Roddy S O'Connor, Omkar U Kawalekar, Saba Ghassemi, and Michael C Milone. "CAR T cell immunotherapy for human cancer". In: *Science* 359.6382 (2018), pp. 1361–1365.

[112] P. L. Kastritis and A. M. J. J. Bonvin. "On the binding affinity of macromolecular interactions: daring to ask why proteins interact". In: *J. R. Soc. Interface* 10.79 (2013), p. 20120835.

[113] J. N. Kather et al. "*In silico* modeling of immunotherapy and stroma-targeting therapies in human colorectal cancer". In: *Cancer Res.* 77.22 (2017), pp. 6442–6452.

[114] D. Kato, T. Yaguchi, Ta. Iwata, K. Morii, T. Nakagawa, R. Nishimura, and Y. Kawakami. "Prospects for personalized combination immunotherapy for solid tumors based on adoptive cell therapies and immune checkpoint blockade therapies". In: *Nihon Rinsho Meneki Gakkai Kaishi* 40.1 (2017), pp. 68–77.

[115] N. W. Kim et al. "Specific association of human telomerase activity with immortal cells and cancer". In: *Science* 266.5193 (1994), pp. 2011–2015.

[116] P. S. Kim and P. P. Lee. “Modeling protective anti-tumor immunity via preventative cancer vaccines using a hybrid agent-based and delay differential equation approach”. In: *PLoS Comput. Biol.* 8.10 (2012), e1002742.

[117] R. Kim. “Cancer immunoediting: from immune surveillance to immune escape”. In: *Cancer Immunotherapy* (2007), pp. 9–27.

[118] D. Kirschner and J. C. Panetta. “Modeling immunotherapy of the tumor–immune interaction”. In: *J. Math. Biol.* 37.3 (1998), pp. 235–252.

[119] C. A. Klebanoff, L. Gattinoni, and N. P. Restifo. “CD8+ T-cell memory in tumor immunology and immunotherapy”. In: *Immunol. Rev.* 211.1 (2006), pp. 214–224.

[120] M. Kolev, S. Nawrocki, and B. Zubik-Kowal. “Numerical simulations for tumor and cellular immune system interactions in lung cancer treatment”. In: *Commun. Nonlinear Sci. Numer. Simul.* 18.6 (2013), pp. 1473–1480.

[121] A. Konstorum, A. T. Vella, A. J. Adler, and R. C. Laubenbacher. “Addressing current challenges in cancer immunotherapy with mathematical and computational modelling”. In: *J. R. Soc. Interface* 14.131 (2017), p. 20170150.

[122] M. Kuznetsov, J. Clairambault, and V. Volpert. “Improving cancer treatments via dynamical biophysical models”. In: *Phys. Life Rev.* 39 (2021), pp. 1–48.

[123] V. A. Kuznetsov, I. A. Makalkin, M. A. Taylor, and A. S. Perelson. “Nonlinear dynamics of immunogenic tumors: parameter estimation and global bifurcation analysis”. In: *Bull. Math. Biol.* 56.2 (1994), pp. 295–321.

[124] J.-W. Lee et al. “Surgical stress promotes tumor growth in ovarian carcinoma”. In: *Clin. Cancer Res.* 15.8 (2009), pp. 2695–2702.

[125] F. Leonard, L. T. Curtis, A. R. Hamed, C. Zhang, E. Chau, D. Sieving, B. Godin, and H. B. Frieboes. “Nonlinear response to cancer nanotherapy due to macrophage interactions revealed by mathematical modeling and evaluated in a murine model via CRISPR-modulated macrophage polarization”. In: *Cancer Immunol. Immunother.* 69.5 (2020), pp. 731–744.

[126] P. Leone, E. C. Shin, F. Perosa, A. Vacca, F. Dammacco, and V. Racanelli. “MHC class I antigen processing and presenting machinery: organization, function, and defects in tumor cells”. In: *J. Natl. Cancer Inst.* 105.16 (2013), pp. 1172–1187.

[127] E. Leschiera, T. Lorenzi, S. Shen, L. Almeida, and C. Audebert. “A mathematical model to study the impact of intra-tumour heterogeneity on anti-tumour CD8+ T cell immune response”. In: *J. Theor. Biol.* (2022), p. 111028.

[128] R. J. LeVeque. *Finite difference methods for ordinary and partial differential equations: steady-state and time-dependent problems*. SIAM, 2007.

[129] D. Li et al. “Genetically engineered T cells for cancer immunotherapy”. In: *Signal Transduct. Target. Ther.* 4.1 (2019), pp. 1–17.

[130] T. Lorenzi. “Cancer modelling as fertile ground for new mathematical challenges. Comment on" Improving cancer treatments via dynamical biophysical models" by M. Kuznetsov, J. Clairambault & V. Volpert”. In: *Phys. Life Rev.* 40 (2022), pp. 3–5.

[131] T. Lorenzi, R. H. Chisholm, L. Desvillettes, and B. D. Hughes. “Dissecting the dynamics of epigenetic changes in phenotype-structured populations exposed to fluctuating environments”. In: *J. Theor. Biol.* 386 (2015), pp. 166–176.

[132] T. Lorenzi, R. H. Chisholm, M. Melensi, A. Lorz, and M. Delitala. "Mathematical model reveals how regulating the three phases of T-cell response could counteract immune evasion". In: *Immunology* 146.2 (2015), pp. 271–280.

[133] T. Lorenzi, P. J. Murray, and M. Ptashnyk. "From individual-based mechanical models of multicellular systems to free-boundary problems". In: *Interfaces Free Boundaries* 22.2 (2020), pp. 205–244.

[134] A. Lorz, T. Lorenzi, J. Clairambault, A. Escargueil, and B. Perthame. "Modeling the effects of space structure and combination therapies on phenotypic heterogeneity and drug resistance in solid tumors". In: *Bull. Math. Biol.* 77.1 (2015), pp. 1–22.

[135] A. Lorz, T. Lorenzi, M. E. Hochberg, J. Clairambault, and B. Perthame. "Populational adaptive evolution, chemotherapeutic resistance and multiple anti-cancer therapies". In: *Esaim Math. Model. Numer. Anal.* 47.2 (2013), pp. 377–399.

[136] M. Łuksza et al. "A neoantigen fitness model predicts tumour response to checkpoint blockade immunotherapy". In: *Nature* 551.7681 (2017), pp. 517–520.

[137] P. M. Lushnikov, N. Chen, and M. Alber. "Macroscopic dynamics of biological cells interacting via chemotaxis and direct contact". In: *Phys. Rev. E* 78.6 (2008), p. 061904.

[138] F. R. Macfarlane, M. A. J. Chaplain, and T. Lorenzi. "A hybrid discrete-continuum approach to model Turing pattern formation". In: *Math. Biosci. Eng.* 17.6 (2020), pp. 7442–7479.

[139] F. R. Macfarlane, M. A. J. Chaplain, and T. Lorenzi. "A stochastic individual-based model to explore the role of spatial interactions and antigen recognition in the immune response against solid tumours". In: *J. Theor. Biol.* 480 (2019), pp. 43–55.

[140] F. R. Macfarlane, T. Lorenzi, and M. A. J. Chaplain. "Modelling the immune response to cancer: an individual-based approach accounting for the difference in movement between inactive and activated T cells". In: *Bull. Math. Biol.* 80.6 (2018), pp. 1539–1562.

[141] P. Maini, K. Painter, and H. P. Chau. "Spatial pattern formation in chemical and biological systems". In: *J. Chem. Soc. Faraday Trans.* 93.20 (1997), pp. 3601–3610.

[142] D. G. Mallet and L. G. De Pillis. "A cellular automata model of tumor–immune system interactions". In: *J. Theor. Biol.* 239.3 (2006), pp. 334–350.

[143] L. Martıénez-Lostao, A. Anel, and J. Pardo. "How do cytotoxic lymphocytes kill cancer cells?" In: *Clinical Cancer Res.* 21.22 (2015), pp. 5047–5056.

[144] D. Mason. "A very high level of crossreactivity is an essential feature of the T-cell receptor". In: *Immunol. Today* 9 (1998), pp. 395–404.

[145] A. Masoudi-Nejad, G. Bidkhori, S. H. Ashtiani, A. Najafi, J. H. Bozorgmehr, and E. Wang. "Cancer systems biology and modeling: microscopic scale and multiscale approaches". In: *Seminars in cancer biology*. Vol. 30. Elsevier. 2015, pp. 60–69.

[146] MATLAB. *9.9.0.1570001 (R2020b)*. Natick, Massachusetts: The MathWorks Inc., 2020.

[147] A. Matzavinos and M. A. J. Chaplain. "Travelling-wave analysis of a model of the immune response to cancer". In: *C. R. Biol.* 327.11 (2004), pp. 995–1008.

[148] A. Matzavinos, M. A. J. Chaplain, and V. A. Kuznetsov. "Mathematical modelling of the spatio-temporal response of cytotoxic T-lymphocytes to a solid tumour". In: *Math. Med. Biol.* 21.1 (2004), pp. 1–34.

[149] K. A. McDonald et al. "Tumor heterogeneity correlates with less immune response and worse survival in breast cancer patients". In: *Annals of Surgical Oncology* 26.7 (2019), pp. 2191–2199.

[150] N. McGranahan et al. "Clonal neoantigens elicit T cell immunoreactivity and sensitivity to immune checkpoint blockade". In: *Science* 351.6280 (2016), pp. 1463–1469.

[151] J. L. Messerschmidt, G. C. Prendergast, and G. L. Messerschmidt. "How cancers escape immune destruction and mechanisms of action for the new significantly active immune therapies: Helping nonimmunologists decipher recent advances". In: *The Oncologist* 21.2 (2016), p. 233.

[152] N. Metropolis, A. W. Rosenbluth, M. N. Rosenbluth, A. H. Teller, and E. Teller. "Equation of state calculations by fast computing machines". In: *J. Chem. Phys.* 21.6 (1953), pp. 1087–1092.

[153] M. J. Miller, S. H. Wei, M. D. Cahalan, and I. Parker. "Autonomous T cell trafficking examined in vivo with intravital two-photon microscopy". In: *Proc. Natl. Acad. Sci. U.S.A.* 100.5 (2003), pp. 2604–2609.

[154] B. Min. "Spontaneous T cell proliferation: a physiologic process to create and maintain homeostatic balance and diversity of the immune system". In: *Front. Immunol.* 9 (2018), p. 547.

[155] G. R. Mirams et al. "Chaste: an open source C++ library for computational physiology and biology". In: *PLOS Comput. Biol.* 9.3 (2013), e1002970.

[156] R. J. Motzer et al. "Nivolumab plus ipilimumab versus sunitinib in advanced renal-cell carcinoma". In: *N. Eng. J. Med.* (2018).

[157] J. D. Murray. *Mathematical biology II: spatial models and biomedical applications*. Vol. 3. Springer New York, 2001.

[158] N. Nagarsheth et al. "PRC2 epigenetically silences Th1-type chemokines to suppress effector T-cell trafficking in colon cancer". In: *Cancer Res.* 76.2 (2016), pp. 275–282.

[159] M Naghavi et al. "Global, regional, and national age-sex specific mortality for 264 causes of death, 1980–2016: a systematic analysis for the Global Burden of Disease Study 2016". In: *Lancet* 390.10100 (2017), pp. 1151–1210.

[160] M. B. Nilsson et al. "Stress hormones regulate interleukin-6 expression by human ovarian carcinoma cells through a Src-dependent mechanism". In: *J. Biol. Chem.* 282.41 (2007), pp. 29919–29926.

[161] P. C. Nowell. "The clonal evolution of tumor cell populations". In: *Science* 194.4260 (1976), pp. 23–28.

[162] E. J. Odes et al. "Earliest hominin cancer: 1.7-million-year-old osteosarcoma from Swartkrans Cave, South Africa". In: *S. Afr. J. Sci.* 112.7-8 (2016), pp. 1–5.

[163] A. Osojnik, E. A. Gaffney, M. Davies, J. W. Yates, and H. M. Byrne. "Identifying and characterising the impact of excitability in a mathematical model of tumour-immune interactions". In: *J. Theor. Biol.* 501 (2020), p. 110250.

[164] Franck Pagès, Jérôme Galon, and Wolf H Fridman. "The essential role of the in situ immune reaction in human colorectal cancer". In: *Journal of leukocyte biology* 84.4 (2008), pp. 981–987.

[165] K. J. Painter. "Mathematical models for chemotaxis and their applications in self-organisation phenomena". In: *J. Theor. Biol.* 481 (2019), pp. 162–182.

[166] K. J. Painter and T. Hillen. "Navigating the flow: individual and continuum models for homing in flowing environments". In: *J. R. Soc. Interface* 12.112 (2015), p. 20150647.

[167] K. J. Painter and T. Hillen. "Volume-filling and quorum-sensing in models for chemosensitive movement". In: *Can. Appl. Math. Quart* 10.4 (2002), pp. 501–543.

[168] K. Pansy et al. "Immune regulatory processes of the tumor microenvironment under malignant conditions". In: *Int. J. Mol. Sci.* 22.24 (2021), p. 13311.

[169] F. Pappalardo, I. M. Forero, M. Pennisi, A. Palazon, I. Melero, and S. Motta. "SimB16: modeling induced immune system response against B16-melanoma". In: *PloS one* 6.10 (2011), e26523.

[170] K. E. Pauken, M. Dougan, N. R. Rose, A. H. Lichtman, and A. H. Sharpe. "Adverse events following cancer immunotherapy: obstacles and opportunities". In: *Trends Immunol.* 40.6 (2019), pp. 511–523.

[171] B. Perthame. "Parabolic equations in biology". In: *Parabolic Equations in Biology*. Springer, 2015, pp. 1–21.

[172] B. Perthame. *Transport equations in biology*. Springer Science & Business Media, 2006.

[173] R. E. Phillips. "Immunology taught by Darwin". In: *Nat. Immunol.* 3.11 (2002), pp. 987–989.

[174] N. Picco, E. Sahai, P. K. Maini, and A. R. A. Anderson. "Integrating models to quantify environment-mediated drug resistance". In: *Cancer Res.* 77.19 (2017), pp. 5409–5418.

[175] L. G. de Pillis, D. G Mallet, and A. E. Radunskaya. "Spatial tumor-immune modeling". In: *Comput. Math. Methods Med.* 7.2-3 (2006), pp. 159–176.

[176] L. G. de Pillis, K. Renee Fister, W. Gu, C. Collins, M. Daub, D. Gross, J. Moore, and B. Preskill. "Mathematical model creation for cancer chemo-immunotherapy". In: *Comput. Math. Methods Med.* 10.3 (2009), pp. 165–184.

[177] Noelia Purroy and Catherine J Wu. "Coevolution of leukemia and host immune cells in chronic lymphocytic leukemia". In: *Cold Spring Harbor perspectives in medicine* 7.4 (2017), a026740.

[178] G. A. Rabinovich, D. Gabrilovich, and E. M. Sotomayor. "Immunosuppressive strategies that are mediated by tumor cells". In: *Annu. Rev. Immunol.* 25 (2007), pp. 267–296.

[179] A. Radunskaya, R. Kim, and T. Woods II. "Mathematical modeling of tumor immune interactions: a closer look at the role of a PD-L1 inhibitor in cancer immunotherapy". In: *Spora: J. Biomat.* 4.1 (2018), pp. 25–41.

[180] A. Reuben et al. "TCR repertoire intratumor heterogeneity in localized lung adenocarcinomas: an association with predicted neoantigen heterogeneity and postsurgical recurrence". In: *Cancer Discov.* 7.10 (2017), pp. 1088–1097.

[181] A. Ribas and J. D. Wolchok. "Cancer immunotherapy using checkpoint blockade". In: *Science* 359.6382 (2018), pp. 1350–1355.

[182] R. M. Samstein et al. "Tumor mutational load predicts survival after immunotherapy across multiple cancer types". In: *Nature Genetics* 51.2 (2019), pp. 202–206.

[183] P. M. Schiltz, G. G. Gomez, S. B. Read, N. V. Kulprathipanja, and C. A. Kruse. "Effects of IFN-γ and Interleukin-1 β on Major Histocompatibility Complex Antigen and Intercellular Adhesion Molecule-1 Expression by 9L Gliosarcoma: Relevance to Its Cytolysis by Alloreactive Cytotoxic T Lymphocytes". In: *J. Interferon Cytokine Res.* 22.12 (2002), pp. 1209–1216.

[184] K. J. Schlesinger, S. P. Stromberg, and J. M. Carlson. "Coevolutionary immune system dynamics driving pathogen speciation". In: *PLoS ONE* 9.7 (2014).

[185] B. L. Segal, V. A. Volpert, and A. Bayliss. "Pattern formation in a model of competing populations with nonlocal interactions". In: *Phys. D* 253 (2013), pp. 12–22.

[186] S. P. Shariatpanahi, K. Madjidzadeh, M. Hassan, and M. Abedi-Valugerdi. "Mathematical modeling of tumor-induced immunosuppression by myeloid-derived suppressor cells: Implications for therapeutic targeting strategies". In: *J. Theor. Biol.* 442 (2018), pp. 1–10.

[187] J. A. Sherratt and M. A. Nowak. "Oncogenes, anti-oncogenes and the immune response to cancer: a mathematical model". In: *Proc. R. Soc. B: Biol. Sci.* 248.1323 (1992), pp. 261–271.

[188] L. Sigalotti et al. "Intratumor heterogeneity of cancer/testis antigens expression in human cutaneous melanoma is methylation-regulated and functionally reverted by 5-Aza-2'-deoxycytidine". In: *Cancer Res.* 64.24 (2004), pp. 9167–9171.

[189] C. Y. Slaney, M. H. Kershaw, and Ph. K. Darcy. "Trafficking of T cells into tumors". In: *Cancer Res.* 74.24 (2014), pp. 7168–7174.

[190] A. Snyder et al. "Genetic basis for clinical response to CTLA-4 blockade in melanoma". In: *N. Engl. J. Med.* 371.23 (2014), pp. 2189–2199.

[191] L. M. Sompayrac. *How the immune system works*. John Wiley & Sons, 2019.

[192] O. Sotolongo-Costa, L. M. Molina, D. R. Perez, J. C. Antoranz, and M. C. Reyes. "Behavior of tumors under nonstationary therapy". In: *Physica D* 178.3-4 (2003), pp. 242–253.

[193] S. Spranger, R. Bao, and T. F. Gajewski. "Melanoma-intrinsic β-catenin signalling prevents anti-tumour immunity". In: *Nature* 523.7559 (2015), pp. 231–235.

[194] R. E. A. Stace, T. Stiehl, M. A. J. Chaplain, A. Marciniak-Czochra, and T. Lorenzi. "Discrete and continuum phenotype-structured models for the evolution of cancer cell populations under chemotherapy". In: *Math. Model. Nat. Phenom.* 15 (2020), p. 14.

[195] N. V. Stepanova. "Course of the immune reaction during the development of a malignant tumour". In: *Biophysics* 24.5 (1979), pp. 917–923.

[196] B. Stockinger, T. Barthlott, and G. Kassiotis. "The concept of space and competition in immune regulation". In: *Immunology* 111.3 (2004), p. 241.

[197] J. D. Stone, A. S. Chervin, and D. M. Kranz. "T-cell receptor binding affinities and kinetics: impact on T-cell activity and specificity". In: *Immunology* 126.2 (2009), pp. 165–176.

[198] S. P. Stromberg and J. Carlson. "Robustness and fragility in immunosenescence". In: *PLOS Comput. Biol.* 2.11 (2006).

[199] S. P. Stromberg and J. M. Carlson. "Diversity of T-cell responses". In: *Phys. Biol.* 10.2 (2013), p. 025002.

[200] M. Al-Tameemi, M. A. J. Chaplain, and A. d'Onofrio. "Evasion of tumours from the control of the immune system: consequences of brief encounters". In: *Biol. Direct* 7.1 (2012), p. 31.

[201] M. Taya. "CT and histopathology used to diagnose osteosarcoma in a dinosaur". In: *Radiol. Imag. Cancer* 2.5 (2020), e209028.

[202] C. Tian, Z. Ling, and L. Zhang. "Nonlocal interaction driven pattern formation in a prey–predator model". In: *Appl. Math. Comput.* 308 (2017), pp. 73–83.

[203] L. Tian et al. “Mutual regulation of tumour vessel normalization and immunostimulatory reprogramming”. In: *Nature* 544.7649 (2017), pp. 250–254.

[204] S. L. Topalian et al. “Safety, activity, and immune correlates of anti–PD-1 antibody in cancer”. In: *N. Engl. J. Med.* 366.26 (2012), pp. 2443–2454.

[205] I. K. Tough. “Mathematical modelling of the immune response to cancer”. PhD thesis. University of Dundee, 2017.

[206] O. Trédan, C. M. Galmarini, K. Patel, and I. F. Tannock. “Drug resistance and the solid tumor microenvironment”. In: *J. Natl. Cancer Inst.* 99.19 (2007), pp. 1441–1454.

[207] A. E. Troy and H. Shen. “Cutting edge: homeostatic proliferation of peripheral T lymphocytes is regulated by clonal competition”. In: *J. Immun.* 170.2 (2003), pp. 672–676.

[208] P. C Tumeh et al. “PD-1 blockade induces responses by inhibiting adaptive immune resistance”. In: *Nature* 515.7528 (2014), pp. 568–571.

[209] M. Urosevic, B. Braun, J. Willers, G. Burg, and R. Dummer. “Expression of melanoma-associated antigens in melanoma cell cultures”. In: *Exp. Dermatol.* 14.7 (2005), pp. 491–497.

[210] R. K. Vaddepally, P. Kharel, R. Pandey, R. Garje, and A. B. Chandra. “Review of indications of FDA-approved immune checkpoint inhibitors per NCCN guidelines with the level of evidence”. In: *Cancers* 12.3 (2020), p. 738.

[211] E. M. Van Allen et al. “Genomic correlates of response to CTLA-4 blockade in metastatic melanoma”. In: *Science* 350.6257 (2015), pp. 207–211.

[212] P. Van Liedekerke, M. M. Palm, N. Jagiella, and D. Drasdo. “Simulating tissue mechanics with agent-based models: concepts, perspectives and some novel results”. In: *Comput. Part. Mech.* 2.4 (2015), pp. 401–444.

[213] M. G. Vander Heiden, L. C. Cantley, and C. B. Thompson. “Understanding the Warburg effect: the metabolic requirements of cell proliferation”. In: *Science* 324.5930 (2009), pp. 1029–1033.

[214] R. Walker and H. Enderling. “From Concept to Clinic: Mathematically Informed Immunotherapy”. In: *Curr. Probl. Cancer* 40.1 (2016), pp. 68–83.

[215] Q. Wang, D. J Klinke, and Z. Wang. “CD8+ T cell response to adenovirus vaccination and subsequent suppression of tumor growth: modeling, simulation and analysis”. In: *BMC Syst. Biol.* 9.1 (2015), pp. 1–19.

[216] X. Wang and I. Rivière. “Clinical manufacturing of CAR T cells: foundation of a promising therapy”. In: *Mol. Ther. Oncolytics* 3 (2016), p. 16015.

[217] Z. Wang and T. Hillen. “Classical solutions and pattern formation for a volume filling chemotaxis model”. In: *Chaos* 17.3 (2007), p. 037108.

[218] J. West, L. You, J. Zhang, R. A. Gatenby, J. S. Brown, P. K. Newton, and A. R. A. Anderson. “Towards multidrug adaptive therapy”. In: *Cancer Res.* 80.7 (2020), pp. 1578–1589.

[219] E. J. Wherry. “T cell exhaustion”. In: *Nat. Immunol.* 12.6 (2011), pp. 492–499.

[220] T. L. Whiteside, S. Demaria, M. E. Rodriguez-Ruiz, H. M. Zarour, and I. Melero. “Emerging opportunities and challenges in cancer immunotherapy”. In: *Clin. Cancer Res.* 22.8 (2016), pp. 1845–1855.

[221] A. Wieland et al. “T cell receptor sequencing of activated CD8 T cells in the blood identifies tumor-infiltrating clones that expand after PD-1 therapy and radiation in a melanoma patient”. In: *Cancer Immunol. Immunother.* 67.11 (2018), pp. 1767–1776.

[222] J. D. Wolchok et al. “Overall survival with combined nivolumab and ipilimumab in advanced melanoma”. In: *N. Eng. J. Med.* 377.14 (2017), pp. 1345–1356.

[223] Y. Wolf et al. “Uvb-induced tumor heterogeneity diminishes immune response in melanoma”. In: *Cell* 179.1 (2019), pp. 219–235.

[224] L. Wooldridge et al. “A single autoimmune T cell receptor recognizes more than a million different peptides”. In: *J. Biol. Chem.* 287.2 (2012), pp. 1168–1177.

[225] L. L van der Woude, M. A. J. Gorris, A. Halilovic, C. G. Figdor, and I. J. M. de Vries. “Migrating into the tumor: a roadmap for T cells”. In: *Trends Cancer* 3.11 (2017), pp. 797–808.

[226] J. S. Yi, M. A. Cox, and A. J. Zajac. “T-cell exhaustion: characteristics, causes and conversion”. In: *Immunology* 129.4 (2010), pp. 474–481.

[227] Y. Yu, X. Ma, R. Gong, J. Zhu, L. Wei, and J. Yao. “Recent advances in CD8+ regulatory T cell research”. In: *Oncol. Lett.* 15.6 (2018), pp. 8187–8194.

[228] J. Zhang, J. J. Cunningham, J. S. Brown, and R. A. Gatenby. “Integrating evolutionary dynamics into treatment of metastatic castrate-resistant prostate cancer”. In: *Nat. Commun.* 8.1 (2017), pp. 1–9.

[229] Q. Zhao et al. “Engineered TCR-T Cell Immunotherapy in Anticancer Precision Medicine: Pros and Cons”. In: *Front. Immunol.* 12 (2021), p. 812.

[230] A. Zlotnik. “Chemokines and cancer”. In: *Int. J. Cancer Res.* 119.9 (2006), pp. 2026–2029.

[231] E. I. Zuniga and J. A. Harker. “T-cell exhaustion due to persistent antigen: Quantity not quality?” In: *Eur. J. Immunol.* 42.9 (2012), pp. 2285–2289.

Mathematical models of tumour-immune interactions: discrete and continuum approaches

Abstract

The past decade's technological advances have led to the development of immunotherapies, which differ from conventional anti-cancer therapies by targeting tumour-immune interactions to enhance the effectiveness of the anti-tumour immune response. However, these interactions are based on complex mechanisms that make it difficult to design treatments to effectively boost the immune response. For this reason, mathematical models are useful tools for reproducing and predicting the spatio-temporal dynamics of interactions between tumour cells and immune cells, in order to test the potential of new therapeutic techniques in a flexible and affordable way. In this thesis, we develop discrete and continuum models to describe the spatio-temporal dynamics of the interactions between a solid tumour and cytotoxic T cells, with the goal to investigate the biological settings which allow for the clearance or the escape of the tumour. The discrete models developed in this work track the dynamics of single cells, thus permitting the representation of single cell-scale mechanisms, and are sufficiently detailed and specific to qualitatively investigate and reproduce empirical observations. The continuum models considered are not formulated on the basis of phenomenological arguments, which can hinder a precise mathematical description of crucial biological and biophysical aspects, but they are formally derived from the discrete models through suitable asymptotic methods. The results of computational simulations of the discrete models show that there is an excellent quantitative agreement between them and numerical solutions of the corresponding continuum models, and further clarify the conditions for successful and unsuccessful immune surveillance. Ultimately, the mathematical models presented in this thesis may provide a framework to help biologists and clinicians gain a better understanding of the mechanisms that are responsible for immune escape, and they may be promising tools in the exploration of therapeutic strategies to improve the effectiveness of the overall anti-tumour immune response.

Keywords: tumour-immune interactions, immunotherapy, discrete models, continuum models, numerical simulations

---

Résumé

Au cours de la dernière décennie, les progrès technologiques ont permis la conception d'immunothérapies qui, contrairement aux thérapies anticancéreuses classiques, ciblent les interactions entre cellules tumorales et cellules immunitaires, dans le but de renforcer l'efficacité de la réponse immunitaire. Cependant, ces interactions reposent sur des mécanismes complexes, ce qui rend difficile la conception de traitements efficaces. Par conséquent, les modèles mathématiques sont des outils utiles pour reproduire la dynamique spatio-temporelle des interactions entre les cellules tumorales et les cellules immunitaires, afin de tester le potentiel de nouvelles techniques thérapeutiques de manière flexible et non coûteuse. Dans cette thèse, nous développons des modèles discrets et continus pour décrire la dynamique spatio-temporelle des interactions entre une tumeur solide et les cellules T cytotoxiques, dans le but d'étudier les paramètres biologiques qui permettent l'élimination, ou bien l'échappement, de la tumeur. Les modèles discrets développés dans ce travail décrivent la dynamique de chaque cellule, permettant ainsi la représentation de mécanismes à l'échelle cellulaire. De plus, ils sont suffisamment détaillés et spécifiques pour reproduire qualitativement les résultats d'études expérimentales. Quant aux modèles continus, ils ne sont pas formulés sur la base d'arguments phénoménologiques, qui peuvent limiter une description mathématique précise d'aspects biologiques et biophysiques cruciaux, mais ils sont dérivés formellement des modèles discrets par le biais de méthodes asymptotiques appropriées. Les résultats des simulations numériques des modèles discrets montrent qu'il existe un excellent accord quantitatif entre eux et les solutions des modèles continus correspondants, et clarifient les conditions de réussite, ou bien d'échec, de la surveillance immunitaire. Enfin, les modèles mathématiques présentés dans cette thèse peuvent fournir un cadre pour aider les biologistes et les cliniciens à mieux comprendre les mécanismes par lesquels les tumeurs échappent au système immunitaire, et peuvent être des outils prometteurs pour explorer des stratégies thérapeutiques conçues pour améliorer l'efficacité de la réponse immunitaire anti-tumorale.

Mots clés : interactions tumeur-système immunitaire, immunothérapie, modèles discrets, modèles continus, simulations numériques

---

Laboratoire Jacques-Louis Lions
Sorbonne Université – Campus Pierre et Marie Curie – 4 place Jussieu – 75005 Paris – France